

# Colloidal Silicon Quantum Dots: From Preparation to the Modifications of Self-Assembled Monolayers for Bio-applications

**Author:**

Cheng, Xiaoyu

**Publication Date:**

2015

**DOI:**

<https://doi.org/10.26190/unsworks/18132>

**License:**

<https://creativecommons.org/licenses/by-nc-nd/3.0/au/>

Link to license to see what you are allowed to do with this resource.

Downloaded from <http://hdl.handle.net/1959.4/54301> in <https://unsworks.unsw.edu.au> on 2024-05-03

# **Colloidal Silicon Quantum Dots: From Preparation to the Modifications of Self-Assembled Monolayers for Bio-applications**

by

Cheng Xiaoyu

A Thesis Submitted in Partial Fulfilment of the Requirements for the Degree of

**DOCTOR OF PHILOSOPHY**

SCHOOL OF CHEMISTRY

THE AUSTRALIAN CENTRE FOR NANOMEDICINE

THE UNIVERSITY OF NEW SOUTH WALES



**UNSW**  
THE UNIVERSITY OF NEW SOUTH WALES

April 2015

**PLEASE TYPE****THE UNIVERSITY OF NEW SOUTH WALES  
Thesis/Dissertation Sheet**

Surname or Family name: Cheng

First name: Xiaoyu

Other name/s:

Abbreviation for degree as given in the University calendar: Ph.D.

School: Chemistry

Faculty: Science

Title: Colloidal silicon quantum dots: from preparation to the modifications of self-assembled monolayers for bio-applications

**Abstract 350 words maximum: (PLEASE TYPE)**

Quantum dots (QDs) are semiconductor nanocrystals with unique photophysical properties. QDs have drawn broad research interests in the past two decades, because of their applications in optoelectronic devices, solar cells and fluorescent imaging agents in biomedicine. However, a major issue for the further development of this new class of materials is that many QDs are composed of heavy metal elements, which are considered unsafe for biological purposes. Therefore, concerns over nanoparticle related toxicity have inspired the design of QDs made from materials with biological benign nature, such as silicon.

The first challenge of working with nanocrystalline silicon quantum dots (SiQDs) is the limited methods available to prepare high quality, surface functionalized nanoparticles. Among the various methods available, chemical synthesis in the colloidal phase is of broad interests, for the simple procedures used and solution based approaches as needed in many applications. In this thesis, chapter three and chapter four describe two new approaches of coping with this challenge, using a one-step thiol-ene method, and a two-step copper catalyzed azide-alkyne cycloaddition (CuAAC) 'click' process respectively.

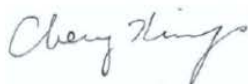
The second challenge of applying solution synthesized SiQDs for bio-imaging is their blue-green photoluminescence that can be affected by biological background signals, as well as the low excitation wavelength which may induce damage to cellular structures. Most responses to this challenge have been focused on material preparation, but limited success has been achieved when solution syntheses are involved. Chapter five presents a different strategy of resolving this issue by focusing on advanced microscopy. Specifically, fluorescence lifetime imaging microscopy (FLIM) is used to observe SiQDs in intracellular contexts, utilizing their long fluorescence lifetime in respect to one-photon FLIM, two-photon FLIM and FLIM-FRET.

Lastly, since surface modified colloidal SiQDs is still in its infancy of development, there are still limited studies showing their applications as biosensors. In chapter six, the efforts toward the preparation of the first SiQDs protease sensor is described. This is based on Förster Resonance Energy Transfer (FRET) process involving SiQDs-dye construct, where SiQDs were used as the donor and conjugated with an organic dye acceptor via an enzyme responsive peptide linker.

**Declaration relating to disposition of project thesis/dissertation**

I hereby grant to the University of New South Wales or its agents the right to archive and to make available my thesis or dissertation in whole or in part in the University libraries in all forms of media, now or here after known, subject to the provisions of the Copyright Act 1968. I retain all property rights, such as patent rights. I also retain the right to use in future works (such as articles or books) all or part of this thesis or dissertation.

I also authorise University Microfilms to use the 350 word abstract of my thesis in Dissertation Abstracts International (this is applicable to doctoral theses only).



Signature



Witness

April 15, 2015

Date

The University recognises that there may be exceptional circumstances requiring restrictions on copying or conditions on use. Requests for restriction for a period of up to 2 years must be made in writing. Requests for a longer period of restriction may be considered in exceptional circumstances and require the approval of the Dean of Graduate Research.

**FOR OFFICE USE ONLY**

Date of completion of requirements for Award:

**THIS SHEET IS TO BE GLUED TO THE INSIDE FRONT COVER OF THE THESIS**

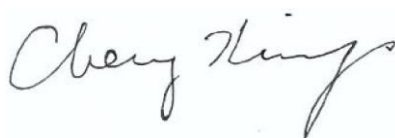
## **COPYRIGHT STATEMENT**

'I hereby grant the University of New South Wales or its agents the right to archive and to make available my thesis or dissertation in whole or part in the University libraries in all forms of media, now or here after known, subject to the provisions of the Copyright Act 1968. I retain all proprietary rights, such as patent rights. I also retain the right to use in future works (such as articles or books) all or part of this thesis or dissertation.

I also authorise University Microfilms to use the 350 word abstract of my thesis in Dissertation Abstract International (this is applicable to doctoral theses only).

I have either used no substantial portions of copyright material in my thesis or I have obtained permission to use copyright material; where permission has not been granted I have applied/will apply for a partial restriction of the digital copy of my thesis or dissertation.'

Signed

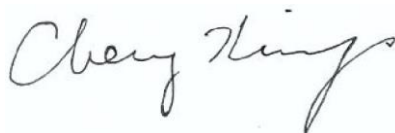


Date April 15, 2015

## **AUTHENTICITY STATEMENT**

'I certify that the Library deposit digital copy is a direct equivalent of the final officially approved version of my thesis. No emendation of content has occurred and if there are any minor variations in formatting, they are the result of the conversion to digital format.'

Signed



Date April 15, 2015

## ORIGINALITY STATEMENT

I hereby declare that this submission is my own work and to the best of my knowledge it contains no materials previously published or written by another person, or substantial proportions of material which have been accepted for the award of any other degree or diploma at UNSW or any other educational institution, except where due acknowledgement is made in the thesis. Any contribution made to the research by others, with whom I have worked at UNSW or elsewhere, is explicitly acknowledged in the thesis. I also declare that the intellectual content of this thesis is the product of my own work, except to the extent that assistance from others in the project's design and conception or in style, presentation and linguistic expression is acknowledged.

Signed

A handwritten signature in cursive script that reads "Cheryl Kings". The signature is written in black ink on a light-colored background.

Date April 15, 2015

## ABSTRACT

Quantum dots (QDs) are semiconductor nanocrystals with unique photophysical properties. Quantum dots have drawn broad research interests in the past three decades, because of their applications in optoelectronic devices, solar cells and fluorescent imaging agents in biomedicine. However, a major issue for the further development of this new class of materials is that many quantum dots are composed of heavy metal elements that are considered unsafe for biological purposes. Therefore, concerns over nanoparticle related toxicity have inspired the design of quantum dots made from materials with biological benign nature, such as crystalline silicon (Si).

The first challenge of working with nanocrystalline silicon quantum dots (SiQDs) is the limited methods available to prepare high quality, surface functionalized nanoparticles. Among the various methods available, colloidal synthesis is of broad interests, for the simple procedures used and solution-based approaches as needed in many applications. In this thesis, chapter three and chapter four describe two new approaches of coping with this challenge, using a one-step method based on thiol-ene chemistry, and a two-step process based on copper catalyzed azide-alkyne cycloaddition (CuAAC) reaction respectively.

The second challenge of applying solution synthesized SiQDs for bio-imaging is their blue photoluminescence that can be affected by biological background signals, as well as the low excitation wavelength that may induce damage to cellular structures. Most responses to this challenge have been focused on material preparation, but limited success has been achieved when solution syntheses are involved. In this thesis, chapter five presents a completely different strategy of resolving this issue by focusing on advanced microscopy. Specifically, fluorescence lifetime imaging microscopy (FLIM) is used to observe SiQDs in intracellular contexts, utilizing their long fluorescence lifetime in the context of one-photon FLIM, two-photon FLIM and energy transfer studies (FLIM-FRET).

Lastly, since surface modified colloidal SiQDs is still in its infancy of development, there are still limited studies showing their applications as biosensors. In chapter six, efforts toward the preparation of the first SiQDs protease sensor is described. This is based on Förster Resonance Energy Transfer (FRET) process involving SiQDs-dye construct, where SiQDs were used as the donor, and conjugated to an organic dye acceptor via an enzyme responsive peptide linker.

## LIST OF PUBLICATIONS

### JOURNAL PUBLICATIONS

(1) **Cheng, X.**; Hinde, E.; Owen D. M.; Lowe, S. B.; Reece, P. J.; Gaus, K.; Gooding, J. J.: Two photon fluorescence lifetime imaging microscopy (FLIM) of SiQDs. *In preparation*.

(1) **Cheng, X.**; *et. al.* A SiQDs protease sensor based on Förster resonance energy transfer (FRET). *In preparation*.

(3) **Cheng, X.**; Lowe, S. B.; Reece, P. J.; Gooding, J. J.: Colloidal SiQDs: from preparation to the modification of self-assembled monolayers (SAMs) for bio-applications. *Chem. Soc. Rev.* **2014**, *43*, 2680-2700.

(4) **Cheng, X.**; Lowe, S. B.; Ciampi, S.; Magenau, A.; Gaus, K.; Reece, P. J.; Gooding, J. J.: Versatile “Click Chemistry” Approach to Functionalizing SiQDs: Applications toward Fluorescent Cellular Imaging. *Langmuir* **2014**, *30*, 5209-5216.

(5) Chen, X.; **Cheng, X.**; Soeriyadi, A. H.; Sagnella, S. M.; Lu, X.; Scott, J. A.; Lowe, S. B.; Kavallaris, M.; Gooding, J. J.: Stimuli-responsive functionalized mesoporous silica nanoparticles for drug release in response to various biological stimuli. *Biomaterials Science* **2014**, *2*, 121-130.

(6) **Cheng, X. Y.**; Gondosiswanto, R.; Ciampi, S.; Reece, P. J.; Gooding, J. J.: One-pot synthesis of colloidal SiQDs and surface functionalization via thiol-ene click chemistry. *Chem Commun* **2012**, *48*, 11874-11876.

(7) Chen, X.; **Cheng, X.**; Gooding, J. J.: Detection of Trace Nitroaromatic Isomers Using Indium Tin Oxide Electrodes Modified Using  $\beta$ -Cyclodextrin and Silver Nanoparticles. *Analytical Chemistry* **2012**.

(8) Chen, X.; **Cheng, X.**; Gooding, J. J.: Multifunctional modified silver nanoparticles as ion and pH sensors in aqueous solution. *Analyst* **2012**, *137*, 2338-2343.

### CONFERENCE PROCEEDINGS

1. **Cheng, X.**; Reece, P.; Gooding, J. J. One pot synthesis of SiQDs passivated with alkanes or alkenes. *Proceedings of APMC 10/ICONN 2012/ACMM 22*, 6-9 Feb. 2012, Perth, Western Australia, Australia. Paper 00468.

2. Chen, X. **Cheng, X. Y.**; Gooding, J. J. Easily prepared mercaptoacetic acid and 2-amino-ethanethiol functionalized silver nanoparticles as ion probes and pH sensors in aqueous solution. *Proceedings of APMC 10/ICONN 2012/ACMM 22*, 6-9 Feb. 2012, Perth, Western Australia, Australia. Paper 00618.

3. **Cheng, X.**; Reece, P.; Gaus, K.; Gooding, J. J. A new route for the efficient synthesis and functionalization of bio-compatible silicon nanocrystals. *Proceedings of 3<sup>rd</sup> International Nanomedicine Conference*, 2-4 Jul. 2012, Sydney New South Wales, Australia.

## ACKNOWLEDGEMENT

Life is a long journey filled with much bitterness and joy, during which one meets many people and experiences many things. This PhD has been the most memorable part of my life. Time may fade its colour, but time will never remove its mark.

There are a number of people I would like to thank upon the completion of this thesis. I would like to begin by acknowledging my supervisor, Scientia Professor J. Justin Gooding, for his guidance and supports for me throughout this project. Justin is an extremely committed scientist and also a creative mentor. He has always tried to push me to think out of the box for the big the picture and I am a better scientist for it. He has profound understanding of diverse cultures, and also someone with lots of sense of humour. This has made the Gooding group an interesting place to work in, with people coming from all walks of life. Some of them will become my lifelong friends. Next, I would like to thank my co-supervisors, Prof. Katharina Gaus (School of Medicine) and Dr. Peter Reece (School of Physics), from both of whom I have learnt massively on biology and optics, to make this project across the traditional boundary of chemistry, where some of the most exciting scientific progresses are happening today. In addition, I would like to thank Prof. Barbara Messerle, Dr. Pall Thordarson, Dr. Till B öcking, Dr. Chuan Zhao, Prof. Bryan Hibbert, Dr. Jonathan Morris, Ms. Carla Gerbo and many other members from the school of chemistry, the ACN, the CVR and the university, for their dedicated support for me in the past four years, especially during the hardest time of this project.

I would like to thank my co-working 'lab-mates' for helping me in numerous ways throughout the project. They have taught me much more than just reading the papers. I would like to acknowledge Dr. Stuart Lowe for his tremendous help in many aspects during this project; Dr. Xin Chen for teaching me his practical knowledge of general experimentations and scientific writing; Dr. Simone Ciampi for his passion with the organic synthesis and the initiation of the first experiment on silicon nanoparticle preparation. I would like to thank Dr. Astrid Magneau for teaching me all the cell culture techniques, Liz, Dylan and Alex, from all of whom I learned much knowledge about microscopy, for helping me with the FLIM experiments and the phasor diagrams. I would like to thank Mr. Andrew Robinson for helping me with the preparation of the FRET conjugate and Dr. Joshua Peterson for preparing the porphyrin complex. I would like to thank all other members in the Gooding/Reece/Gaus Lab, for their continuing support for me throughout the project.

Lastly, but definitely not the least, I would like to give my sincere gratitude to my parents, for their tremendous efforts/sacrifices made since I was born. I went through much up and down moments in my life, but they are always there, giving their loving supports for me and I am a better person for it. I would like to thank all of my friends and other important figures in my life especially those who helped me finish this hard journey including Xun, Pengfei and Ying, Fan, Rain, Sam, Yu, Elva, Andrew, and many others for their sincere accompany and hope they brought to me during the most desperate moments of this PhD.

## TABLE OF CONTENTS

COPYRIGHT STATEMENT .....	3
AUTHENTICITY STATEMENT .....	3
ORIGINALITY STATEMENT.....	4
ABSTRACT.....	5
LIST OF PUBLICATIONS.....	6
ACKNOWLEDGEMENT .....	7
TABLE OF CONTENTS .....	8
LIST OF ABBREVIATIONS.....	12
CHAPTER 1 INTRODUCTION .....	14
1.1    GENERAL INTRODUCTION TO SEMICONDUCTOR QUANTUM DOTS .....	15
1.2    PHYSICAL PROPERTIES .....	17
1.2.1    Comparison between quantum dots and organic dyes .....	19
1.2.2    Important physical properties of silicon quantum dots.....	22
1.3    METHODS OF PREPARATION .....	26
1.3.1    The top-down approach .....	26
1.3.2    The bottom-up approach.....	27
1.3.2.1    Solution based precursor reduction .....	27
1.3.2.2    Development of Zintl-salt based approaches .....	29
1.3.2.3    Advantages and disadvantages.....	30
1.3.3    Precursor decomposition and re-assembly.....	31
1.4    SURFACE MODIFICATIONS .....	32
1.4.1.1    Wet-chemical based modification strategies .....	33
1.4.1.2    Formation of SAMs by hydrosilylation.....	33
1.4.1.3    Modification of halogen coated silicon quantum dots .....	36
1.4.1.4    Advantages and drawbacks .....	38
1.4.2    Surface passivation by plasma-surface interactions.....	39
1.4.2.1    Aerosol-based plasma modification .....	39
1.4.2.2    Plasma functionalization in the liquid phase.....	40
1.4.2.3    Advantages and drawbacks .....	41
1.4.3    Multi-step surface modifications .....	42
1.4.4    Characterizing the surface.....	44
1.5    SILICON QUANTUM DOTS FOR BIO-APPLICATIONS .....	45
1.5.1    Fluorescent Imaging.....	45
1.5.2    Silicon quantum dots as a less toxic alternative to conventional quantum dots	
48	
1.6    SUMMARY AND SCOPE OF THIS THESIS .....	52
1.7    REFERENCES .....	54
CHAPTER 2 METHODS AND MATERIALS .....	68

2.1	CHEMICALS AND MATERIALS .....	69
2.2	PREPARATION OF HYDROGEN TERMINATED SILICON QUANTUM DOTS .....	70
2.3	SURFACE PASSIVATION OF HYDROGEN TERMINATED SILICON QUANTUM DOTS .	72
2.4	PURIFICATION OF SURFACE PASSIVATED SILICON QUANTUM DOTS .....	73
2.5	FURTHER MODIFICATION OF SURFACE PASSIVATED SILICON QUANTUM DOTS ...	74
2.6	CHARACTERIZATION OF MORPHOLOGY .....	74
2.7	CHARACTERIZATION OF SURFACE PROPERTIES .....	75
2.7.1	Fourier transform infrared (FT-IR) spectroscopy .....	75
2.7.2	Nuclear magnetic resonance (NMR) spectroscopy.....	75
2.7.3	X-ray photoelectron spectroscopy (XPS) spectroscopy.....	76
2.8	CHARACTERIZATION OF OPTICAL PROPERTIES .....	76
2.8.1	Ultraviolet-visible spectroscopy .....	77
2.8.2	Fluorescence spectroscopy.....	77
2.8.3	Quantum yields measurements .....	77
2.9	CELL CULTURE AND FLUORESCENT CELLULAR IMAGING.....	78
2.10	CYTOTOXICITY EVALUATION .....	78
2.11	REFERENCES .....	79
PART I PREPARATION & SURFACE MODIFICATIONS .....		81
CHAPTER 3 ONE-POT SYNTHESIS OF COLLOIDAL SILICON QUANTUM DOTS AND SURFACE FUNCTIONALIZATION VIA THIOL-ENE CLICK CHEMISTRY... 81		
3.1	INTRODUCTION .....	82
3.2	METHODS AND MATERIALS .....	83
3.2.1	Chemicals and Materials.....	83
3.2.2	One pot synthesis of allyl functionalized silicon quantum dots.....	84
3.2.3	Surface functionalization of silicon quantum dots via thiol-ene click reactions 84	
3.2.4	Characterization of morphology .....	85
3.2.5	Characterization of optical properties .....	85
3.2.6	Characterization of surface properties .....	85
3.3	RESULTS AND DISCUSSIONS .....	86
3.3.1	Characterization of morphology by transmission electron microscopy.....	86
3.3.2	Characterization of surface properties .....	89
3.3.2.1	Phasor transfer after surface modification with thiol-ene reaction.....	89
3.3.2.2	FT-IR spectroscopy of surface modified silicon quantum dots .....	90
3.3.2.3	<sup>1</sup> H-NMR spectra of surface functionalized SiQDs.....	91
3.3.3	Characterization of optical properties .....	93
3.3.3.1	UV absorption and photoluminescence (PL) properties.....	93
3.3.3.2	Measurements of quantum yields.....	95
3.4	CONCLUSIONS .....	97
3.5	REFERENCES .....	98
CHAPTER 4 VERSATILE “CLICK CHEMISTRY” APPROACH TO FUNCTIONALIZING SILICON QUANTUM DOTS: APPLICATIONS TOWARD FLUORESCENT CELLULAR IMAGING.....		100

4.1	INTRODUCTION .....	101
4.2	METHODS AND MATERIALS .....	103
4.2.1	Chemicals and Materials.....	103
4.2.2	Synthesis of azides.....	103
4.2.3	Synthesis and purification of nonadiyne modified silicon quantum dots ....	104
4.2.4	Surface functionalization via CuAAC click reaction.....	104
4.2.5	Characterization of morphology .....	105
4.2.6	Characterization of optical properties.....	105
4.2.7	Characterization of surface properties .....	105
4.2.8	Fluorescence cellular imaging .....	105
4.2.9	Cytotoxicity evaluations .....	106
4.3	RESULTS AND DISCUSSIONS.....	106
4.3.1	Characterization of morphology .....	106
4.3.2	Characterization of surface properties .....	109
4.3.2.1	FT-IR measurements .....	109
4.3.2.2	<sup>1</sup> H -NMR measurements and effects of column purification .....	112
4.3.2.3	XPS measurements and surface coverage .....	113
4.3.2.4	Phase transfer .....	116
4.3.3	Characterization of optical properties.....	117
4.3.4	Photostability studies.....	120
4.3.5	Fluorescent cellular imaging studies.....	121
4.3.6	MTT toxicology studies.....	123
4.4	CONCLUSIONS.....	124
4.5	REFERENCES .....	126
CHAPTER 5 FLUORESCENCE IMAGING MICROSCOPY (FLIM) OF SILICON QUANTUM DOTS (SIQDS) .....		131
5.1	INTRODUCTION .....	132
5.2	METHODS AND MATERIALS .....	134
5.2.1	Chemicals and Materials.....	134
5.2.2	Synthesis and purification of allylamine modified silicon quantum dots ....	134
5.2.3	Preparation of SiQDs–DY485 conjugate for FRET measurements.....	134
5.2.4	Characterization of morphology .....	135
5.2.5	Characterization of optical properties.....	135
5.2.6	Preparation of HeLa cell samples .....	135
5.2.7	Fluorescent lifetime imaging microscopy (FLIM).....	135
5.2.8	FLIM data analysis and phasor transformation.....	136
5.2.9	Calculation of FRET efficiency and Förster distance .....	137
5.3	RESULTS AND DISCUSSIONS.....	139
5.3.1	Characterization of allylamine modified SiQDs.....	139
5.3.2	One-photon FLIM of HeLa cells incubated with SiQDs .....	140
5.3.3	Analysis of lifetime components of allylamine modified SiQDs .....	143
5.3.4	Two-photon FLIM of HeLa cells incubated with SiQDs.....	144
5.3.5	FLIM-FRET study using SiQDs-DY485 conjugate .....	146
5.4	CONCLUSIONS.....	151
5.5	REFERENCES .....	152

CHAPTER 6 A SILICON QUANTUM DOTS PROTEASE SENSOR BASED ON FÖRSTER RESONANCE ENERGY TRANSFER (FRET) .....	155
6.1 INTRODUCTION .....	156
6.2 METHODS AND MATERIALS .....	158
6.2.1 Chemicals and Materials.....	158
6.2.2 Synthesis and purification of allylamine modified silicon quantum dots ....	159
6.2.3 Preparation and characterization of dye labelled peptides.....	159
6.2.4 Preparation of the FRET conjugates .....	160
6.2.5 Characterization of optical properties of surface modified SiQDs .....	160
6.2.6 Calculation of FRET efficiency and Förster distance .....	161
6.2.7 Trypsin enzyme assay .....	161
6.3 RESULTS AND DISCUSSIONS .....	162
6.3.1 Characterization of surface groups by FT-IR.....	162
6.3.2 Characterization of DY485 labelled peptides .....	165
6.3.3 Optical properties of the FRET conjugate .....	166
6.3.4 Trypsin assay with FRET conjugate .....	169
6.3.5 Ab initio calculation of separation distance between donor/acceptor.....	171
6.4 CONCLUSIONS .....	174
6.5 REFERENCES .....	174
CHAPTER 7 CONCLUSIONS AND FUTURE PERSPECTIVES .....	179
7.1 SUMMARY OF RESULTS.....	180
7.2 FUTURE WORK .....	182
7.3 CONCLUDING REMARKS.....	185
7.4 REFERENCES .....	186
APPENDIX.....	187
APPENDIX I CHARACTERIZATION OF DYE LABELLED PEPTIDES BY HPLC-MS.....	187
APPENDIX II OPTICAL PROPERTIES OF SIQDS-PORPHYRIN CONJUGATES.....	189
APPENDIX III FLIM STUDY OF SIQDS-PORPHYRIN CONJUGATES .....	190

## LIST OF ABBREVIATIONS

### Abbreviations of amino acids

One-letter code	Three-letter code	Amino Acid
A	Ala	Alanine
C	Cys	Cysteine
D	Asp	Aspartate
E	Glu	Glutamate
F	Phe	Phenylalanine
G	Gly	Glycine
H	His	Histidine
I	Ile	Isoleucine
K	Lys	Lysine
L	Leu	Leucine
M	Met	Methionine
N	Asn	Asparagine
P	Pro	Proline
Q	Gln	Glutamine
R	Arg	Arginine
S	Ser	Serine
T	Thr	Threonine
V	Val	Valine
W	Trp	Tryptophan
Y	Tyr	Tyrosine

### Abbreviation of Units

Symbol	Units
Å	Angstrom
°C	Degree Celsius
Da	Dalton
g	Gram
kDa	Kilo-Dalton
l	Litre(s)
M	Mol l <sup>-1</sup>
m	Metre(s)
mg	Milligram(s)
min	Minute(s)
ml	Milliliter(s)
mM	millimol l <sup>-1</sup>
mol	Mole(s)
µl	Microlitre(s)

---

$\mu\text{M}$	Micromol $\text{l}^{-1}$
nm	Nanometer(s)
ppm	Parts per million
s	Second(s)

---

#### Other Abbreviations

---

Symbol	Units
Fig.	Figure
FLIM	Fluorescence lifetime imaging microscopy
FRET	Förster resonance energy transfer
<i>in situ</i>	In the reaction mixture
<i>in vivo</i>	Taking place inside a living organism
<i>in vitro</i>	Taking place outside a living organism
QY or $\phi$	Quantum yield
PL	Photoluminescence
Ref.	Reference
SiQDs	Silicon quantum dots
UV	Ultraviolet

---

## Chapter 1 Introduction

**Part of this chapter has been published in**

**Cheng, X.;** Lowe, S. B.; Reece, P. J.; Gooding, J. J.: Colloidal silicon quantum dots: from preparation to the modification of self-assembled monolayers (SAMs) for bio-applications. *Chem. Soc. Rev.* **2014**, *43*, 2680-2700.

## 1.1 General introduction to semiconductor quantum dots

Semiconductor nanocrystals, or quantum dots (QDs), are attractive nanomaterials because of their unique optoelectronic properties. They possess strong absorption, size-tunable photoluminescent (PL) emission, high quantum yield (QY) and high stability against photobleaching<sup>1</sup>. This is primarily due to the confinement of charge carriers within the small physical dimensions (usually in the range of several to tens of nanometers) defined by particle size, or the quantum confinement effect.<sup>2,3</sup> The methods of preparation, surface properties and fundamental physics of compound semiconductor quantum dots have been well explored, including II-VI (e.g., CdX, X = Se, S, Te)<sup>4-7</sup>, III-V (e.g., InP, InAs, GaAs)<sup>8-10</sup>, and IV-VI (e.g., PbX, X = Se, S) quantum dots<sup>11-13</sup>. More recently, their applications in solar cells<sup>14-16</sup>, optoelectronic devices<sup>17-19</sup> and fluorescent labelling agents<sup>20-24</sup> have been recognized and studied extensively, suggesting enormous potential for this class of material for a number of applications. However, one problem associated with traditional quantum dots is the use of heavy metal elements, such as cadmium which is known to be toxic to biological systems<sup>25-27</sup>. Safety issues therefore have hampered their development to some extent due to the current regulation on the use of heavy metals for commercial products<sup>27,28</sup>, which is particularly relevant with medically related products for *in vivo* purposes<sup>29-31</sup>.

Silicon is one of the most important materials on earth. It is abundant, relatively benign and widely used in microelectronic industry. Although an *indirect bandgap semiconductor* material Although an *indirect bandgap semiconductor* material due to band mismatch between the minimum-energy state of the valence band and

maximum-energy state of the conduction band, hence less interesting for light emitting device applications in the bulk form, the quantum confinement effect has allowed efficient photoluminescence (PL) emission from silicon quantum dots (SiNCs, silicon quantum dots or SiQDs)<sup>32,33</sup>, with photoluminescence (PL) quantum yield (QY) up to 60-75%<sup>34,35</sup>. What is emphasized here are ‘*colloidal*’ silicon quantum dots, or *freestanding* silicon nanocrystals<sup>36</sup>, as particles embedded in matrices such as thin films are another significant area of studies and beyond the scope of this thesis. Two decades have passed since the first reports on silicon quantum dots,<sup>32,33</sup> but challenges still remain in various aspects of working with this type of material. The first challenge is how to efficiently prepare high quality colloidal silicon quantum dots. This requires the particles to be made relatively simply with controlled size, shape, composition, surface properties, crystallinity and optical properties. For this aim size tunable within 1 – 5 nm<sup>37</sup>, emission wavelength spanning from blue to near-IR (NIR) and QY above 10-15 % are essential<sup>38,39</sup>. Another challenge is how to effectively modify the surface of silicon quantum dots, as freshly prepared silicon surface is prone to oxidation<sup>40,41</sup>. The impact of surface states is also significant for particles at this dimension<sup>42</sup>, due to the small exciton Bohr radius for silicon of merely 4.2 nm<sup>43</sup>. Both challenges, combined with difficulties in characterization, make SiQDs considerably more difficult to work with compared with conventional metal based quantum dots.

In spite of these challenges, the past two decades have seen rapid progress in methodologies in the preparation and surface modification of silicon quantum dots. Colloidal silicon quantum dots can now be made with a range of optical properties

and with reasonably complex surface architectures. For the sections below, critical steps of recent advancements in these areas are reviewed. Section 1.1.2 gives a review on the distinct physical features of silicon quantum dots. In section 1.1.3 and 1.1.4, methods of preparation and strategies for surface modification are reviewed respectively. In section 1.1.5, the focus is on recent developments in the applications of silicon quantum dots, highlighting fluorescent imaging studies in biological contexts.

## **1.2 Physical properties**

Semiconductor quantum dots (QDs) are considered as artificial atoms: they exhibit discrete atomic-like density-of-states where the physical dimensions of the particle strongly affect the allowed energies of free electrons and holes (Figure 1.1A)<sup>5</sup>. Relaxation of free carriers across these discrete energy levels is a radiative process and yields the emission of a photon of equivalent energy.<sup>44</sup> The degree of confinement experienced by the electrons and holes, and hence emission wavelength, along with rates of radiative recombination, lifetimes, and quantum efficiency are largely governed by the dimensions of the particle, as well as the properties of the host material and surrounding barrier<sup>5,45</sup>. In an idealized scenario (e.g. a cubic dot with infinite potential barriers) the separation between energy states of electrons and holes can be described as the sum of the band gap energy of the host material  $E_g$  and energy contributions for each of the confined dimensions (x, y, z) for the conduction and valence bands<sup>46</sup>, as well as a small contribution from exciton binding (not included)<sup>47</sup>:

$$\Delta E = E_g + \sum_{i=x,y,z} \frac{\hbar^2 \pi^2 n_i^2}{2d_i^2} \left( \frac{1}{m_e} + \frac{1}{m_h} \right)$$

Here  $d_i$  is the size of the QD in the  $i$ th dimension,  $n$  is the quantum number, and  $m_e$  and  $m_h$  are the effective masses of the conduction band electrons and valence band holes, respectively. For large nanocrystals the confinement energies are negligible, however when the dimensions become comparable to the exciton Bohr radius of the host material the confinement energies become significant<sup>5</sup>. These size-tunable alterations of electronic states, and thus optical features of the particle, make quantum dots a distinct class of fluorophores (Figure 1.1B)<sup>48</sup>. In practice there are many physical factors that complicate the expected behaviour of electronic states and optical properties in quantum dots; they include finite potential barriers, band-offsets<sup>49</sup>, surface mediated effects<sup>50</sup>, band-structure related effects (degeneracy, critical points)<sup>51</sup>, dark states, etc<sup>52,53</sup>. These must all be considered in understanding the details of the observed behaviour of the light emission process in quantum dots.

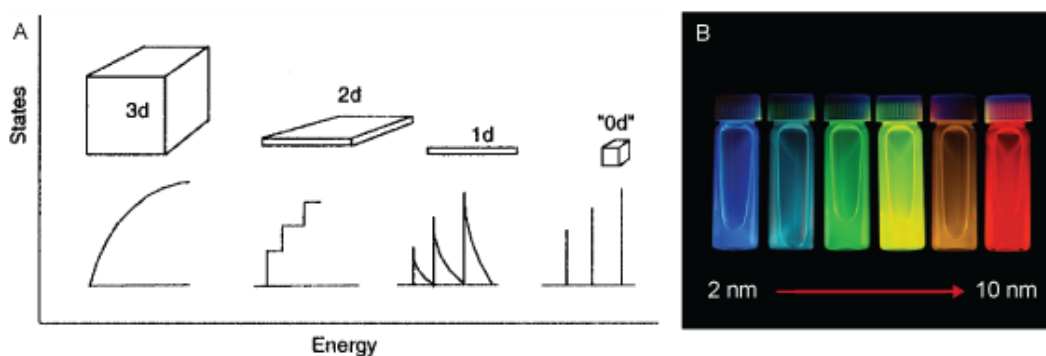


Figure 1.1 A: Idealized density of states for one band for a material which has 3,2,1 and 0 dimensions. B: Change of PL colour of CdSe quantum dots with size ranging from 2 nm to 10 nm. Reprinted with permission from Alivisatos *et. al.*<sup>5</sup> Copyright 1996 American Chemical Society.

The physical properties of quantum confined semiconductor heterostructures have been investigated extensively in compound materials systems, such as III-V and II-VI quantum dots in colloidal or matrix-embedded form. Precise physical deposition methods, such as molecular beam epitaxy, have allowed the growth defect-free islands of low energy band gap material (e.g. InAs) inside a wider band gap host (e.g. GaAs)<sup>54,55</sup>. The host material acts as a potential barrier that confines conduction band electrons and valence band holes within the dots and also acts to passivate the structures against surface related effects<sup>54</sup>. III-V quantum dots, whilst having no utility in bio-labelling applications, have provided a great deal of fundamental information on the nature of quantum confinement in solid state systems and have significant applications in technological areas of optoelectronics and quantum information<sup>56,57</sup>. Chemically synthesised II-VI compound quantum dots are a colloidal analogue of conventional III-V quantum dots: they have a core-shell structure, where the wider band-gap semiconductor (e.g. ZnS) provides a confining potential for the smaller band gap (i.e. CdSe, CdTe etc.) core region<sup>4,8</sup>, although it is not always the situation where certain inorganic systems are used<sup>7,52</sup>. In addition, II-VI quantum dots have an organic capping layer that stabilises the colloid in solution and can be used for further functionalization for specific applications<sup>45</sup>. Synthesis is based on a mature process where size dispersity and optical properties can be controlled with excellent precision<sup>45</sup>.

### **1.2.1 Comparison between quantum dots and organic dyes**

In general, essential physical features for fluorophores include the absorption and

emission profiles, spectral position, blinking, full width at half maximum (FWHM), brightness, fluorescence lifetime, quantum yield and the Stokes shift (Table 1.1)<sup>1</sup>.

Table 1.1 Glossary of terms used

Absorption/emission band	A range of wavelengths in the spectrum where a particular photon can be absorbed/emitted from a substance
Blinking	Excited fluorophores emit light for limited time, disrupted by periods when no emission occurs.
Full width at half maximum	Width of the emission peak at which half of its intensity is observed
Brightness	Product of the molar extinction coefficient and quantum yield, measured at the excitation wavelength.
Fluorescence life time	Time needed for intensity of fluorescence to decay to 1/e of its maximum value
Photostability	Resistance of photoluminescence to change under influence of external factors, such as light
Quantum yield	Efficiency of the fluorescence process, defined as ratio of the number of photons emitted to the number of photons absorbed.
Stokes shift	Difference of wavelength between the absorption/emission peaks.

The most frequently used fluorophores today are organic dyes, which are widely used in various biological and biochemical assays<sup>58</sup>. Although there are several reviews in literature comparing the properties of quantum dots and organic dyes<sup>1,45</sup>, emphasis is still given here due to the importance of the topic. In comparison to conventional organic dyes, fluorescent quantum dots are endowed with several attractive properties (Table 1.2).

One critical property of quantum dots as fluorophore is related to the broad absorption profile accompanied by a narrow, wavelength-tunable emission peak<sup>59</sup>. This is a key advantage of quantum dots over organic fluorophores. The broad absorption spectrum allows efficient excitation, which is desirable when the number of available photons for excitation is limited. In fact, the broad absorption spectrum

has allowed much larger molar absorption coefficient (up to  $100,000,000 \text{ M}^{-1}\text{cm}^{-1}$ )<sup>59,60</sup> of quantum dots compared with organic fluorophores (up to  $250,000 \text{ M}^{-1}\text{cm}^{-1}$ )<sup>61,62</sup>. In addition, the emission band of organic dyes are often unsymmetrical<sup>63</sup>, whose red ‘tail’ is not seen in the emission profiles of quantum dots. Position of the emission peak in quantum dots is also tunable in a wide range by varying size of the particle<sup>64</sup>, which is not possible for most organic dyes. This has made multicolour imaging using quantum dots by the same incidence light source possible, whereas only limited wavelength choices are available for dye staining<sup>64</sup>.

Table 1.2 Comparison between quantum dots and organic dyes

Property	Organic dyes	QDs
Absorption profile	Narrow, discrete bands, FWHM ranges from 35 nm to 80 – 100nm	Broad, unsymmetrical profile, increase steadily towards UV region
Emission profile	Asymmetric, FWHM 35 nm to 70 – 100 nm	Nearly symmetrical, FWHM, 30 nm – 90 nm
Stokes shift	Usually less than 50 nm	Usually less than 100 nm
Quantum yield	0.5 – 1 (visible), 0.05 – 0.2 (NIR)	0.1 – 0.8 (visible), 0.2 – 0.7 (NIR)
Fluorescent lifetimes	1 – 5 ns	5 – 100 ns, up to $\mu\text{s}$ for some red SiQD
Photochemical Stability	Sufficient in the visible region, but can be insufficient for NIR dyes	High, sufficient in both visible and NIR regions
Multiple colours	Possible by varying molecular structure	Adjustable by varying size

An additional advantage of quantum dots over organic dyes is its high quantum yield, especially in the near infrared (NIR) region. For organic dyes, QY is usually high in the visible region, but below 20% in the NIR region<sup>63</sup>. In the case of quantum dots, quantum yield can reach up to 60% to 80% in both the visible and NIR region depending on the core materials<sup>65-68</sup>. A third major difference is the significantly longer fluorescent lifetime of quantum dots compared with organic

dyes. Fluorescent lifetimes for most organic dyes are less than 5 ns in the visible region and sometimes less than 1 ns in the NIR region<sup>69</sup>, causing difficulties for temporal discrimination between fluorescence interference and scattering from the excitation wave<sup>69</sup>. In contrast, most quantum dots have fluorescent lifetimes to 10 ns, sometimes reaching several tens of ns even  $\mu$ s for red emitting silicon quantum dots, allowing sensitive separation between signals from auto-fluorescence and scattered excitation light by time-gated imaging techniques<sup>70</sup>.

Due to the use of heavy metal elements in conventional quantum dots, they are considered by many to be not suitable for large scale bio-applications, particularly for *in vivo* applications.<sup>23</sup> Therefore, this chapter concentrates on the bio-applications of SiQDs. However, SiQDs possess distinct physical properties compared with conventional quantum dots, as will be explain in section 1.2.2.

### 1.2.2 Important physical properties of silicon quantum dots

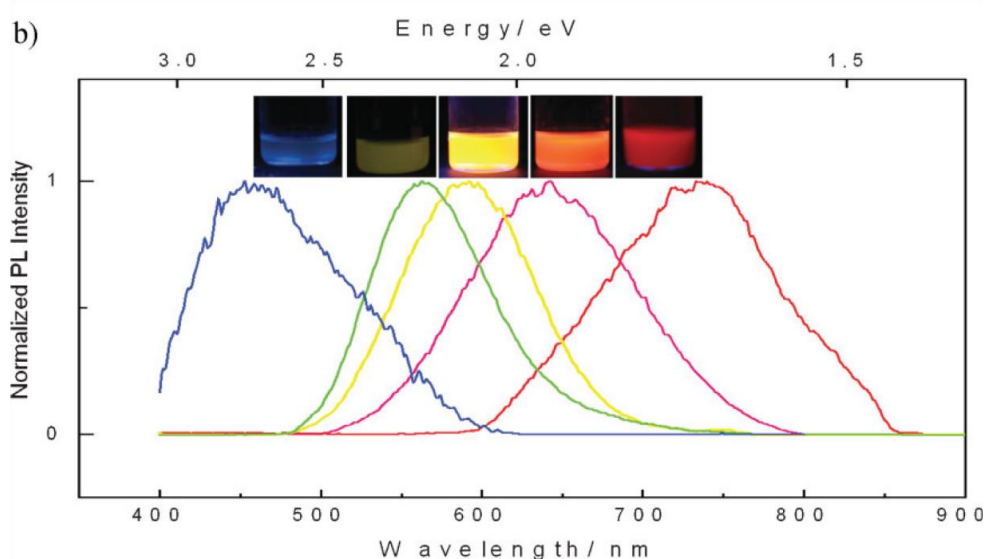


Figure 1.2 Photoluminescence spectra and corresponding fluorescence colors of SiQDs produced by controlled etching conditions. The SiQDs were excited at 350

Unlike conventional core-shell QDs, SiQDs are usually prepared with hydrogen, halogen, oxide or alkyl surface. Due to the lack of a lattice-matched semiconductor barrier layer, surface properties are of particular significance in defining the photophysics of SiQDs<sup>72</sup>. The different potential barriers affect the photoluminescence (PL) properties, including wavelength of the emission peak, appearance of subsidiary peaks, quantum yield (QY) and fluorescence lifetime ( $\tau$ )<sup>73</sup>. In terms of the emission profile, absence of a semiconductor shell reduces the degree of exciton confinement in the core and broadens the emission peak.<sup>74</sup> In practice, SiQDs prepared via colloidal solution methods were predominantly blue-green in colour, whilst red dots with broad emission can only be prepared via high temperature or etching related methods thus far (Figure 1.2). In addition, there have been attempts to red-shift the emission profile of blue emitting SiQDs by doping with substituent atoms<sup>75,76</sup>. Noticeably, because of the small size of SiQDs, any dopant atoms incorporated are present at concentrations that would be considered 'heavy doping' and furthermore SiQDs may be doped stochastically, resulting in sub-populations of doped and undoped SiQDs<sup>77,78</sup>. In terms of QY, the existence of imperfections and defects at the surface of SiQDs can affect QY by providing alternative decay pathways. In most cases, additional decay pathways associated with surface capping ligands may become the dominant factor of causing reduction in QY<sup>79</sup>, and can lead to the appearance of subsidiary blue/green emission peaks via surface-associated recombination<sup>73,80,81</sup>. Interestingly, certain electron donating,

nitrogen containing species at particle surface strongly increase QY of SiQDs, as was shown in a recent study<sup>35</sup>. It was suggested that surface capping of SiQDs with organic ligands has led to distortion of electronic structure, which was evidenced by scanning tunnelling microscopy<sup>80</sup>. Oxidation of larger SiQDs has been shown to affect the crystallinity and core diameter of the Si nanocrystals, reducing the QY and blue-shifting the wavelength of emission peak<sup>34,71</sup>. However, modification of the SiQD surface with an organic monolayer can prevent the long-term oxidation, providing more stable PL properties<sup>82</sup>. In terms of lifetime, short fluorescence lifetime (order of ns) in SiQDs is often associated with core-related recombination<sup>83</sup>. Much longer lifetime (order of  $\mu$ s) in SiQDs has been observed, which was suggested to be due to the existence of ultrafast trapping of excited carriers in surface states, preventing core recombination<sup>84</sup>.

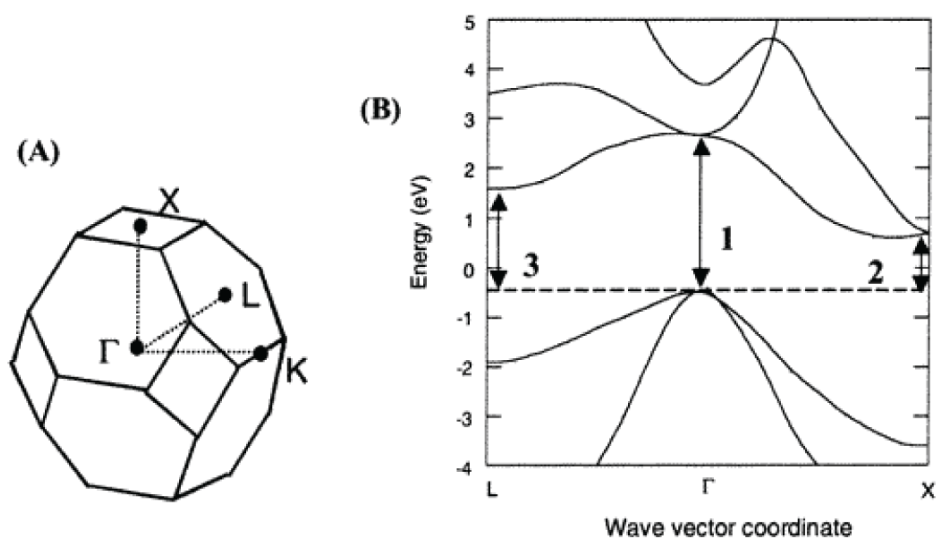


Figure 1.3 Crystalline silicon as an indirect bandgap semiconductor. (A) Brillouin zone of zinc blende diamond crystal. (B) Band structure of bulk crystalline silicon. Copyright 2001 American Chemical Society<sup>85</sup>.

Conventional QDs are usually made from semiconductor materials with a

direct bandgap, which indicates there is no band mismatch between the minimum-energy state of the valence band and maximum-energy state of the conduction band. The radiative transition pathway in SiQDs is different in character from that of conventional QDs because bulk silicon is an indirect bandgap semiconductor (Figure 1.3). In terms of the bio-applications of SiQDs, a detailed discussion of the SiQD electronic structure, which describes the state of motion of electrons within the electrostatic field created by QDs, is beyond the scope of this chapter. However, it is worth mentioning that the exciton recombination rate is higher than that observed in bulk silicon because quantum confinement increases the uncertainty in  $k$  vector, meaning that previously unflavoured transitions are accessible. Veinot *et al.* suggest that,<sup>36,42</sup> as well as confinement, surface effects may also be responsible for the observed rate of dipole-mediated radiative decay. Because it can be difficult to separate surface and confinement effects in free-standing colloidal nanocrystals, some work has been done to study this transition in systems where the SiQDs are embedded in a matrix.<sup>86</sup>

Similarly to conventional quantum dots, many preparations of SiQDs display decreased PL when transferred into aqueous solution.<sup>87</sup> But the PL could be maintained by encapsulating SiQDs in phospholipid micelles.<sup>87</sup> A likely origin of PL quenching of SiQDs upon transfer to aqueous media has been suggested to originate from the formation of non-radiative oxide-related states during surface treatments designed to render the SiQDs water soluble.<sup>88</sup> Despite this, water-soluble SiQDs do not photobleach under conditions that photobleached conventional organic dyes<sup>83</sup>. Blinking of PL fluorescence is a commonly-observed phenomenon

in fluorescent molecules including SiQDs<sup>89</sup>. Galland *et al.* have suggested that the origin of blinking in semiconductor QDs is due to a combination of multiple effects; i) non-radiative recombination caused by excess charges; and ii) charge fluctuations in electron-accepting surface sites<sup>90</sup>.

Although SiQDs possess many of the desired physical properties for bio-applications, including fluorescence colour, long PL lifetime and stability against photobleaching, in order for them to be effective in practical contexts, the impact of preparation method and surface functionalization must be considered with respect to both photophysical features and biological interactions. These aspects will be covered in the following sections.

### **1.3 Methods of preparation**

Numerous methods have been developed for preparing colloidal silicon quantum dots (SiQDs). Similar to the methods of preparing many types of nanostructures, these methods can be roughly classified as either ‘top-down’ approaches, i.e. breaking down large pieces of silicon to smaller nanoscale pieces, or ‘bottom-up’ approaches that primarily rely on self-assembly processes using molecule silicon precursor species. Due to the interdisciplinary nature of some methods, a third class of methods can be classified based on the involvement of both ‘top-down’ and ‘bottom-up’ components. Here, developments of methods for preparing colloidal SiQDs are summarized.

#### **1.3.1 The top-down approach**

The first class of methods, namely the ‘top-down’ approach, is represented by etching of bulk silicon or breaking down silicon rich oxides containing SiQDs. The etching method was first developed by Heinrich *et. al.*<sup>91</sup> and have been adopted by several groups<sup>92-94</sup>. SiQDs could also be obtained from breaking silicon rich oxides ( $\text{Si}_m\text{O}_n$ ) that contains nanoparticles after an initial annealing step, as represented by the Veinot group<sup>95-97</sup>. Since these methods are not used in this thesis and there are several comprehensive reviews on them,<sup>36,98</sup> they are only briefly mentioned here.

### 1.3.2 The bottom-up approach

The alternative to the top-down routes mentioned above to prepare colloidal silicon quantum dots is via assembly of small molecular precursors. That is, via a bottom-up approach.

#### 1.3.2.1 Solution based precursor reduction

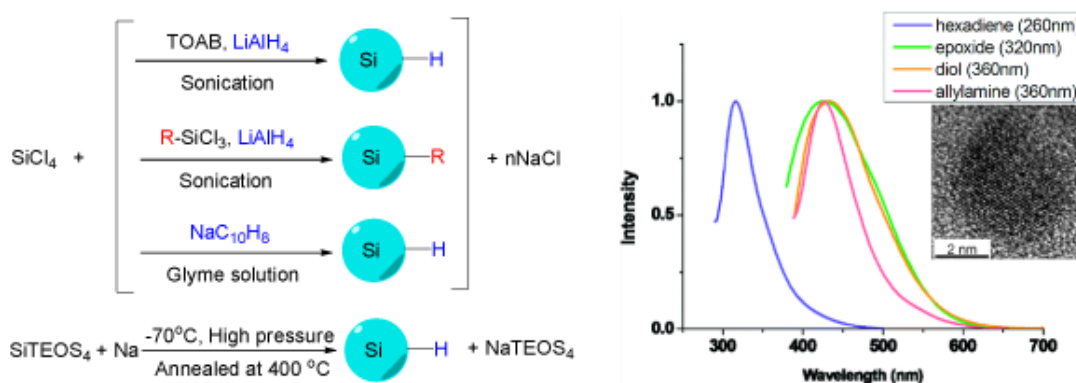


Figure 1.4 Preparation of colloidal silicon quantum dots via solution based precursor reduction. HR-TEM images confirm crystal structure of the particles obtained, with fluorescence in the UV-blue region under UV excitation. Copyright 2010 American Chemical Society.<sup>99,100</sup>

One class of bottom-up procedures uses reducing agents in the presence of

silane precursors in solution (Figure 1.4). The method was initially demonstrated by Heath in 1992, who showed that mixing  $\text{SiCl}_4$  and octyltrichlorosilane with sodium metal under high temperature and pressure produced polydispersed silicon nanoparticles<sup>101</sup>. Due to the relative simplicity of the approach, numerous variants of this method have been established. Examples include the use of sodium naphthalenide ( $\text{NaC}_{10}\text{H}_8$ ) as the reducing agent and  $\text{SiCl}_4$  in glyme solution<sup>102</sup>, or sodium (Na) as the reducing agent and tetraethyl orthosilicate (TEOS) in a bomb reactor<sup>103</sup>. Both methods yielded silicon quantum dots with size of several nanometers with visible blue luminescence<sup>102</sup>. However, one disadvantage was the poor control of particle size, with particle diameter usually ranging over tens of nanometers within a single batch<sup>102</sup>. To assist with reducing particle size distribution, it was reported that addition of surfactant molecules to the reaction mixture, to create inverse micelle environments, provided a greater ability to control the size. This remarkable improvement was recently demonstrated by Tilley *et al.*<sup>83,99</sup>. In a typical experiment, tetraoctylammonia bromide (TOAB), a phase transfer agent and surfactant, stabilized the halogenated silane precursors in toluene, allowing relatively homogeneous precipitation of silicon quantum dots within the inverse micelle upon addition of lithium aluminum bromide<sup>83,99</sup>. This method generated hydrogen terminated silicon quantum dots with narrow size distribution, i.e. FWHM of emission peak below 80 nm and size of 2 – 3 nm within one batch<sup>83,100,104,105</sup>. Generally this method produces only blue luminescent colloidal silicon quantum dots. To date it is still difficult to obtain a full range of colours with the reduction method. Furthermore, separating the surfactant from the reaction

mixture is not a trivial task<sup>100</sup>, albeit not impossible with size-exclusion chromatography<sup>105</sup>. To avoid the tedious purification steps, it was recently shown that halogenated silanes with carbon rich side chains can function as a replacement for the surfactant TOAB<sup>106</sup>. This led to very facile methods of preparing surface passivated silicon quantum dots at a rate of several tens milligrams per batch with essentially no purification processes<sup>106</sup>, while at the same time giving easily accessible surface moieties for further functionalization<sup>107</sup>. Again however the quantum dots obtained are only blue in colour.

### 1.3.2.2 Development of Zintl-salt based approaches

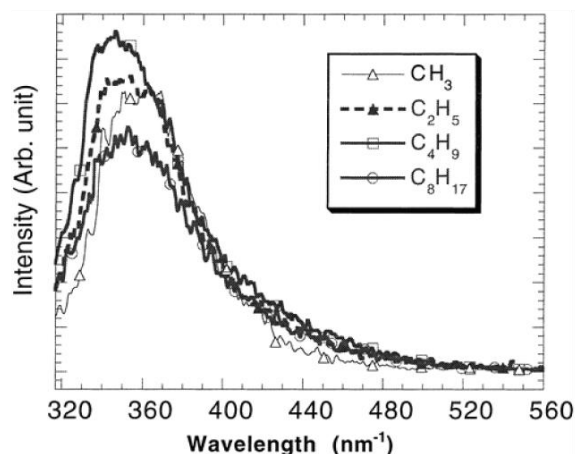
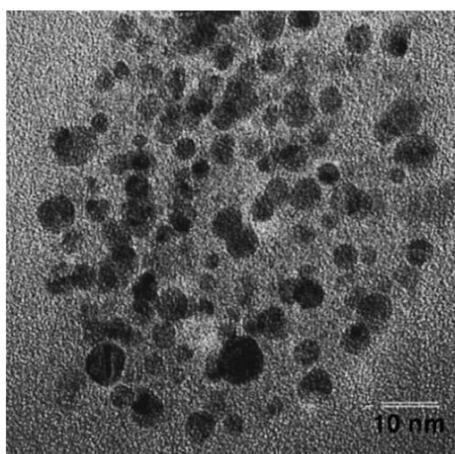
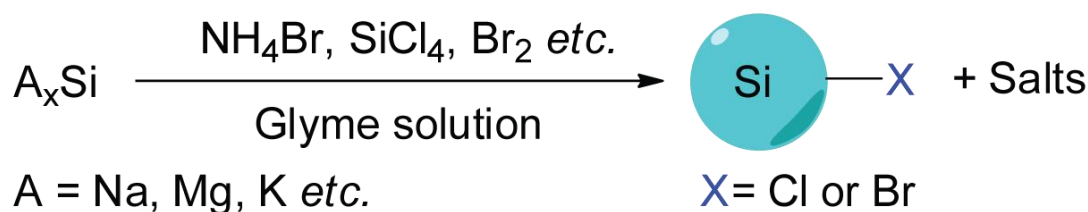


Figure 1.5 Zintl salts based synthetic methods of preparing SiQDs. A: Represented TEM images and B: PL spectra of synthesized SiQDs. Copyright 1999 American Chemical Society<sup>108</sup>

A second class of reaction for the bottom-up preparation of silicon quantum dots utilizes silicon Zintl salts (*i.e.* ASi<sub>x</sub>, A = Na, K, Mg *etc.*). Typically with this

class of method a silicon Zintl salt is reacted with silicon halides, or bromine gas. For instance, Kauzlarich *et al.* prepared silicon quantum dots *via* reactions between potassium silicide (KSi) and SiCl<sub>4</sub> in boiling glyme or diglyme solution<sup>109,116–120</sup> (Figure 1.5). Relevant FT-IR analysis confirmed that the prepared nanoparticles were initially halogen species coated but further functionalized with methoxy groups during the work up step in which methanol was used for washing.<sup>119</sup> A comparable method was developed by using sodium silicide (NaSi) and ammonium bromide (NH<sub>4</sub>Br). The method also gave blue luminescent silicon quantum dots with average size of ~4–5 nm but with reasonably large amounts of tens of milligrams per batch.<sup>121</sup> Comparative results were obtained for reaction between magnesium silicide (MgSi<sub>2</sub>) and bromine gas (Br<sub>2</sub>),<sup>122</sup> as well as between NaSi and SiCl<sub>4</sub> in boiling glyme solution.<sup>117</sup>

### 1.3.2.3 Advantages and disadvantages

Recognized features of the bottom-up methods are: First, they are more often performed in solution which is favourable in many industrial applications. Second, usually common reagents and equipment that are compatible with conventional bench top chemistry are used. This also made surface chemistry of the particles more easily accessible, which is essential for both preparation and characterization. Finally, it is not uncommon with these methods to yield reasonable amount of SiQDs (i.e. tens of milligrams per batch) with reasonable quality, an important factor to consider when scaling up the production for application contexts.

In contrast, an obvious disadvantage with solution bottom-up methods is the lack of full spectrum of colour, with only blue-green colour accessible to date. Regardless the fact that red emitting dots can be made with laser pyrolysis and non-thermal plasma synthesis, variation of particle emission wavelength with the bottom-up approach has this far only been achieved by further etching the particles with concentrated HF, which is essentially a top-down approach. Purity is another issue, as purification of SiQDs synthesized by this class of methods can become quite complicated and time consuming. Also, although there are recent reports demonstrating SiQDs with very high quantum yield can be synthesized by this class of method,<sup>35</sup> particles prepared using bottom up approaches usually exhibited much lower quantum yield compared with top-down approaches, with quantum yield rarely exceeds 15%.

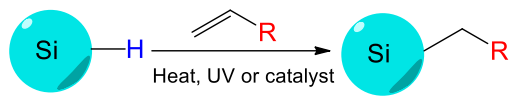
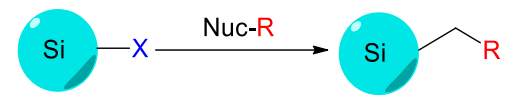
### **1.3.3 Precursor decomposition and re-assembly**

A third class of methods typically involves the decomposition precursor species containing silicon heteroatoms and a re-assembly processes to form SiQDs. Here, the term ‘re-assembly’ refers to the re-organization of the silicon atoms in ordered forms to form nanoparticles with controlled size, composition and morphology<sup>5</sup>. Methods belonging to this class are distinct to previously discussed methods due to the multiple processes needed, which usually involve both the top-down and bottom-up steps. Represented studies involve the use of supercritical fluids,<sup>85</sup> laser pyrolysis<sup>38,41,109</sup> and plasma synthesis.<sup>34,110,111</sup> Similar to section 1.3.1, since these methods are not used in this thesis and they have been extensively reviewed

elsewhere,<sup>112,113</sup> they are only briefly mentioned here in this section.

#### 1.4 Surface modifications

Table 1.3 Schematic of strategies of surface modification of colloidal SiQDs by forming covalent linkages

Surface of SiQDs	Surface modification strategies	Example of distal moieties
Hydride terminated surface	<p style="text-align: center;">Hydrosilylation</p>  <p style="text-align: center;">Heat, UV or catalyst</p>	Alkane Alkene NH <sub>2</sub> COOH
Halogen terminated surface	<p style="text-align: center;">Nucleophilic Substitution</p>  <p style="text-align: center;">Nuc-R = LiAlH<sub>4</sub>, Butyl-NH<sub>2</sub>, RMgX, RLi, CH<sub>3</sub>OH/H<sub>2</sub>O</p>	Hydrogen Alkane -OH

In contrast to the well-established methods of surface modification for II-IV semiconductor quantum dots<sup>114</sup>, very different procedures are used for forming self-assembled monolayers (SAMs) on colloidal silicon quantum dots. Despite the use of a silica shell for surface modification in some cases<sup>115-117</sup>, probably the most common approach for introducing surface moieties to colloidal II-IV quantum dots is still via ligand exchange<sup>118</sup>. The ligand exchange principle relies on replacing surfactant molecules with ligands with strong affinity with surface of quantum dots, using thiols<sup>119-122</sup>, polymers<sup>123-125</sup>, or certain inorganic systems<sup>126</sup>. However, comparable surface modification techniques for SiQDs typically require the

formation of robust covalent linkages, usually between surface silicon atoms and carbon, nitrogen or oxygen species (Table 1.3)<sup>127</sup>. This is particularly important in preventing the oxidation of silicon surfaces. Despite increasing interests in the surface passivation of SiQDs, complete characterization of the surface remains a challenge. The challenge is particularly evident when considering the incomplete coverage of organic monolayers on flat and porous silicon surfaces<sup>127-132</sup>. In this section, recent methodological advances in surface modification of colloidal SiQDs are discussed.

#### 1.4.1.1 Wet-chemical based modification strategies

#### 1.4.1.2 Formation of SAMs by hydrosilylation

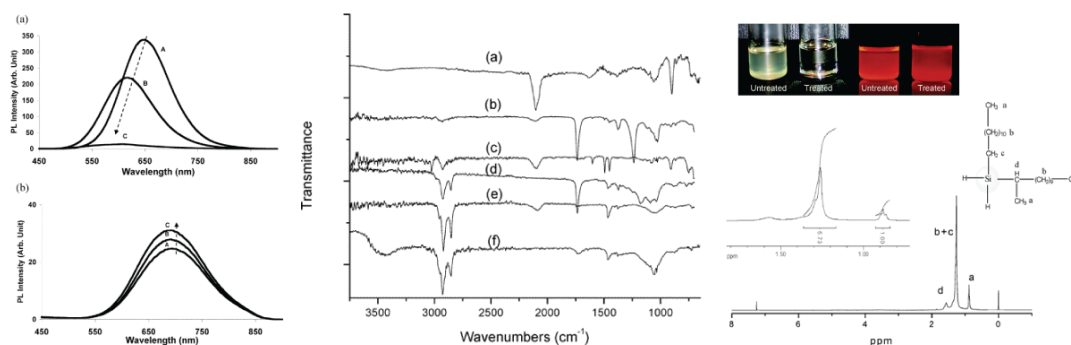


Figure 1.6 Attachment of different surface moieties to SiQDs via hydrosilylation. The reaction is initiated by photo-, thermal or catalytical treatment. *Left:* (a) unmodified SiQDs showed instable photoluminescence. (A) immediately after preparation, (B) after 1 day, (C) after 12 days in toluene. (b) grafted particles with improved PL stability. (A) immediately after preparation, (B) after 35 days, (C) after 60 days in toluene. *Middle:* FT-IR spectra of SiQDs with a range of surface groups (a) hydrogen, (b) vinyl acetate, (c) styrene, (d) ethyl undecylenate, (e) 1-dodecene and (f) undecanol. *Right:* modified SiQDs have improved dispersity in solvents and strong fluorescence (top). The surface groups were characterized by <sup>1</sup>H-NMR spectroscopy (bottom). Copyright 2004 & 2005 American Chemical Society.<sup>38,109</sup>

Hydrosilylation is arguably the most important method of surface modification for colloidal SiQDs (Figure 1.6). Performing hydrosilylation reaction on SiQDs is similar to the widely used approach for assembling organic monolayers on bulk silicon surfaces, as first demonstrated by Linford and Chidsey<sup>133,134</sup>. Hydrosilylation requires the preparation of hydrogen terminated colloidal SiQDs. This step can be achieved by solution based reduction<sup>100-102</sup>, use of silicon Zintl salts<sup>135-138</sup>, HF based etching<sup>38,88,93,109,139</sup>, or the use of non-thermal plasma<sup>34,39,94,140,141</sup>, as described in Section 1.3.. The prepared hydrogen- terminated silicon nanoparticles processes a distinct Si-H peak at  $\sim 2100\text{ cm}^{-1}$  by FT-IR measurements<sup>38,39,109,136,137,140,142</sup>. This absorption band is not necessarily shown on all ports. For example, direct evidence for the formation of bond is still absent with some solution reduction based methods, regardless of strong indication of Si-H presence according to subsequent chemistries of successful grafting of surface molecules<sup>83,99,100,104,105,143</sup>. Interestingly, the Si-H bond on silicon quantum dots exhibits subtle differences compared with its bulk counterparts. For instance, the HF etching rate on silicon quantum dots was shown to be much slower than that on bulk silicon, with only several nanometers per minute on particles versus micrometers per minutes on bulk<sup>38,109,144</sup>. It was argued that a likely cause for the slow rate is the presence of fluorinated ions on the curved surface<sup>38,145</sup>. Furthermore, it was reported that HF alone often could not completely remove all oxides<sup>38</sup>, but the addition of ethanol and HNO<sub>3</sub> to the etching mixture assisted the production of oxide free particle surface<sup>95,145</sup>.

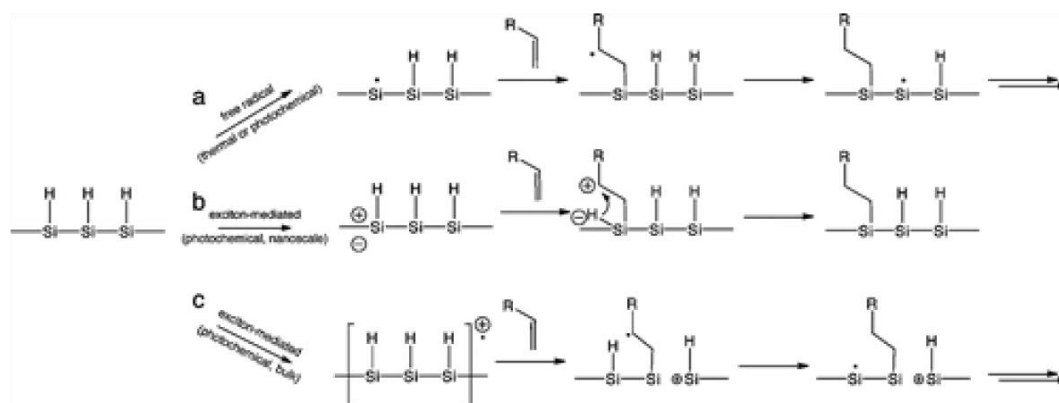


Figure 1.7 Proposed mechanism of hydrosilylation on silicon nanocrystals as a free radical (a) or exciton (b) initiated processes, in comparison with exciton mediated hydrosilylation on bulk silicon (c). Reprinted with permission from Kelly *et al.*<sup>146</sup>, Copyright 2011 American Chemical Society

The Si-H bonds on nanocrystals then readily react with alkene or alkyne moieties to form robust Si-C bonds on silicon quantum dots under thermal, photochemical, or in rarer cases catalytical treatment (Figure 1.7)<sup>143</sup>. It was shown that both UV and near-UV irradiation allowed the attachment of alkenes on SiQDs' surface<sup>88,146,147</sup>, but the reaction rate was slower on larger particles using near-UV light of 365 nm<sup>88,146</sup>. Thermal methods have been equally successful with the hydrosilylation processes, with heating at 140 °C for 20 hours shown to attach alkenes on hydrogen terminated silicon quantum dots<sup>98</sup>, while a recent paper from the Veinot group suggested the formation of oligomers.<sup>81</sup> In addition, common catalyst for hydrosilylation reaction, such as chloroplatinic acid ( $\text{H}_2\text{PtCl}_6$ ) was used to initiate the reaction<sup>100</sup>, though at a rate slower than thermal or photochemical activation<sup>143</sup>. In a recent report by Korgel *et al.*, it was shown that the process could occur even at room temperature with certain biofunctional alkenes, arguably because of the carboxylic acid facilitated nucleophilic attack on the curved

surface<sup>148</sup>. Due to the wide choices of the distal moieties of the surface molecules, it has been demonstrated that hydrosilylation allowed direct coupling of various polar (i.e.  $-\text{NH}_2$ ,  $-\text{COOH}$ ,  $-\text{SO}_3^{2-}$ ) or non-polar (i.e. alkyl, alkenyl) moieties to the surface of silicon quantum dots<sup>107,149-151</sup>. Understanding the details of the mechanism of hydrosilylation is still the focus of intense studies and debates on bulk silicon surfaces, and few work has been done with silicon quantum dots. However, increasing evidence suggested that hydrosilylation on silicon quantum dots happened in a comparable manner to flat or porous silicon<sup>88,139,146</sup> (Figure 1.7). Recently, it was depicted that hydrosilylation occurred via either a free radical or exciton mediated mechanism on particle surface<sup>88,146</sup>. In the free radical initiated process (Figure 1.7, a), a hydride homolysis step due to thermal or photochemical treatment leads to the generation of free radicals, which allow the addition of alkene moiety in a chain of propagation process. In the exciton activated mechanism (Figure 1.7, b), no radical is generated, but photochemical generated excitations allow directly addition of nearby alkene moieties with the Si-H bonds, a comparable process to what happens on bulk silicon (Figure 1.7, c)<sup>88,146</sup>.

#### **1.4.1.3 Modification of halogen coated silicon quantum dots**

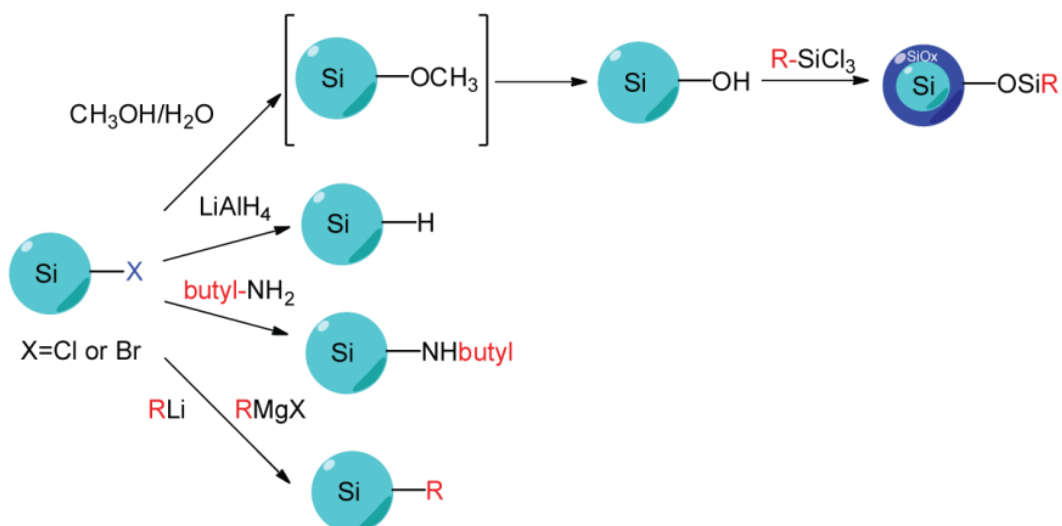


Figure 1.8 Modification of halide-terminated silicon nanocrystals. The electrophilic reactivity and versatility of the Si-X moieties are used to introduce various surface groups.

Another route of surface modification for silicon nanocrystals is based on reactions of the surface Si-Cl or Si-Br moieties (Figure 1.8). Silicon quantum dots with chloride surface are usually prepared by the reaction of silicon Zintl salt (ASi: A=Na, Mg, K) and  $\text{SiCl}_4$ , as discussed in Section 1.3.2.2<sup>102,108,136,137</sup>. Since the surface was Lewis acidic, the strong electrophilic reactivity and versatility of the Si-Cl bond were utilized for the attachment of a range of surface molecules. For example, rinsing chloride coated particles with methanol/water resulted in hydrophobic methoxy surfaces; common nucleophilic reagents such as alkyl lithium and Grignard reagents allow alkyl attachments<sup>108,135</sup>; treatment of Si-Cl terminated particles with  $\text{LiAlH}_4$  or butyl-amine produced Si-H and Si-NH-butyl terminated particles, respectively<sup>83,99,143,152</sup>. Furthermore, the methoxy functionalized particles were subjects for further modifications, in a serendipitous discovery by Kauzlarich *et al.*, hydrolysis of surface Si-Cl occurred with

methanol/water washing<sup>138</sup>, and dots were further functionalized with alkyl-trichlorosilanes, generating particles with siloxane-alkyl surfaces<sup>138</sup>. Noticeably, silicon nanoparticles with siloxane cross-linked surfaces exhibit much higher stability of blue fluorescence for several months, in a sharp contrast to particles terminated with chloride or alkoxy surface that only lasted for two weeks<sup>138</sup>.

#### **1.4.1.4 Advantages and drawbacks**

Wet-chemical approaches of surface modification to colloidal silicon nanocrystals has shown notable advantages: they are compatible with conventional bench-top chemistry allow relatively simple experimental set-ups; procedures are performed in solution, which is fundamentally important for applications such as ink printing and fluorescent labelling agents. However, such strategies suffer a few drawbacks. For instance, problems are sometimes encountered with complications of the air-sensitive techniques, which usually require the use of a Schlenk line or glove box. Another downside is the low boiling point of many small organic molecules that may be employed for the modification reaction, which often leads to reduction of reaction temperature to minimize evaporation. The resultant lower temperature in many cases extends reaction time, which can be for tens of hours before the final products are ready for collection. Furthermore, a minor disadvantage is the occasional agglomeration of the functionalized silicon nanocrystals in solvents, seen as a cloudy suspension from a macroscopic point of view. This phenomenon is primarily caused by the non-equilibrium competition between the attractive van der Waals forces and the interactions of the organic

surface groups that stabilize particles in solution.

## 1.4.2 Surface passivation by plasma-surface interactions

In view of the above mentioned issues, and to explore new routes of surface modification for colloidal silicon nanocrystals, plasma assisted passivation has emerged as an alternative route to the wet-chemical approach. Based on the state of the plasma environment used, here these methods are classified as either aerosol, or liquid-phase plasma methods, respectively.

### 1.4.2.1 Aerosol-based plasma modification

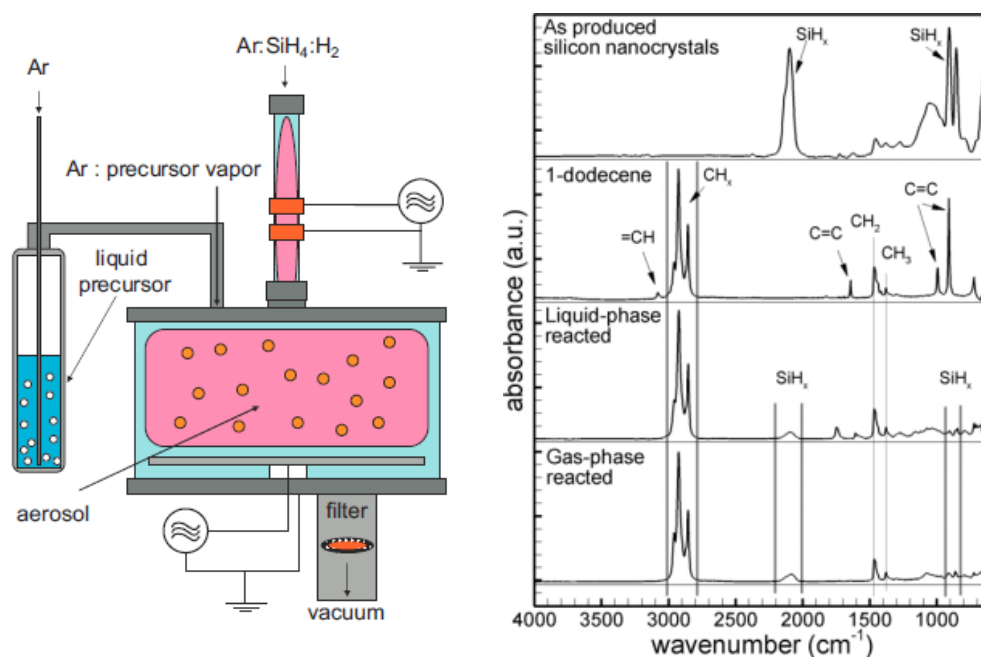


Figure 1.9 Typical experimental set-up for aerosol plasma functionalization of silicon nanocrystals (left). Silicon nanocrystals functionalized by this method showed similar FT-IR features compared with liquid-phase methods. Copyright 2007 Wiley-VCH.<sup>140</sup>

One class of plasma-aided method of grafting molecules to the surface of silicon quantum dots involves gas-phase plasma grafting. The procedure was first

demonstrated by Liao and Robert<sup>153</sup>, who showed assembly of alkene, alkyne, amine and aldehyde molecules on to aerosolized silicon nanocrystals<sup>153</sup>. The method was recently further developed by Kortshagen *et al.*<sup>34,39,110,111,140,142</sup>. Typically, an aerosol-based functionalization procedure requires a two part system. The first part is a synthesis component with the principle described in Section 1.3.3 (Figure 1.9). In the second part, silicon nanocrystals are transferred in an argon gas stream into a chamber reactor, into which a vapour mixture containing desired organic molecules and argon gas was injected<sup>140</sup>. Vapor pressure and flow rate could be controlled by changing the bubbler equipped on the flow tap. Due to the continuous flow of the gas mixture, silicon nanocrystals were eventually collected on the filter as an orange and fluffy powder film<sup>140</sup>. The obtained particles were surface-functionalized, showing organic surface moieties with confirmed by related FT-IR features, which were similar to liquid-phase modifications<sup>140</sup>.

#### **1.4.2.2 Plasma functionalization in the liquid phase**

In addition to the aerosol-based functionalization, coupling plasma with silicon nanocrystals in the liquid phase has been shown to modify the surface of particles with organic monolayers<sup>154-159</sup>. Several approaches were developed for liquid-phase plasma functionalization, including the use of pulsed laser<sup>160</sup>, direct current<sup>161</sup>, and the use of high frequency microplasma<sup>159</sup>. In particular, one technique utilized direct current to generate atmospheric pressure plasma between the electrode and surface of the colloidal dispersion<sup>161</sup>. In a typical set-up, the distance between end of the metal electrode and liquid surface was maintained between 0.5 – 1 mm. A

counter electrode made of a carbon rod was placed ~ 2 cm away from the metal tube, inside which was supplied with Ar or He gas. With the application of high voltage of up to 2 kV, plasma was sustained and current was maintained between 0.5 mA and 5 mA<sup>161</sup>. This allowed the grafting of a number of molecules to the surface of silicon quantum dots<sup>161</sup>. Comparatively, microplasma was shown to be generated within a thin quartz capillary using a set of ring electrode made from copper<sup>162</sup>. Surface grafting of organic molecules were confirmed by FT-IR studies, which were similar to the direct-current microplasma approach<sup>162</sup>.

Although surface engineering on silicon nanocrystals using plasma in the liquid phase is a relatively new concept, the available data still gave some mechanistic insights into how the modification reaction occurs. It was argued that using direct current to generate the plasma may externally ‘inject’ electrons in the liquid phase, which induces a cascade of radical events on the particle surface, allowing the addition of organic molecules<sup>162</sup>. There has been no report so far showing the exact mechanism of how ultra-high frequency microplasma initiated any subsequent chemical reactions, but comparable characterization data of particle surface chemistry suggests a dominant role of plasma-electron interactions at the particle surface<sup>162</sup>

#### **1.4.2.3 Advantages and drawbacks**

As an alternative approach to the wet-chemical methods, one advantage of the plasma method is that the particles are negatively charged throughout the grafting process. Due to the inter-particle repulsion, the aggregation of nanocrystals clusters

is minimized<sup>110</sup>. A second advantage is the particle confinement to the central part of the reactor. This is primarily caused by charged reactor wall that minimizes diffusion loss between particle-wall interactions, which could significantly influence the yield of the final products<sup>110</sup>. A third advantage is the selective particle heating so that the actual operation temperature does not need to be very high. This is particularly true for non-thermal plasma functionalization, as the particles can be selectively heated up to hundreds of Kelvins higher compared to the surrounding gas<sup>39</sup>. This allowed the actual operation temperature of the equipment to be quite low, sometimes close to the room temperature<sup>110</sup>. Last but not least, once set-up, the experiment is usually very rapid, with grafting process usually take only a few minutes, compared to normally hours of reaction time needed for wet-chemical methods. The major disadvantage of the plasma method is the particular expertise needed to construct the entire set-up. Another issue is the non-solution environment which is unfavoured for industrial purposes. Both aspects are critical factors to consider for large-scale, low cost processing in applications such as ink printing and fluorescence imaging agents.

### **1.4.3 Multi-step surface modifications**

There is increasing interests in further engineering of the SAM architecture after the initial modification process. Two issues are identified for single stepped surface passivations: First, as the reactivity of different functional groups may differ significantly, when the desired surface molecules have more than one functional group, it is more favoured to use a multi-step approach than a single-step strategy,

so that competition of reactions between the reactive moieties can be minimized. Second, some surface molecules are hard to synthesize and often obtained in small quantity, it is therefore easier to attach these molecule onto the first SAM, rather than directly coupling with surface silicon species. In practice, the most challenging aspect of surface passivation is often how to preserve optical properties of the particles and introduce surface functionalities at the same time<sup>127</sup>. This problem can be better addressed with a multi-step process. An early example of direct modification on the first SAM layer was shown by Kauzlarich *et al.*, who demonstrated successful synthesis siloxane coated particles via an intermediate hydroxyl terminated step<sup>138</sup>.

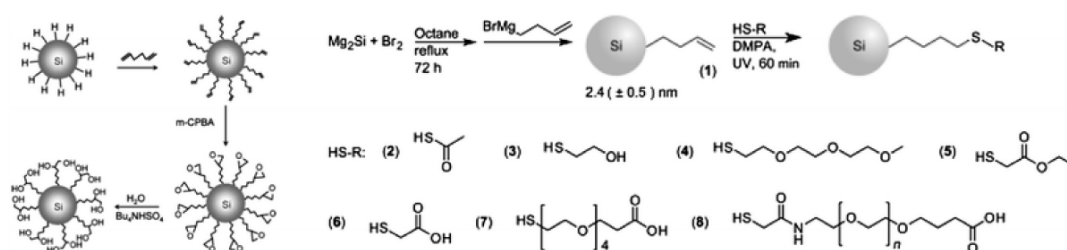


Figure 1.10 Several multiple-step modification strategies. Both methods shown here rely on the preparation of alkene-functionalized particles. Reprinted with permission from Shiohara *et al.*<sup>100</sup>(left) and Ruizendaal *et al.*<sup>151</sup>(right). Copyright 2010 American Chemical Society. Copyright 2011 Wiley-VCH.

Recently, Shiohara *et al.* reported a reaction chain by first modifying hydrogen terminated particles with hexadiene molecule (Figure 1.10)<sup>100</sup>, then further utilized the distal alkene group to produce epoxy, then diol functionalized particles<sup>100</sup>. In addition, Ruizendaal *et al.* and Cheng *et al.* used thiol-ene ‘click’ approach of functionalization (Figure 1.10), first prepared alkene-passivated silicon quantum dots, then further reacted the terminal alkene moieties with thiol molecules with a

number of distal groups<sup>107,151</sup>. Due to the broad choices of commercially available thiols, this has allowed the production of colloidal silicon nanocrystals with a range of choice of surface functionalities.

#### 1.4.4 Characterizing the surface

When characterizing the surface chemistry of colloidal silicon quantum dots, two questions are of immediate concern. The first is what molecular species are actually present on the surface. A combination of NMR, IR and XPS studies can generally give a picture of the molecular species present.<sup>127</sup> The second is the degree of surface coverage of the SAM. It was reported that surface coverage of the organic monolayer was from ~55 % on average to ~80 % at best for flat silicon (1,0,0) and silicon (1,1,1) surface<sup>127</sup>, respectively. Porous silicon showed similar degree of coverage with highest reported value being 60 %<sup>130</sup>. However, studies on the level of monolayer coverage for silicon quantum dots are still rare, though several reports are present across the literature.<sup>147</sup> One study by Hua *et al.* used XPS integrated peak area to indicate approximately 50 % of monolayer coverage for 1.5 nm nanocrystals in plasma assisted modification of particle surface<sup>147</sup>. Another study for estimating the level of surface coverage was reported by Swihart *et al.*, who used thermo-gravimetric analysis (TGA) and <sup>1</sup>H-NMR with an internal standard to show almost complete coverage of surface silicon atoms by photo-initiated hydrosilylation<sup>36,85,147</sup>. However, to date no single method has been widely adopted to determine surface coverage rate for silicon nanoparticles, arguably due to the difficulty in accurate size measurement and complication of the actual surface

chemistry, which could be different to what was observed for flat silicon surfaces

## **1.5 Silicon quantum dots for bio-applications**

### **1.5.1 Fluorescent Imaging**

The potential of colloidal quantum dots in fluorescent bio-imaging applications has been well recognized. Such application is particularly relevant to quantum dots emit in the near infrared (NIR) region of 650 nm to 900 nm, due to the existence of tissue window in which light absorption and scattering is minimized. In spite of the numerous studies of fluorescence imaging using CdSe quantum dots, the first report involving SiNCs was not published until 2004 by Li and Ruckenstein<sup>163</sup>. This work rapidly attracted much attention, and a number of reports have been published ever since<sup>87,99,164-167</sup>.

The most typical approach for bio-imaging using silicon nanocrystals is *in vitro* studies that show the uptake of particles by cell via endocytosis. For instance, Alsharif *et al.* reported the intracellular internalization of alkyl-functionalized SiNCs in human neoplastic and normal primary cells<sup>168</sup>. It was found that cellular uptake rate was significantly faster for malignant cells in comparison with normal cells, and endocytosis was influenced by certain cholesterol derivatives<sup>168</sup>. Warner *et al.* reported cellular uptake of blue-luminescent, amine coated quantum dots, with no acute cellular toxicity observed<sup>99,104</sup>. He *et al.* used silicon quantum dots embedded in oxide to form nanoparticle spheres, demonstrated several endocytosis processes<sup>37,166</sup>. Importantly, silicon quantum dots in these studies were functionalized with any bio-functional moieties to target the particles to any specific

locations in the cell. Hence, particles simply are located throughout the cell and therefore further modification of the particles to ensure targeted interactions are required for practical considerations.

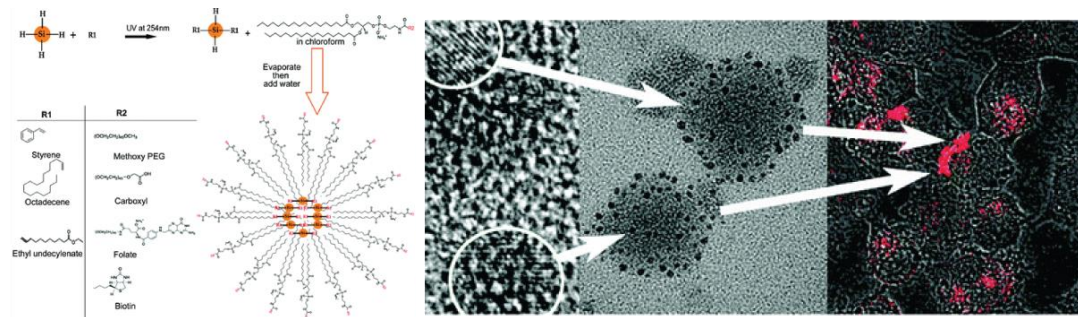


Figure 1.11 Silicon nanocrystals encapsulated within phospholipid micelles. TEM images suggest silicon nanocrystals containing phospholipid is several tens of nanometers in diameters in size. Uptake of the micelles is demonstrated by fluorescence imaging of HeLa cells incubated with the particles. Copyright 2008 American Chemical Society.<sup>87</sup>

Phospholipid-encapsulated systems have shown promise in bio-imaging applications of fluorescent nanoparticles (Figure 1.11). The advantages of using phospholipids include the good colloidal stability and low non-specific adsorption<sup>22</sup>. Erogbogbo *et al.* first demonstrated this process for SiNCs using hydrophobic SiNCs encapsulated in phospholipids to form micelle-type structures<sup>87</sup> (Figure 1). The particle-micelle system exhibited reasonable quantum efficiency (2%) and biocompatibility, as demonstrated by *in vitro* imaging studies with HeLa cells<sup>87</sup>. A major benefit of this technique is that it offers a range of engineering choices on the micelle shell. For example, it was shown that modifying the phospholipid layer with 1,4,7,10-tetraazacyclododecane-1,4,7,10-tetraacetic acid (DOTA) ligands allowed the chelate of paramagnetic Gd ion<sup>169</sup>. Alternatively, coupling the micelle layer with a dye donor allowed fluorescent resonance energy transfer (FRET) to happen<sup>170</sup>,

improving the undesired situation of fluorescence loss after encapsulation<sup>170</sup>.

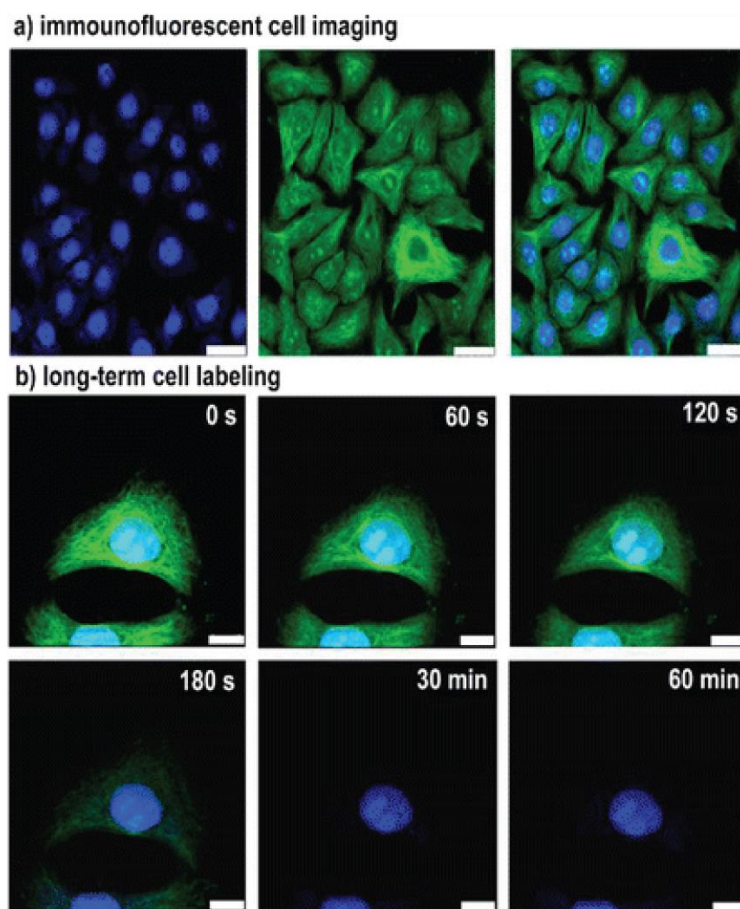


Figure 1.12 Immunofluorescent cell imaging by confocal microscopy. Illustrated as staining of microtubules by FITC (Green) and nucleus by silicon nanocrystals (Blue), showing no photo-bleaching of SiNCs under one hour constant illumination. Reprinted with permission from Zhong *et al.*<sup>171</sup> Copyright 2013 American Chemical Society.

One issue with fluorescent bio-imaging using silicon nanocrystals is the low excitation wavelength. The excitation wavelength for SiNCs is often in the UV-blue, a region that is outside of the tissue window (650 - 900 nm) so relevant to *in vivo* applications. One strategy to avoid the low wavelength excitation is using two photon techniques<sup>172</sup>, where particles are simultaneously excited by two photons of half the energy to the excited state<sup>172</sup>. It was shown that both excitation and

emission can be achieved in the NIR wavelength<sup>173</sup>. Another issue is sometimes the large hydrodynamic diameters (> 10 nm) for phospholipid-coated dots that could potentially lead to slow degradation rate<sup>174</sup>. Since most bio-imaging applications require the fluorescent label to be selectively attached with a biological entity, small particle radius, good colloidal stability and bio-active surfaces are equally important for bio-applicable silicon nanocrystals. It seems that these criteria can be best met with functionalization with self-assembled monolayers (SAMs)<sup>171,175</sup>. For instance, a recent report by Zhong *et al.* showed long term cellular imaging of cell nuclei for up to 60 min with no photo bleaching<sup>171</sup>. Erogbogbo *et al.* showed selective uptake of colloidal silicon nanocrystals by cancer cells<sup>175</sup>. That was achieved by covalently modifying the particles via EDC/NHS reaction with biomolecules including lysine, folate, antimesothelin and transferrin<sup>175</sup>. After incubation with pancreatic cancer cells, folate and antimesothelin conjugated particles were selectively internalized by the cell<sup>175</sup>.

### **1.5.2 Silicon quantum dots as a less toxic alternative to conventional quantum dots**

One of the more attractive aspects of SiQDs for use *in vivo* is the low intrinsic toxicity of silicon as a material<sup>176</sup>. During the past-decade, advances in synthetic and surface chemistry have allowed the preparation of monodisperse, photostable quantum dots(QDs) in aqueous solutions, inspiring the design of novel fluorescent labelling agents<sup>20,23,114,177</sup>. However, the core materials of these quantum dots often contain heavy metal elements, such as cadmium (Cd). Due to the known toxicity of

the Cd element to biological systems, there have been intense debates over whether to use them in imaging contexts<sup>178,179</sup>. Although the toxicity issue of QDs has been extensively reviewed elsewhere<sup>27</sup>, some of the most critical aspects here due to the importance of this topic are still highlighted.

Investigations into the toxicity of quantum dots began with studying *in vitro* effects. Those studies indicate that QDs associated cytotoxicity may be primarily caused by release of cadmium ions, or the generation of free radicals<sup>180</sup>. On the one hand, the cadmium core may contribute to biological damage caused by the QDs. One of the first systematic investigations was performed by Derfus and coworkers, who reported DNA/cell damage employing CdSe quantum dots with a variety of coating ligands<sup>25</sup>. In particular, it was shown that CdSe release cadmium ions after UV exposure, leading to cell and DNA damage<sup>25</sup>. This result was supported by several other reports, suggesting the cytotoxic effects may be reduced to some extent by the coating with different surface ligands, such as mercaptoacetic acid (MAA), bovine serum albumin (BSA), mercaptoundecanoic acid (MUA), cysteamine (QD-NH<sub>2</sub>) or thioglycerol (QD-OH), mercaptopropionic acid (MPA) and polyethylene glycol (PEG)<sup>27,31</sup>. However, cytotoxicity cannot be completely eliminated as cell/DNA damage was observed after long term exposure to high concentration of surface coated QDs<sup>25,27,31</sup>. On the other hand, another series of in-depth studies showed the generation of reactive oxygen intermediates (ROI) under UV may also contribute to the quantum dots (QDs) toxicity. Inspired by the work of Green and Howman, who demonstrated DNA nicking takes place immediately upon the addition of QDs in dark conditions<sup>181</sup>, electron paramagnetic resonance

(EPR) studies suggested the formation of superoxide radicals from CdS dots, and hydroxyl radicals from CdSe dots respectively<sup>182</sup>. Based on their results, Ipe *et al.* concluded that although type and amount of radicals differ from each dot, ROI is indeed produced by QDs<sup>182</sup>.

Concerns about the toxicity of ‘conventional’ QDs steered researchers towards finding cadmium-free alternatives, and in recent years a plethora of candidates have been brought to light. Indium-based QDs including InP and InP/ZnS QDs with the latter being demonstrated for pancreatic cancer imaging<sup>183,184</sup>. Alternatively, CuInS<sub>2</sub>/ZnS core-shell QDs have been demonstrated for sentinel lymph node imaging in both visible and near-IR region<sup>185-187</sup>. Zinc compounds that are often used as the shell material in conventional QDs have been put forward as a cadmium-free core material. By doping zinc-based QDs with heavy metal ions, strong emission in the visible region has been achieved<sup>188</sup>. ZnS:Mn/ZnS core-doped core/shell QDs were used *in vivo* for tumour imaging<sup>189</sup>, and recently Maity *et al.* compared the performance of three doped QD materials (Mn doped ZnS, Mn doped ZnSe and Cu doped InZnS) *in vitro*<sup>190</sup>.

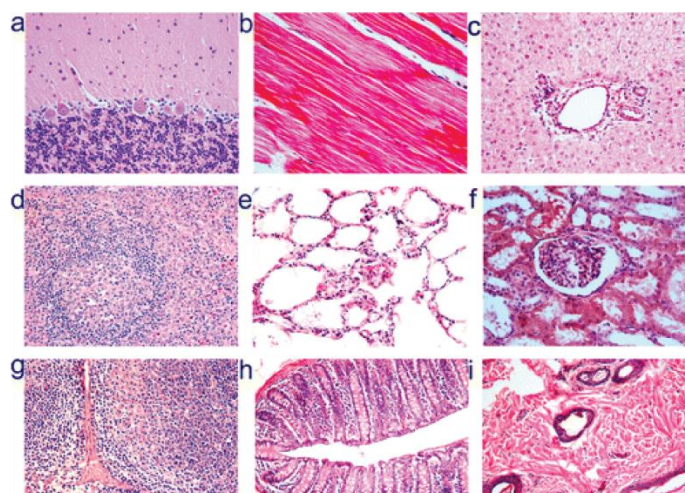


Figure 1.13 Histological images of rhesus macaques indicate no toxicity of silicon nanoparticles after 3 months of injection at dose of 200 mg/kg. Images shown were tissues sample obtained from (a) brain, (b) heart, (c) liver, (d) spleen, (e) lung, (f) kidney, (g) lymph, (h) intestine and (i) skin at 40 times magnification. Reprinted with permission from Liu *et. al.*<sup>191</sup> Copyright 2013 American Chemical Society

Silicon is an attractive material for the preparation of cadmium-free QDs because it is non-toxic in its bulk form and is readily degraded to silicic acid, which can be excreted in the urine<sup>192</sup>. Silicon has even been suggested as a trace nutrient or food additive<sup>193,194</sup>. Recently, a number of studies have demonstrated the low *in vitro* toxicity of SiQDs<sup>168,195,196</sup>. With respect to *in vivo* studies, silicon's benign nature has inspired applications in tumour vasculature targeting, sentinel lymph node mapping and multicolour imaging in mice<sup>174</sup>. It was shown that phospholipid encapsulated silicon quantum dots showed minimal *in vivo* toxicity at particle concentration up to ~380 mg/kg, a much higher value compared with studies performed with CdSe/ZnS quantum dots<sup>174,197</sup>. Recently, Liu *et. al.* performed *in vivo* toxicity studies of SiQDs in mice and monkeys and found no overt signs of toxicity at dose of 200 mg/kg<sup>191</sup>. Neither monkey nor mice showed signs of toxicity at this dose. However SiQDs did not seem to degrade as expected, and histological

tests did not indicate any toxicity in monkey (Figure 1.13)<sup>191</sup>. Positron emission tomography (PET) analysis suggested that after injection, most SiQDs are rapidly excreted via renal filtration with the remainder accumulating in the liver for weeks with no acute toxicity observed, regardless a level of inflammation response was observed<sup>191,198</sup>. With all nanoparticle toxicity studies it is important to note that capping ligands, targeting moieties, nanoparticle shape, size and surface chemistry can all elicit a cellular response<sup>199</sup>. For example, it was suggested that the surface chemistry of semiconductor QDs may significantly alter the potential for aggregation, and control of interface architecture have a significant impact on particle clearance from the body<sup>200</sup>. Hence it is vital to perform a full toxicological characterization of the nanomaterial system as it will be used in the clinic in order to elicit a full picture of the organism's response.

## **1.6 Summary and scope of this thesis**

This chapter has given a general review of the current research on the topic of colloidal silicon quantum dots. Generally speaking, the intrinsic optoelectronic properties of silicon quantum dots have made this type of nanomaterial a potential candidate in a number of applications including fluorescent imaging agent for biomedicine. However the small size of SiQDs, limited methods of preparation and complicated surface chemistry have made them much harder to work compared with their heavy metal counterparts.

This thesis is concerned with the further exploration of this topic. The results

chapters are divided into two parts. In the first part, namely ‘synthesis and surface modifications’ including chapter three and chapter four, the main focus is on development of new methodologies of preparing and surface modification of colloidal SiQDs. Specifically, chapter three describes a ‘one pot’ synthesis method of preparing alkene terminated colloidal SiQDs that are modified with thiol-ene ‘click’ chemistry. Chapter four describes a comparable, but two-step procedure using copper catalysed azide-alkyne cycloaddition approach with demonstration of these SiQDs in biological fluorescence imaging contexts.

In the second part of the thesis, namely ‘bio-applications’ including chapter 5 and chapter 6, the use of SiQDs in biological applications is emphasized. In chapter six, SiQDs are used for cellular fluorescence imaging in the context of fluorescence lifetime imaging microscopy (FLIM). The long fluorescence lifetime of the nanoparticles is utilized to obtain deconvoluted signals using both one and two photon FLIM. Using the phasor approach of FLIM data analysis, it is demonstrated that the multiple components of lifetime decay can be easily separated using limited photons available in each pixel. In chapter six, the first silicon quantum dots protease sensor is described. This is based on Förster resonance energy transfer (FRET) process using a SiQDs-dye conjugate, where SiQDs were conjugated to a dye acceptor via an enzyme responsive peptide linker.

## 1.7 References

- (1) Resch-Genger, U.; Grabolle, M.; Cavaliere-Jaricot, S.; Nitschke, R.; Nann, T. Quantum dots versus organic dyes as fluorescent labels. *Nat Methods* **2008**, *5*, 763-775.
- (2) Brus, L. Electronic wave-functions in semiconductor clusters - experiment and theory. *J Phys Chem-US* **1986**, *90*, 2555-2560.
- (3) Brus, L. E. Electron electron and electron-hole interactions in small semiconductor crystallites - the size dependence of the lowest excited electronic state. *J. Chem. Phys.* **1984**, *80*, 4403-4409.
- (4) Peng, X.; Manna, L.; Yang, W.; Wickham, J.; Scher, E.; Kadavanich, A.; Alivisatos, A. P. Shape control of CdSe nanocrystals. *Nature* **2000**, *404*, 59-61.
- (5) Alivisatos, A. P. Perspectives on the physical chemistry of semiconductor nanocrystals. *J Phys Chem-US* **1996**, *100*, 13226-13239.
- (6) Peng, Z. A.; Peng, X. G. Formation of high-quality CdTe, CdSe, and CdS nanocrystals using CdO as precursor. *Journal of the American Chemical Society* **2001**, *123*, 183-184.
- (7) Murray, C. B.; Norris, D. J.; Bawendi, M. G. Synthesis and characterization of nearly monodisperse CdE (E = sulfur, selenium, tellurium) semiconductor nanocrystallites. *Journal of the American Chemical Society* **1993**, *115*, 8706-8715.
- (8) Peng, X. G.; Wickham, J.; Alivisatos, A. P. Kinetics of II-VI and III-V colloidal semiconductor nanocrystal growth: "Focusing" of size distributions. *Journal of the American Chemical Society* **1998**, *120*, 5343-5344.
- (9) Garcia, J. M.; MedeirosRibeiro, G.; Schmidt, K.; Ngo, T.; Feng, J. L.; Lorke, A.; Kotthaus, J.; Petroff, P. M. Intermixing and shape changes during the formation of InAs self-assembled quantum dots. *Appl Phys Lett* **1997**, *71*, 2014-2016.
- (10) Marzin, J. Y.; Gerard, J. M.; Izrael, A.; Barrier, D.; Bastard, G. Photoluminescence of single InAs quantum dots obtained by self-organized growth GaAs. *Phys. Rev. Lett.* **1994**, *73*, 716-719.
- (11) Wise, F. W. Lead Salt Quantum Dots: the Limit of Strong Quantum Confinement. *Accounts Chem Res* **2000**, *33*, 773-780.
- (12) Talapin, D. V.; Rogach, A. L.; Shevchenko, E. V.; Kornowski, A.; Haase, M.; Weller, H. Dynamic distribution of growth rates within the ensembles of colloidal II-VI and III-V semiconductor nanocrystals as a factor governing their photoluminescence efficiency. *Journal of the American Chemical Society* **2002**, *124*, 5782-5790.
- (13) Ellingson, R. J.; Beard, M. C.; Johnson, J. C.; Yu, P. R.; Micic, O. I.; Nozik, A. J.; Shabaev, A.; Efros, A. L. Highly efficient multiple exciton generation in colloidal PbSe and PbS quantum dots. *Nano Letters* **2005**, *5*, 865-871.
- (14) Robel, I.; Subramanian, V.; Kuno, M.; Kamat, P. V. Quantum dot solar cells. Harvesting light energy with CdSe nanocrystals molecularly linked to mesoscopic TiO<sub>2</sub> films. *Journal of the American Chemical Society* **2006**, *128*, 2385-2393.
- (15) Kamat, P. V. Quantum Dot Solar Cells. Semiconductor Nanocrystals as

Light Harvesters. *J Phys Chem C* **2008**, *112*, 18737-18753.

(16)Conibeer, G.; Green, M.; Cho, E.-C.; König, D.; Cho, Y.-H.; Fangsuwannarak, T.; Scardera, G.; Pink, E.; Huang, Y.; Puzzer, T.; Huang, S.; Song, D.; Flynn, C.; Park, S.; Hao, X.; Mansfield, D. Silicon quantum dot nanostructures for tandem photovoltaic cells. *Thin Solid Films* **2008**, *516*, 6748-6756.

(17)Huffaker, D. L.; Park, G.; Zou, Z.; Shchekin, O. B.; Deppe, D. G. 1.3  $\mu\text{m}$  room-temperature GaAs-based quantum-dot laser. *Appl Phys Lett* **1998**, *73*, 2564-2566.

(18)Strauf, S.; Hennessy, K.; Rakher, M. T.; Choi, Y. S.; Badolato, A.; Andreani, L. C.; Hu, E. L.; Petroff, P. M.; Bouwmeester, D. Self-tuned quantum dot gain in photonic crystal lasers. *Phys. Rev. Lett.* **2006**, *96*.

(19)Sun, Q.; Wang, Y. A.; Li, L. S.; Wang, D. Y.; Zhu, T.; Xu, J.; Yang, C. H.; Li, Y. F. Bright, multicoloured light-emitting diodes based on quantum dots. *Nat Photonics* **2007**, *1*, 717-722.

(20)Michalet, X.; Pinaud, F. F.; Bentolila, L. A.; Tsay, J. M.; Doose, S.; Li, J. J.; Sundaresan, G.; Wu, A. M.; Gambhir, S. S.; Weiss, S. Quantum Dots for Live Cells, in Vivo Imaging, and Diagnostics. *Science* **2005**, *307*, 538-544.

(21)Medintz, I. L.; Uyeda, H. T.; Goldman, E. R.; Mattoussi, H. Quantum dot bioconjugates for imaging, labelling and sensing. *Nat. Mater.* **2005**, *4*, 435-446.

(22)Dubertret, B.; Skourides, P.; Norris, D. J.; Noireaux, V.; Brivanlou, A. H.; Libchaber, A. In Vivo Imaging of Quantum Dots Encapsulated in Phospholipid Micelles. *Science* **2002**, *298*, 1759-1762.

(23)Bruchez, M.; Moronne, M.; Gin, P.; Weiss, S.; Alivisatos, A. P. Semiconductor nanocrystals as fluorescent biological labels. *Science* **1998**, *281*, 2013-2016.

(24)Chan, W. C. W.; Nie, S. Quantum Dot Bioconjugates for Ultrasensitive Nonisotopic Detection. *Science* **1998**, *281*, 2016-2018.

(25)Derfus, A. M.; Chan, W. C. W.; Bhatia, S. N. Probing the cytotoxicity of semiconductor quantum dots. *Nano Letters* **2004**, *4*, 11-18.

(26)Lewinski, N.; Colvin, V.; Drezek, R. Cytotoxicity of nanoparticles. *Small* **2008**, *4*, 26-49.

(27)Kirchner, C.; Liedl, T.; Kudera, S.; Pellegrino, T.; Javier, A. M.; Gaub, H. E.; Stolzle, S.; Fertig, N.; Parak, W. J. Cytotoxicity of colloidal CdSe and CdSe/ZnS nanoparticles. *Nano Letters* **2005**, *5*, 331-338.

(28)Oberdorster, G.; Oberdorster, E.; Oberdorster, J. Nanotoxicology: An emerging discipline evolving from studies of ultrafine particles. *Environ Health Persp* **2005**, *113*, 823-839.

(29)Hardman, R. A toxicologic review of quantum dots: Toxicity depends on physicochemical and environmental factors. *Environ Health Persp* **2006**, *114*, 165-172.

(30)Gao, X. H.; Yang, L. L.; Petros, J. A.; Marshal, F. F.; Simons, J. W.; Nie, S. M. In vivo molecular and cellular imaging with quantum dots. *Curr. Opin. Biotechnol.* **2005**, *16*, 63-72.

(31)Hoshino, A.; Fujioka, K.; Oku, T.; Suga, M.; Sasaki, Y. F.; Ohta, T.; Yasuhara, M.; Suzuki, K.; Yamamoto, K. Physicochemical properties and cellular

toxicity of nanocrystal quantum dots depend on their surface modification. *Nano Letters* **2004**, *4*, 2163-2169.

(32) Wilson, W. L.; Szajowski, P. F.; Brus, L. E. Quantum confinement in size-selected, surface-oxidized silicon nanocrystals. *Science* **1993**, *262*, 1242-1244.

(33) Delley, B.; Steigmeier, E. F. Quantum confinement in Si nanocrystals. *Phys Rev B* **1993**, *47*, 1397-1400.

(34) Jurbergs, D.; Rogojina, E.; Mangolini, L.; Kortshagen, U. Silicon nanocrystals with ensemble quantum yields exceeding 60%. *Appl Phys Lett* **2006**, *88*.

(35) Li, Q.; He, Y.; Chang, J.; Wang, L.; Chen, H.; Tan, Y.-W.; Wang, H.; Shao, Z. Surface-Modified Silicon Nanoparticles with Ultrabright Photoluminescence and Single-Exponential Decay for Nanoscale Fluorescence Lifetime Imaging of Temperature. *Journal of the American Chemical Society* **2013**, *135*, 14924-14927.

(36) Veinot, J. G. Synthesis, surface functionalization, and properties of freestanding silicon nanocrystals. *Chem Commun (Camb)* **2006**, 4160-4168.

(37) He, Y.; Kang, Z.-H.; Li, Q.-S.; Tsang, C. H. A.; Fan, C.-H.; Lee, S.-T. Ultrastable, Highly Fluorescent, and Water-Dispersed Silicon-Based Nanospheres as Cellular Probes. *Angewandte Chemie International Edition* **2009**, *48*, 128-132.

(38) Li, X. G.; He, Y. Q.; Swihart, M. T. Surface functionalization of silicon nanoparticles produced by laser-driven pyrolysis of silane followed by HF-HNO<sub>3</sub> etching. *Langmuir* **2004**, *20*, 4720-4727.

(39) Mangolini, L.; Thimsen, E.; Kortshagen, U. High-yield plasma synthesis of luminescent silicon nanocrystals. *Nano Letters* **2005**, *5*, 655-659.

(40) Ciampi, S.; Harper, J. B.; Gooding, J. J. Wet chemical routes to the assembly of organic monolayers on silicon surfaces via the formation of Si-C bonds: surface preparation, passivation and functionalization. *Chem. Soc. Rev.* **2010**, *39*, 2158-2183.

(41) Erogbogbo, F.; Yong, K. T.; Hu, R.; Law, W. C.; Ding, H.; Chang, C. W.; Prasad, P. N.; Swihart, M. T. Biocompatible Magnetofluorescent Probes: Luminescent Silicon Quantum Dots Coupled with Superparamagnetic Iron(III) Oxide. *Acs Nano* **2010**, *4*, 5131-5138.

(42) Dasog, M.; Yang, Z. Y.; Regli, S.; Atkins, T. M.; Faramus, A.; Singh, M. P.; Muthuswamy, E.; Kauzlarich, S. M.; Tilley, R. D.; Veinot, J. G. C. Chemical Insight into the Origin of Red and Blue Photoluminescence Arising from Freestanding Silicon Nanocrystals. *Acs Nano* **2013**, *7*, 2676-2685.

(43) Yoffe, A. D. Low-dimensional systems - quantum-size effects and electronic properties of semiconductor microcrystallites (zero-dimensional systems) and some quasi-2-dimensional systems. *Adv Phys* **1993**, *42*, 173-266.

(44) Lannoo, M.; Delerue, C.; Allan, G.; Niquet, Y. M. Confinement effects and tunnelling through quantum dots. *Philos Transact A Math Phys Eng Sci* **2003**, *361*, 259-272; discussion 272-253.

(45) Yin, Y.; Alivisatos, A. P. Colloidal nanocrystal synthesis and the organic-inorganic interface. *Nature* **2005**, *437*, 664-670.

(46) Mansur, H. S. Quantum dots and nanocomposites. *Wiley Interdiscip Rev Nanomed Nanobiotechnol* **2010**, *2*, 113-129.

- (47) Scholes, G. D.; Rumbles, G. Excitons in nanoscale systems. *Nat Mater* **2006**, *5*, 683-696.
- (48) Medintz, I. L.; Uyeda, H. T.; Goldman, E. R.; Mattoussi, H. Quantum dot bioconjugates for imaging, labelling and sensing. *Nat Mater* **2005**, *4*, 435-446.
- (49) Liu, H. Y.; Steer, M. J.; Badcock, T. J.; Mowbray, D. J.; Skolnick, M. S.; Navaretti, P.; Groom, K. M.; Hopkinson, M.; Hogg, R. A. Long-wavelength light emission and lasing from InAs/GaAs quantum dots covered by a GaAsSb strain-reducing layer. *Appl Phys Lett* **2005**, *86*, -.
- (50) Allan, G.; Delerue, C.; Lannoo, M. Nature of Luminescent Surface States of Semiconductor Nanocrystallites. *Phys. Rev. Lett.* **1996**, *76*, 2961-2964.
- (51) Tolbert, S. H.; Herhold, A. B.; Johnson, C. S.; Alivisatos, A. P. Comparison of Quantum Confinement Effects on the Electronic Absorption Spectra of Direct and Indirect Gap Semiconductor Nanocrystals. *Phys. Rev. Lett.* **1994**, *73*, 3266-3269.
- (52) Efros, A. L.; Rosen, M.; Kuno, M.; Nirmal, M.; Norris, D. J.; Bawendi, M. Band-edge exciton in quantum dots of semiconductors with a degenerate valence band: Dark and bright exciton states. *Phys Rev B* **1996**, *54*, 4843-4856.
- (53) Trindade, T.; O'Brien, P.; Pickett, N. L. Nanocrystalline semiconductors: Synthesis, properties, and perspectives. *Chem Mater* **2001**, *13*, 3843-3858.
- (54) Yoffe, A. D. Semiconductor quantum dots and related systems: Electronic, optical, luminescence and related properties of low dimensional systems. *Adv Phys* **2001**, *50*, 1-208.
- (55) Landin, L.; Miller, M. S.; Pistol, M. E.; Pryor, C. E.; Samuelson, L. Optical studies of individual InAs quantum dots in GaAs: Few-particle effects. *Science* **1998**, *280*, 262-264.
- (56) Bimberg, D.; Grundmann, M.; Heinrichsdorff, F.; Ledentsov, N. N.; Ustinov, V. M.; Zhukov, A. E.; Kovsh, A. R.; Maximov, M. V.; Shernyakov, Y. M.; Volovik, B. V.; Tsatsul'nikov, A. F.; Kop'ev, P. S.; Alferov, Z. I. Quantum dot lasers: breakthrough in optoelectronics. *Thin Solid Films* **2000**, *367*, 235-249.
- (57) Patel, R. B.; Bennett, A. J.; Farrer, I.; Nicoll, C. A.; Ritchie, D. A.; Shields, A. J. Two-photon interference of the emission from electrically tunable remote quantum dots. *Nat Photonics* **2010**, *4*, 632-635.
- (58) Frangioni, J. V. In vivo near-infrared fluorescence imaging. *Curr Opin Chem Biol* **2003**, *7*, 626-634.
- (59) Yu, W. W.; Qu, L. H.; Guo, W. Z.; Peng, X. G. Experimental determination of the extinction coefficient of CdTe, CdSe and CdS nanocrystals (vol 15, pg 2854, 2003). *Chem Mater* **2004**, *16*, 560-560.
- (60) Kucur, E.; Boldt, F. M.; Cavaliere-Jaricot, S.; Ziegler, J.; Nann, T. Quantitative analysis of cadmium selenide nanocrystal concentration by comparative techniques. *Anal Chem* **2007**, *79*, 8987-8993.
- (61) Rueda, D.; Walter, N. G. Fluorescent energy transfer readout of an aptazyme-based biosensor. *Methods Mol Biol* **2006**, *335*, 289-310.
- (62) Gruber, H. J.; Hahn, C. D.; Kada, G.; Riener, C. K.; Harms, G. S.; Ahrer, W.; Dax, T. G.; Knaus, H. G. Anomalous fluorescence enhancement of Cy3 and cy3.5 versus anomalous fluorescence loss of Cy5 and Cy7 upon covalent linking to

- IgG and noncovalent binding to avidin. *Bioconjug Chem* **2000**, *11*, 696-704.
- (63) Soper, S. A.; Mattingly, Q. L. Steady-State and Picosecond Laser Fluorescence Studies of Nonradiative Pathways in Tricarbocyanine Dyes - Implications to the Design of near-IR Fluorochromes with High Fluorescence Efficiencies. *Journal of the American Chemical Society* **1994**, *116*, 3744-3752.
- (64) Alivisatos, A. P.; Gu, W.; Larabell, C. Quantum dots as cellular probes. *Annu Rev Biomed Eng* **2005**, *7*, 55-76.
- (65) Wang, X. Y.; Qu, L. H.; Zhang, J. Y.; Peng, X. G.; Xiao, M. Surface-related emission in highly luminescent CdSe quantum dots. *Nano Letters* **2003**, *3*, 1103-1106.
- (66) Talapin, D. V.; Mekis, I.; Gotzinger, S.; Kornowski, A.; Benson, O.; Weller, H. CdSe/CdS/ZnS and CdSe/ZnSe/ZnS core-shell-shell nanocrystals. *Journal of Physical Chemistry B* **2004**, *108*, 18826-18831.
- (67) Spanhel, L.; Haase, M.; Weller, H.; Henglein, A. Photochemistry of Colloidal Semiconductors .20. Surface Modification and Stability of Strong Luminescing Cds Particles. *Journal of the American Chemical Society* **1987**, *109*, 5649-5655.
- (68) Xu, S.; Kumar, S.; Nann, T. Rapid synthesis of high-quality InP nanocrystals. *Journal of the American Chemical Society* **2006**, *128*, 1054-1055.
- (69) Mihindukulasuriya, S. H.; Morcone, T. K.; McGown, L. B. Characterization of acridone dyes for use in four-decay detection in DNA sequencing. *Electrophoresis* **2003**, *24*, 20-25.
- (70) Dahan, M.; Laurence, T.; Pinaud, F.; Chemla, D. S.; Alivisatos, A. P.; Sauer, M.; Weiss, S. Time-gated biological imaging by use of colloidal quantum dots. *Optics Letters* **2001**, *26*, 825-827.
- (71) Gupta, A.; Swihart, M. T.; Wiggers, H. Luminescent Colloidal Dispersion of Silicon Quantum Dots from Microwave Plasma Synthesis: Exploring the Photoluminescence Behavior Across the Visible Spectrum. *Adv Funct Mater* **2009**, *19*, 696-703.
- (72) Wheeler, L. M.; Neale, N. R.; Chen, T.; Kortshagen, U. R. Hypervalent surface interactions for colloidal stability and doping of silicon nanocrystals. *Nat Commun* **2013**, *4*.
- (73) Takeoka, S.; Fujii, M.; Hayashi, S. Size-dependent photoluminescence from surface-oxidized Si nanocrystals in a weak confinement regime. *Phys Rev B* **2000**, *62*, 16820-16825.
- (74) Sychugov, I.; Fucikova, A.; Pevero, F.; Yang, Z.; Veinot, J. G. C.; Linnros, J. Ultranarrow Luminescence Linewidth of Silicon Nanocrystals and Influence of Matrix. *ACS Photonics* **2014**, *1*, 998-1005.
- (75) Zhang, X. M.; Neiner, D.; Wang, S. Z.; Louie, A. Y.; Kauzlarich, S. M. A new solution route to hydrogen-terminated silicon nanoparticles: synthesis, functionalization and water stability. *Nanotechnology* **2007**, *18*.
- (76) Sugimoto, H.; Fujii, M.; Imakita, K.; Hayashi, S.; Akamatsu, K. Phosphorus and Boron Codoped Colloidal Silicon Nanocrystals with Inorganic Atomic Ligands. *The Journal of Physical Chemistry C* **2013**, *117*, 6807-6813.
- (77) Norris, D. J.; Efros, A. L.; Erwin, S. C. Doped Nanocrystals. *Science* **2008**,

319, 1776-1779.

(78)Mocatta, D.; Cohen, G.; Schattner, J.; Millo, O.; Rabani, E.; Banin, U. Heavily Doped Semiconductor Nanocrystal Quantum Dots. *Science* **2011**, *332*, 77-81.

(79)Mastronardi, M. L.; Maier-Flaig, F.; Faulkner, D.; Henderson, E. J.; Kübel, C.; Lemmer, U.; Ozin, G. A. Size-Dependent Absolute Quantum Yields for Size-Separated Colloidally-Stable Silicon Nanocrystals. *Nano Letters* **2011**, *12*, 337-342.

(80)Wolf, O.; Dasog, M.; Yang, Z.; Balberg, I.; Veinot, J. G. C.; Millo, O. Doping and Quantum Confinement Effects in Single Si Nanocrystals Observed by Scanning Tunneling Spectroscopy. *Nano Letters* **2013**.

(81)Dasog, M.; Yang, Z.; Regli, S.; Atkins, T. M.; Faramus, A.; Singh, M. P.; Muthuswamy, E.; Kauzlarich, S. M.; Tilley, R. D.; Veinot, J. G. C. Chemical Insight into the Origin of Red and Blue Photoluminescence Arising from Freestanding Silicon Nanocrystals. *ACS Nano* **2013**, *7*, 2676-2685.

(82)Shirahata, N. Colloidal Si nanocrystals: a controlled organic-inorganic interface and its implications of color-tuning and chemical design toward sophisticated architectures. *Physical Chemistry Chemical Physics* **2011**, *13*, 7284-7294.

(83)Warner, J. H.; Hoshino, A.; Yamamoto, K.; Tilley, R. D. Water-Soluble Photoluminescent Silicon Quantum Dots. *Angewandte Chemie International Edition* **2005**, *44*, 4550-4554.

(84)Dohnalova, K.; Poddubny, A. N.; Prokofiev, A. A.; de Boer, W. D. A. M.; Umesh, C. P.; Paulusse, J. M. J.; Zuilhof, H.; Gregorkiewicz, T. Surface brightens up Si quantum dots: direct bandgap-like size-tunable emission. *Light-Sci Appl* **2013**, *2*.

(85)Holmes, J. D.; Ziegler, K. J.; Doty, R. C.; Pell, L. E.; Johnston, K. P.; Korgel, B. A. Highly luminescent silicon nanocrystals with discrete optical transitions. *Journal of the American Chemical Society* **2001**, *123*, 3743-3748.

(86)Ding, L.; Chen, T. P.; Liu, Y.; Ng, C. Y.; Fung, S. Optical properties of silicon nanocrystals embedded in a SiO<sub>2</sub> matrix. *Phys Rev B* **2005**, *72*.

(87)Erogbogbo, F.; Yong, K. T.; Roy, I.; Xu, G.; Prasad, P. N.; Swihart, M. T. Biocompatible luminescent silicon quantum dots for imaging of cancer cells. *ACS Nano* **2008**, *2*, 873-878.

(88)Kelly, J. A.; Veinot, J. G. C. An Investigation into Near-UV Hydrosilylation of Freestanding Silicon Nanocrystals. *ACS Nano* **2010**, *4*, 4645-4656.

(89)Bruhn, B.; Valenta, J.; Sanghaleh, F.; Linnros, J. Blinking Statistics of Silicon Quantum Dots. *Nano Letters* **2011**, *11*, 5574-5580.

(90)Galland, C.; Ghosh, Y.; Steinbruck, A.; Sykora, M.; Hollingsworth, J. A.; Klimov, V. I.; Htoon, H. Two types of luminescence blinking revealed by spectroelectrochemistry of single quantum dots. *Nature* **2011**, *479*, 203-U275.

(91)HEINRICH, J. L.; CURTIS, C. L.; CREDO, G. M.; SAILOR, M. J.; KAVANAGH, K. L. Luminescent Colloidal Silicon Suspensions from Porous Silicon. *Science* **1992**, *255*, 66-68.

(92)Kang, Z.; Tsang, C. H.; Zhang, Z.; Zhang, M.; Wong, N. B.; Zapien, J. A.;

Shan, Y.; Lee, S. T. A polyoxometalate-assisted electrochemical method for silicon nanostructures preparation: from quantum dots to nanowires. *J Am Chem Soc* **2007**, *129*, 5326-5327.

(93) Kang, Z.; Liu, Y.; Tsang, C. H. A.; Ma, D. D. D.; Fan, X.; Wong, N.-B.; Lee, S.-T. Water-Soluble Silicon Quantum Dots with Wavelength-Tunable Photoluminescence. *Advanced Materials* **2009**, *21*, 661-664.

(94) Kang, Z. H.; Tsang, C. H. A.; Wong, N. B.; Zhang, Z. D.; Lee, S. T. Silicon quantum dots: A general photocatalyst for reduction, decomposition, and selective oxidation reactions. *Journal of the American Chemical Society* **2007**, *129*, 12090-+.

(95) Henderson, E. J.; Veinot, J. G. C. Synthesis of Oxide Encapsulated and Freestanding Hydride Surface Terminated Si<sub>1-x</sub>Ge<sub>x</sub> Nanocrystals. *Chem Mater* **2007**, *19*, 1886-1888.

(96) Hessel, C. M.; Henderson, E. J.; Veinot, J. G. C. Hydrogen silsesquioxane: A molecular precursor for nanocrystalline Si-SiO<sub>2</sub> composites and freestanding hydride-surface-terminated silicon nanoparticles. *Chem Mater* **2006**, *18*, 6139-6146.

(97) Hessel, C. M.; Henderson, E. J.; Veinot, J. G. C. An investigation of the formation and growth of oxide-embedded silicon nanocrystals in hydrogen silsesquioxane-derived nanocomposites. *J Phys Chem C* **2007**, *111*, 6956-6961.

(98) Kelly, J. A.; Henderson, E. J.; Veinot, J. G. Sol-gel precursors for group 14 nanocrystals. *Chem Commun (Camb)* **2010**, *46*, 8704-8718.

(99) Tilley, R. D.; Yamamoto, K. The microemulsion synthesis of hydrophobic and hydrophilic silicon nanocrystals. *Advanced Materials* **2006**, *18*, 2053-2056.

(100) Shiohara, A.; Hanada, S.; Prabakar, S.; Fujioka, K.; Lim, T. H.; Yamamoto, K.; Northcote, P. T.; Tilley, R. D. Chemical Reactions on Surface Molecules Attached to Silicon Quantum Dots. *Journal of the American Chemical Society* **2010**, *132*, 248-253.

(101) Heath, J. R. A LIQUID-SOLUTION-PHASE SYNTHESIS OF CRYSTALLINE SILICON. *Science* **1992**, *258*, 1131-1133.

(102) Baldwin, R. K.; Pettigrew, K. A.; Ratai, E.; Augustine, M. P.; Kauzlarich, S. M. Solution reduction synthesis of surface stabilized silicon nanoparticles. *Chem Commun* **2002**, 1822-1823.

(103) Arul Dhas, N.; Raj, C. P.; Gedanken, A. Preparation of Luminescent Silicon Nanoparticles: A Novel Sonochemical Approach. *Chem Mater* **1998**, *10*, 3278-3281.

(104) Prabakar, S.; Shiohara, A.; Hanada, S.; Fujioka, K.; Yamamoto, K.; Tilley, R. D. Size Controlled Synthesis of Germanium Nanocrystals by Hydride Reducing Agents and Their Biological Applications. *Chem Mater* **2010**, *22*, 482-486.

(105) Shiohara, A.; Prabakar, S.; Faramus, A.; Hsu, C. Y.; Lai, P. S.; Northcote, P. T.; Tilley, R. D. Sized controlled synthesis, purification, and cell studies with silicon quantum dots. *Nanoscale* **2011**, *3*, 3364-3370.

(106) Wang, J.; Sun, S.; Peng, F.; Cao, L.; Sun, L. Efficient one-pot synthesis of highly photoluminescent alkyl-functionalised silicon nanocrystals. *Chem Commun (Camb)* **2011**, *47*, 4941-4943.

- (107) Cheng, X. Y.; Gondosiswanto, R.; Ciampi, S.; Reece, P. J.; Gooding, J. J. One-pot synthesis of colloidal silicon quantum dots and surface functionalization via thiol-ene click chemistry. *Chem Commun* **2012**, *48*, 11874-11876.
- (108) Yang, C. S.; Bley, R. A.; Kauzlarich, S. M.; Lee, H. W. H.; Delgado, G. R. Synthesis of alkyl-terminated silicon nanoclusters by a solution route. *Journal of the American Chemical Society* **1999**, *121*, 5191-5195.
- (109) Hua, F.; Swihart, M. T.; Ruckenstein, E. Efficient surface grafting of luminescent silicon quantum dots by photoinitiated hydrosilylation. *Langmuir* **2005**, *21*, 6054-6062.
- (110) Kortshagen, U. Nonthermal plasma synthesis of semiconductor nanocrystals. *J Phys D Appl Phys* **2009**, *42*.
- (111) Kortshagen, U.; Mangolini, L.; Bapat, A. Plasma synthesis of semiconductor nanocrystals for nanoelectronics and luminescence applications. *J Nanopart Res* **2007**, *9*, 39-52.
- (112) Bapat, A.; Gatti, M.; Ding, Y.-P.; Campbell, S. A.; Kortshagen, U. A plasma process for the synthesis of cubic-shaped silicon nanocrystals for nanoelectronic devices. *J Phys D Appl Phys* **2007**, *40*, 2247-2257.
- (113) Cheng, X.; Lowe, S. B.; Reece, P. J.; Gooding, J. J. Colloidal silicon quantum dots: from preparation to the modification of self-assembled monolayers (SAMs) for bio-applications. *Chem. Soc. Rev.* **2014**, *43*, 2680-2700.
- (114) Medintz, I. L.; Uyeda, H. T.; Goldman, E. R.; Mattoussi, H. Quantum dot bioconjugates for imaging, labelling and sensing. *Nat Mater* **2005**, *4*, 435-446.
- (115) Gerion, D.; Pinaud, F.; Williams, S. C.; Parak, W. J.; Zanchet, D.; Weiss, S.; Alivisatos, A. P. Synthesis and properties of biocompatible water-soluble silica-coated CdSe/ZnS semiconductor quantum dots. *J. Phys. Chem. B* **2001**, *105*, 8861-8871.
- (116) Burns, A.; Ow, H.; Wiesner, U. Fluorescent core-shell silica nanoparticles: towards "Lab on a Particle" architectures for nanobiotechnology. *Chem. Soc. Rev.* **2006**, *35*, 1028-1042.
- (117) Mulvaney, P.; Liz-Marzan, L. M.; Giersig, M.; Ung, T. Silica encapsulation of quantum dots and metal clusters. *J Mater Chem* **2000**, *10*, 1259-1270.
- (118) Dubois, F.; Mahler, B.; Dubertret, B.; Doris, E.; Mioskowski, C. A versatile strategy for quantum dot ligand exchange. *Journal of the American Chemical Society* **2007**, *129*, 482-483.
- (119) Wuister, S. F.; Donega, C. D.; Meijerink, A. Influence of thiol capping on the exciton luminescence and decay kinetics of CdTe and CdSe quantum. *J. Phys. Chem. B* **2004**, *108*, 17393-17397.
- (120) Gaponik, N.; Talapin, D. V.; Rogach, A. L.; Hoppe, K.; Shevchenko, E. V.; Kornowski, A.; Eychmuller, A.; Weller, H. Thiol-capping of CdTe nanocrystals: An alternative to organometallic synthetic routes. *J. Phys. Chem. B* **2002**, *106*, 7177-7185.
- (121) Shavel, A.; Gaponik, N.; Eychmuller, A. Factors governing the quality of aqueous CdTe nanocrystals: Calculations and experiment. *J. Phys. Chem. B* **2006**,

110, 19280-19284.

(122) Eychmuller, A.; Rogach, A. L. Chemistry and photophysics of thiol-stabilized II-VI semiconductor nanocrystals. *Pure Appl Chem* **2000**, *72*, 179-188.

(123) Lin, C.-A. J.; Sperling, R. A.; Li, J. K.; Yang, T.-Y.; Li, P.-Y.; Zanella, M.; Chang, W. H.; Parak, W. J. Design of an Amphiphilic Polymer for Nanoparticle Coating and Functionalization. *Small* **2008**, *4*, 334-341.

(124) Tomczak, N.; Janczewski, D.; Han, M. Y.; Vancso, G. J. Designer polymer-quantum dot architectures. *Prog. Polym. Sci.* **2009**, *34*, 393-430.

(125) Yu, W. W.; Chang, E.; Falkner, J. C.; Zhang, J. Y.; Al-Somali, A. M.; Sayes, C. M.; Johns, J.; Drezek, R.; Colvin, V. L. Forming biocompatible and nonaggregated nanocrystals in water using amphiphilic polymers. *Journal of the American Chemical Society* **2007**, *129*, 2871-2879.

(126) Tang, J.; Kemp, K. W.; Hoogland, S.; Jeong, K. S.; Liu, H.; Levina, L.; Furukawa, M.; Wang, X. H.; Debnath, R.; Cha, D. K.; Chou, K. W.; Fischer, A.; Amassian, A.; Asbury, J. B.; Sargent, E. H. Colloidal-quantum-dot photovoltaics using atomic-ligand passivation. *Nat. Mater.* **2011**, *10*, 765-771.

(127) Ciampi, S.; Harper, J. B.; Gooding, J. J. Wet chemical routes to the assembly of organic monolayers on silicon surfaces via the formation of Si-C bonds: surface preparation, passivation and functionalization. *Chem Soc Rev* **2010**, *39*, 2158-2183.

(128) Bhairamadgi, N. S.; Gangarapu, S.; Campos, M. A. C.; Paulusse, J. M. J.; van Rijn, C. J. M.; Zuilhof, H. Efficient Functionalization of Oxide-Free Silicon(111) Surfaces: Thiol-yne versus Thiol-ene Click Chemistry. *Langmuir* **2013**, *29*, 4535-4542.

(129) Ciampi, S.; Bocking, T.; Kilian, K. A.; James, M.; Harper, J. B.; Gooding, J. J. Functionalization of acetylene-terminated monolayers on Si(100) surfaces: A click chemistry approach. *Langmuir* **2007**, *23*, 9320-9329.

(130) Bocking, T.; Kilian, K. A.; Gaus, K.; Gooding, J. J. Modifying Porous Silicon with Self-Assembled Monolayers for Biomedical Applications: The Influence of Surface Coverage on Stability and Biomolecule Coupling. *Adv Funct Mater* **2008**, *18*, 3827-3833.

(131) Anglin, E. J.; Cheng, L. Y.; Freeman, W. R.; Sailor, M. J. Porous silicon in drug delivery devices and materials. *Adv Drug Deliver Rev* **2008**, *60*, 1266-1277.

(132) Kilian, K. A.; Bocking, T.; Gaus, K.; Gal, M.; Gooding, J. J. Si-C linked oligo(ethylene glycol) layers in silicon-based photonic crystals: Optimization for implantable optical materials. *Biomaterials* **2007**, *28*, 3055-3062.

(133) Linford, M. R.; Chidsey, C. E. D. ALKYL MONOLAYERS COVALENTLY BONDED TO SILICON SURFACES. *Journal of the American Chemical Society* **1993**, *115*, 12631-12632.

(134) Linford, M. R.; Fenter, P.; Eisenberger, P. M.; Chidsey, C. E. D. Alkyl monolayers on silicon prepared from 1-alkenes and hydrogen-terminated silicon. *Journal of the American Chemical Society* **1995**, *117*, 3145-3155.

(135) Mayeri, D.; Phillips, B. L.; Augustine, M. P.; Kauzlarich, S. M. NMR Study of the Synthesis of Alkyl-Terminated Silicon Nanoparticles from the

Reaction of SiCl<sub>4</sub> with the Zintl Salt, NaSi. *Chem Mater* **2001**, *13*, 765-770.

(136) Baldwin, R. K.; Pettigrew, K. A.; Garno, J. C.; Power, P. P.; Liu, G. Y.; Kauzlarich, S. M. Room temperature solution synthesis of alkyl-capped tetrahedral shaped silicon nanocrystals. *Journal of the American Chemical Society* **2002**, *124*, 1150-1151.

(137) Bley, R. A.; Kauzlarich, S. M. A low-temperature solution phase route for the synthesis of silicon nanoclusters. *Journal of the American Chemical Society* **1996**, *118*, 12461-12462.

(138) Zou, J.; Baldwin, R. K.; Pettigrew, K. A.; Kauzlarich, S. M. Solution synthesis of ultrastable luminescent siloxane-coated silicon nanoparticles. *Nano Letters* **2004**, *4*, 1181-1186.

(139) Rodríguez Núñez, J. R.; Kelly, J. A.; Henderson, E. J.; Veinot, J. G. C. Wavelength-Controlled Etching of Silicon Nanocrystals. *Chem Mater* **2011**, *24*, 346-352.

(140) Mangolini, L.; Kortshagen, U. Plasma-assisted synthesis of silicon nanocrystal inks. *Advanced Materials* **2007**, *19*, 2513-+.

(141) Mangolini, L.; Thimsen, E.; Kortshagen, U.: High-yield synthesis of luminescent silicon quantum dots in a continuous flow non-thermal plasma reactor. In *Amorphous and Nanocrystalline Silicon Science and Technology-2005*; Collins, R. W., Taylor, P. C., Kondo, M., Carius, R., Biswas, R., Eds.; Materials Research Society Symposium Proceedings, 2005; Vol. 862; pp 307-312.

(142) Mangolini, L.; Thimsen, E.; Kortshagen, U. High-yield synthesis of luminescent silicon quantum dots in a continuous flow non-thermal plasma reactor. *Amorphous and Nanocrystalline Silicon Science and Technology-2005* **2005**, *862*, 307-312.

(143) Tilley, R. D.; Warner, J. H.; Yamamoto, K.; Matsui, I.; Fujimori, H. Micro-emulsion synthesis of monodisperse surface stabilized silicon nanocrystals. *Chem Commun* **2005**, *0*, 1833-1835.

(144) Li, X.; Bohn, P. W. Metal-assisted chemical etching in HF/H<sub>2</sub>O(2) produces porous silicon. *Appl Phys Lett* **2000**, *77*, 2572-2574.

(145) Hessel, C. M.; Henderson, E. J.; Kelly, J. A.; Cavell, R. G.; Sham, T.-K.; Veinot, J. G. C. Origin of luminescence from silicon nanocrystals: a near edge X-ray absorption fine structure (NEXAFS) and X-ray excited optical luminescence (XEOL) study of oxide-embedded and free-standing systems. *J Phys Chem C* **2008**, *112*, 14247-14254.

(146) Kelly, J. A.; Shukaliak, A. M.; Fleischauer, M. D.; Veinot, J. G. C. Size-Dependent Reactivity in Hydrosilylation of Silicon Nanocrystals. *Journal of the American Chemical Society* **2011**, *133*, 9564-9571.

(147) Hua, F. J.; Swihart, M. T.; Ruckenstein, E. Efficient surface grafting of luminescent silicon quantum dots by photoinitiated hydrosilylation. *Langmuir* **2005**, *21*, 6054-6062.

(148) Yu, Y.; Hessel, C. M.; Bogart, T. D.; Panthani, M. G.; Rasch, M. R.; Korgel, B. A. Room Temperature Hydrosilylation of Silicon Nanocrystals with Bifunctional Terminal Alkenes. *Langmuir* **2013**, *29*, 1533-1540.

(149) Rosso-Vasic, M.; Spruijt, E.; Popovic, Z.; Overgaag, K.; van Lagen,

B.; Grandidier, B.; Vanmaekelbergh, D.; Dominguez-Gutierrez, D.; De Cola, L.; Zuilhof, H. Amine-terminated silicon nanoparticles: synthesis, optical properties and their use in bioimaging. *J Mater Chem* **2009**, *19*, 5926-5933.

(150) Siekierzycka, J. R.; Rosso-Vasic, M.; Zuilhof, H.; Brouwer, A. M. Photophysics of n-Butyl-Capped Silicon Nanoparticles. *J Phys Chem C* **2011**, *115*, 20888-20895.

(151) Ruizendaal, L.; Pujari, S. P.; Gevaerts, V.; Paulusse, J. M.; Zuilhof, H. Biofunctional silicon nanoparticles by means of thiol-ene click chemistry. *Chem Asian J* **2011**, *6*, 2776-2786.

(152) Rogozhina, E.; Belomoin, G.; Smith, A.; Abuhassan, L.; Barry, N.; Akcakir, O.; Braun, P. V.; Nayfeh, M. H. Si-N linkage in ultrabright, ultrasmall Si nanoparticles. *Appl Phys Lett* **2001**, *78*, 3711-3713.

(153) Liao, Y.-C.; Roberts, J. T. Self-assembly of organic monolayers on aerosolized silicon nanoparticles. *Journal of the American Chemical Society* **2006**, *128*, 9061-9065.

(154) Svrcek, V.; Mariotti, D.; Kondo, M. Microplasma-induced surface engineering of silicon nanocrystals in colloidal dispersion. *Appl Phys Lett* **2010**, *97*.

(155) Svrcek, V.; Yamanari, T.; Mariotti, D.; Matsubara, K.; Kondo, M. Enhancement of hybrid solar cell performance by polythieno 3,4-b thiophenebenzodithiophene and microplasma-induced surface engineering of silicon nanocrystals. *Appl Phys Lett* **2012**, *100*.

(156) McKenna, J.; Patel, J.; Mitra, S.; Soin, N.; Svrcek, V.; Maguire, P.; Mariotti, D. Synthesis and surface engineering of nanomaterials by atmospheric-pressure microplasmas. *Eur Phys J-Appl Phys* **2011**, *56*.

(157) Mariotti, D.; Sankaran, R. M. Microplasmas for nanomaterials synthesis. *J Phys D Appl Phys* **2010**, *43*.

(158) Mariotti, D.; Sankaran, R. M. Perspectives on atmospheric-pressure plasmas for nanofabrication. *J Phys D Appl Phys* **2011**, *44*.

(159) Mariotti, D.; Patel, J.; Svrcek, V.; Maguire, P. Plasma-Liquid Interactions at Atmospheric Pressure for Nanomaterials Synthesis and Surface Engineering. *Plasma Process Polym* **2012**, *9*, 1074-1085.

(160) Svrcek, V.; Mariotti, D.; Shibata, Y.; Kondo, M. A hybrid heterojunction based on fullerenes and surfactant-free, self-assembled, closely packed silicon nanocrystals. *J Phys D Appl Phys* **2010**, *43*.

(161) Mariotti, D.; Svrcek, V.; Hamilton, J. W. J.; Schmidt, M.; Kondo, M. Silicon Nanocrystals in Liquid Media: Optical Properties and Surface Stabilization by Microplasma-Induced Non-Equilibrium Liquid Chemistry. *Adv Funct Mater* **2012**, *22*, 954-964.

(162) Mariotti, D.; Mitra, S.; Svrcek, V. Surface-engineered silicon nanocrystals. *Nanoscale* **2013**, *5*, 1385-1398.

(163) Li, Z. F.; Ruckenstein, E. Water-Soluble Poly(acrylic acid) Grafted Luminescent Silicon Nanoparticles and Their Use as Fluorescent Biological Staining Labels. *Nano Letters* **2004**, *4*, 1463-1467.

(164) Henderson, E. J.; Shuhendler, A. J.; Prasad, P.; Baumann, V.; Maier-Flaig, F.; Faulkner, D. O.; Lemmer, U.; Wu, X. Y.; Ozin, G. A. Colloidally Stable

Silicon Nanocrystals with Near-Infrared Photoluminescence for Biological Fluorescence Imaging. *Small* **2011**, *7*, 2507-2516.

(165) Manhat, B. A.; Brown, A. L.; Black, L. A.; Ross, J. B. A.; Fichter, K.; Vu, T.; Richman, E.; Goforth, A. M. One-Step Melt Synthesis of Water-Soluble, Photoluminescent, Surface-Oxidized Silicon Nanoparticles for Cellular Imaging Applications. *Chem Mater* **2011**, *23*, 2407-2418.

(166) He, Y.; Su, Y.; Yang, X.; Kang, Z.; Xu, T.; Zhang, R.; Fan, C.; Lee, S.-T. Photo and pH Stable, Highly-Luminescent Silicon Nanospheres and Their Bioconjugates for Immunofluorescent Cell Imaging. *Journal of the American Chemical Society* **2009**, *131*, 4434-4438.

(167) McVey, B. F. P.; Tilley, R. D. Solution Synthesis, Optical Properties, and Bioimaging Applications of Silicon Nanocrystals. *Accounts Chem Res* **2014**, *47*, 3045-3051.

(168) Alsharif, N. H.; Berger, C. E. M.; Varanasi, S. S.; Chao, Y.; Horrocks, B. R.; Datta, H. K. Alkyl-Capped Silicon Nanocrystals Lack Cytotoxicity and have Enhanced Intracellular Accumulation in Malignant Cells via Cholesterol-Dependent Endocytosis. *Small* **2009**, *5*, 221-228.

(169) Erogbogbo, F.; Chang, C. W.; May, J. L.; Liu, L.; Kumar, R.; Law, W. C.; Ding, H.; Yong, K. T.; Roy, I.; Sheshadri, M.; Swihart, M. T.; Prasad, P. N. Bioconjugation of luminescent silicon quantum dots to gadolinium ions for bioimaging applications. *Nanoscale* **2012**, *4*, 5483-5489.

(170) Erogbogbo, F.; Chang, C. W.; May, J.; Prasad, P. N.; Swihart, M. T. Energy transfer from a dye donor to enhance the luminescence of silicon quantum dots. *Nanoscale* **2012**, *4*, 5163-5168.

(171) Zhong, Y.; Peng, F.; Bao, F.; Wang, S.; Ji, X.; Yang, L.; Su, Y.; Lee, S.-T.; He, Y. Large-Scale Aqueous Synthesis of Fluorescent and Biocompatible Silicon Nanoparticles and Their Use as Highly Photostable Biological Probes. *Journal of the American Chemical Society* **2013**.

(172) Tu, C. Q.; Ma, X. C.; Pantazis, P.; Kauzlarich, S. M.; Louie, A. Y. Paramagnetic, Silicon Quantum Dots for Magnetic Resonance and Two-Photon Imaging of Macrophages. *Journal of the American Chemical Society* **2010**, *132*, 2016-2023.

(173) Liu, J.; Erogbogbo, F.; Yong, K.-T.; Ye, L.; Liu, J.; Hu, R.; Chen, H.; Hu, Y.; Yang, Y.; Yang, J.; Roy, I.; Karker, N. A.; Swihart, M. T.; Prasad, P. N. Assessing Clinical Prospects of Silicon Quantum Dots: Studies in Mice and Monkeys. *ACS Nano* **2013**, *7*, 7303-7310.

(174) Erogbogbo, F.; Yong, K. T.; Roy, I.; Hu, R.; Law, W. C.; Zhao, W.; Ding, H.; Wu, F.; Kumar, R.; Swihart, M. T.; Prasad, P. N. In vivo targeted cancer imaging, sentinel lymph node mapping and multi-channel imaging with biocompatible silicon nanocrystals. *ACS Nano* **2011**, *5*, 413-423.

(175) Erogbogbo, F.; Tien, C. A.; Chang, C. W.; Yong, K. T.; Law, W. C.; Ding, H.; Roy, I.; Swihart, M. T.; Prasad, P. N. Bioconjugation of luminescent silicon quantum dots for selective uptake by cancer cells. *Bioconjug Chem* **2011**, *22*, 1081-1088.

(176) Kilian, K. A.; Bocking, T.; Gooding, J. J. The importance of surface

chemistry in mesoporous materials: lessons from porous silicon biosensors. *Chem Commun* **2009**, 630-640.

(177) Smith, A. M.; Duan, H.; Mohs, A. M.; Nie, S. Bioconjugated quantum dots for in vivo molecular and cellular imaging. *Adv Drug Deliver Rev* **2008**, *60*, 1226-1240.

(178) Hardman, R. A toxicologic review of quantum dots: toxicity depends on physicochemical and environmental factors. *Environ Health Perspect* **2006**, *114*, 165-172.

(179) Hauck, T. S.; Anderson, R. E.; Fischer, H. C.; Newbigging, S.; Chan, W. C. In vivo quantum-dot toxicity assessment. *Small* **2010**, *6*, 138-144.

(180) Bottrill, M.; Green, M. Some aspects of quantum dot toxicity. *Chem Commun (Camb)* **2011**.

(181) Green, M.; Howman, E. Semiconductor quantum dots and free radical induced DNA nicking. *Chem Commun (Camb)* **2005**, 121-123.

(182) Ipe, B. I.; Lehnig, M.; Niemeyer, C. M. On the generation of free radical species from quantum dots. *Small* **2005**, *1*, 706-709.

(183) Bharali, D. J.; Lucey, D. W.; Jayakumar, H.; Pudavar, H. E.; Prasad, P. N. Folate-Receptor-Mediated Delivery of InP Quantum Dots for Bioimaging Using Confocal and Two-Photon Microscopy. *Journal of the American Chemical Society* **2005**, *127*, 11364-11371.

(184) Yong, K.-T.; Ding, H.; Roy, I.; Law, W.-C.; Bergey, E. J.; Maitra, A.; Prasad, P. N. Imaging Pancreatic Cancer Using Bioconjugated InP Quantum Dots. *ACS Nano* **2009**, *3*, 502-510.

(185) Li, L.; Daou, T. J.; Texier, I.; Kim Chi, T. T.; Liem, N. Q.; Reiss, P. Highly Luminescent CuInS<sub>2</sub>/ZnS Core/Shell Nanocrystals: Cadmium-Free Quantum Dots for In Vivo Imaging. *Chem Mater* **2009**, *21*, 2422-2429.

(186) Pons, T.; Pic, E.; Lequeux, N.; Cassette, E.; Bezdetnaya, L.; Guillemin, F.; Marchal, F.; Dubertret, B. Cadmium-free CuInS<sub>2</sub>/ZnS quantum dots for sentinel lymph node imaging with reduced toxicity. *ACS Nano* **2010**, *4*, 2531-2538.

(187) Helle, M.; Cassette, E.; Bezdetnaya, L.; Pons, T.; Leroux, A.; Pléat, F.; Guillemin, F.; Dubertret, B.; Marchal, F. Visualisation of Sentinel Lymph Node with Indium-Based near Infrared Emitting Quantum Dots in a Murine Metastatic Breast Cancer Model. *PLoS ONE* **2012**, *7*, e44433.

(188) Pradhan, N.; Goorskey, D.; Thessing, J.; Peng, X. G. An alternative of CdSe nanocrystal emitters: Pure and tunable impurity emissions in ZnSe nanocrystals. *Journal of the American Chemical Society* **2005**, *127*, 17586-17587.

(189) Yu, Z.; Ma, X.; Yu, B.; Pan, Y.; Liu, Z. Synthesis and characterization of ZnS:Mn/ZnS core/shell nanoparticles for tumor targeting and imaging in vivo. *Journal of Biomaterials Applications* **2013**, *28*, 232-240.

(190) Maity, A. R.; Palmal, S.; Basiruddin, S. K.; Karan, N. S.; Sarkar, S.; Pradhan, N.; Jana, N. R. Doped semiconductor nanocrystal based fluorescent cellular imaging probes. *Nanoscale* **2013**, *5*, 5506-5513.

(191) Liu, J.; Erogbogbo, F.; Yong, K.-T.; Ye, L.; Liu, J.; Hu, R.; Chen, H.; Hu, Y.; Yang, Y.; Yang, J.; Roy, I.; Karker, N. A.; Swihart, M. T.; Prasad, P. N. Assessing Clinical Prospects of Silicon Quantum Dots: Studies in Mice and

Monkeys. *ACS Nano* **2013**.

(192) Fujioka, K.; Hiruoka, M.; Sato, K.; Manabe, N.; Miyasaka, R.; Hanada, S.; Hoshino, A.; Tilley, R. D.; Manome, Y.; Hirakuri, K.; Yamamoto, K. Luminescent passive-oxidized silicon quantum dots as biological staining labels and their cytotoxicity effects at high concentration. *Nanotechnology* **2008**, *19*.

(193) Sripanyakorn, S.; Jugdaohsingh, R.; Thompson, R. P. H.; Powell, J. J. Dietary silicon and bone health. *Nutrition Bulletin* **2005**, *30*, 222-230.

(194) Canham, L. T. Nanoscale semiconducting silicon as a nutritional food additive. *Nanotechnology* **2007**, *18*.

(195) Choi, J.; Zhang, Q.; Reipa, V.; Wang, N. S.; Stratmeyer, M. E.; Hitchins, V. M.; Goering, P. L. Comparison of cytotoxic and inflammatory responses of photoluminescent silicon nanoparticles with silicon micron-sized particles in RAW 264.7 macrophages. *J Appl Toxicol* **2009**, *29*, 52-60.

(196) Wang, Q.; Bao, Y.; Zhang, X.; Coxon, P. R.; Jayasooriya, U. A.; Chao, Y. Uptake and Toxicity Studies of Poly-Acrylic Acid Functionalized Silicon Nanoparticles in Cultured Mammalian Cells. *Advanced healthcare materials* **2012**, *1*, 189-198.

(197) Gao, X.; Cui, Y.; Levenson, R. M.; Chung, L. W. K.; Nie, S. In vivo cancer targeting and imaging with semiconductor quantum dots. *Nat Biotech* **2004**, *22*, 969-976.

(198) Tu, C.; Ma, X.; House, A.; Kauzlarich, S. M.; Louie, A. Y. PET Imaging and Biodistribution of Silicon Quantum Dots in Mice. *ACS Medicinal Chemistry Letters* **2011**, *2*, 285-288.

(199) Nel, A.; Xia, T.; Moller, L.; Li, N. Toxic Potential of Materials at the Nanolevel. *Science* **2006**, *311*, 622-627.

(200) Fischer, H. C.; Liu, L. C.; Pang, K. S.; Chan, W. C. W. Pharmacokinetics of nanoscale quantum dots: In vivo distribution, sequestration, and clearance in the rat. *Adv Funct Mater* **2006**, *16*, 1299-1305.

## **Chapter 2 Methods and Materials**

## 2.1 Chemicals and Materials

All chemicals and materials used in this thesis are listed in Table 2.1

Table 2.1 Chemicals and materials used in this thesis

<b>Name</b>	<b>Purity/Specification</b>	<b>Supplier</b>
Acetone	H <sub>2</sub> O < 10 ppm	Innovative Technology
Allylamine	99%	Sigma Aldrich
Allyltrichlorosilane	95%	Sigma Aldrich
Arg-Gly-Asp-Cys	95%	Genscript
11-Azido-3,6,9-trioxaundecan-1-amine	90%	Sigma Aldrich
Bio-Beads S-X Media	99%	Bio-Rad
Butanethiol	99%	Sigma Aldrich
3-Bromopropionic acid	97%	Sigma Aldrich
3-Bromopropylamine hydrobromide	98%	Sigma Aldrich
Copper(II) sulfate hexahydrate	98%	Sigma Aldrich
Cysteamine hydrochloride	97%	Sigma Aldrich
Dichloromethane	Distilled/stored in molecular sieves	Ajax Finechem
Dimethylformamide	Distilled/stored in molecular sieves	Ajax Finechem
Dimethyl sulfoxide	Distilled/stored in molecular sieves	Ajax Finechem
Dulbecco's modified eagle medium (DMEM)	[+] 4.5g/L D-glucose [+] L-glutamine [-] Sodium pyruvate	Life Technologies
Dulbecco's phosphate buffer saline (PBS)	No Ca, No Mg	Life Technologies
DY485-NHS	90%	Dyomics GmbH
Ethanol	Distilled/stored in molecular sieves	Ajax Finechem
Ethyl acetate	Distilled/stored in molecular sieves	Ajax Finechem
Fetal bovine serum	Sterile-filtered, suitable for cell culture	Sigma Aldrich
1,5-Hexadiene	≥ 97%	Sigma Aldrich
Hexane	Distilled/stored in molecular sieves	Ajax Finechem
Hexyltrichlorosilane	97%	Sigma Aldrich
Hydrochloric acid	32%	Ajax Finechem

Lithium Aluminum Hydride	1M solution in THF	Sigma Aldrich
Milli-Q™ water	>18Ω	Millipore Corp.
Molecular sieves	4 Å pore diameter 8-12 mesh beads	Sigma Aldrich
1,8-Nonadiyne	≥ 97%	Alfa Aesar
Octyltrichlorosilane	≥ 98%	Sigma Aldrich
Oxalyl chloride	99%	Sigma Aldrich
Potassium carbonate	99.99%	Sigma Aldrich
Polyvinylidene fluoride (PVDF) membrane	0.45 μm pore	Invitrogen
Sephadex® LH-20 Media	25-100 μm beads	Sigma Aldrich
Sodium azide	99%	Sigma Aldrich
Sodium L-ascorbate	≥ 98%	Sigma Aldrich
Sodium 2-mercaptoethanesulfonate	≥ 98%	Sigma Aldrich
Sodium sulfate	99%	Sigma Aldrich
Tetrahydrofuran	H <sub>2</sub> O < 10 ppm	Innovative Technology
Tetraoctylammonium bromide	98%	Sigma Aldrich
Thiazolyl Blue Tetrazolium Bromide	97.5%	Sigma Aldrich
Thioglycolic acid	98%	Sigma Aldrich
Toluene	H <sub>2</sub> O < 10 ppm	Innovative Technology
Trichloro(hexyl)silane	97%	Sigma Aldrich
Trypsin EDTA	10 times, 1 mM	Life Technologies
Silicon tetrabromide	99%	Sigma Aldrich
Silicon tetrachloride	99.998%	Sigma Aldrich
(+)-Sodium L-ascorbate	≥ 98%	Sigma Aldrich
N-Succinimidyl 4-(maleimidomethyl)cyclohexanecarboxylate	98%, powder	Sigma Aldrich

## 2.2 Preparation of hydrogen terminated silicon quantum dots

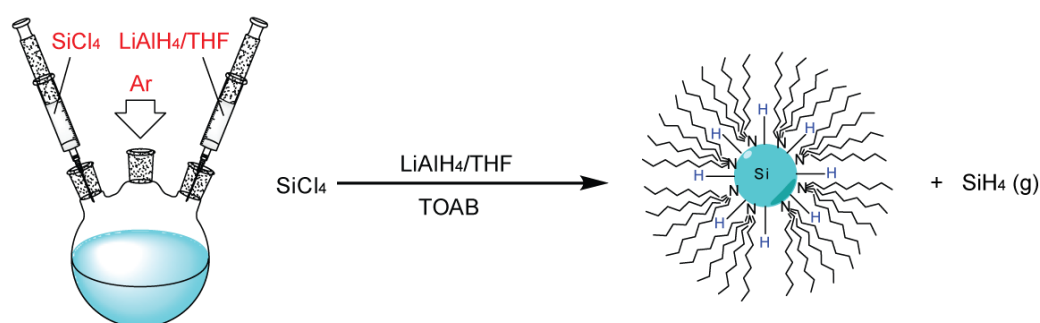


Figure 2.1 Schematics of solution synthesis of silicon quantum dots by reduction of silanes precursors. A strong reducing agent, LiAlH<sub>4</sub>, is used to reduce halogenated

silane precursors to produce hydrogen terminated SiQDs. **Caution: be aware that silane gas (SiH<sub>4</sub>) is highly flammable and the reaction should be performed in a fume hood with airflow rate above 80 fpm.**

Hydrogen-terminated SiQDs were prepared based on modifications of a published method (Figure 2.1).<sup>1-4</sup> All experiments were performed under Ar using a standard Schlenk line setup. In a typical experiment, 300  $\mu\text{L}$  of silicon tetrachloride (SiCl<sub>4</sub>,  $2.6 \times 10^{-3}$  mol) and 1.5 g tetraoctylammonium bromide (TOAB,  $2.7 \times 10^{-3}$  mol) were dissolved in 100 mL of dry toluene (obtained from PURE-SOLV solvent purification system without further treatment) in a 250 mL three-neck flask. The mixture was sonicated for 20 min. An excess amount of LiAlH<sub>4</sub> (200 mg,  $5.4 \times 10^{-3}$  mol) in 4 mL of dry THF was then added, and the mixture was further stirred and sonicated for 45 min. The reaction was then quenched with ~30 mL dry ethanol and kept under argon. The particles were further modified immediately after synthesis without weighing according to procedures described in 2.3.

### 2.3 Surface passivation of hydrogen terminated silicon quantum dots

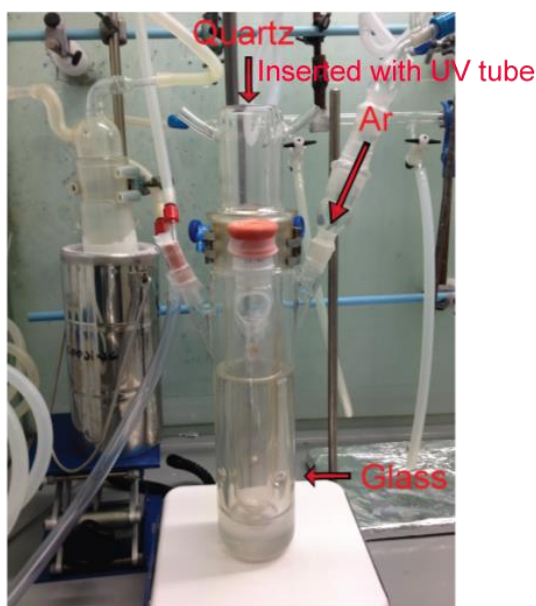


Figure 2.2 Photo for the set-up of surface modifications of hydrogen terminated SiQDs. The photochemical reactor was purchase from ACE Glass Inc. (Product Code 7861). The reactor assembly was composed of a quartz core and a glass shell. During the reaction, a UV lamp (8 W) was inserted at the centre to catalyse the hydrosilylation reaction that occurred between the core and within the shell.

Hydrogen terminated silicon quantum dots were passivated by hydrosilylation with alkenyl or alkynyl molecules<sup>2,4-6</sup> (Figure 2.2). After the initial preparation of hydrogen terminated silicon quantum dots, the hydrogen-terminated SiQDs were transferred to a quartz reaction vessel (250 mL) via cannula under Ar protection. For each hydrosilylation reaction, 4 - 8 mL of alkene or alkyne was added, using chemicals as received without further purifications, and the mixture was treated with ultraviolet (UV) (254 nm) for 15 h. After the reaction, all solvent and unreacted alkene or alkyne were evaporated under reduced pressure and elevated temperature, with the crude product obtained as yellow oil. To the mixture was then added water (3 × 20 mL) and hexane (10 mL). Depending on the surface group of SiQDs, the

desired solvent layer was obtained and then passed through a polyvinylidene difluoride (PVDF) membrane with a 0.45  $\mu\text{m}$  pore size. Approximately 10 – 20 mg of surface modified SiQDs were obtained per batch.

#### 2.4 Purification of surface passivated silicon quantum dots

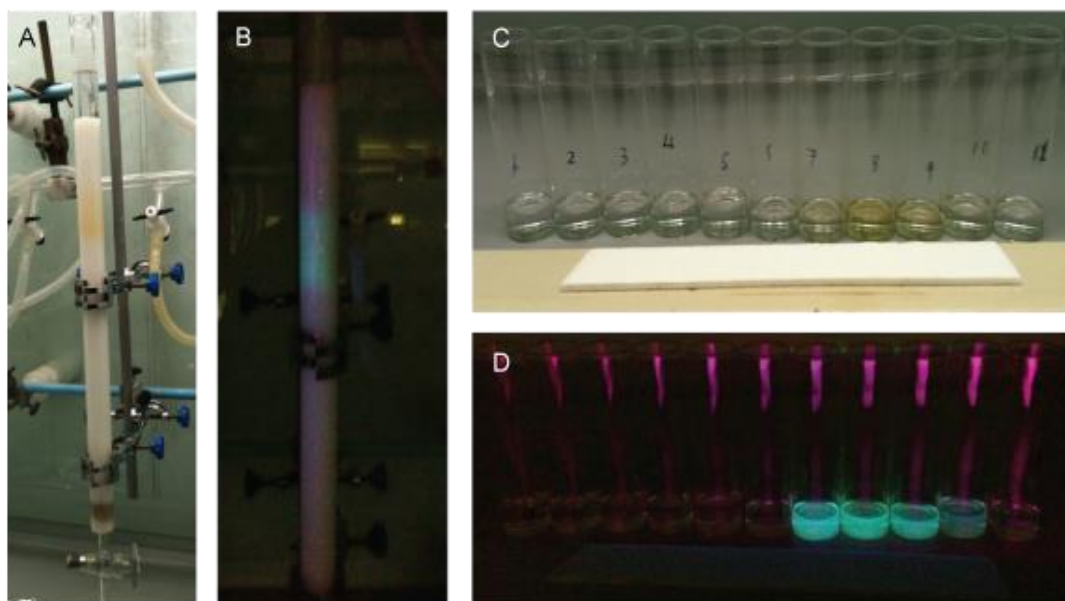


Figure 2.3 Illustration for the purification of surface modified SiQDs. After extraction and passing through the PVDF membrane, the crude SiQDs were purified by size exclusion chromatography (A-B). Sephadex-LH20 was used for SiQDs with hydrophilic surfaces and water was used as the eluent. Bio-beads S-X was used for SiQDs with hydrophobic surfaces and toluene was used as the eluent. Only the fluorescent portions containing the nanoparticles were collected (C-D).

To further purify surface passivated SiQDs, size-exclusion chromatography was used (Figure 2.3).<sup>7</sup> To do this, all hexane was evaporated, and particles were resuspended in 3 mL of toluene or water depending on the surface groups. Bio-Beads SX was used as the stationary phase for toluene dispersible SiQDs and toluene was used as the eluent. Sephadex-LH 20 was used as the stationary phase for water dispersible SiQDs and water was used as the eluent. After loading the

sample, SiQDs were allowed to enter the media slowly without any pressure applied. After all of the sample entered the media, extra solvent was added and a small amount of pressure could be applied for LH-20 column. Care was taken as the addition of solvent would not disturb the top part of the resin, in which case SiQDs already entered the resin could be lost during the process. Fractions that showed blue fluorescence under UV lamp were collected.

## **2.5 Further modification of surface passivated silicon quantum dots**

For one pot synthesis and further surface functionalization with thiol molecules, details of experiments were described in chapter 3. For functionalization with azide molecules *via* copper catalyzed azide-alkyne (CuAAC) ‘click’ chemistry, details of experiments were described in chapter 4. For further functionalization for the attachment of acceptor dye molecules for FLIM imaging or protease assay, details of experiments were described in chapter 5 and chapter 6.

## **2.6 Characterization of morphology**

Morphology of the prepared SiQDs was characterized by transmission electron microscopy (TEM) and dynamic light scattering (DLS) measurements. The SiQDs stock was prepared at a concentration of 10 mg/mL as a light yellow colloidal solution. For TEM sample preparation, a small amount (~5  $\mu$ L) of SiQDs sample was placed on a carbon coated copper grid that was fixed by self-closing tweezers, and dried under room temperature. TEM measurements were performed on a Philip CM 200 microscope operated at 200 kV. The start-up voltage used was tuned to

the maximum at 4.48 kV, and sample was loaded when the vacuum indicator (IPG) was below 27. Eucentric height was adjusted to make sure the position of the sample was optimal. Beam alignment was then performed so that the beam was circular in shape, with focus at the centre of the field. All TEM images were visualized without staining. Digital images were recorded with Digital Micrograph with Camera length of 420 mm and exposure time of 0.5 s. DLS measurements were performed on a Brookhaven 90 Plus Instrument. A background scan with the solvent only was performed prior to sample measurement, and each sample was measured three times to obtain an average reading of the particle size.

## **2.7 Characterization of surface properties**

### **2.7.1 Fourier transform infrared (FT-IR) spectroscopy**

FT-IR measurements were performed on an Avartar 320 FT-IR spectrometer. Measurements were performed by dropping 10  $\mu\text{L}$  of concentrated SiQDs dispersion in hexane or dry ethanol onto a pellet premade by grinding powder of KBr. The pellet was dried completely to ensure no solvent peak was observed. All FT-IR results were analysed with Omnic<sup>TM</sup>.

### **2.7.2 Nuclear magnetic resonance (NMR) spectroscopy**

<sup>1</sup>H-NMR experiments were run on a Bruker DPX 300MHz spectrometer equipped with an auto-sampler. NMR spectra of organic molecules were using ~ 5 mg compounds in CDCl<sub>3</sub> with 32 scans. NMR spectra of silicon quantum dots were prepared by adding ~ 5 mg silicon quantum dots to deuterated solvents (i.e. CDCl<sub>3</sub>

or D<sub>2</sub>O depending on surface group and solvent dispersity). All spectral results were analysed with TopSpin™ or SpinWorks.

### **2.7.3 X-ray photoelectron spectroscopy (XPS) spectroscopy**

XPS measurements were performed by dropping SiQDs dispersion on indium tin oxide (ITO) surfaces and all solvent were dried before measurements. Measurements were performed in a similar manner to measuring flat or porous surfaces.<sup>8-11</sup> Specifically, an ESCALAB 200iXL spectrometer equipped with a monochromatic Al K $\alpha$  source (1486.6 eV) hemispherical analyser and six multichannel detectors was used. During acquisition of the XPS spectra, background pressure in the analysis chamber was maintained below the 10<sup>-10</sup> range. The X-ray incidence angle was set to 58 ° relative to the analyser lens and the beam size on the sample was approximately 100  $\mu$ m in diameter. The resolution of the XPS spectrometer was about 0.6 eV measured from the Ag 3d<sub>5/2</sub> signal using full width at half maximum (FWHM) with a 20 eV pass energy. Survey scans were carried out over 1100 – 0 eV range with a 1.0 eV step size, a 10 ms dwell time and analyser pass energy of 100 eV. High-resolution scans were run with 0.1 eV step size, dwell time of 100 ms and the analyser pass energy set to 20 eV. Spectra were fitted with a convolution of Lorentzian and Gaussian profiles. All energies are reported as binding energies in eV and referenced to the C1s signal corrected to 285 eV.

## **2.8 Characterization of optical properties**

### **2.8.1 Ultraviolet-visible spectroscopy**

The absorption properties were characterized by ultraviolet–visible (UV–vis) measurements. UV–vis spectra were recorded on a Cary 50 UV–vis spectrometer using quartz cell with volume of 100  $\mu\text{L}$  or 3 mL. A baseline scan with the solvent used was performed prior to absorption measurements of all samples. Concentration of the sample was controlled so that the absorption unit does not exceed 1.0 for all measurements.

### **2.8.2 Fluorescence spectroscopy**

The photoluminescent properties of SiQDs were characterized by fluorescence spectroscopy. The fluorescence spectra were measured on a Cary Eclipse fluorescence spectrometer using quartz cell with volume of 100  $\mu\text{L}$  or 3 mL. The Slit width was chosen between 5 to 20  $\mu\text{m}$  depending on the concentration of the samples. Line smoothing was performed during the measurement with the moving average mode.

### **2.8.3 Quantum yields measurements**

Quantum yields (QY or  $\Phi$ ) were measured in accordance with a published method,<sup>12-14</sup> where comparison was made to a reference dye 4',6-diamidino-2-phenylindole (DAPI). This particular reference dye was chosen due to its comparable absorption and emission profile to the SiQDs synthesized.<sup>15-17</sup> DAPI had a reported  $\Phi$  of  $\sim 4.5\%$  in water.<sup>15-17</sup> For each sample of SiQDs,  $\Phi$  was determined as the ratio of integrated PL intensity vs. absorbance with a range of

diluted samples. i.e. the sum of the emission intensity at each wavelength was used as the vertical axis, and the absorbance was used as the horizontal axis. The gradient of the line generated was used in comparison to the reference line of DAPI.

## **2.9 Cell culture and fluorescent cellular imaging**

HeLa cells were cultured in a 75 cm<sup>2</sup> incubation flask with ~12 mL of medium [500 mL of Dulbecco's modified Eagle's medium (DMEM), 10% fetal calf serum, and 4 mM L-glutamine]. Cells were incubated at 37 °C, with CO<sub>2</sub> level of 5% and split regularly to prevent overgrowth. For imaging, cells were fluorescently labelled using surface-functionalized SiQDs. At 1 day prior to the imaging, the cells were plated at a density of ~50 000/plate in a Petri dish with 2 mL of medium. On the day of imaging, cells were grown to at least 80% confluence. To allow uptake of SiQDs, nanoparticle dispersion in 1× phosphate-buffered saline (PBS) was added to the medium to reach a final concentration of 50–100 µg/mL before further incubating the cells at 37 °C for 2–3 h. Before imaging, the medium was removed and cells were carefully washed 3 times with fresh PBS solution. The cells were imaged using a Zeiss Axiovert 200 M inverted microscope fitted with a 20×, 40×, and 60× immersion objective and a 4',6-diamidino-2-phenylindole (DAPI) filter. For FLIM imaging, details of experiments were described in chapter 5 and chapter 6.

## **2.10 Cytotoxicity evaluation**

Toxicity was assessed by 3-[4,5-dimethylthiazol-2-yl]-2,5-diphenyltetrazolium

bromide (MTT) assay (Sigma-Aldrich). HeLa cells were cultured to 70–80% confluence in a 96-well plate prior to the experiment. In a typical experiment, 20  $\mu$ L of SiQDs was added to each well and incubated for 24 h. After the incubation, the MTT reagent (5 mg/mL) was reconstituted in PBS and added in an equal volume. The cells were further incubated for 3 h. After the incubation period, the resulting formazan crystals were dissolved by adding an equal volume of dimethyl sulfoxide (DMSO) to the original culture medium volume. The mixture was gently mixed in a gyratory shaker with occasional pipetting to help fully dissolve the crystals. The absorption measurements were performed using a FLUOstar fluorescence plate reader (BMG Labtech) at 570 nm and background at 690 nm.

## 2.11 References

- (1) Wilcoxon, J. P.; Samara, G. A.; Provencio, P. N.: Optical and electronic properties of Si nanoclusters synthesized in inverse micelles. *Phys Rev B* **1999**, *60*, 2704-2714.
- (2) Tilley, R. D.; Yamamoto, K.: The microemulsion synthesis of hydrophobic and hydrophilic silicon nanocrystals. *Advanced Materials* **2006**, *18*, 2053-2056.
- (3) Warner, J. H.; Hoshino, A.; Yamamoto, K.; Tilley, R. D.: Water-Soluble Photoluminescent Silicon Quantum Dots. *Angewandte Chemie International Edition* **2005**, *44*, 4550-4554.
- (4) Shiohara, A.; Hanada, S.; Prabakar, S.; Fujioka, K.; Lim, T. H.; Yamamoto, K.; Northcote, P. T.; Tilley, R. D.: Chemical Reactions on Surface Molecules Attached to Silicon Quantum Dots. *Journal of the American Chemical Society* **2010**, *132*, 248-253.
- (5) Warner, J. H.; Hoshino, A.; Yamamoto, K.; Tilley, R. D.: Water-soluble photoluminescent silicon quantum dots. *Angew Chem Int Ed Engl* **2005**, *44*, 4550-4.
- (6) Tilley, R. D.; Warner, J. H.; Yamamoto, K.; Matsui, I.; Fujimori, H.: Microemulsion synthesis of monodisperse surface stabilized silicon nanocrystals. *Chem Commun* **2005**, 1833-1835.
- (7) Shiohara, A.; Prabakar, S.; Faramus, A.; Hsu, C. Y.; Lai, P. S.; Northcote, P. T.; Tilley, R. D.: Sized controlled synthesis, purification, and cell studies with silicon quantum dots. *Nanoscale* **2011**, *3*, 3364-70.
- (8) Le Saux, G.; Ciampi, S.; Gaus, K.; Gooding, J. J.: Electrochemical

Behavior of Gold Colloidal Alkyl Modified Silicon Surfaces. *Acs Appl Mater Inter* **2009**, *1*, 2477-2483.

(9) Ciampi, S.; Bocking, T.; Kilian, K. A.; Harper, J. B.; Gooding, J. J.: Click chemistry in mesoporous materials: Functionalization of porous silicon rugate filters. *Langmuir* **2008**, *24*, 5888-5892.

(10) Ciampi, S.; Bocking, T.; Kilian, K. A.; James, M.; Harper, J. B.; Gooding, J. J.: Functionalization of acetylene-terminated monolayers on Si(100) surfaces: A click chemistry approach. *Langmuir* **2007**, *23*, 9320-9329.

(11) Ng, C. C. A.; Ciampi, S.; Harper, J. B.; Gooding, J. J.: Antifouling behaviour of silicon surfaces modified with self-assembled monolayers containing both ethylene glycol and charged moieties. *Surf Sci* **2010**, *604*, 1388-1394.

(12) Brouwer, A. M.: Standards for photoluminescence quantum yield measurements in solution (IUPAC Technical Report). *Pure Appl Chem* **2011**, *83*, 2213-2228.

(13) Williams, A. T. R.; Winfield, S. A.; Miller, J. N.: Relative Fluorescence Quantum Yields Using a Computer-Controlled Luminescence Spectrometer. *Analyst* **1983**, *108*, 1067-1071.

(14) Dhami, S.; Demello, A. J.; Rumbles, G.; Bishop, S. M.; Phillips, D.; Beeby, A.: Phthalocyanine Fluorescence at High-Concentration - Dimers or Reabsorption Effect. *Photochemistry and Photobiology* **1995**, *61*, 341-346.

(15) Du, H.; Fuh, R. C. A.; Li, J. Z.; Corkan, L. A.; Lindsey, J. S.: PhotochemCAD: A computer-aided design and research tool in photochemistry. *Photochemistry and Photobiology* **1998**, *68*, 141-142.

(16) Hard, T.; Fan, P.; Kearns, D. R.: A Fluorescence Study of the binding of hoechst 33258 and DAPI to halogenated DNAs. *Photochemistry and Photobiology* **1990**, *51*, 77-86.

(17) Dixon, J. M.; Taniguchi, M.; Lindsey, J. S.: PhotochemCAD 2: A Refined Program with Accompanying Spectral Databases for Photochemical Calculations. *Photochemistry and Photobiology* **2005**, *81*, 212-213.

## **Part I Preparation & Surface Modifications**

### **Chapter 3 One-Pot Synthesis of Colloidal Silicon Quantum Dots and Surface Functionalization *via* Thiol-Ene Click Chemistry**

**Part of this chapter has been published in:**

**Cheng, X. Y.;** Gondosiswanto, R.; Ciampi, S.; Reece, P. J.; Gooding, J. J.: One-pot synthesis of colloidal silicon quantum dots and surface functionalization via thiol-ene click chemistry. *Chem Commun* 2012, 48, 11874-11876.

### 3.1 Introduction

As introduced in chapter 1, Tilley *et. al.* developed a reverse-micelle method of preparing silicon quantum dots by reduction of halogenated silane precursors using  $\text{LiAlH}_4$ , where no highly hazardous material or procedure was used, although small amount of silane is produced<sup>1</sup>. This approach of preparing SiQDs has attracted broad attentions<sup>1-11</sup>, due to the simplicity of the method used and good quality of the SiQDs obtained. It was shown that gram scale of oxide-free SiQDs could be prepared by this method<sup>2</sup>. It was also shown that the hydrogen terminated SiQDs were modifiable with molecules possessing a terminal alkene with various distal moieties.<sup>4,10</sup> A study by Ruizendaal and co-workers is particularly relevant in that it demonstrated further functionalization of alkene terminated SiQDs using thiol-ene click reactions<sup>17</sup>. Despite the good particle monodispersity, simple experimental set-up given by this procedure, monolayer surface coverage and purification from surfactants can both be problematic.<sup>10,11</sup> To tackle these issues, Wang *et. al.* advanced a method using hexyl-trichlorosilane as both the surfactant and the reactant, showing a fabrication strategy with simplified purification steps.<sup>12</sup> However, the resultant functionalized SiQDs were terminated with methyl distal moieties; a surface functionality in which further modification is difficult at best. Therefore only hexane dispersible quantum dots with hydrophobic surface were made, and the emission peak was restricted largely in the UV region.<sup>12</sup>

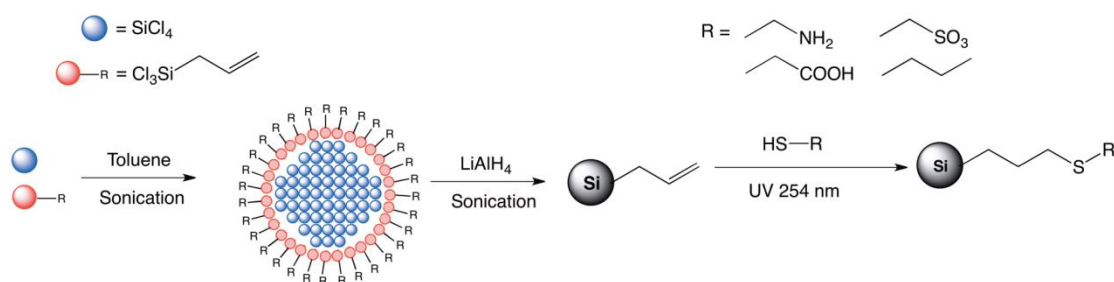


Figure 3.1 One-pot synthesis of alkene coated SiQDs and further functionalization via thiol-ene click chemistry.

In view of the above mentioned issues, and using these previous methods as inspiration, in this chapter an efficient one-pot method of fabricating colloidal SiQDs with modifiable surface is presented (Figure 3.1). In particular, allyl trichlorosilanes is used as both the surfactant and the reactant, self-assembling around halogenated silane precursors ( $\text{SiX}_4$ ,  $\text{X} = \text{Cl}, \text{Br}$ ) in toluene. The formed reverse micelle contains a  $\text{SiX}_4$  core and allyl trichlorosilanes, which is then treated with  $\text{LiAlH}_4$  to yield SiQDs with alkene groups covering the surface. The residue lithium salts was washed through in the water layer. We further demonstrate that SiQDs prepared by this method can be reacted with thiol bearing molecules, rendering the particles functionalized with a wide choice of distal groups, using the thiol-ene click reaction. By using different surface alkanethiols, we show that the particles can be dispersed in water or hexane phase, as well as have their emission properties altered.

## 3.2 Methods and Materials

### 3.2.1 Chemicals and Materials

All chemicals and solvent used were obtained and prepared as described in

chapter 2 unless otherwise stated.

### **3.2.2 One pot synthesis of allyl functionalized silicon quantum dots**

All experiments were conducted using standard Schlenk techniques. In a typical experiment, silicon tetrachloride ( $\text{SiCl}_4$ , 100  $\mu\text{L}$ ) and allyl trichlorosilane ( $\text{SiCl}_3\text{-CH}_2\text{CH=CH}_2$ , 175  $\mu\text{L}$ ) were mixed in 100 mL dry toluene (shown above) and sonicated for 20 min. An excess amount of  $\text{LiAlH}_4$  in dry THF was then added, and the mixture further sonicated for another 30 min. The reaction was quenched by adding dry ethanol (~30 mL). All solvents were then evaporated under reduced pressure, and 10 mL hexane was added to disperse the particles. The mixture was washed with 30 mL MilliQ water, the organic layer was obtained and passed through PVDF membrane with 0.45 $\mu\text{m}$  pore size. If further functionalization was performed, the hexane solvent was evaporated under reduced pressure. SiQDs was obtained in the form of an odourless, colourless oil with weight in the range of ~20 – 40 mg per batch.

### **3.2.3 Surface functionalization of silicon quantum dots via thiol-ene click reactions**

The allyl terminated silicon quantum dots were dissolved in 10 mL DMF, and thiol molecules were added to the mixture in 1:5 ratio. The reaction was left in a UV chamber (254 nm) for 5 h. After the reaction, all of the solvent was removed by evaporation under reduced pressure. For purification, the particle mixtures were either dialyzed in semi-permeable membrane with 1.5-3 kDa cut off against MilliQ

water for 24 h, or heated under reduced pressure in the case of thiol-butane. Purified quantum dots were dispersed in 5 mL of water or hexane depending on the surface groups. Approximately 5 – 10 mg of functionalized SiQDs were obtained after surface modification.

### **3.2.4 Characterization of morphology**

Morphology and size distribution of silicon quantum dots were characterized by transmission electron microscopy (TEM) as described in chapter 2.

### **3.2.5 Characterization of optical properties**

Optical properties of synthesized silicon quantum dots, including UV-Vis absorption spectra, photoluminescence (PL) spectra, PL quantum yields (QY), were characterized in accordance to methods described in chapter 2.

### **3.2.6 Characterization of surface properties**

Surface properties of synthesized silicon quantum dots, including FT-IR spectra and NMR spectra were recorded as described in chapter 2.

### 3.3 Results and Discussions

#### 3.3.1 Characterization of morphology by transmission electron microscopy

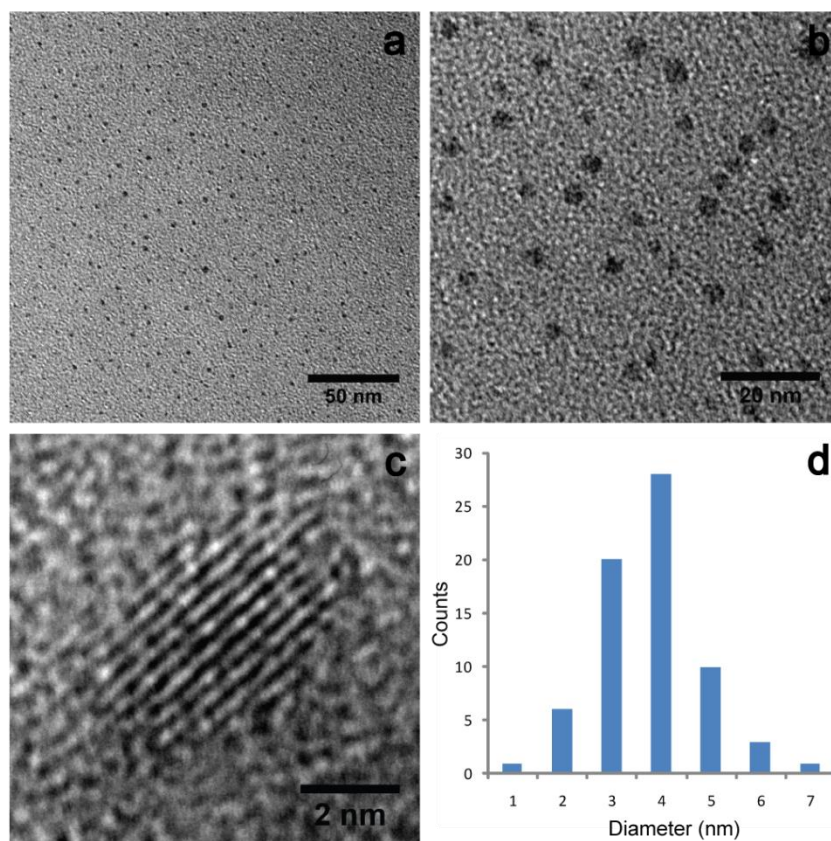


Figure 3.2 Representative TEM images and size distribution analysis of silicon quantum dots synthesized by the one pot method.

The obtained transmission electron microscopy (TEM) images show that synthesized SiQDs are reasonably mono-disperse, with only small amounts of aggregations seen in an area of  $\sim 200 \times 200$  nm. High resolution (HR-TEM) images (Figure 3.2c) shows lattice structures within the spheres. (Figure 3.2, middle), indicating the obtained particles are crystalline. Based on the TEM results, size distribution analysis indicates the average particle size is  $3.7 \pm 1.0$  nm for allyl functionalized particles, with similar results observed for SiQD with other functional groups.

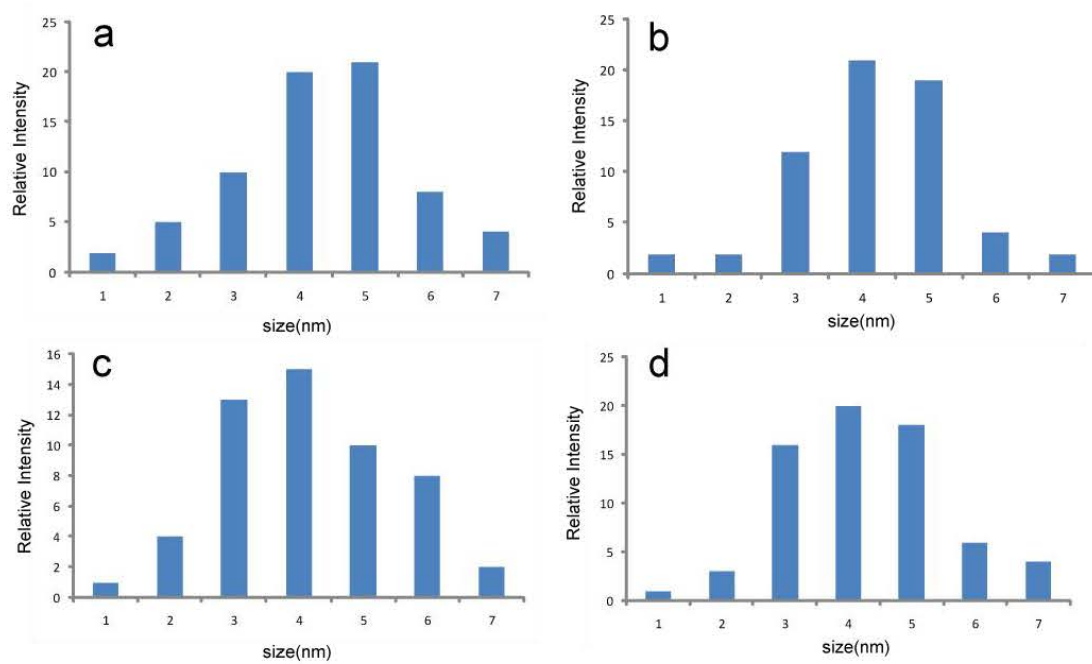
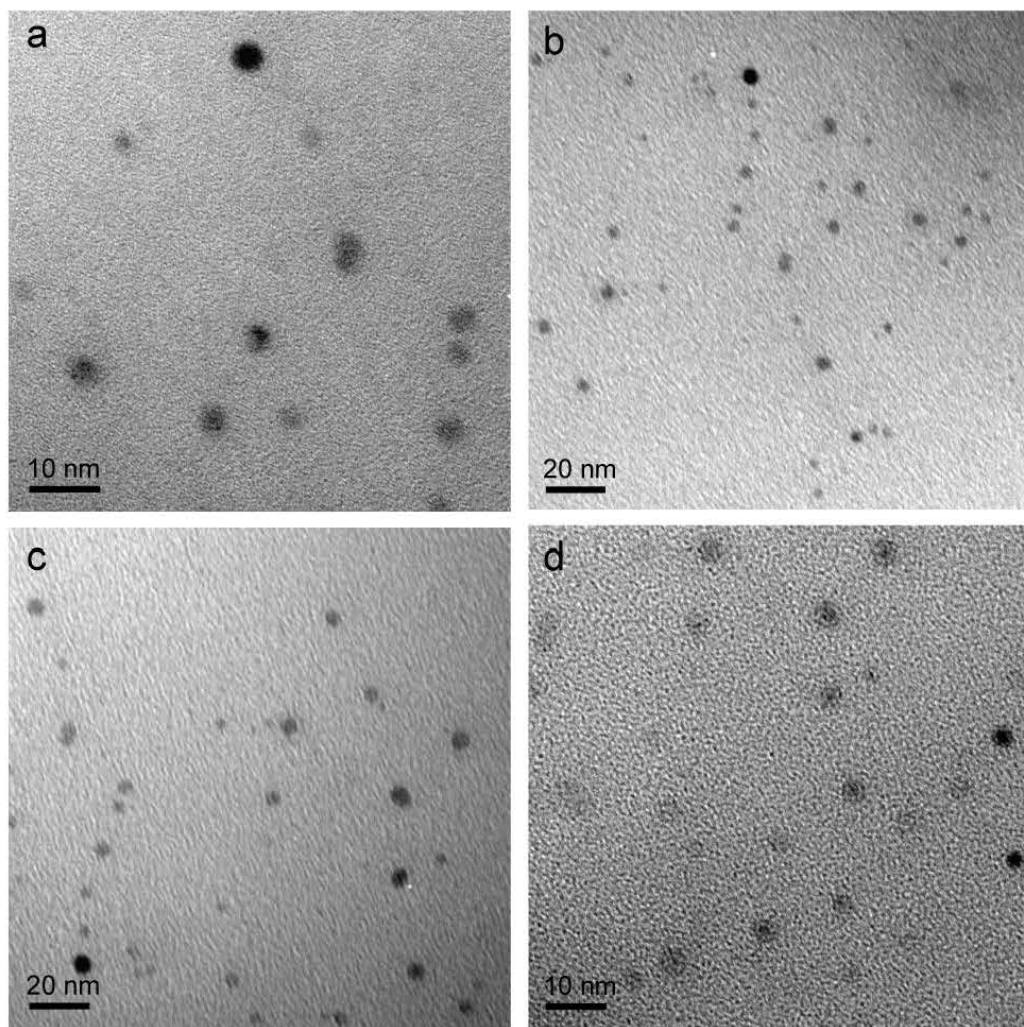


Figure 3.3 Representative TEM images and size distribution analysis of SiQDs after thiol-ene click reaction.

Additional TEM results suggested that there is no major change of size or morphology after modification (Figure 3.3). From a-d showing terminal groups as: a) SiQD-NH<sub>2</sub> (4.3 ± 1.4 nm), b) SiQD-COOH (4.2 ± 1.1 nm), c) SiQD-SO<sub>3</sub><sup>-</sup> (4.1 ± 1.3 nm), d) SiQD-butane (4.2 ± 1.3 nm).

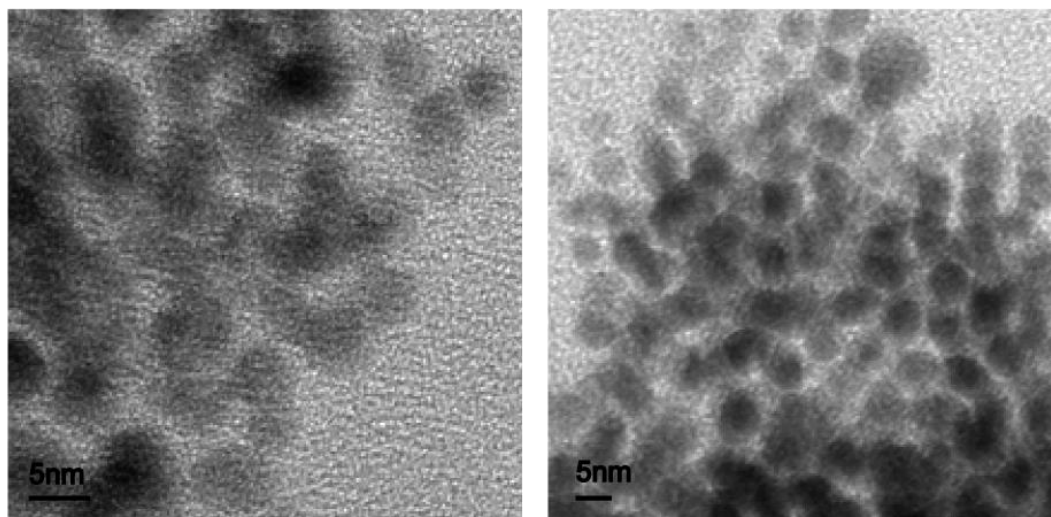


Figure 3.4 TEM images showing occasional aggregations of allyl functionalized silicon quantum dots.

During the TEM studies, it was noted that although SiQDs synthesized were generally monodisperse, aggregations were occasionally seen (Figure 3.4). One of the main factors that govern the monodispersity, and thus colloidal stability of nanoparticles in solution is the interactions of surface molecules<sup>13-15</sup>. i.e. charge repulsions or attractions. In this case, the length of the allyl group only contained three carbon atoms therefore offered weaker interactions between the chains in comparison to literature<sup>12</sup>. It is anticipated that the monodispersity and colloidal stability of SiQDs synthesized by this method improve when the chain length is increased.

### 3.3.2 Characterization of surface properties

#### 3.3.2.1 Phase transfer after surface modification with thiol-ene reaction

For nanoparticles in general, it is known that particle dispersity in solvents is governed primarily by surface properties, such as the polarity of the distal moieties of the surface-modifying molecules. Here, when coated with non-polar allyl molecules, the surface of the SiQDs was hydrophobic and the particles were only dispersible in non-polar solvents such as hexane or toluene. Upon functionalization with thiol-molecules, the surface of the SiQDs became hydrophilic upon attachment with polar molecules, and remained hydrophobic with non-polar molecules (Figure 3.5). The water dispersity is favored in several contexts particularly bio-imaging related applications where the environment is predominantly surrounded by water.

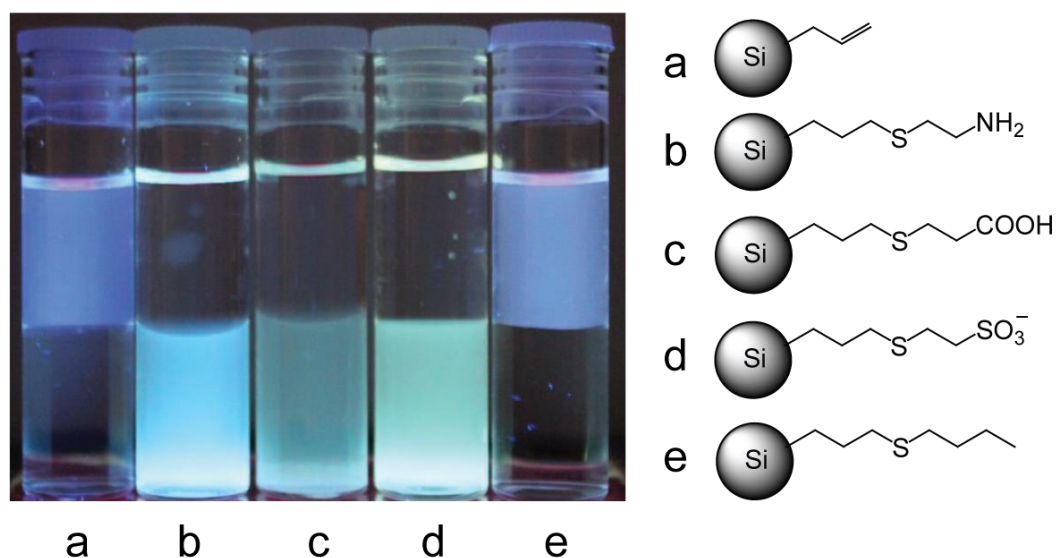


Figure 3.5 Phase transfer as the result of thiol-ene click reaction. In each tube, the upper layer contains hexane and the bottom layer contains dH<sub>2</sub>O.

### 3.3.2.2 FT-IR spectroscopy of surface modified silicon quantum dots

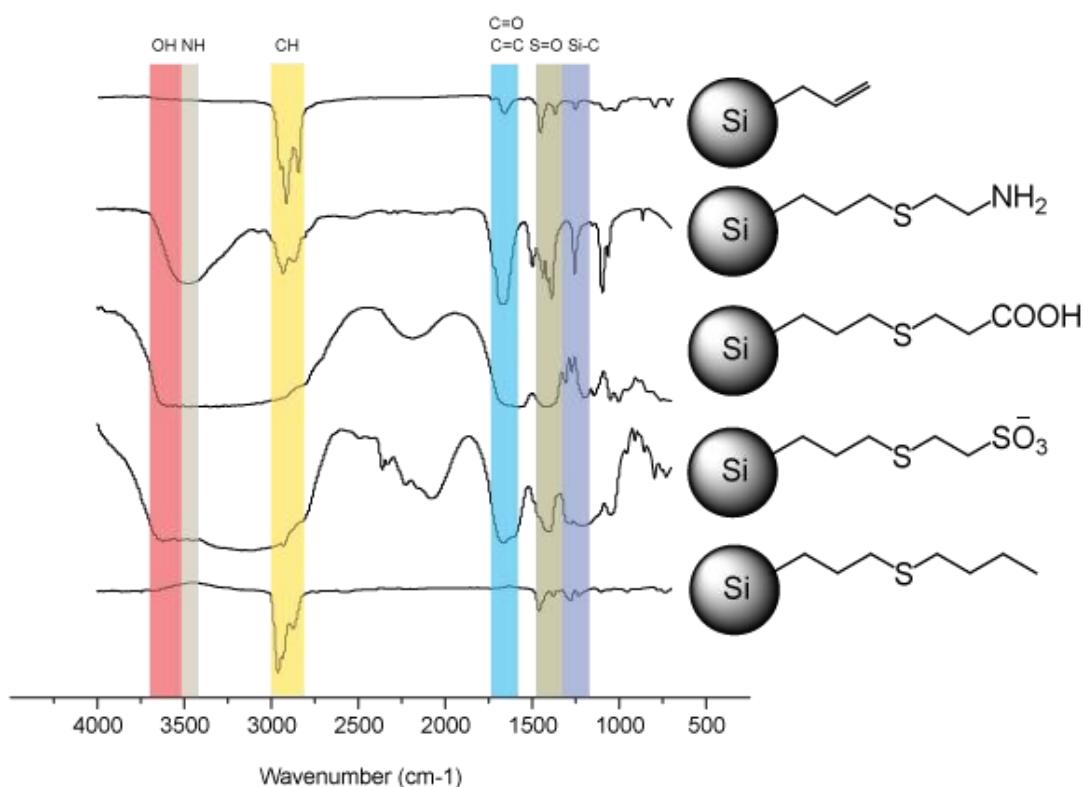


Figure 3.6 FT-IR spectra of silicon quantum dots synthesized by one-pot method and modified with thiol-ene click reaction.

To characterize the alkanethiols attached onto the surface of SiQDs, FT-IR and NMR measurements were performed. The FT-IR spectra show distinct bands from the surface molecules attached to SiQDs (Figure 3.6). The peak at  $\sim 1257\text{-}1268\text{ cm}^{-1}$  is typical for Si-C stretch and is seen in all spectra. After the thiol-ene click reaction, no typical S-H stretch in the region of  $\sim 2530\text{-}2590\text{ cm}^{-1}$  is observed, while signature bands associated with the distal groups are seen in all spectra. For allyl terminated SiQDs, the peak at  $1630\text{ cm}^{-1}$  indicates C=C stretch due to allyl group on the surface. The peak disappears after thiol-ene click reaction, which is seen most clearly for butanethiol functionalized molecule. For amine functionalized SiQDs, the broad peak at  $3470\text{ cm}^{-1}$  is due to the N-H stretch in the  $\text{-NH}_2$  group.

The peak at  $\sim 1635\text{ cm}^{-1}$  is due to the N-H bending. For carboxyl terminated quantum dots, the peak at  $1650\text{ cm}^{-1}$  and the broad peak at  $3580\text{ cm}^{-1}$  are due to the C=O stretch and O-H stretch in the  $-\text{COOH}$  group. For sulfonate functionalized SiQDs, the peak at  $1370\text{ cm}^{-1}$  is due to the S=O stretch in the  $-\text{SO}_3^-$  group. The peak at  $\sim 2200\text{ cm}^{-1}$  seen on  $-\text{COOH}$  and  $\text{SO}_3^-$  functionalized SiQDs is uncharacteristic, its origin is unclear. The surface chemistry is further confirmed by  $^1\text{H-NMR}$  experiments. In general, the double bond signal that is seen for allyl group disappears after grafting of alkanethiols, and proton signal close to the thiol groups are seen after the thiol-ene click reaction. These results provide evidence that the surface molecules are attached to the SiQDs via covalent bonds.

### 3.3.2.3 $^1\text{H-NMR}$ spectra of surface functionalized SiQDs

NMR measurements were performed to further verify the surface groups of silicon quantum dots synthesized by the one-pot method (Figure 3.7). Peaks from the surface groups of SiQDs were significantly broadened, similar to NMR measurements of large molecules where slow tumbling speed of particles in solution leads to significantly prolonged relaxation time<sup>16-18</sup>. This caused considerable difficulties in resolving some of the splitting patterns. For allyl terminated SiQDs, two peaks at 5.8 ppm (singlet) and 5.0 ppm (doublet) were typical for terminal alkene groups. These two peaks disappeared after performing the click reaction, indicating reaction of the alkene with the SH group. In addition, for thiol-amine terminated quantum dots, the two peaks at 2.97 ppm (triplet) and 3.34 ppm (triplet) were due to the  $\text{CH}_2$  protons on the attached thiol-amine

molecules. Similarly, For thiol-carboxyl terminated quantum dots, the two peaks at 2.85 ppm (triplet) and 2.51 ppm (triplet) are due to the CH<sub>2</sub> protons on the attached thiol-carboxyl molecules. For thiol-sulfonate terminated quantum dots, the two peaks at 3.25 ppm (multiplet) and 3.05 ppm (multiplet) were due to the CH<sub>2</sub> protons on the attached thiol-sulfonate molecules. For thiol-butane terminated quantum dots, the two peaks at 2.55 ppm and 2.42 ppm were due to the CH<sub>2</sub> protons next to the thiol groups.

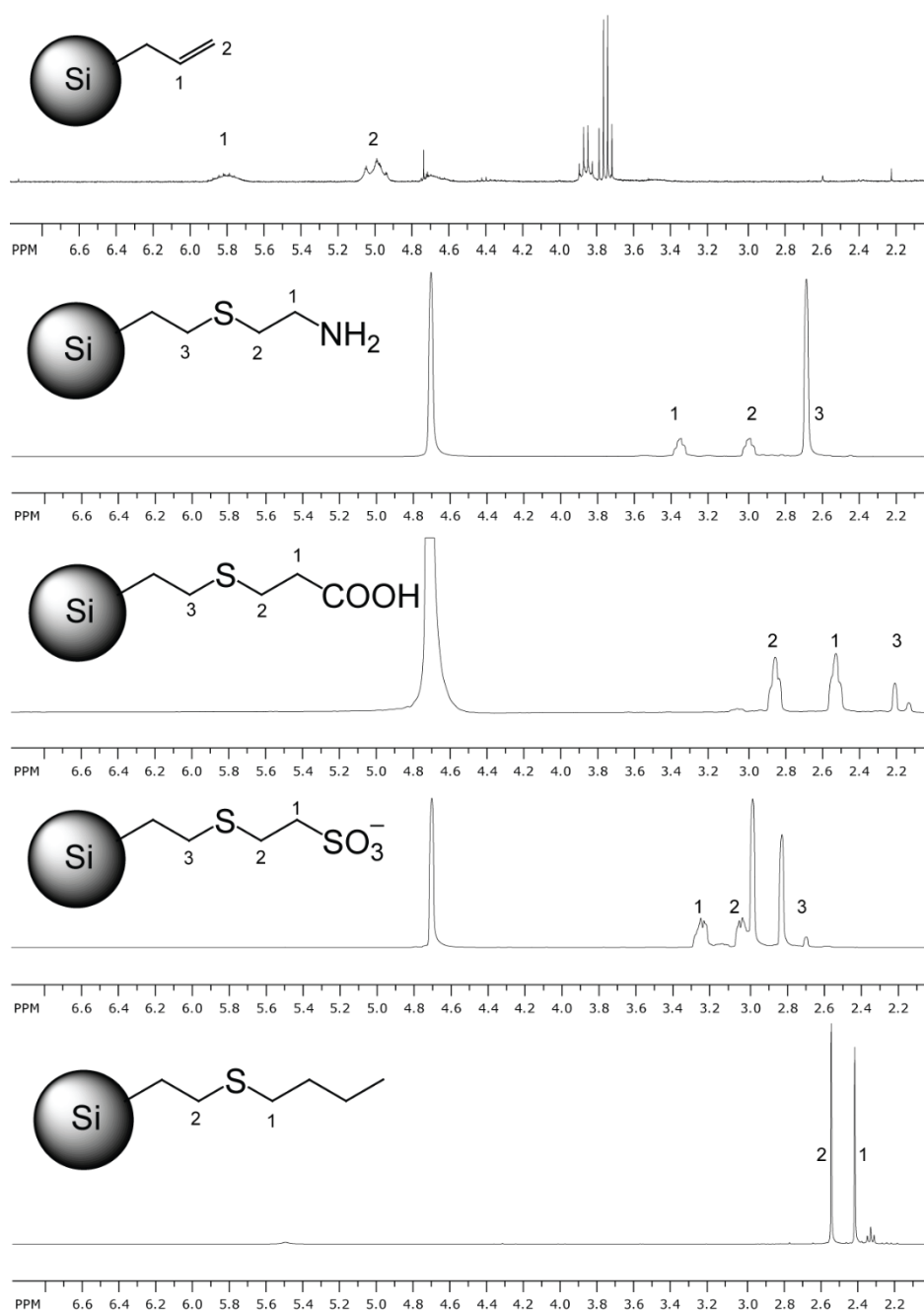


Figure 3.7  $^1\text{H-NMR}$  spectra of silicon quantum dots synthesized by one-pot method and modified with thiol-ene click reaction.

### 3.3.3 Characterization of optical properties

#### 3.3.3.1 UV absorption and photoluminescence (PL) properties

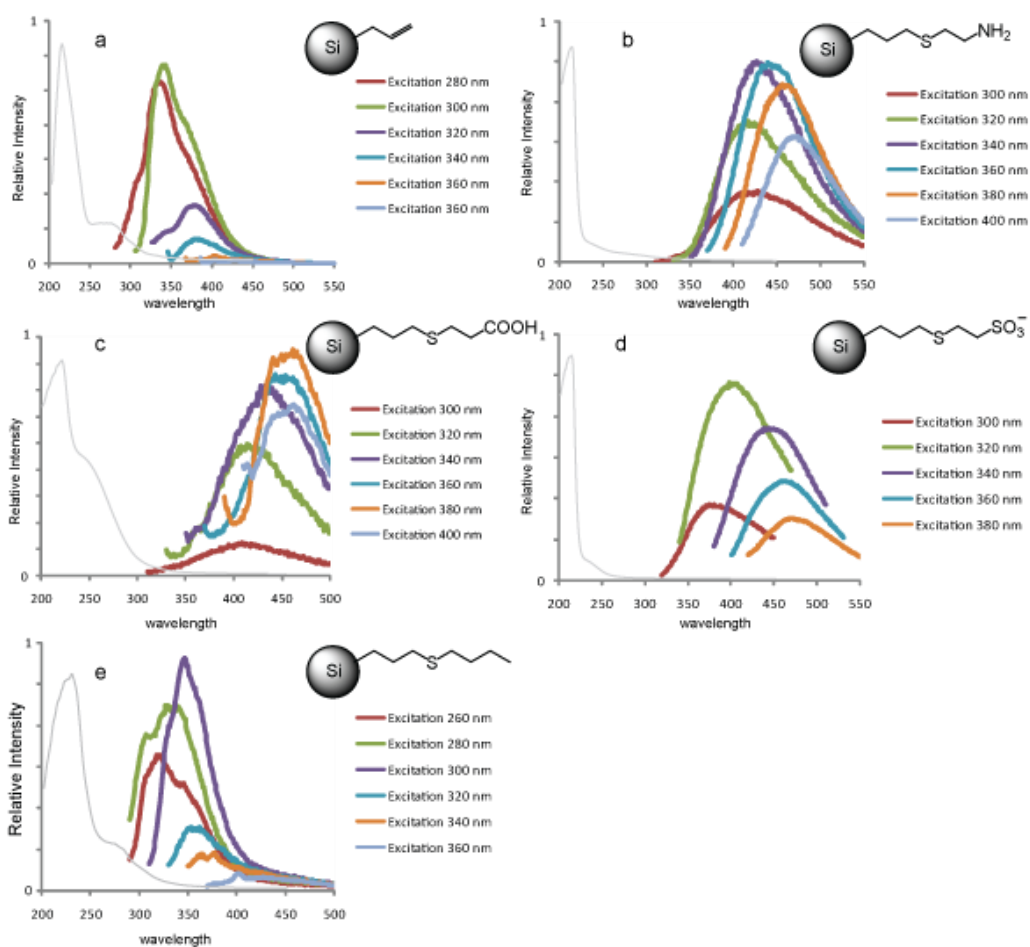
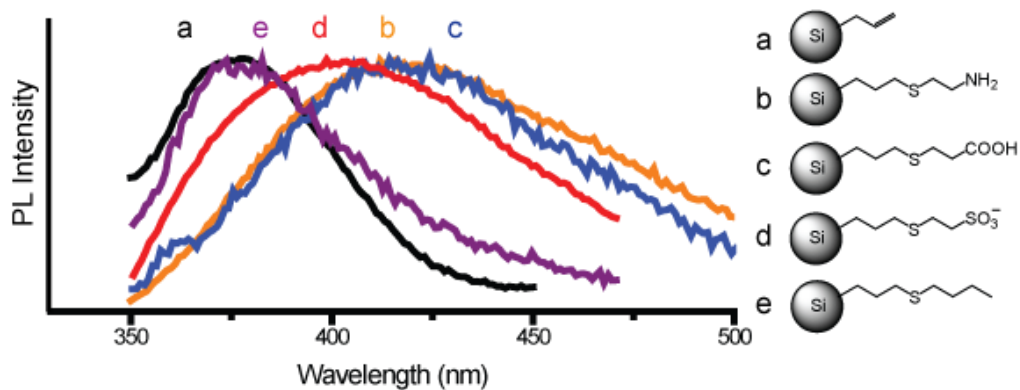


Figure 3.8 Optical properties of silicon quantum dots synthesized by one-pot method and modified with thiol-ene click reaction. Top: emission spectra with excitation at 320 nm. Bottom: change of emission profile with excitation at different wavelengths.

To study the optical properties of synthesized SiQDs, UV absorption and photoluminescence (PL) spectra were recorded. In particular, particles absorb

mainly in the UV region below 400 nm. This is typical for SiQDs synthesized by similar approaches.<sup>1</sup> The newly synthesized, allyl coated particles showed emission peak in the UV region at 375 nm with full width at half maximum (FWHM) of ~70 nm, upon excitation at 320 nm (Figure 3.8), similar to that observed with similar approaches.<sup>4,10,12</sup> The emission peak is red shifted with increasing wavelength of the excitation source, which is possibility due to the slight variation of particle size in the system. The high energy emission profile is comparable to what had been observed for oxide-free alkyl terminated quantum dot.<sup>19</sup> This suggests that surface defect level is low in particles synthesized by this method, and the allyl group well protects the particle core and optical signature is preserved. After the thiol-ene click reaction, as surface alkanethiol molecules with polar or charged end groups are attached on the particle surface, the emission peak is red shifted for 50-70 nm (Figure 3.8). The peaks are also broadened with FWHM of ~100-120 nm. These are in contrast to the butane thiol terminated particles, where no significant shift of emission peak is observed. These observations were consistent with several recent reports. For instance, Dasog *et. al.* reported blue PL with short excited states of TOAB treated SiQDs that could be affected by solvent conditions. i.e. a red shift of ~50 nm was observed when solvent was changed from pentane to chloroform, suggesting a possible of charge transfer mechanism on the surface of the nanoparticles<sup>20</sup>.

### **3.3.3.2 Measurements of quantum yields**

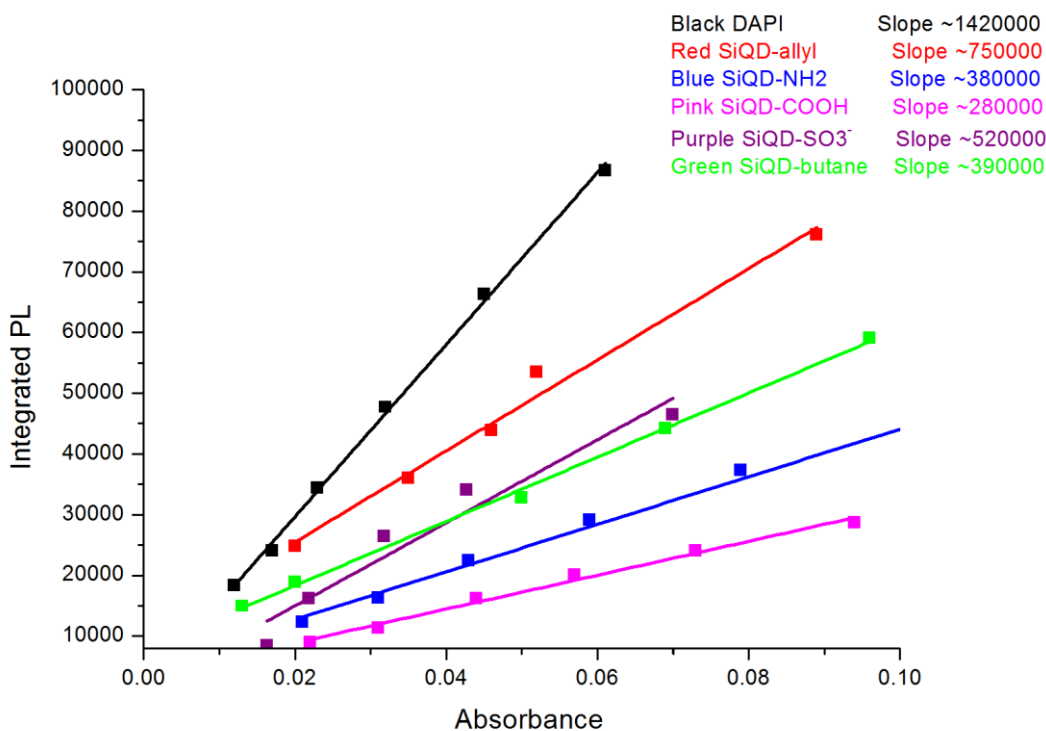


Figure 3.9 Quantum yields ( $\Phi$ ) of silicon quantum dots synthesized by the one-pot method and functionalized by thiol-ene click reaction.

To further investigate the effect of surface groups on fluorescence efficiency of SiQDs, quantum yield ( $\Phi$ ) were performed with a published method<sup>21</sup> (Figure 3.9). Quantum yield is defined as the ratio of the number of photons emitted versus the number of photons absorbed<sup>22</sup>. Here, 4',6-diamidino-2-phenylindole (DAPI) is chosen as the reference dye. The dye has comparable absorption and emission profiles with the dots, with a reported quantum yield of 4.5% in water<sup>23</sup>. Specifically,  $\Phi$  is determined as the ratio of integrated PL intensity vs. absorbance with a range of diluted samples in each case. The measured quantum yield of newly synthesized, allyl coated quantum dots is measured to be 2.5%. The quantum yield decreases to various extents as thiol groups are attached, with the most significant drop seen with -COOH terminated particles to only 0.9%.

Table 3.1 Quantum yield of one-pot synthesized SiQDs with different surface groups

Fluorophores	Quantum Yield ( $\Phi$ )
DAPI	4.5 %
SiQD-Allyl	2.5 %
SiQD-NH <sub>2</sub>	1.2 %
SiQD-COOH	0.9 %
SiQD-SO <sub>3</sub> <sup>-</sup>	1.6 %
SiQD-butane	1.2 %

### 3.4 Conclusions

In summary, this chapter shows an efficient one-pot synthetic method of preparing colloidal silicon nanocrystals in solution. It is demonstrated that silicon quantum dots synthesized by this method are reasonably monodisperse, and can be further modified with a range of different thiol molecules. This process gives nanocrystals the surface groups in need and good dispersity in water as favored in biological applications. This advance is important as it provides a simple route by which SiQDs with a range of functionalities can easily be fabricated without the need of purification from surfactant molecules where column chromatography is used.

### 3.5 References

- (1) Tilley, R. D.; Yamamoto, K. The microemulsion synthesis of hydrophobic and hydrophilic silicon nanocrystals. *Advanced Materials* **2006**, *18*, 2053-2056.
- (2) Rosso-Vasic, M.; Spruijt, E.; van Lagen, B.; De Cola, L.; Zuilhof, H. Alkyl-functionalized oxide-free silicon nanoparticles: synthesis and optical properties. *Small* **2008**, *4*, 1835-1841.
- (3) Rosso-Vasic, M.; Spruijt, E.; Popovic, Z.; Overgaag, K.; van Lagen, B.; Grandidier, B.; Vanmaekelbergh, D.; Dominguez-Gutierrez, D.; De Cola, L.; Zuilhof, H. Amine-terminated silicon nanoparticles: synthesis, optical properties and their use in bioimaging. *J Mater Chem* **2009**, *19*, 5926-5933.
- (4) Ruizendaal, L.; Pujari, S. P.; Gevaerts, V.; Paulusse, J. M.; Zuilhof, H. Biofunctional silicon nanoparticles by means of thiol-ene click chemistry. *Chem Asian J* **2011**, *6*, 2776-2786.
- (5) Siekierzycka, J. R.; Rosso-Vasic, M.; Zuilhof, H.; Brouwer, A. M. Photophysics of n-Butyl-Capped Silicon Nanoparticles. *J Phys Chem C* **2011**, *115*, 20888-20895.
- (6) Tilley, R. D.; Warner, J. H.; Yamamoto, K.; Matsui, I.; Fujimori, H. Microemulsion synthesis of monodisperse surface stabilized silicon nanocrystals. *Chem Commun* **2005**, *0*, 1833-1835.
- (7) Warner, J. H.; Hoshino, A.; Yamamoto, K.; Tilley, R. D. Water-soluble photoluminescent silicon quantum dots. *Angew Chem Int Ed Engl* **2005**, *44*, 4550-4554.
- (8) Warner, J. H.; Hoshino, A.; Yamamoto, K.; Tilley, R. D. Water-Soluble Photoluminescent Silicon Quantum Dots. *Angewandte Chemie International Edition* **2005**, *44*, 4550-4554.
- (9) Prabakar, S.; Shiohara, A.; Hanada, S.; Fujioka, K.; Yamamoto, K.; Tilley, R. D. Size Controlled Synthesis of Germanium Nanocrystals by Hydride Reducing Agents and Their Biological Applications. *Chem Mater* **2010**, *22*, 482-486.
- (10) Shiohara, A.; Hanada, S.; Prabakar, S.; Fujioka, K.; Lim, T. H.; Yamamoto, K.; Northcote, P. T.; Tilley, R. D. Chemical Reactions on Surface Molecules Attached to Silicon Quantum Dots. *Journal of the American Chemical Society* **2010**, *132*, 248-253.
- (11) Shiohara, A.; Prabakar, S.; Faramus, A.; Hsu, C. Y.; Lai, P. S.; Northcote, P. T.; Tilley, R. D. Sized controlled synthesis, purification, and cell studies with silicon quantum dots. *Nanoscale* **2011**, *3*, 3364-3370.
- (12) Wang, J.; Sun, S.; Peng, F.; Cao, L.; Sun, L. Efficient one-pot synthesis of highly photoluminescent alkyl-functionalised silicon nanocrystals. *Chem Commun (Camb)* **2011**, *47*, 4941-4943.
- (13) Aveyard, R.; Binks, B. P.; Clint, J. H. Emulsions stabilised solely by colloidal particles. *Adv. Colloid Interface Sci.* **2003**, *100-102*, 503-546.
- (14) Kirchner, C.; Liedl, T.; Kudera, S.; Pellegrino, T.; Javier, A. M.; Gaub, H. E.; Stolzle, S.; Fertig, N.; Parak, W. J. Cytotoxicity of colloidal CdSe and CdSe/ZnS nanoparticles. *Nano Letters* **2005**, *5*, 331-338.
- (15) Ghosh, P.; Han, G.; De, M.; Kim, C. K.; Rotello, V. M. Gold nanoparticles

in delivery applications. *Adv Drug Deliver Rev* **2008**, *60*, 1307-1315.

(16)Mayeri, D.; Phillips, B. L.; Augustine, M. P.; Kauzlarich, S. M. NMR Study of the Synthesis of Alkyl-Terminated Silicon Nanoparticles from the Reaction of SiCl<sub>4</sub> with the Zintl Salt, NaSi. *Chem Mater* **2001**, *13*, 765-770.

(17)Tu, C. Q.; Ma, X. C.; Pantazis, P.; Kauzlarich, S. M.; Louie, A. Y. Paramagnetic, Silicon Quantum Dots for Magnetic Resonance and Two-Photon Imaging of Macrophages. *Journal of the American Chemical Society* **2010**, *132*, 2016-2023.

(18)Hua, F.; Swihart, M. T.; Ruckenstein, E. Efficient surface grafting of luminescent silicon quantum dots by photoinitiated hydrosilylation. *Langmuir* **2005**, *21*, 6054-6062.

(19)Resch-Genger, U.; Grabolle, M.; Cavaliere-Jaricot, S.; Nitschke, R.; Nann, T. Quantum dots versus organic dyes as fluorescent labels. *Nat Methods* **2008**, *5*, 763-775.

(20)Dasog, M.; Yang, Z.; Regli, S.; Atkins, T. M.; Faramus, A.; Singh, M. P.; Muthuswamy, E.; Kauzlarich, S. M.; Tilley, R. D.; Veinot, J. G. C. Chemical Insight into the Origin of Red and Blue Photoluminescence Arising from Freestanding Silicon Nanocrystals. *ACS Nano* **2013**, *7*, 2676-2685.

(21)Sankaran, R. M.; Holunga, D.; Flagan, R. C.; Giapis, K. P. Synthesis of Blue Luminescent Si Nanoparticles Using Atmospheric-Pressure Microdischarges. *Nano Letters* **2005**, *5*, 537-541.

(22)Jurbergs, D.; Rogojina, E.; Mangolini, L.; Kortshagen, U. Silicon nanocrystals with ensemble quantum yields exceeding 60%. *Appl Phys Lett* **2006**, *88*.

(23)Hard, T.; Fan, P.; Kearns, D. R. A FLUORESCENCE STUDY OF THE BINDING OF HOECHST 33258 and DAPI TO HALOGENATED DNAs. *Photochemistry and Photobiology* **1990**, *51*, 77-86.

**Chapter 4 Versatile “Click Chemistry” Approach to  
Functionalizing Silicon Quantum Dots:  
Applications Toward Fluorescent Cellular Imaging**

**Part of this chapter has been published in**

**Cheng, X.;** Lowe, S. B.; Ciampi, S.; Magenau, A.; Gaus, K.; Reece, P. J.; Gooding, J. J.: Versatile “Click Chemistry” Approach to Functionalizing Silicon Quantum Dots: Applications toward Fluorescent Cellular Imaging. *Langmuir* **2014**, *30*, 5209-5216.

## 4.1 Introduction

Since most currently available methods of modifying the surface of SiQDs are single-step processes, two issues are present for their use in practical contexts. First, if the molecule used to functionalize the SiQDs surface is heterobifunctional, competition of reactions between the reactive moieties at the surface could lead to undesired moieties being presented on the functionalized SiQDs<sup>1</sup>. Second, certain molecules for surface functionalization are difficult to synthesize and are often obtained in small quantities, such as proteins and DNAs, therefore directly passivating the surface of SiQDs presenting the desired surface groups. In both situations, using a multiple-step modification strategy instead of a single-step process would help to produce SiQDs presenting the desired surface groups. Despite some methods being reported in the literature<sup>1-4</sup>, to date there are still limited examples of modifying SiQDs using a multiple-step strategy.

Recent progresses in click chemistry, in which modular molecular building blocks are joined together with high specificity and yields to produce complex structures have inspired growing applications in many fields such as drug discovery<sup>5</sup>, materials synthesis<sup>6</sup>, bioconjugation<sup>7</sup>, supramolecular chemistry<sup>8</sup> and polymer sciences<sup>6</sup>. This is represented by the copper catalyzed azide-alkyne cycloaddition (CuAAC) reaction, which a massive library of products has been produced in mild conditions. Importantly, the CuAAC reaction has been demonstrated with the surface modifications of various types of nanoparticles<sup>5-10</sup>, as well as silicon surfaces high degree of control of surface architecture could be obtained<sup>11-15</sup>.

This chapter describes a new approach of modifying the surface of silicon quantum dots in solution (Figure 4.1). Specifically, hydrogen terminated silicon quantum dots were first modified by hydrosilylation with 1,8-nonadiyne under UV

irradiation to produce particles with alkyne terminated surface. Nonadiyne functionalized dots were further reacted with azide molecules via CuAAC click reaction to introduce desired functionalities. The resulting water soluble SiQDs were then used for fluorescent imaging of HeLa cells, where no severe cytotoxicity was observed. By using a multiple-step, click approach, it is demonstrate that SiQDs can be uniformly functionalized with a range of desired surface groups, due to the existence of a large number of different azide species.

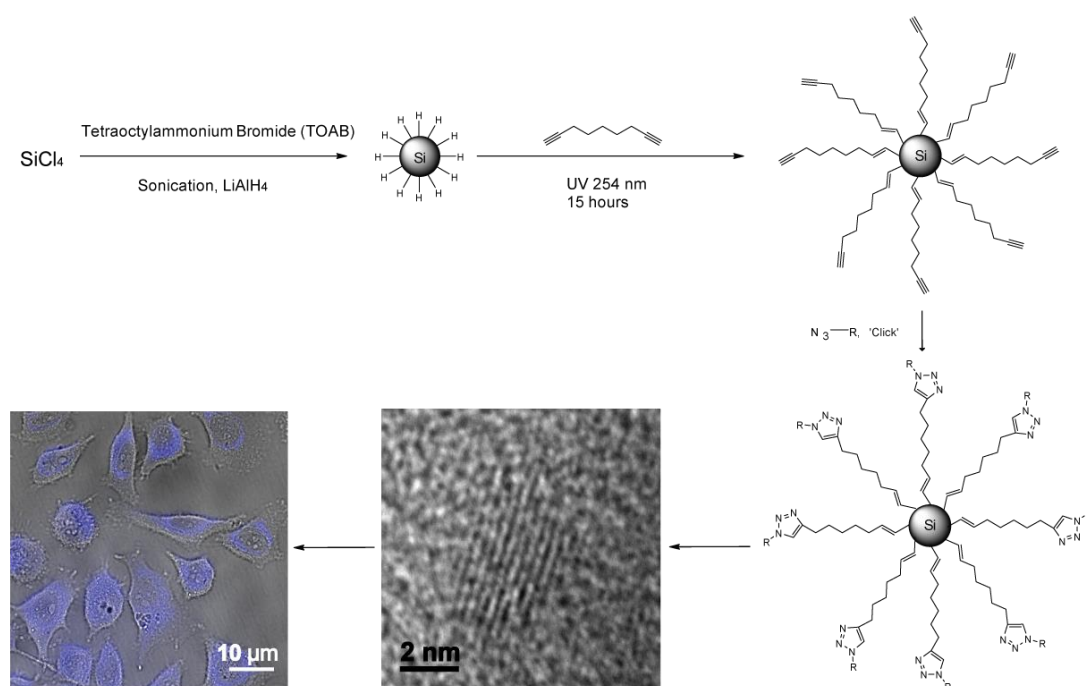


Figure 4.1 Strategies of synthesis and surface modification of silicon quantum dots for cellular fluorescent imaging.

## 4.2 Methods and Materials

### 4.2.1 Chemicals and Materials

All chemicals and solvent used were obtained and prepared as described in chapter 2 unless otherwise stated.

### 4.2.2 Synthesis of azides

#### *Synthesis and <sup>1</sup>H NMR of 3-azido-1-propan-1-amine*

This compound was synthesized by a published method<sup>16</sup>. In brief, to a solution of 3-bromopropylamine hydrobromide (1 g) in water (3.125 mL) was added a solution of sodium azide (1.04 g) in water (5 mL) in one portion while stirring under argon. The reaction was heated to reflux for 16 hours while stirred. After reaction, the mixture was put in an ice/water bath and added diethyl ether (16 mL). Potassium hydroxide pellets (1.25 g) was added whilst keeping the mixture temperature below 10 °C. The mixture was stirred for further 30 mins and extracted with diethyl ether (2 x 5 mL), and organic layer washed with water (5 mL). The obtained mixture was dried over potassium carbonate, filtered through celite and concentrated to give a volatile, slightly yellow oil.

<sup>1</sup>H NMR (300 MHz, H<sub>2</sub>O): 3.38 (t, J = 6.7 Hz, 2H; CH<sub>2</sub>), 2.70 ppm (t, J = 6.8 Hz, 2H; CH<sub>2</sub>), 1.64 (quin (tt), J = 6.8, 6.8 Hz, 2H; CH<sub>2</sub>).

#### *Synthesis and <sup>1</sup>H NMR of 3-azido-propanonic acid*

The product was synthesized with a published method<sup>17</sup>. In brief, 3-bromopropionic acid (25 mmol) was dissolved in acetonitrile (40 mL) and Sodium azide was (50 mmol) added to the solution, the mixture was refluxed for 4 hours after which acetonitrile was removed *in vacuo*

and the resulting residue was suspended in ethyl acetate (50 mL) and extracted with 0.1 M HCl (3 x 40 mL), water (3 x 40 mL) and brine (1 x 30 mL). The organic layer was dried using anhydrous Na<sub>2</sub>SO<sub>4</sub> to afford the 3-azidopropionic acid in 87% yield. 3-Azidopropionic acid (20 mmol) was dissolved in DCM (40 mL) and treated with oxalyl chloride (20 mmol). The reaction was allowed to stir for 6 hours at room temperature to afford 3-azido propyl chloride 5b, which was used directly without any further purification.

<sup>1</sup>H-NMR (300 MHz, D<sub>2</sub>O) δ 3.61-3.57 (t, J = 6.4 Hz, 2H), 2.66-2.62 (t, J = 6.4 Hz, 2H).

#### *Synthesis and 1H NMR of 11-azido-3,6,9-trioxaudecan-1-ol*

The product was purchased from Sigma Aldrich (744336) and used as received

<sup>1</sup>H-NMR (300 MHz, CDCl<sub>3</sub>) δ 3.61-3.57 (t, J = 6.4 Hz, 2H), 2.66-2.62 (t, J = 6.4 Hz, 2H).

### **4.2.3 Synthesis and purification of nonadiyne modified silicon quantum dots**

Hydrogen terminated SiQDs were prepared as described in chapter 2. Surface modification and purification were prepared using procedures as described in chapter 2, using ~4 mL of nonadiyne (2.7 × 10<sup>-2</sup> mol) added per 100 mL of solution.

### **4.2.4 Surface functionalization via CuAAC click reaction**

For a typical click reaction on the alkyne functionalized SiQDs, a dispersion of SiQDs-nonadiyne containing ~ 10 mg particles was transferred into a 25 mL round bottom flask and all of the solvent evaporated using a rotatory evaporator. To the flask 3 mL of DMF and 3 mL of water were added to fully disperse the nanoparticles. To the mixture were then added with CuSO<sub>4</sub>, L-sodium ascorbate and azides in

1:20:100 molar ratios. The reaction was stirred overnight under room temperature before removing all the solvent in vacuo. The obtained click product was purified by dialysis using Tube-O-Dialyzer with MWCO of 1.5 kDa, and the process was performed over 12 hours in Milli-Q water. After dialysis, all solvent was again evaporated and particles dispersed in 1 mL of the desired solvent.

#### **4.2.5 Characterization of morphology**

Morphology and size distribution of silicon quantum dots were characterized by transmission electron microscopy (TEM) and dynamic light scattering (DLS) measurements as described in chapter 2.

#### **4.2.6 Characterization of optical properties**

Optical properties of synthesized silicon quantum dots, including UV-Vis absorption spectra, photoluminescence (PL) spectra, quantum yields (QY), were characterized as described in chapter 2.

#### **4.2.7 Characterization of surface properties**

Surface properties of synthesized silicon quantum dots, including FT-IR measurements, NMR measurements and XPS measurements were performed as described in chapter 2.

#### **4.2.8 Fluorescence cellular imaging**

Fluorescent labelling experiments of SiQDs using HeLa cells was performed

as described in chapter 2.

#### 4.2.9 Cytotoxicity evaluations

Cytotoxicity evaluations of SiQDs were performed using MTT assays as described in chapter 2.

### 4.3 Results and Discussions

#### 4.3.1 Characterization of morphology

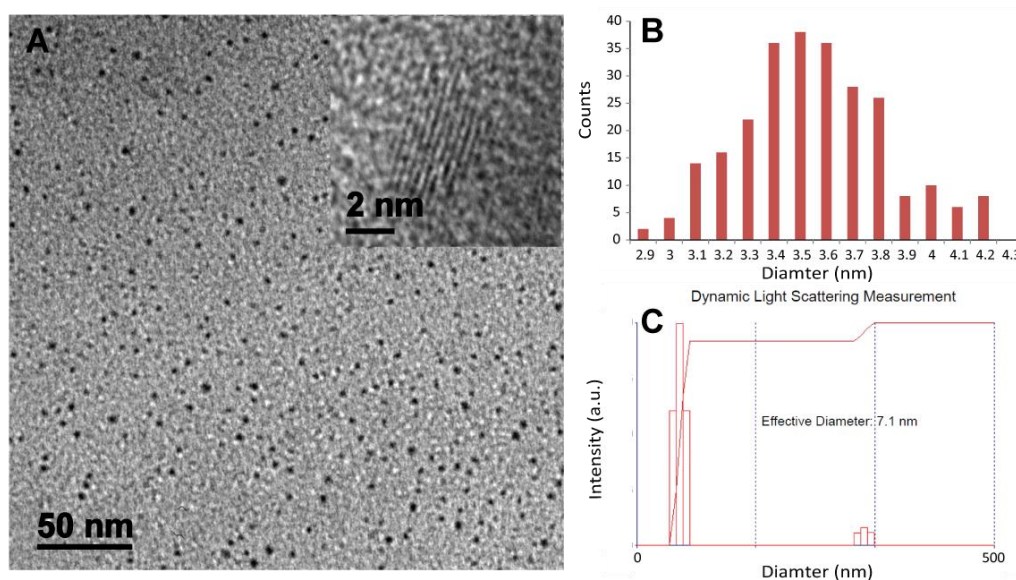


Figure 4.2 Morphology of surface-functionalized SiQDs. (A) TEM images of SiQD–nonadiyne. (Inset) HR-TEM images demonstrate the crystal structure of the particles obtained. (B) Size distribution analysis of particles based on TEM images. (C) DLS results showing narrow size distribution.

The morphology of the synthesized SiQDs prepared was characterized by TEM (Figure 4.2) and DLS (Figure 4.2C) measurements. The results indicated that the SiQDs synthesized had similar morphology with comparative methods<sup>18-28</sup>. From the TEM images, it was seen that SiQDs synthesized were nearly spherical in shape.

The SiQDs showed reasonable monodispersity with an absence of aggregates. High-resolution TEM (HR-TEM) images indicated lattice fringes within the nanoparticles (inset of Figure 4.2A), demonstrating that the particles synthesized were indeed nanocrystalline silicon. The size distribution determined from the TEM images suggests that the average size of the nanoparticles was  $3.5 \pm 0.6$  nm (Figure 4.2B). DLS indicates that the average hydrodynamic diameter of the SiQDs was  $7.1 \pm 0.5$  nm, with only a small fraction of aggregation observed (Figure 4.2C). Interestingly, the obtained DLS value was larger than the TEM results. The difference between the two measurements reflects the fact that the hydrodynamic radius measured by DLS incorporates the contributions of surface functionalization and any associated solvents, whereas for TEM measurements, all solvent were evaporated.

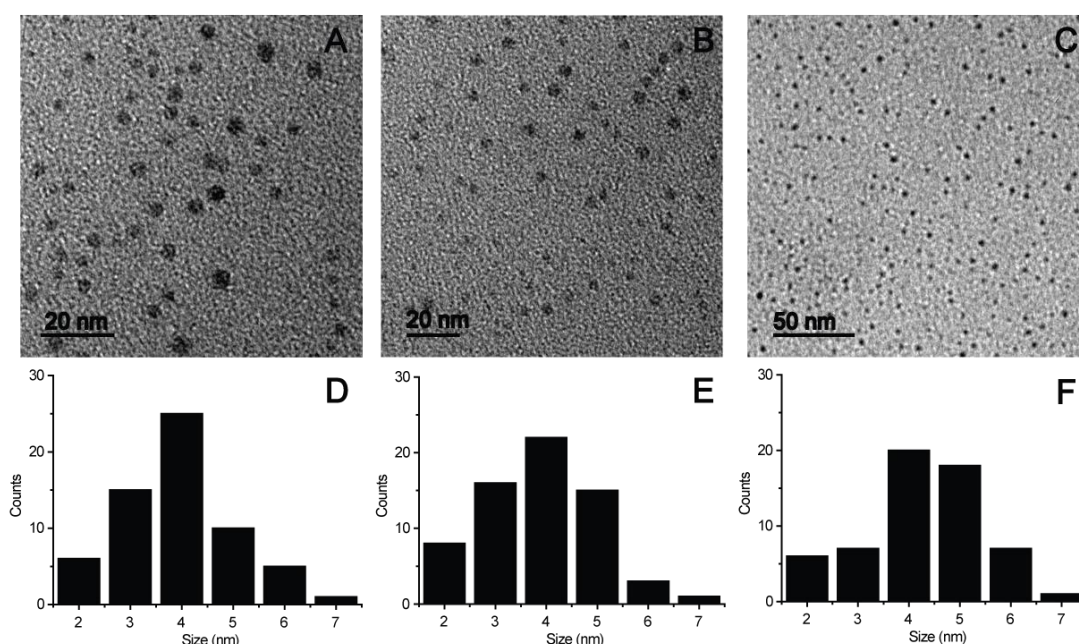


Figure 4.3 TEM images (A-C) and size distribution analysis (D-F) of SiQDs functionalized with different azide groups. From A-C: TEM image of (A) SiQDs-NH<sub>2</sub>, (B) SiQDs-COOH and (C) SiQDs-(EO)<sub>3</sub>. From D-F: Size distribution analysis of (D) SiQDs-NH<sub>2</sub>, (E) SiQDs-COOH and (F) SiQDs-(EO)<sub>3</sub>.

After the additional modification process with the different azides, the TEM images showed similar features to alkyne-passivated dots (Figure 4.3). The measured particle sizes were  $3.9 \pm 1.0$  nm for azido-propylamine-modified particles,  $3.8 \pm 0.9$  nm for azido-propionic-acid-modified particles, and  $4.3 \pm 1.2$  nm for (EO)<sub>3</sub>-azide-modified particles. The length of the capping molecules in their lowest energy form (MM2 level) were calculated in ChemDraw as: nonadiyne: 1.0 nm; azido-propylamine: 1.7 nm; azido-propionic acid: 1.6 nm; azido-ethylene oxide: 2.1 nm. By considering the length of the capping molecules, i.e. adding twice the length of the capping molecules onto the core of the corrected size of the SiQDs were: SiQDs-nonadiyne:  $5.5 \pm 0.6$  nm; SiQDs-NH<sub>2</sub>:  $7.3 \pm 1.0$  nm; SiQDs-COOH:  $7.0 \pm 0.9$  nm; SiQDs-(EO)<sub>3</sub>:  $8.5 \pm 1.2$  nm. It is realized that the DLS and TEM measurements of the size of SiQDs-nondaiyne were very close considering that the measurements were close to the lower limit of DLS measurements.

## 4.3.2 Characterization of surface properties

### 4.3.2.1 FT-IR measurements

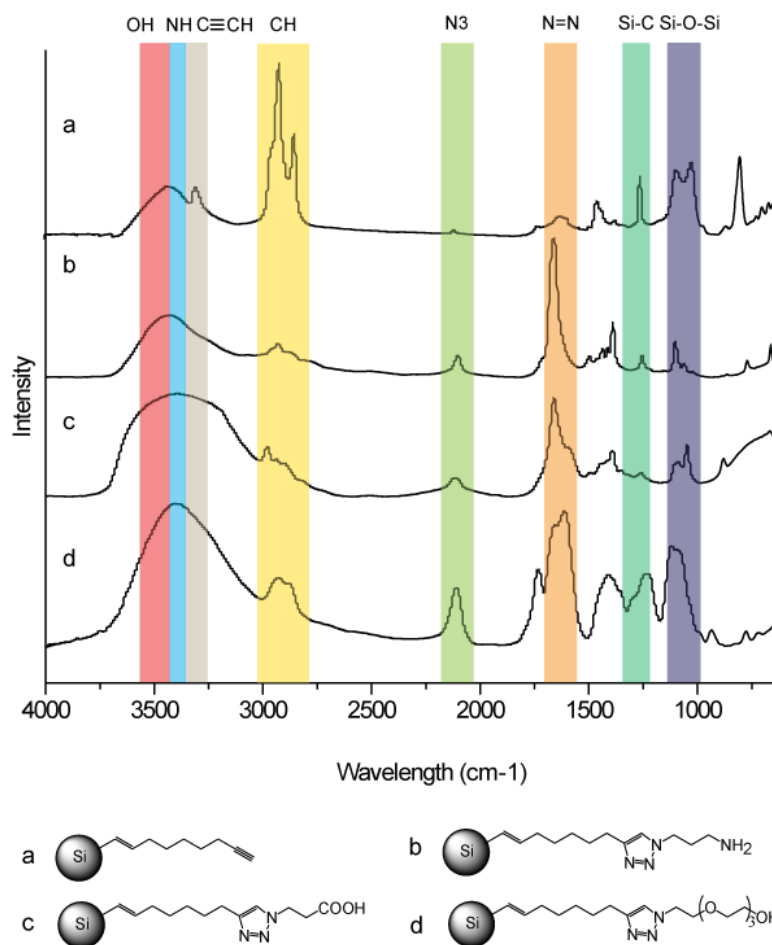


Figure 4.4 FTIR spectra of SiQDs modified with different surface groups. (a) SiQD–nonadiyne, (b) SiQD–NH<sub>2</sub>, (c) SiQD–COOH, and (d) SiQD–(EO)<sub>3</sub>.

To characterize surface groups of the modified SiQDs, FTIR measurements were performed on the click-functionalized SiQDs, showing spectral signatures from the surface moieties. The peaks at ~1260 cm<sup>-1</sup> (medium) were seen in all spectra and attributed to the CH<sub>3</sub> symmetrical deformation from the Si–C bond on the particle surface. For SiQD–nonadiyne (Figure 4.4a), two peaks at 3290 cm<sup>-1</sup> (medium) and 2115 cm<sup>-1</sup> (weak) were attributed to the terminal ≡C–H stretch and the C≡C stretch, respectively. Because all solvents and unreacted nonadiyne were

evaporated under reduced pressure after hydrosilylation and the SiQDs further purified *via* size-exclusion chromatography, the  $\equiv\text{C-H}$  stretch and  $\text{C}\equiv\text{C}$  stretch signals were evidence of the successful attachment of nonadiyne onto the surface of SiQDs. The attachment of nonadiyne was also confirmed by proton nuclear magnetic resonance ( $^1\text{H}$  NMR) studies (see Figure 4.6), although peak assignment was influenced by significant peak broadening, possibly because of the extended relaxation time as a result of slow tumbling of particles in solution. The peaks between  $1000$  and  $1100\text{ cm}^{-1}$  were due to the formation of oxides, most likely  $\text{Si-O-Si}$  from surface siloxanes, which were observed in a number of other studies<sup>1,3</sup>. The peak at  $810\text{ cm}^{-1}$  was attributed to the rocking modes in the surface  $\text{Si-CH}_3$  bonds. After performing the click reaction (panels b–d of Figure 4.4), the alkyne peak in FTIR disappeared, while peaks as a result of the presence of triazoles could be observed. The broad features around  $1600\text{ cm}^{-1}$  were due to the  $\text{N}=\text{N}$  stretch, as observed elsewhere<sup>10</sup>. Also, after the click reaction, peaks at  $2110\text{ cm}^{-1}$  (weak) originated from an alkyl azide antisymmetric stretch indicated some level of physical adsorption of azides on the particle surface. Because this feature was very clear in azide molecules (see Figure 4.5), usually stronger than the  $\text{C-H}$  stretch at  $2900\text{ cm}^{-1}$ , the observed peaks on SiQDs suggest only weak physical adsorption of azides. For  $\text{SiQD-NH}_2$ , the broad peak at  $3410\text{ cm}^{-1}$  was due to the  $\text{N-H}$  stretch. The peak at  $1590\text{ cm}^{-1}$  (strong) was due to the  $\text{N-H}$  bend in the amine molecule. For  $\text{SiQD-COOH}$ , the broad peak at  $3442\text{ cm}^{-1}$  (broad) was due to the  $\text{OH}$  stretch, while  $1721\text{ cm}^{-1}$  (strong) was caused by the  $\text{C=O}$  stretch in the distal  $-\text{COOH}$  group. For  $\text{SiQD-(EO)}_3$ , the peak at  $\sim 1122\text{ cm}^{-1}$  was a result of the  $\text{C-O}$  stretch in

the (EO)<sub>3</sub> molecules.

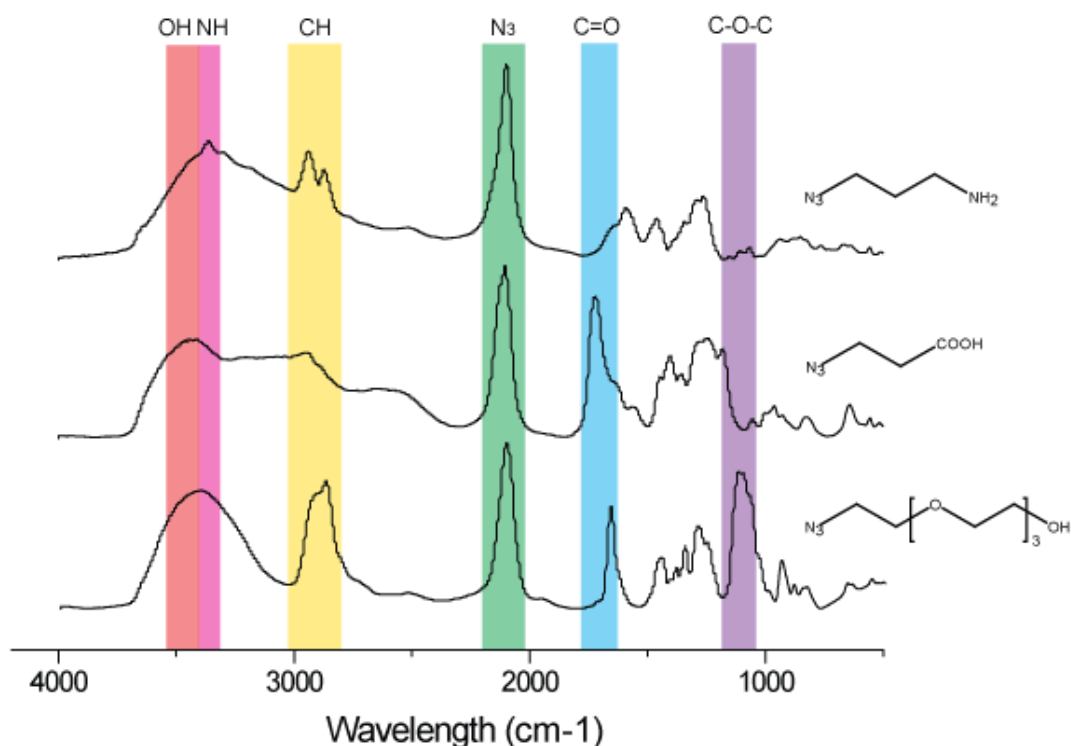


Figure 4.5 IR spectra of azide molecules used for click reaction on the surface of silicon quantum dots. Characteristic peaks are highlighted with different colors.

All azide molecules used for click reactions on silicon quantum dots show strong absorption peaks at  $\sim 2100\text{ cm}^{-1}$ , which are attributed to the  $\text{N}=\text{N}=\text{N}$  antisym stretch in azides. In particular, this peak is present at  $2099\text{ cm}^{-1}$  for 3-azido-1-propan-1-amine,  $2104\text{ cm}^{-1}$  for 3-azido-propanoic acid,  $2107\text{ cm}^{-1}$  for 11-azido-3,6,9-trioxaudecan-1-ol and  $2095\text{ cm}^{-1}$  for 1-azidodecane. Characteristic peaks for each molecule are also observed. For 3-azido-1-propan-1-amine, the broad peak at  $\sim 3364\text{ cm}^{-1}$  is due to the N-H stretch in the terminal amine group. For 3-azido-propanoic acid, the C=O group shows strong absorption at  $1721\text{ cm}^{-1}$ , and the broad peak at  $\sim 3442\text{ cm}^{-1}$  is due to the O-H stretch of the end group. For 11-azido-3,6,9-trioxaudecan-1-ol, the C-O-C stretch is observed at  $1122\text{ cm}^{-1}$ , and the terminal O-H shows broad feature at  $\sim 3404\text{ cm}^{-1}$ .

#### 4.3.2.2 $^1\text{H}$ -NMR measurements and effects of column purification

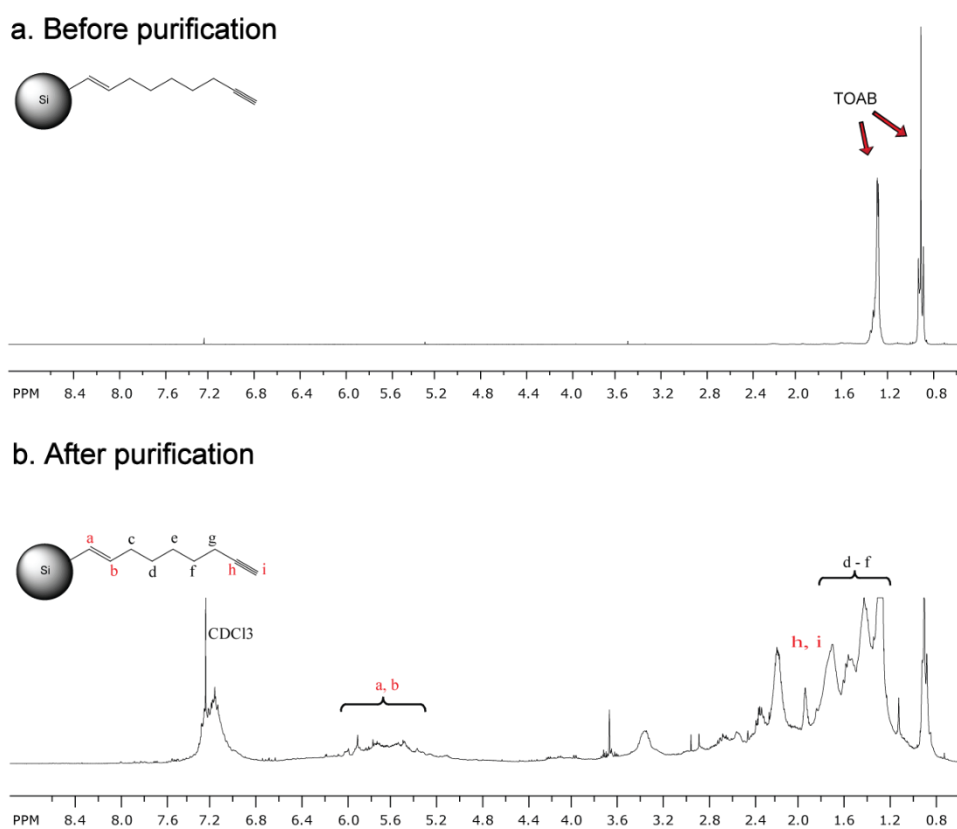


Figure 4.6  $^1\text{H}$ -NMR of SiQDs-nonadiyne and effects of size-exclusion column chromatography. (a) Before purification and (b) after purification by Bio-Beads column.

The attachment of nonadiyne was also confirmed by proton nuclear magnetic resonance ( $^1\text{H}$  NMR) studies (see Figure 4.6). It was noticed that before purification by size-exclusion column, signals were dominated by the surfactant TOAB molecules, which and signals from the surface groups were hardly seen. After purification, however, it was noted that most of the surfactants were removed and the resulting signals were better resolved and were assigned to the surface groups, a similar observation to comparative studies<sup>21,29</sup>. Also, significant peak broadening

was observed, which was probably due to the extended relaxation time as a result of slow tumbling of particles in solution. This was also observed in a few comparative studies<sup>25,27,30-33</sup>. Several peaks related with surface attached nonadiyne could still be identified. The peak observed at ~5.5 – 6 ppm was related with proton *a* and proton *b*. The peak observed at ~1.9 ppm was caused by the distal alkyne proton. However, after the click reaction, the peaks were further broadened and no peak was clearly identified. The obtained NMR results indicated that the attachment of alkyne on the surface of SiQDs was indeed via hydrosilylation, and that the actual surface structure was more complicated than the model proposed here.

#### **4.3.2.3 XPS measurements and surface coverage**

To further explore the surface structure of nonadiyne modified SiQDs, XPS measurements were performed. Figure 4.7 showed typical XPS spectra of nonadiyne passivated silicon quantum dots after column purification. In the survey scan (A), no nitrogen 1s peak at ~401 eV was observed. Since a large amount of surfactants that contain nitrogen (TOAB, tetraoctylammonium bromide) was added during the synthesis, the absence of this peak suggested that most of the surfactants were removed during purification, and the carbon 1s peak observed at 285 eV (Figure 4.7C) was primarily related with surface bound alkyne. It was noticed that although the TEM results confirmed the crystal structure of silicon quantum dots synthesized, the Si 2p peak (Figure 4.7B) observed at 102.5 eV indicated that the existence of oxides rather than non-oxidized crystalline silicon. In fact, this observation was previously reported by a few groups<sup>22,34,35</sup>. A likely source of this

feature could be related to the surface Si-O-Si structures, as was further confirmed by the FT-IR studies as shown in Figure 4.4. This feature is interesting as from the integrated peak intensity, the oxygen peak would be much larger than observed if the synthesized particles were completely oxides (Table 2.1).

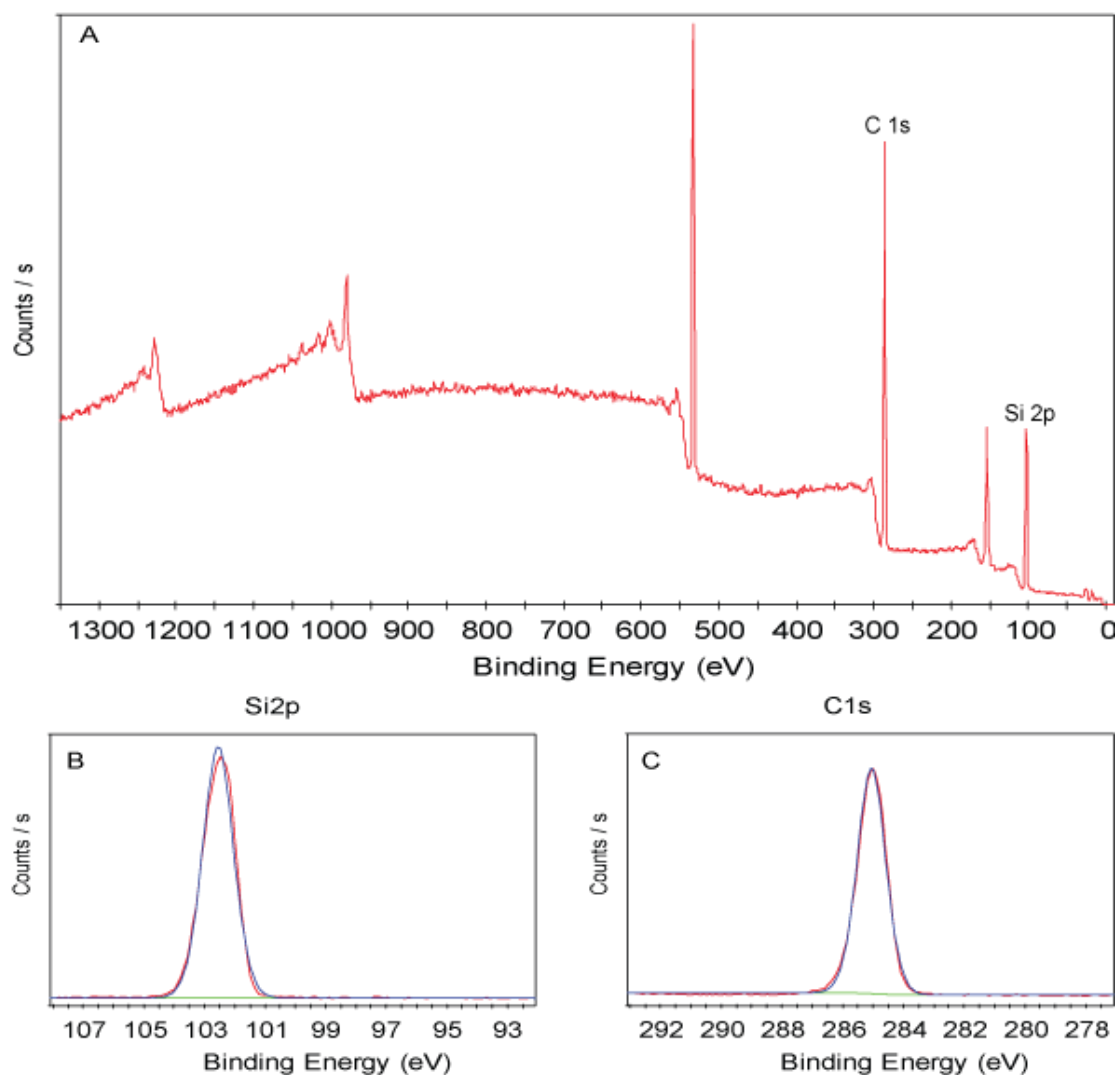


Figure 4.7 XPS spectra of silicon quantum dots functionalized with nonadiyne.

Using XPS integrated peak area, an attempt on determining surface coverage of nonadiyne on silicon quantum dots was made. This was done by firstly calculating the number of silicon atoms in each silicon quantum dots. Since there

are 4 atoms completely inside the unit cell, 8 on the corners, 6 on the faces, there are  $4 + 1 + 3 = 8$  atoms in a unit cell. Therefore, the cell volume =  $(0.543 \text{ nm})^3 = 1.6 \times 10^{-22} \text{ cm}^3$ . For crystalline silicon which had a cubic diamond structure, the lattice constant is  $5.431 \text{ \AA}$ . The density of silicon atoms =  $8 \text{ atoms}/(\text{cell volume}) = 50 \text{ atoms/nm}^3$ . Assuming the nanoparticle is spherical, i.e., radius  $r = 1 \text{ nm}$ , then the volume =  $\frac{4}{3}\pi r^3 = 4.19 \text{ nm}^3$ , which contains  $4.19 \times 50 = 209$  silicon atoms. By comparable methods, the number of silicon atoms in spherical silicon nanocrystals of different sizes can be calculated (Figure 4.8B).

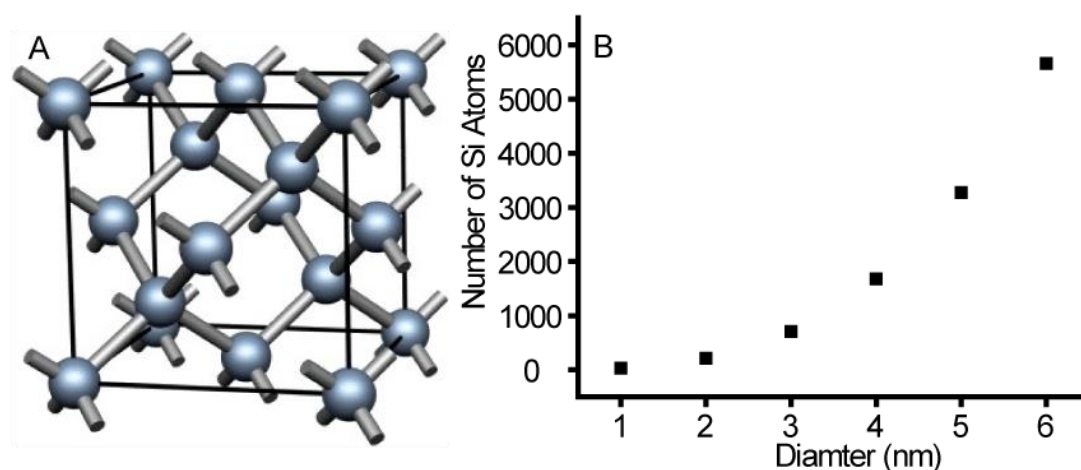


Figure 4.8 Correlation of number of silicon atoms and particle size. A: Unit cell of silicon crystal (cubic diamond). B: Correlation between number of atoms and particle size, assuming particles are spherical.

Table 2.4 Atomic percentage of alkyne modified silicon quantum dots by XPS

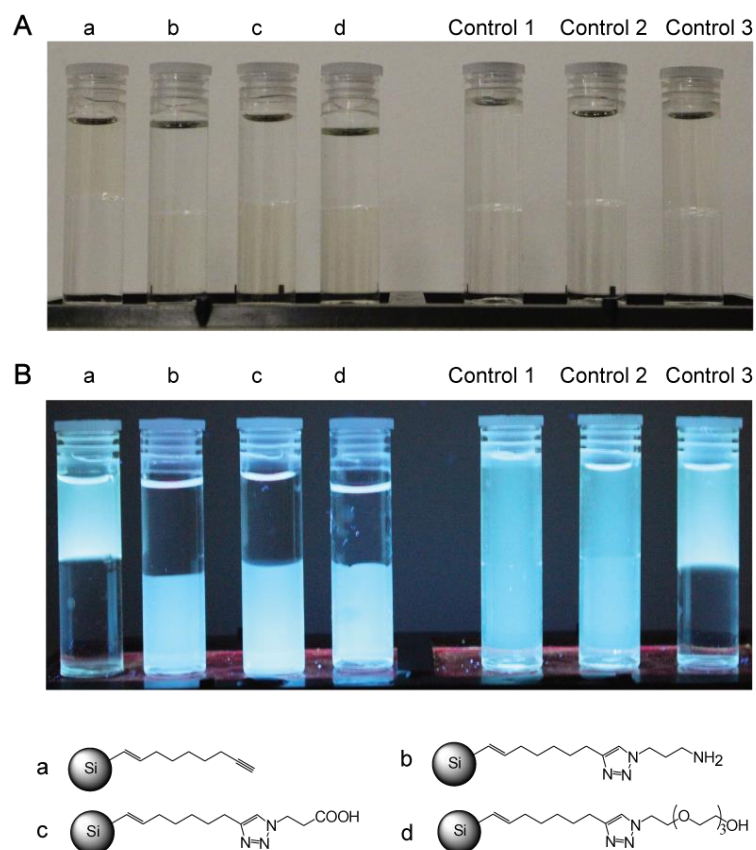
Sample	Substrate	Si %	O %	C %	Si/O Ratio	Si/C Ratio
1	In	23.39	19.97	46.6	1.1713	0.5019
2	ITO	24.97	21.53	53.5	1.1598	0.4667
3	ITO	25.23	21.65	52.9	1.1653	0.4769
Mean		24.53	21.05	51	1.1654	0.4809
S.D		0.9957	0.9377	3.8223	0.0057	0.2605

The second step is to calculate the surface coverage of the nonadiyne molecule.

For silicon nanoparticle of 4 nm in size approximately half of the atoms were

located on the surface<sup>36-41</sup>. According to the XPS results, 24% of all atoms in the sample were Si, therefore on 12% were surface Si atoms. Also, 51% of all atoms in the sample were C, which were all surface bound. Hence the surface coverage of nonadiyne molecules was  $(51/9)/12 = \sim 48\%$ . From the TEM and DLS results, silicon quantum dots synthesized had an average diameter of 3.5 nm. From the results obtained (Figure 4.8), approximately 1200 Si atoms were contained in each sphere, among which  $\sim 600$  were on the surface. Hence for silicon quantum dots synthesized with the method presented here, there are approximately  $600 \times 0.48 = 288$  nonadiyne molecules attached on the surface.

#### 4.3.2.4 Phase transfer



Control 1 No Copper; Control 2 No Sodium Ascorbate; Control 3 No Azides

Figure 4.9 Dispersivity of SiQDs in polar and nonpolar solvents changes upon the introduction

of different surface groups. Each vial contained water (bottom layer) and hexane (top layer), under (A) visible and (B) 365 nm UV excitation conditions. Control 1, no copper; control 2, no sodium ascorbate; and control 3, no azides.

For nanoparticles in general, it is known that particle dispersity in solvents is governed by the surface properties, such as the polarity of the distal moieties of the surface-modifying molecules.<sup>42</sup> In this study, it was shown that, when coated with nonpolar nonadiyne molecules, the surface of SiQDs was hydrophobic and the dots were only dispersible in nonpolar solvents, such as hexane or toluene. After functionalization with azide-bearing molecules with hydrophilic distal moieties, the surface of the dots became hydrophilic and dots were dispersible in water (Figure 3A). When controls were performed in which only two of CuSO<sub>4</sub>, sodium ascorbate, or azides were added, it was shown that some of the azide molecules adsorbed onto the particle surface (controls 1–3, Figure 4.9). Specifically, as soon as azides were added, some of the particles immediately became water-dispersible, regardless of the addition of copper or sodium ascorbate. Simply adding azides alone did not completely change the dispersity of the entire SiQDs, with some particles still remaining in the hexane phase.

### 4.3.3 Characterization of optical properties

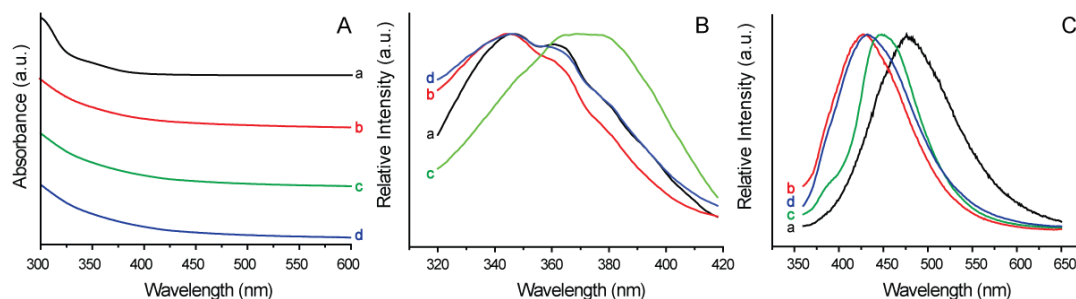


Figure 4.10 Optical properties of surface-functionalized SiQDs. (A) UV absorption spectra, (B) excitation spectra, and (C) PL emission spectra of surface-functionalized SiQDs (excitation at 350 nm): (a) SiQD–nonadiyne, (b) SiQD–NH<sub>2</sub>, (c) SiQD–COOH, and (d) SiQD–(EO)<sub>3</sub>. In panel A, spectra b–d were shifted

upward for clarity.

The absorption and PL properties of the synthesized SiQDs were measured, as shown in Figure 4.10. The particles predominantly absorbed in the UV region (Figure 4.10A) and emitted in the blue region of the visible spectrum. Although an indirect bandgap semiconductor and, therefore, not commonly considered a fluorescent material in bulk, nanoscale silicon exhibits quantum confinement and radiative recombination, in good agreement with previous reports.<sup>18,24,25,33,43,44</sup>

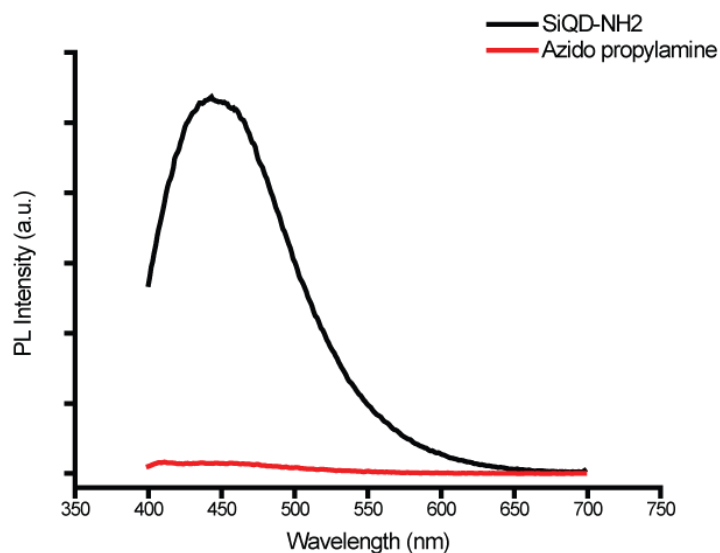


Figure 4.11 Comparison of PL between silicon quantum dots and azido-propylamine. The amine molecule is not fluorescent, indicating that the fluorescence signal observed were from the SiQDs. Excitation: 360 nm.

Since some nitrogen containing species are by themselves fluorescent, the control experiment with azido propylamine (Figure 4.11) suggested that fluorescence indeed originated from the SiQDs. The absorption profile of the particles did not change significantly upon the introduction of surface groups (Figure 4.10A); however, the emission peak maximum was blue-shifted by up to 50

nm (Figure 4.10C). This blue shift may be due to adsorbed azides inducing the surface effect, as observed by Dasog et al.,<sup>45</sup> where exposure of SiQDs to nitrogen species in the presence of oxygen induced a fluorescence blue shift<sup>36,46</sup>.

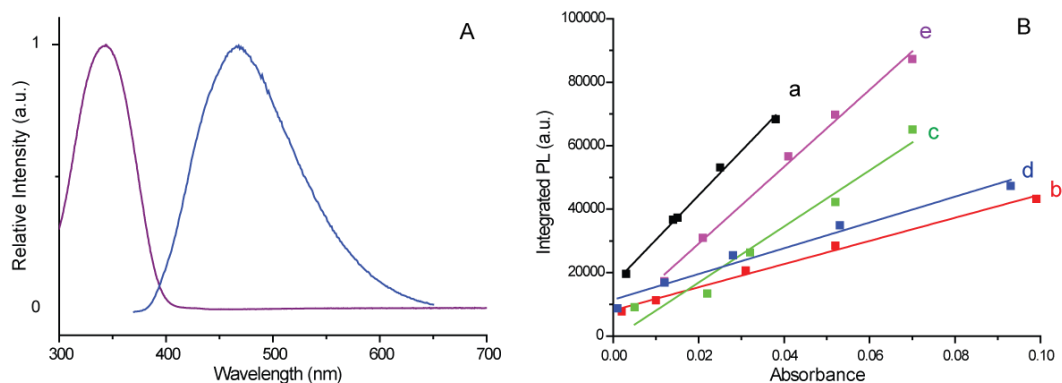


Figure 4.12 Optical properties of 4,6-diamidino-2-phenylindole (*DAPI*) (A), and determination of quantum yields ( $\Phi$ ) of SiQDs (B).

Quantum yields ( $\Phi$ ) of the surface-functionalized SiQDs were measured (Figure 4.12). Calculations are based on the Eq. 4.1, based on a reported method<sup>47,48</sup>.

$$\Phi_{\text{SiQD}} = \Phi_{\text{DAPI}} \frac{\text{Em}_{\text{QDs}}/\text{Em}_{\text{DAPI}}}{\text{Abs}_{\text{QDs}}/\text{Abs}_{\text{DAPI}}} \quad (\text{Eq. 4.1})$$

Here, DAPI was used as a reference because of its comparable absorption/emission profile to the dots (Figure 4.12A)<sup>49-52</sup>. The  $\Phi$  of alkyne-functionalized SiQDs was measured as 5.2%, with the  $\Phi$  of the click-functionalized SiQDs found to decrease to 1.4–3.3% (

Table 2.5). The observed decrease in  $\Phi$  was consistent with comparable studies of the modification of SiQDs with thiols<sup>2,53</sup>, in which additional non-radiative decay pathways were introduced by the functionalization procedures, through either surface traps and defects or vibrational energy states introduced by the

functionalization molecules<sup>54</sup>.

Table 2.5 Quantum Yield of SiQDs with Different Surface Groups

Fluorophores	Slope	Quantum Yield ( $\Phi$ )
a. SiQDs-Nonadiyne	1.40E6	5.2%
b. SiQDs-NH <sub>2</sub>	3.65E5	1.4%
c. SiQDs-COOH	8.83E5	3.3%
d. SiQDs-(EO) <sub>3</sub>	4.06E5	1.5%
e. DAPI	1.21E6	4.5%

#### 4.3.4 Photostability studies

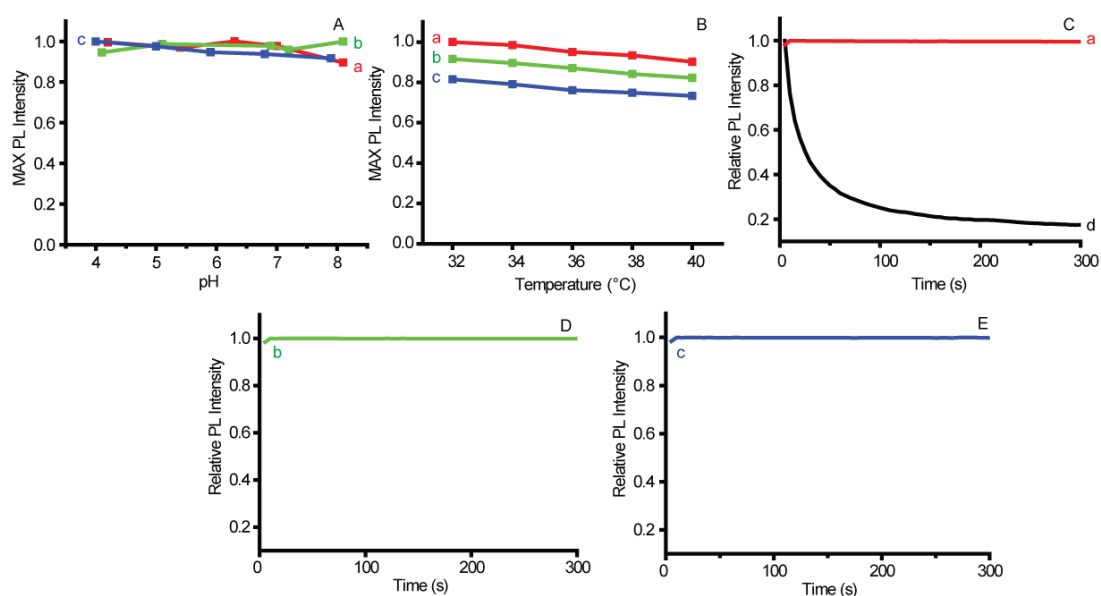


Figure 4.13 Photostability of azide-functionalized SiQDs with respect to (A) pH, (B) temperature, and (C-E) prolonged photoexcitation conditions: (a) SiQD–NH<sub>2</sub>, (b) SiQD–COOH, (c) SiQD–(EO)<sub>3</sub>, and (d) FITC. Measurements were performed in a UV reactor equipped with 4×6W UV lamps. Samples were placed directly below the lamps at a distance of ~20cm.

Photostability of the azide-functionalized SiQDs was tested with respect to pH, temperature, and constant photoexcitation conditions (Figure 4.13). It was shown that PL from SiQDs was stable in a range of physiologically relevant pH (4–8) and temperature (32–40 °C) conditions, with less than 10% of change in maximum PL

intensity observed throughout the experimental ranges. Also, in photobleaching experiments, the PL from the dots remained stable under constant photoexcitation, with less than a 2% drop in intensity after excitation for 5 min (Figure 4.13). This was in contrast to typical organic fluorophores, such as fluorescein isothiocyanate (FITC), whose PL rapidly decreased to less than 20% of the initial intensity because of photobleaching<sup>55-59</sup>. The photostability of the SiQDs (in comparison to organic dyes) was particularly notable, because the hydrosilylation of the dialkynes on the surface of the SiQDs was a UV (365 nm)-promoted process and the PL from the SiQDs was recorded after at least 15 h of constant photoexcitation. Because most organic dyes would photobleach over such a long period of excitation time, the PL of SiQDs showed much higher stability.<sup>60</sup> The demonstrated photostability of SiQDs would be strongly favored for bioimaging applications, where the loss of fluorescence because of photobleaching often hampers signal detection in fluorescence microscopy.<sup>60</sup>

#### **4.3.5 Fluorescent cellular imaging studies**

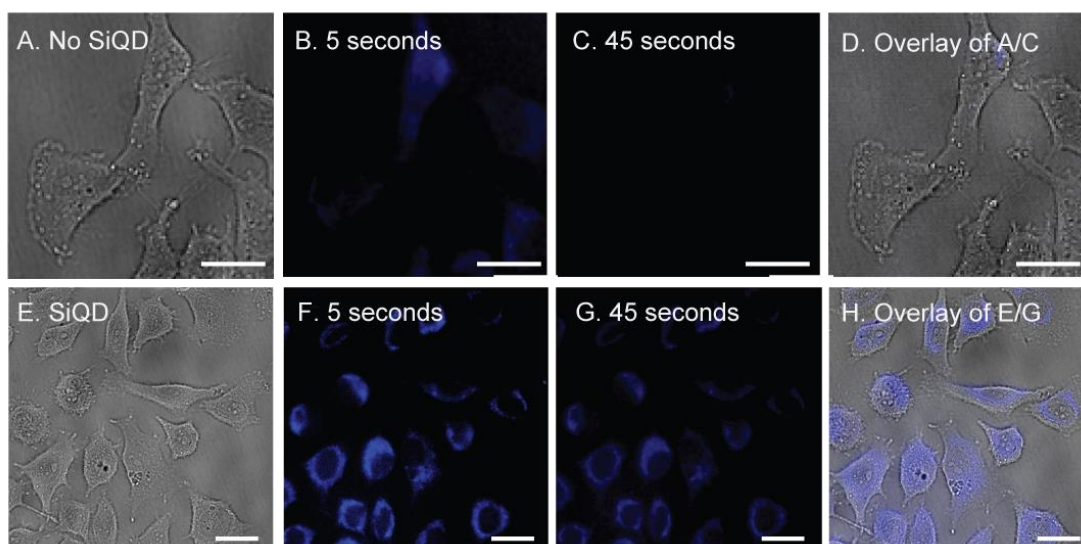


Figure 4.14 Fluorescence microscopy images show the presence of amine-modified SiQDs in HeLa cells under constant excitation. Cells were grown to at least 70% confluence and then incubated with amine-functionalized SiQDs for 2–3 h. HeLa cells were images by phase contrast and SiQDs excited at 405 nm, and fluorescence images were collected using a DAPI filter. Scale bar = 10  $\mu$ m. From A to D, control group with no SiQDs added, and from E to H, cells incubated with SiQDs. Panels A and E are bright-field images, and panels B, C, F, and G are fluorescent images with indicated excitation time.

To further demonstrate the use of surface-functionalized SiQDs for bioimaging applications, amine-functionalized SiQDs were used for *in vitro* fluorescent labeling of HeLa cells (Figure 4.14). Panels A–D show the bright-field and fluorescence imaging of HeLa cells without SiQDs as a control. From Figure 4.14C, it was seen that, after 45 s of constant excitation, the cellular autofluorescence has been photobleached. In Figure 4.14G, it was noted that because of the high photostability of the SiQDs, it was possible to photobleach the cellular autofluorescence while still maintaining emission from the SiQDs. The amine-functionalized SiQDs were observed to be distributed throughout the cytoplasm, indicating efficient uptake by HeLa cells. The ability to distinguish SiQD fluorescence from cellular autofluorescence and the uptake of QDs by cells

demonstrated the potential utility of SiQDs for cellular imaging studies, which is comparable to similar studies<sup>23</sup>. This further provided evidence that SiQDs modified by the approach reported here could be a good candidate for fluorescent cellular imaging.

#### 4.3.6 MTT toxicology studies

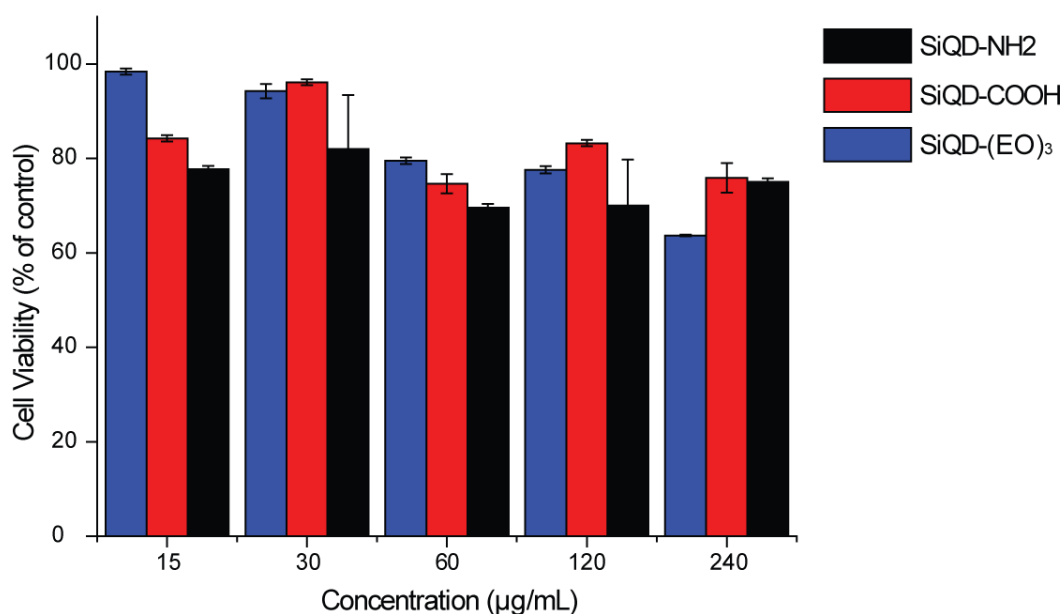


Figure 4.15 Cytotoxicity toxicity of SiQDs measured by the MTT assay. Functionalized SiQDs with different surface groups [blue, SiQD-(EO)<sub>3</sub>; red, SiQD-COOH; and black, SiQD-NH<sub>2</sub>] were incubated with HeLa cells for 24 h, and then cell viability was tested using the colorimetric MTT assay. For the control group, cells were incubated under the same conditions but without SiQDs.

The cytotoxicity of functionalized SiQDs was tested to determine whether the SiQDs would be harmful to cells when used in bioapplications. Figure 4.15 shows the results of the MTT cytotoxicity assay for different SiQD concentrations. Over the concentration range used here, a decrease of up to 20–30% in cell viability (mitochondrial activity) was observed. Even at concentrations as high as 240 µg/mL,

cellular viability remained at ~65% of the control for (EO)<sub>3</sub>-functionalized SiQDs. By comparison, the concentration of SiQDs used to acquire the fluorescence images in Figure 4.14 was 50–100 µg/mL. Hence, the functionalized SiQDs were found to possess low cytotoxicity, indicating that they would be suitable for use in cellular imaging studies.

#### 4.4 Conclusions

In this work, colloidal SiQDs were prepared by reduction of halogenated silane precursors in solution. The dots were functionalized with dialkyne molecules via UV-promoted hydrosilylation and then modified with azides via CuAAC click reaction. A combination of FT-IR, NMR and XPS techniques were used to characterize the surface of nonadiyne modified SiQDs, indicating successful grafting of the alkyne molecule with ~ 48% surface coverage rate. Attachment of azides was demonstrated via FT-IR measurements, and the functionalized SiQDs were shown to be water-soluble. The functionalized SiQDs were relatively monodisperse and showed bright blue PL under UV excitation, with quantum yields being up to 5.2%. PL of functionalized SiQDs showed good stability against photobleaching and biologically relevant pH and temperature conditions. Water-soluble SiQDs were used for fluorescent cellular imaging using HeLa cells. Cell viability studies indicated that the functionalized SiQDs possessed low cytotoxicity up to concentrations of 240 µg/mL. This work demonstrates a facile method for surface modification of SiQDs, with water-soluble surface groups amenable to bio-functionalization. We envisage wide applicability of these QDs in bio-applications

using their photostable fluorescence emission *in vitro* and potentially *in vivo*.

## 4.5 References

- (1) Shiohara, A.; Hanada, S.; Prabakar, S.; Fujioka, K.; Lim, T. H.; Yamamoto, K.; Northcote, P. T.; Tilley, R. D. Chemical Reactions on Surface Molecules Attached to Silicon Quantum Dots. *Journal of the American Chemical Society* **2010**, *132*, 248-253.
- (2) Ruizendaal, L.; Pujari, S. P.; Gevaerts, V.; Paulusse, J. M.; Zuilhof, H. Biofunctional silicon nanoparticles by means of thiol-ene click chemistry. *Chem Asian J* **2011**, *6*, 2776-2786.
- (3) Biesta, W.; van Lagen, B.; Gevaert, V. S.; Marcelis, A. T. M.; Paulusse, J. M. J.; Nielen, M. W. F.; Zuilhof, H. Preparation, Characterization, and Surface Modification of Trifluoroethyl Ester-Terminated Silicon Nanoparticles. *Chem Mater* **2012**, *24*, 4311-4318.
- (4) Cheng, X. Y.; Gondosiswanto, R.; Ciampi, S.; Reece, P. J.; Gooding, J. J. One-pot synthesis of colloidal silicon quantum dots and surface functionalization via thiol-ene click chemistry. *Chem Commun* **2012**, *48*, 11874-11876.
- (5) Kolb, H. C.; Sharpless, K. B. The growing impact of click chemistry on drug discovery. *Drug Discovery Today* **2003**, *8*, 1128-1137.
- (6) Lutz, J.-F. 1,3-Dipolar Cycloadditions of Azides and Alkynes: A Universal Ligation Tool in Polymer and Materials Science. *Angewandte Chemie International Edition* **2007**, *46*, 1018-1025.
- (7) Jewett, J. C.; Bertozzi, C. R. Cu-free click cycloaddition reactions in chemical biology. *Chem. Soc. Rev.* **2010**, *39*, 1272-1279.
- (8) Wu, P.; Feldman, A. K.; Nugent, A. K.; Hawker, C. J.; Scheel, A.; Voit, B.; Pyun, J.; Fréchet, J. M. J.; Sharpless, K. B.; Fokin, V. V. Efficiency and Fidelity in a Click-Chemistry Route to Triazole Dendrimers by the Copper(I)-Catalyzed Ligation of Azides and Alkynes. *Angewandte Chemie International Edition* **2004**, *43*, 3928-3932.
- (9) Achatz, D. E.; Mezö, G.; Kele, P.; Wolfbeis, O. S. Probing the Activity of Matrix Metalloproteinase II with a Sequentially Click-Labeled Silica Nanoparticle FRET Probe. *ChemBioChem* **2009**, *10*, 2316-2320.
- (10) Pandey, P.; Farha, O. K.; Spokoyny, A. M.; Mirkin, C. A.; Kanatzidis, M. G.; Hupp, J. T.; Nguyen, S. T. A "click-based" porous organic polymer from tetrahedral building blocks. *J Mater Chem* **2011**, *21*, 1700-1703.
- (11) Ciampi, S.; Harper, J. B.; Gooding, J. J. Wet chemical routes to the assembly of organic monolayers on silicon surfaces via the formation of Si-C bonds: surface preparation, passivation and functionalization. *Chem Soc Rev* **2010**, *39*, 2158-2183.
- (12) Gooding, J. J.; Ciampi, S. The molecular level modification of surfaces: from self-assembled monolayers to complex molecular assemblies. *Chem Soc Rev* **2011**, *40*, 2704-2718.
- (13) Guan, B.; Magenau, A.; Kilian, K. A.; Ciampi, S.; Gaus, K.; Reece, P. J.; Gooding, J. J. Mesoporous silicon photonic crystal microparticles: towards single-cell optical biosensors. *Faraday Discuss* **2011**, *149*, 301-317; discussion 333-356.
- (14) Ciampi, S.; Bocking, T.; Kilian, K. A.; James, M.; Harper, J. B.; Gooding,

J. J. Functionalization of acetylene-terminated monolayers on Si(100) surfaces: A click chemistry approach. *Langmuir* **2007**, *23*, 9320-9329.

(15) Ciampi, S.; James, M.; Michaels, P.; Gooding, J. J. Tandem "click" reactions at acetylene-terminated Si(100) monolayers. *Langmuir* **2011**, *27*, 6940-6949.

(16) Hannant, J.; Hedley, J. H.; Pate, J.; Walli, A.; Farha Al-Said, S. A.; Galindo, M. A.; Connolly, B. A.; Horrocks, B. R.; Houlton, A.; Pike, A. R. Modification of DNA-templated conductive polymer nanowires via click chemistry. *Chem Commun* **2010**, *46*, 5870-5872.

(17) Srinivasan, R.; Tan, L. P.; Wu, H.; Yang, P.-Y.; Kalesh, K. A.; Yao, S. Q. High-throughput synthesis of azide libraries suitable for direct "click" chemistry and in situ screening. *Organic & Biomolecular Chemistry* **2009**, *7*, 1821-1828.

(18) Tilley, R. D.; Yamamoto, K. The microemulsion synthesis of hydrophobic and hydrophilic silicon nanocrystals. *Advanced Materials* **2006**, *18*, 2053-2056.

(19) Warner, J. H.; Hoshino, A.; Yamamoto, K.; Tilley, R. D. Water-soluble photoluminescent silicon quantum dots. *Angew Chem Int Ed Engl* **2005**, *44*, 4550-4554.

(20) Tilley, R. D.; Warner, J. H.; Yamamoto, K.; Matsui, I.; Fujimori, H. Microemulsion synthesis of monodisperse surface stabilized silicon nanocrystals. *Chem Commun* **2005**, *0*, 1833-1835.

(21) Shiohara, A.; Hanada, S.; Prabakar, S.; Fujioka, K.; Lim, T. H.; Yamamoto, K.; Northcote, P. T.; Tilley, R. D. Chemical reactions on surface molecules attached to silicon quantum dots. *J Am Chem Soc* **2010**, *132*, 248-253.

(22) Rosso-Vasic, M.; Spruijt, E.; van Lagen, B.; De Cola, L.; Zuilhof, H. Alkyl-functionalized oxide-free silicon nanoparticles: synthesis and optical properties. *Small* **2008**, *4*, 1835-1841.

(23) Li, Q.; He, Y.; Chang, J.; Wang, L.; Chen, H.; Tan, Y.-W.; Wang, H.; Shao, Z. Surface-Modified Silicon Nanoparticles with Ultrabright Photoluminescence and Single-Exponential Decay for Nanoscale Fluorescence Lifetime Imaging of Temperature. *Journal of the American Chemical Society* **2013**, *135*, 14924-14927.

(24) Baldwin, R. K.; Pettigrew, K. A.; Ratai, E.; Augustine, M. P.; Kauzlarich, S. M. Solution reduction synthesis of surface stabilized silicon nanoparticles. *Chem Commun* **2002**, 1822-1823.

(25) Baldwin, R. K.; Pettigrew, K. A.; Garno, J. C.; Power, P. P.; Liu, G. Y.; Kauzlarich, S. M. Room temperature solution synthesis of alkyl-capped tetrahedral shaped silicon nanocrystals. *Journal of the American Chemical Society* **2002**, *124*, 1150-1151.

(26) Yang, C. S.; Bley, R. A.; Kauzlarich, S. M.; Lee, H. W. H.; Delgado, G. R. Synthesis of alkyl-terminated silicon nanoclusters by a solution route. *Journal of the American Chemical Society* **1999**, *121*, 5191-5195.

(27) Zou, J.; Baldwin, R. K.; Pettigrew, K. A.; Kauzlarich, S. M. Solution synthesis of ultrastable luminescent siloxane-coated silicon nanoparticles. *Nano Letters* **2004**, *4*, 1181-1186.

(28) Zhang, X. M.; Neiner, D.; Wang, S. Z.; Louie, A. Y.; Kauzlarich, S. M. A new solution route to hydrogen-terminated silicon nanoparticles: synthesis,

functionalization and water stability. *Nanotechnology* **2007**, *18*.

(29)Shiohara, A.; Prabakar, S.; Faramus, A.; Hsu, C. Y.; Lai, P. S.; Northcote, P. T.; Tilley, R. D. Sized controlled synthesis, purification, and cell studies with silicon quantum dots. *Nanoscale* **2011**, *3*, 3364-3370.

(30)Mayeri, D.; Phillips, B. L.; Augustine, M. P.; Kauzlarich, S. M. NMR Study of the Synthesis of Alkyl-Terminated Silicon Nanoparticles from the Reaction of SiCl<sub>4</sub> with the Zintl Salt, NaSi. *Chem Mater* **2001**, *13*, 765-770.

(31)Atkins, T. M.; Cassidy, M. C.; Lee, M.; Ganguly, S.; Marcus, C. M.; Kauzlarich, S. M. Synthesis of Long T-1 Silicon Nanoparticles for Hyperpolarized Si-29 Magnetic Resonance Imaging. *Acs Nano* **2013**, *7*, 1609-1617.

(32)Hua, F.; Swihart, M. T.; Ruckenstein, E. Efficient surface grafting of luminescent silicon quantum dots by photoinitiated hydrosilylation. *Langmuir* **2005**, *21*, 6054-6062.

(33)Li, X. G.; He, Y. Q.; Swihart, M. T. Surface functionalization of silicon nanoparticles produced by laser-driven pyrolysis of silane followed by HF-HNO<sub>3</sub> etching. *Langmuir* **2004**, *20*, 4720-4727.

(34)Veinot, J. G. Synthesis, surface functionalization, and properties of freestanding silicon nanocrystals. *Chem Commun (Camb)* **2006**, 4160-4168.

(35)Ondic, L.; Kusova, K.; Ziegler, M.; Fekete, L.; Gartnerova, V.; Chab, V.; Holy, V.; Cibulka, O.; Herynkova, K.; Gallart, M.; Gilliot, P.; Honerlage, B.; Pelant, I. A complex study of the fast blue luminescence of oxidized silicon nanocrystals: the role of the core. *Nanoscale* **2014**, *6*, 3837-3845.

(36)Chen, X.; Pi, X.; Yang, D. Bonding of Oxygen at the Oxide/Nanocrystal Interface of Oxidized Silicon Nanocrystals: An Ab Initio Study. *The Journal of Physical Chemistry C* **2010**, *114*, 8774-8781.

(37)Ma, Y.; Pi, X.; Yang, D. Fluorine-Passivated Silicon Nanocrystals: Surface Chemistry versus Quantum Confinement. *The Journal of Physical Chemistry C* **2012**, *116*, 5401-5406.

(38)Wang, R.; Pi, X.; Yang, D. Surface modification of chlorine-passivated silicon nanocrystals. *Physical Chemistry Chemical Physics* **2013**, *15*, 1815-1820.

(39)Wang, J.; Sun, S.; Peng, F.; Cao, L.; Sun, L. Efficient one-pot synthesis of highly photoluminescent alkyl-functionalised silicon nanocrystals. *Chem Commun (Camb)* **2011**, *47*, 4941-4943.

(40)Ma, Y.; Chen, X.; Pi, X.; Yang, D. Lightly boron and phosphorus co-doped silicon nanocrystals. *J Nanopart Res* **2012**, *14*, 1-7.

(41)Chen, X.; Pi, X.; Yang, D. Critical Role of Dopant Location for P-Doped Si Nanocrystals. *The Journal of Physical Chemistry C* **2010**, *115*, 661-666.

(42)Yin, Y.; Alivisatos, A. P. Colloidal nanocrystal synthesis and the organic-inorganic interface. *Nature* **2005**, *437*, 664-670.

(43)Hessel, C. M.; Henderson, E. J.; Veinot, J. G. C. Hydrogen silsesquioxane: A molecular precursor for nanocrystalline Si-SiO<sub>2</sub> composites and freestanding hydride-surface-terminated silicon nanoparticles. *Chem Mater* **2006**, *18*, 6139-6146.

(44)Pi, X. D.; Mangolini, L.; Campbell, S. A.; Kortshagen, U. Room-temperature atmospheric oxidation of Si nanocrystals after HF etching. *Phys Rev B* **2007**, *75*, 085423.

- (45) Dasog, M.; Yang, Z.; Regli, S.; Atkins, T. M.; Faramus, A.; Singh, M. P.; Muthuswamy, E.; Kauzlarich, S. M.; Tilley, R. D.; Veinot, J. G. C. Chemical Insight into the Origin of Red and Blue Photoluminescence Arising from Freestanding Silicon Nanocrystals. *ACS Nano* **2013**, *7*, 2676-2685.
- (46) Wang, R.; Pi, X. D.; Yang, D. R. First-Principles Study on the Surface Chemistry of 1.4 nm Silicon Nanocrystals: Case of Hydrosilylation. *J Phys Chem C* **2012**, *116*, 19434-19443.
- (47) Skillman, J. B. Quantum yield variation across the three pathways of photosynthesis: not yet out of the dark. *J Exp Bot* **2008**, *59*, 1647-1661.
- (48) Brouwer, A. M. Standards for photoluminescence quantum yield measurements in solution (IUPAC Technical Report). *Pure Appl Chem* **2011**, *83*, 2213-2228.
- (49) Dixon, J. M.; Taniguchi, M.; Lindsey, J. S. PhotochemCAD 2: A Refined Program with Accompanying Spectral Databases for Photochemical Calculations. *Photochemistry and Photobiology* **2005**, *81*, 212-213.
- (50) Du, H.; Fuh, R. C. A.; Li, J. Z.; Corkan, L. A.; Lindsey, J. S. PhotochemCAD: A computer-aided design and research tool in photochemistry. *Photochemistry and Photobiology* **1998**, *68*, 141-142.
- (51) Hard, T.; Fan, P.; Kearns, D. R. A fluorescence study of the binding of hoechst 33258 and DAPI to halogenated DNAs. *Photochemistry and Photobiology* **1990**, *51*, 77-86.
- (52) Hard, T.; Fan, P.; Kearns, D. R. A Fluorescence Study of the Binding of Hoechst-33258 and Dapi to Halogenated Dnas. *Photochemistry and Photobiology* **1990**, *51*, 77-86.
- (53) Cheng, X.; Gondosiswanto, R.; Ciampi, S.; Reece, P. J.; Gooding, J. J. One-pot synthesis of colloidal silicon quantum dots and surface functionalization via thiol-ene click chemistry. *Chem Commun (Camb)* **2012**, *48*, 11874-11876.
- (54) Mastronardi, M. L.; Henderson, E. J.; Puzzo, D. P.; Ozin, G. A. Small Silicon, Big Opportunities: The Development and Future of Colloidally-Stable Monodisperse Silicon Nanocrystals. *Advanced Materials* **2012**, *24*, 5890-5898.
- (55) Gaponik, N.; Talapin, D. V.; Rogach, A. L.; Hoppe, K.; Shevchenko, E. V.; Kornowski, A.; Eychmuller, A.; Weller, H. Thiol-capping of CdTe nanocrystals: An alternative to organometallic synthetic routes. *J. Phys. Chem. B* **2002**, *106*, 7177-7185.
- (56) Zhong, Y.; Peng, F.; Bao, F.; Wang, S.; Ji, X.; Yang, L.; Su, Y.; Lee, S.-T.; He, Y. Large-Scale Aqueous Synthesis of Fluorescent and Biocompatible Silicon Nanoparticles and Their Use as Highly Photostable Biological Probes. *Journal of the American Chemical Society* **2013**.
- (57) Derfus, A. M.; Chan, W. C. W.; Bhatia, S. N. Probing the cytotoxicity of semiconductor quantum dots. *Nano Letters* **2004**, *4*, 11-18.
- (58) Zhu, Z. J.; Yeh, Y. C.; Tang, R.; Yan, B.; Tamayo, J.; Vachet, R. W.; Rotello, V. M. Stability of quantum dots in live cells. *Nat Chem* **2011**, *3*, 963-968.
- (59) Kim, M.; Yoda, M. Using Quantum Dots for Liquid-Phase Thermometry at near-Infrared Wavelengths in Silicon Devices. *Proceedings of the Asme International Heat Transfer Conference - 2010, Vol 4* **2010**, 75-81.

(60)Gao, X. H.; Yang, L. L.; Petros, J. A.; Marshal, F. F.; Simons, J. W.; Nie, S. M. In vivo molecular and cellular imaging with quantum dots. *Curr. Opin. Biotechnol.* **2005**, *16*, 63-72.

**Chapter 5 Fluorescence imaging microscopy (FLIM)  
of silicon quantum dots (SiQDs)**

## 5.1 Introduction

As discussed in previous chapters, considerable efforts have been made towards the preparations and applications of SiQDs since their discovery<sup>1-10</sup>, but challenges still remain. The first is the limited choice of colour for solution-based methods of preparation. Although colloidal synthesis is the preferred method of fabrication due to its simplicity, a major downside of the current bottom-up solution methods is that only blue-green SiQDs can be made<sup>7,11</sup>. In fact, SiQDs emitting in the red end of the spectrum are obtainable only by laser, plasma or etching based processes, where high temperature, complicated instrumentations or highly toxic materials such as hydrofluoric acid (HF) are used<sup>1,12-14</sup>. It has been shown that the interaction of the SiQDs surfaces with nitrogen containing species, for instance surfactant molecules which were used in many surface modification routes<sup>15-17</sup>, inevitably leads to blue emitting SiQDs regardless of their colour prior to modification<sup>18</sup>. This blue-shift of emission is likely to be associated with surface mediated radiative pathways<sup>18</sup>, possibly because of the absence of a lattice matched barrier layer as seen in CdS/ZnS quantum dots. This has led to a second challenge of using SiQDs for bio-imaging, which is the signal overlap with tissue scattering and biological autofluorescence due to the requirement for a short (UV to near UV) wavelength of excitation light<sup>19,20</sup>. The presence of background signals can cause difficulties in the distinction of signals from the blue SiQDs and thus has greatly limited their use in biological contexts. Furthermore, long term exposure time is often needed for tracking of fluorescent species, and excitation in the UV to near UV region can damage cellular structures.

In this chapter, a completely different strategy to resolve the issues is demonstrated. This strategy focuses on advanced microscopy (Figure 5.1). Specifically, fluorescence lifetime

imaging microscopy (FLIM) is used to deconvolute the signals of SiQDs from background signals. Although multi-photon excitation has been shown to be able to excite SiQDs<sup>21,22</sup>, there are still limited examples of applying such laser sources in intracellular contexts and to our knowledge there is no demonstration for two-photon FLIM for colloidal SiQDs. Here, two-photon excitation with FLIM is used to avoid the high energy excitation associated with the one-photon laser sources. Finally, the SiQDs were conjugated to a dye acceptor to produce SiQDs with different colours as a result of Förster Resonance Energy Transfer (FRET) demonstrated with FLIM measurements.

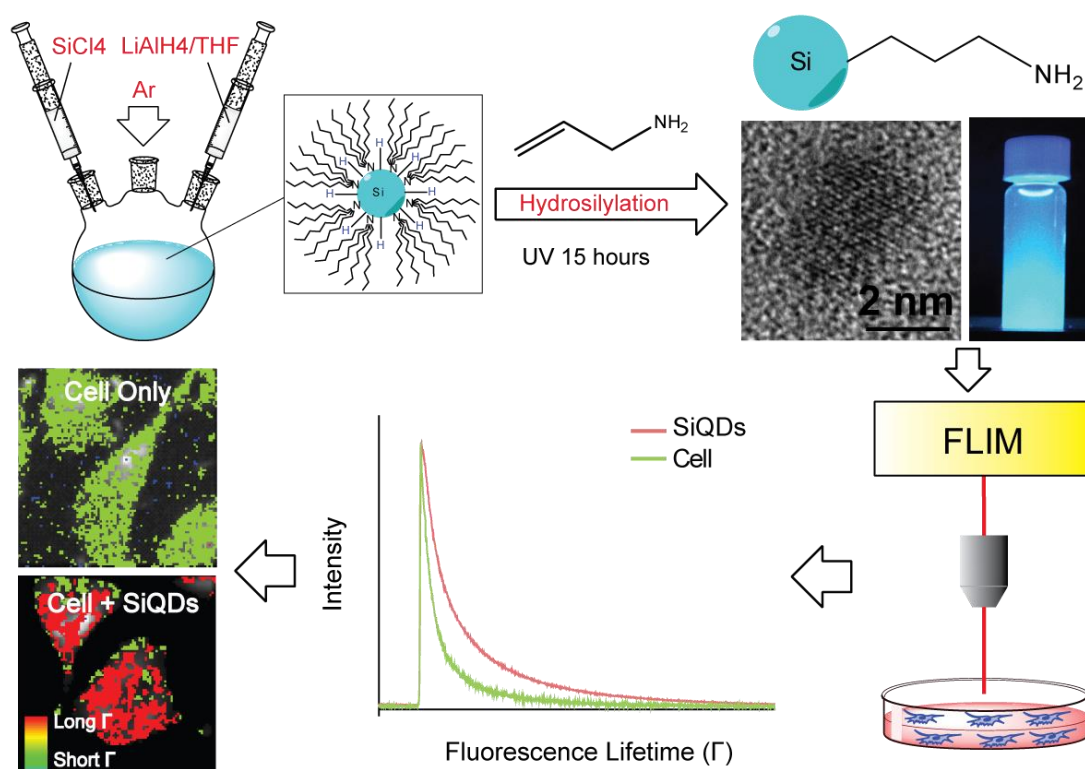
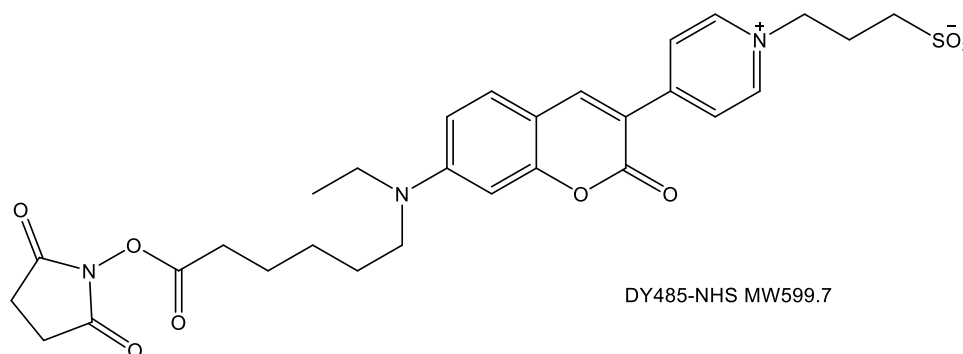


Figure 5.1 Schematic for FLIM imaging of silicon quantum dots (SiQDs). Photoluminescent SiQDs were synthesized in the solution phase via reduction of silane precursors. The obtained SiQDs were used for the fluorescent imaging of HeLa cells. The SiQDs have a longer fluorescence lifetime than the typical cellular autofluorescence, which can be used to deconvolute the FLIM signals.

## 5.2 Methods and Materials

### 5.2.1 Chemicals and Materials

All chemicals and solvent used were obtained and prepared as described in chapter 2 unless otherwise stated. The organic dye acceptor DY485-NHS was purchased from Dyomics (GmbH) with the following structure:



### 5.2.2 Synthesis and purification of allylamine modified silicon quantum dots

Hydrogen terminated SiQDs were prepared as described in chapter 2. Surface modification and purification were prepared using procedures as described in chapter 2, using ~4 mL of allylamine ( $5.3 \times 10^{-2}$  mol) added per 100 mL of solution.

### 5.2.3 Preparation of SiQDs–DY485 conjugate for FRET measurements

To prepare SiQDs-DY485 conjugates for FRET measurements, a solution of 10 mg/mL of allylamine functionalized SiQDs were prepared in 1×PBS at pH 7.2. NHS activated dye was stored in dry form at  $-20$  °C and a 10 mM solution was prepared in dry DMF immediately before use. Different amount of dye was added to surface functionalized SiQDs to reach the desired concentration, and the reaction was left for 2 hours before FLIM measurements.

#### **5.2.4 Characterization of morphology**

Morphology and size distribution of silicon quantum dots were characterized by transmission electron microscopy (TEM) measurements as described in chapter 2.

#### **5.2.5 Characterization of optical properties**

Optical properties of synthesized silicon quantum dots, including UV-Vis absorption spectra, photoluminescence (PL) and photoluminescence excitation spectra were characterized as described in chapter 2.

#### **5.2.6 Preparation of HeLa cell samples**

Preparation of HeLa cell cultures for all imaging experiments was performed as described in chapter 2.

#### **5.2.7 Fluorescent lifetime imaging microscopy (FLIM)**

FLIM was performed on a Microtime 200 microscope (PicoQuant, GmbH). Lifetime images were recorded using a 60 $\times$ , 1.2 NA water-immersion objective (Olympus). Single photon excitation was conducted *via* a fiber coupled, picosecond pulsed diode laser operating at 405 nm for picosecond pulsed excitation and two-photon excitation was performed at wavelength of 740 nm and 800 nm. The wavelength of the band pass filters used were: 435 nm, 447 nm, 483 nm, 510 nm, 525 nm, 585 nm, 617 nm and 690 nm.

For the one and two-photon FLIM experiments the emission was collected

using a 450 nm long-pass filter and a single photon avalanche diode (PDM, Microphoton Devices, for a ‘stop’ signal) connected to time correlated single-photon counting electronics (PicoHarp 300, Picoquant, for a ‘start’ signal). For the one-photon FLIM-FRET experiment the fluorescence signal was directed through a 538 nm beam splitter, and the donor and acceptor signal split between two single-photon avalanche diodes with the following bandwidth filters in front of each: 460/40 nm, 585/40 respectively. Atto 425 was used to calibrate the phasor plot to a monoexponential lifetime of 3.6 ns. The data was acquired and analyzed using SymphoTime (PicoQuant, GmbH) and phasor analysis performed using SimFCS (Laboratory of Fluorescence Dynamics, University of California at Irvine, downloadable from [www.lfd.uci.edu](http://www.lfd.uci.edu)).

### 5.2.8 FLIM data analysis and phasor transformation

Fitting the data using a 3-component exponential was performed using Picoquant software.

The phasor analysis of FLIM data was performed using SimFCS with a published method<sup>24</sup>.

As the experiments were performed in the time domain, the  $s$  (vertical) and  $g$  (horizontal) coordinates in the phasor plot corresponding to a decay  $I(t)$  were given as:

$$g_{i,j}(\omega) = \int_0^{\infty} I_{i,j}(t) \cos(\omega t) dt / \int_0^{\infty} I_{i,j}(t) dt \quad (\text{Eq. 5.1})$$

$$s_{i,j}(\omega) = \int_0^{\infty} I_{i,j}(t) \sin(\omega t) dt / \int_0^{\infty} I_{i,j}(t) dt \quad (\text{Eq. 5.2})$$

Where  $\omega$  is the angular frequency of the laser repetition,  $i$  and  $j$  define a pixel of the FLIM image. Hence in the case if the decay curve is single exponential, the coordinates of the phasor are given by:

$$g_{i,j}(\omega) = \frac{1}{1+(\omega\tau)^2} \quad (\text{Eq. 5.3})$$

$$s_{i,j}(\omega) = \frac{\omega\tau}{1+(\omega\tau)^2} \quad (\text{Eq. 5.4})$$

In the case when several exponential components are present, the coordinates of the phasor at pixel (i, j) were given by:

$$g_{i,j}(\omega) = \sum_k \frac{f_k}{1+(\omega\tau_k)^2} \quad (\text{Eq. 5.5})$$

$$s_{i,j}(\omega) = \sum_k \frac{f_k\omega\tau_k}{1+(\omega\tau_k)^2} \quad (\text{Eq. 5.6})$$

Where  $f_k$  is the intensity weighted fractional contribution of the components.  $\tau_k$  is the lifetime. For single exponential decay,  $f_k = 1$ . By this way, all single exponential phasors are represented by a semicircle with centre at (1/2, 0) and radius 1/2 on the phasor plot, namely the universal circle, and phasors with multi-exponential components are located within the universal circle. A phasor of short lifetime is close to the bottom right corner (1,0), and a phasor of long lifetime is close to the bottom left corner (0,0). To resolve the fractional contributions of two phasor components in a cluster Eq. 5.5 and Eq. 5.6 are graphically solved.

### 5.2.9 Calculation of FRET efficiency and Förster distance

The FRET efficiency was defined based on the following relationship:

$$E = 1 - \frac{\tau}{\tau_{donor}} \quad (\text{Equ. 5.7})$$

Instead of directly measuring the fluorescence lifetime of the donor/acceptor, in this chapter, FRET efficiencies were calculated graphically from the phasor plot. For instance, when the lifetime of the SiQDs (donor) was changed upon interaction with the dye molecule (acceptor), the realization of all possible FRET phasors with the different efficiencies was described with a curved trajectory in the phasor plot (black curve in Figure 5.8D-H for an example). The experimental position of the phasor of a given pixel was then plotted directly onto the trajectory to determine

the FRET efficiency. The contributions of the background and of the donor without acceptor were evaluated using the rule of the linear combination (Eq. 5.5 and Eq. 5.6), where the background phasor and the donor alone (SiQDs alone) were recorded in independent measurements under comparable conditions to FRET studies of molecular species<sup>26</sup>.

The FRET efficiency depends on the distance between donor and acceptor:

$$E = \frac{1}{1+(r/R_0)^6} \quad (\text{Equ. 5.8}), \text{ where:}$$

E = FRET efficiency

r = distance between the donor and acceptor

R<sub>0</sub> = Förster distance

The Förster distance is determined by the following relationship:

$$R_0 = 0.211 * [\kappa^2 n^{-4} Q_D \int_0^\infty F_D(\lambda) \epsilon_A(\lambda) \lambda^4 d\lambda]^{1/6} \quad (\text{Equ. 5.9}), \text{ where}$$

$\kappa$  = dipole orientation factor,  $\kappa^2 \approx 2/3$  for randomly oriented molecules

n = refractive index of the medium ( n = 1.33 for H<sub>2</sub>O)

Q<sub>D</sub> = quantum yield of the donor (between 0 – 100 %)

F<sub>D</sub>( $\lambda$ ) = normalized emission spectrum of the donor (unit: none)

$\epsilon_A(\lambda)$  = wavelength dependent extinction coefficient of the acceptor (unit: M<sup>-1</sup>\*cm<sup>-1</sup>)

1)

Within the universal circle. A phasor of short lifetime is close to the bottom right corner (1,0), and a phasor of long lifetime is close to the bottom left corner (0,0).

To resolve the fractional contributions of two phasor components in a cluster Eq.

5.5 and Eq. 5.6 are graphically solved.

## 5.3 Results and Discussions

### 5.3.1 Characterization of allylamine modified SiQDs

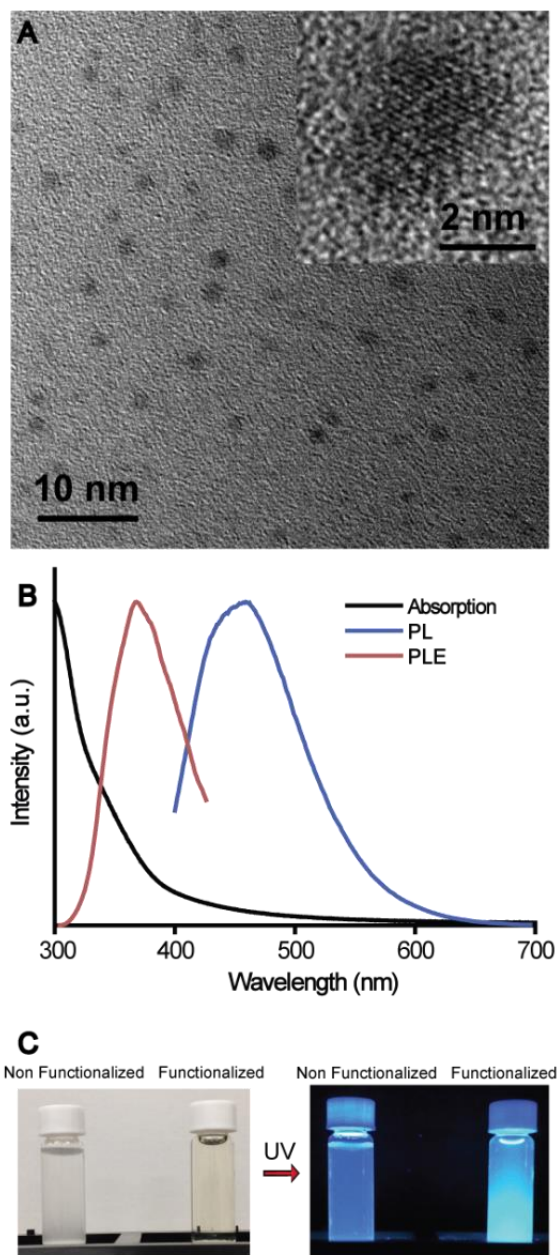


Figure 5.2 Characterization of colloidal SiQDs synthesized in the solution phase. Synthesized nanoparticles were characterized by TEM (A). Optical properties (B) of the particles were characterized in respect to absorption (black), photoluminescence (PL) with excitation wavelength at 375 nm and photoluminescence excitation (PLE) measurements. After functionalization with surface molecules, particles emitted strong blue luminescence under UV excitation (C).

Colloidal SiQDs used for FLIM studies were prepared in the solution phase<sup>4,11,15,16,27,28</sup>. In brief, the SiQDs were synthesized by reacting surfactants (tetraoctylammonium bromide, TOAB) stabilized silane precursors ( $\text{SiX}_4$ , X = Cl or Br) with lithium aluminium hydride ( $\text{LiAlH}_4$ ). The process was performed in dry toluene under inert condition with strict removal of oxygen and water to avoid surface oxidation. The resulting crystalline SiQDs were formed inside the reverse micelles in a uniform manner. The initial Si-H surface of the SiQDs is prone to oxidation, so the nanoparticles were then modified with unsaturated amine terminated molecules via UV promoted hydrosilylation to produce surface passivated particles. The crude product was purified by size-exclusion chromatography, and the resulting blue-luminescent SiQDs showed an average diameter of  $2.5 \pm 0.7$  nm based on the TEM results (Figure 5.2). The lattice fringes within the particles were clearly observable from the high-resolution images, suggesting the crystalline nature of the particles (Figure 5.2A). The synthesized SiQDs absorb predominantly in the UV end of the spectrum, with a broad blue emission peak observed at  $\sim 460$  nm (FWHM  $\sim 90$  nm) and excitation peak at 370 nm (Figure 5.2B). After surface modifications, SiQDs became dispersible in polar solvents such as phosphate buffer saline (PBS) or water, which was in contrast to a cloudy dispersion in those solvents for non-modified particles (Figure 5.2C).

### **5.3.2 One-photon FLIM of HeLa cells incubated with SiQDs**

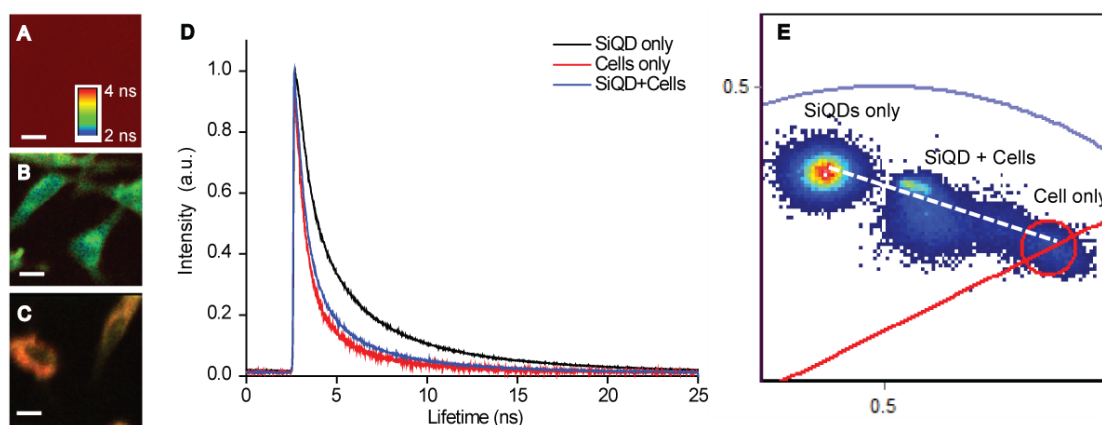


Figure 5.3 One-photon FLIM imaging (excitation wavelength: 405 nm) and phasor approach of data analysis using HeLa cells incubated with SiQDs. From A-C, FLIM images of (A) SiQDs alone, (B) HeLa cells alone and (C) HeLa cells incubated with SiQDs. Autofluorescence from the cells with short lifetime ( $< 2.5$  ns) were pseudo coloured in green, whereas signals with longer lifetime ( $> 4$  ns) due to the presence of the SiQDs were pseudo coloured in red. Scale Bar:  $10\ \mu\text{m}$ . (D). The lifetime decay curves showing the lifetime of SiQDs alone, cells alone and combination of the two, which are difficult to distinguish. (E) As contrast, lifetime distributions in each image were transformed to a single phasor diagram, where the *cos* and *sin* component of the decay were used as the vertical and horizontal axis respectively. The resulting phasor plot indicating the phasor of the SiQDs emission could be resolved from the autofluorescence of the cells. Upon incubation with SiQDs, cells gave rise to a lifetime distribution as a linear combination of the two terminal phasors.

The prepared amine functionalized SiQDs were used to label HeLa cells for FLIM imaging (Figure 5.3). The cellular autofluorescence exhibited much shorter lifetime ( $< 2.5$  ns) in comparison with the SiQDs ( $> 4$  ns). Although the brightness of the SiQDs was inadequate to be distinctive from autofluorescence of the cells by intensity based imaging methods (Figure 5.4), this problem can be avoided using FLIM where deconvoluted images could be obtained (Figure 5.3A-C). For instance, in (C), although the autofluorescence of the cell is still present, the lifetime signals of the SiQDs were sufficient to cover the background signals therefore the ‘green’ colour can be hardly seen.

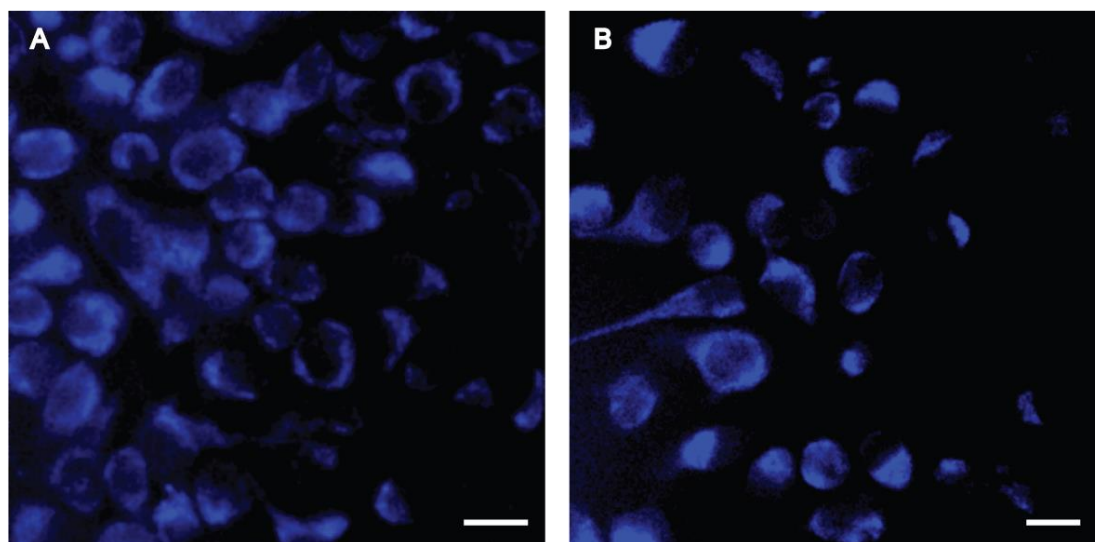


Figure 5.4 Fluorescence image of HeLa cells incubated with SiQDs. (A) HeLa cells alone and (B) after incubation with SiQDs for 2 hours. The autofluorescence from the cell affected signal detection of the nanoparticles due to their comparable blue colour, although the influence could be reduced by constant excitation<sup>28</sup>. Images were taken with a Zeiss Axiovert 200M inverted microscope fitted with a 20 $\times$ , 40 $\times$  or 60 $\times$  immersion objective and a DAPI filter with excitation at 405 nm. Scale Bar: 10  $\mu$ m.

In cellular FLIM images, the signal from each pixel typically contains multiple fluorescent species, with each species being single or multi-exponential. In a typical FLIM experiment only limited photons are collected, usually in the range of 500-1000 per pixel. This is often not enough to separate these decay components, and fitting the exponential decay, such as seen in Figure 5.3D has its own challenges. To overcome this limitation, the histograms of the time delays in each pixel in the FLIM images were Fourier-transformed onto a phasor diagram, where the *cos* and *sin* components of the decay in each pixel was plotted as the vertical and horizontal coordinates<sup>24</sup> (Figure 5.3E). In the phasor plot, three distinctive phasor clusters corresponding to SiQDs, cellular autofluorescence and combination of the two were seen. The resolution of the phasors depends on the photon counts per pixel and diversity of the decay

components. After incubating with the nanoparticles, the phasors spread in a larger area compared with the cells alone probably due to the extra diversity in decay components. The phasor corresponding to the combination of signals was located in the middle of a straight line connecting the other two phasor clusters (Figure 5.3D, dashed line). Since signals from both the cellular autofluorescence and SiQDs co-existed in the same pixel, and no fluorescence was detected outside of the cell, this indicated that fluorescence observed in Figure 5.3C was indeed a combination of signals from both the SiQDs and cellular autofluorescence, with no energy transfer process occurring.

### 5.3.3 Analysis of lifetime components of allylamine modified SiQDs

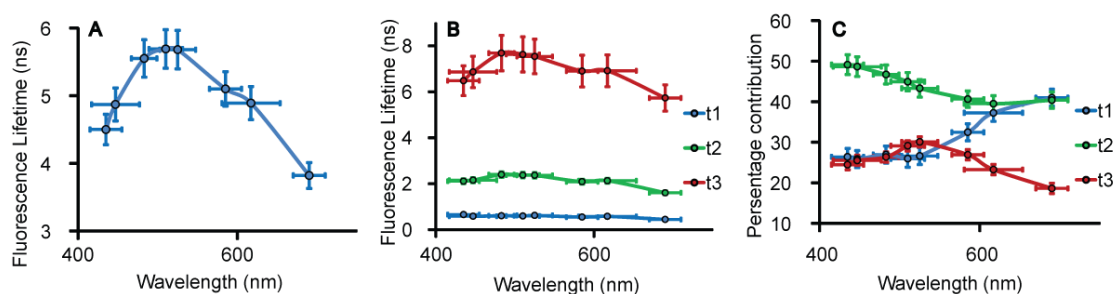


Figure 5.5 Analysis of the FLIM decay components by 3-component exponential fitting. The mean lifetime (A) of the three fitted component was expressed as a function of emission wavelength. These decay components (B) and their relative contributions (C) were graphed in relation to the emission wavelength. Horizontal bars reflect the emission filter pass width used during the measurements.

For a particular fluorophore that has multiple lifetime components, the contribution of each component gives important insights to the status of the fluorophore and its environments<sup>23-25,29</sup>. In this case, analysis of the various lifetime components was performed by fitting the decay curve (Figure 5.5). Here, three distinct components of SiQDs were found to best fit to the data (Figure 5.5B-C), with a fast decay of <math><1\text{ ns}</math> (~30 %), a medium decay of ~2.2 ns (~40 %) and a

slow decay of  $>6$  ns ( $\sim 30\%$ ). The photoluminescence kinetics of quantum dots is primarily governed by the radiative and non-radiative pathways that an exciton undergoes to achieve electron-hole recombination. The observed different decay components were associated with their corresponding radiative recombination pathways. As silicon is an indirect band-gap semiconductor and in this case, a lattice matched barrier structure as used in CdSe/ZnS quantum dots is absent, these radiative pathways were more likely to be associated with surface mediated transition rather than simply by quantum confinement<sup>30,31</sup>. In practice, as both of the fast and medium lifetime components could be filtered by time-gated acquisition steps, for imaging purposes, the PL signals from SiQDs could be obtained distinctively without the interference of the background noise.

#### 5.3.4 Two-photon FLIM of HeLa cells incubated with SiQDs

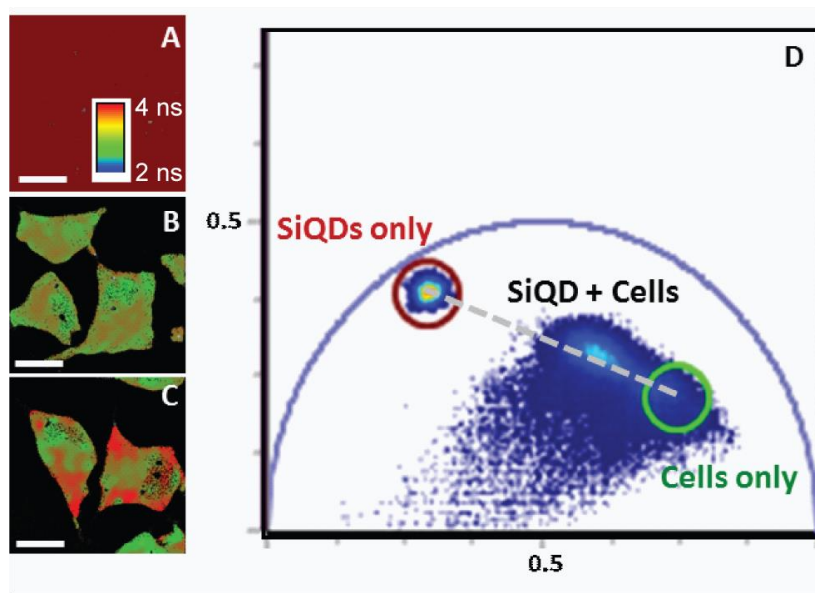


Figure 5.6 Two-photon FLIM imaging (excitation wavelength in A-D and H-J: 800 nm in E-G: 740 nm) and phasor analysis of HeLa cells incubated with SiQDs. From A-C, (A) SiQDs alone, (B) HeLa cells alone and (C) HeLa cells labelled with SiQDs. (D) Lifetime distribution of the experiments presented in (A)-(C) transformed into the phasor plot are similarly to the one-photon experiment presented in Figure 5.3. The auto-fluorescent signal of the cells only (B) can be

resolved from the SiQDs emission (A) in cells incubated with SiQDs (C), where the lifetime distribution that is a linear combination of the signals from the cells and SiQDs only. Autofluorescence were pseudo coloured in green, whereas fluorescence from the SiQDs was pseudo coloured in red. Scale Bar: 10  $\mu\text{m}$ .

Figure 5.6 shows the two-photon FLIM images and the phasor plot of SiQDs, cellular autofluorescence and combination of the two. Similar to the one-photon data shown above, SiQDs exhibited much longer fluorescence lifetime compared with their biological background (Figure 5.6, A-C). Three distinct phasor clusters were observed (Figure 5.6D), where combination of the signals were located in the middle of a straight line connecting the SiQDs and autofluorescence. Similar to the one-photon FLIM studies, the linear combination of signals suggested no energy transfer process in the system. It was noted that when two-photon excitation at 740 nm was used, cellular autofluorescence still influenced signal detection and differentiation of phasor clusters were not obvious (Figure 5.7A-C). However, excitation at longer wavelength (800 nm) favoured excitation of the SiQDs, with almost no autofluorescence observed (Figure 5.7D-F). In addition, it was evident from both one and two-photon FLIM experiments that SiQDs were located throughout the cytoplasm with no signal detected inside the nucleus, indicating that SiQDs did not pass through the nuclear membrane.

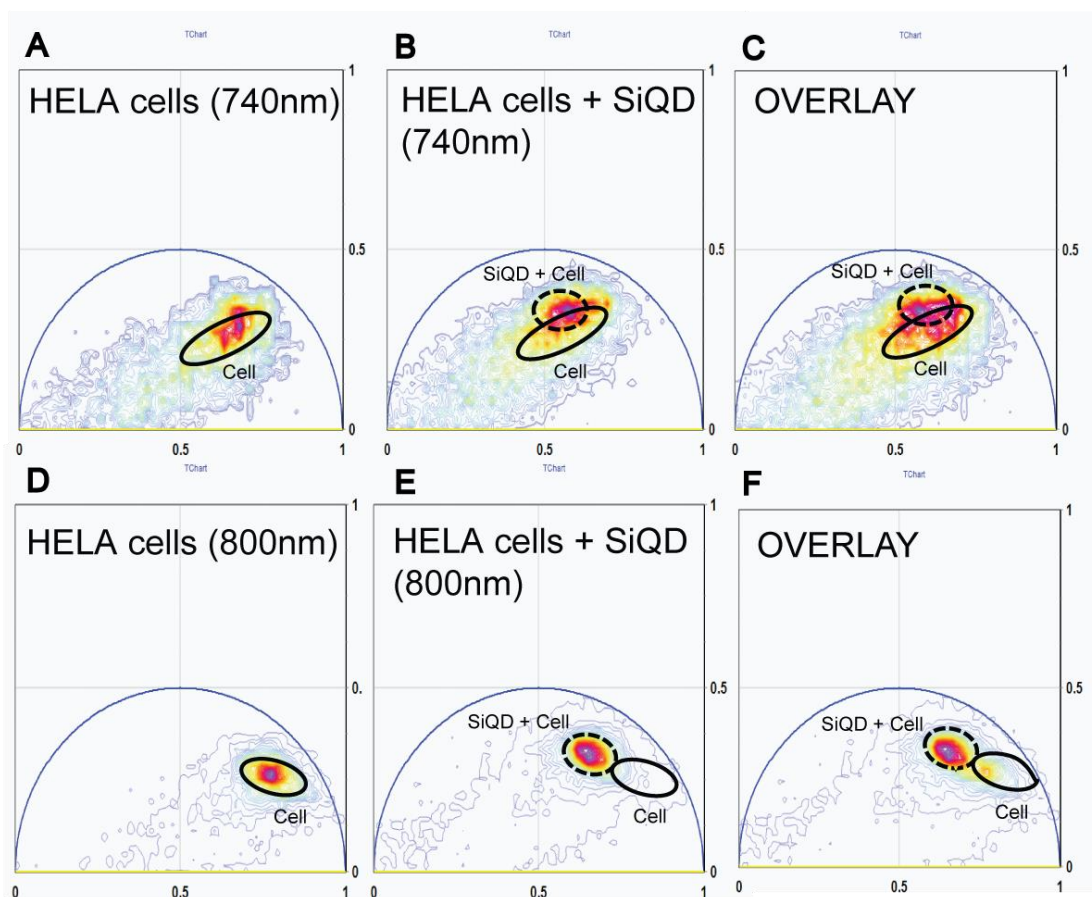


Figure 5.7 Comparison of two-photon FLIM results using 740 nm and 800 nm excitations. A-C: Phasor diagrams using excitation source of 740 nm, where autofluorescence is still present. D-F: Phasor diagrams using excitation source of 800 nm, where cellular autofluorescence is almost completely removed.

The results so far demonstrated that one and two-photon excitations can be used to acquire FLIM data of SiQDs in live cells without the interference of cellular autofluorescence, with the latter also avoiding the phototoxic effect of near-UV laser. In fact, as the excitation wavelength of the two-photon FLIM experiments was located in the near infrared (NIR) region ( $\geq 650$  nm), this approach may be suitable for *in vivo* studies where the tissue window enables deeper penetration into the sample.

### 5.3.5 FLIM-FRET study using SiQDs-DY485 conjugate

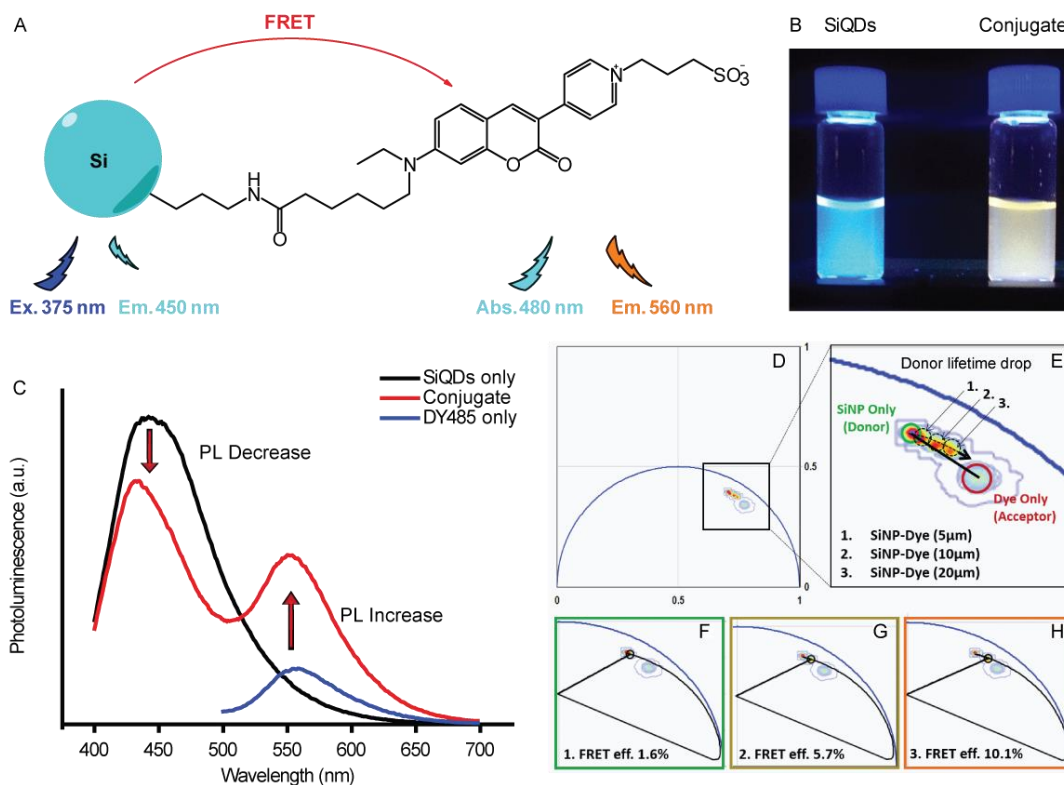


Figure 5.8 Study of Förster resonance energy transfer (FRET) between SiQDs donor and an organic dye (DY485) acceptor using FLIM analysed in the phasor space. (A) SiQDs were used as the donor and were conjugated with an acceptor dye molecule (DY485) through an amide bond. (B) The resulting conjugate showed orange fluorescence upon excitation with a UV lamp. (C) Photoluminescence spectra of the SiQDs alone, the conjugate and the dye alone. Excitation wavelength: 375 nm. D-E Phasor diagrams showing the decrease of donor (SiQDs) lifetime in the presence of an increasing amount of the acceptor (DY485). The quenched trajectory is characteristic of FRET and is distinct from the linear combination of lifetimes that would result from non-interacting donor-acceptor pair. F-H Theoretical FRET trajectory superimposed (black line) to determine the FRET efficiency of the SiQDs with the three different concentrations of the dye. The indicated concentration refers to the concentration of the dye used during surface modification step, as it was difficult to measure the amount of dyes on particle surface directly.

One of the main applications of FLIM is in Förster resonance energy transfer (FRET) measurements<sup>29,32</sup>. As fluorescence lifetime of a fluorophore depends on both the radiative (i.e. fluorescence) and non-radiative (i.e. quenching) processes,

energy transfer from the donor to the acceptor during FRET leads to decrease of lifetime for the donor and increase of lifetime for the acceptor<sup>29,32-34</sup>. Compared with intensity based FRET measurements, the FLIM approach is insensitive to the concentration of the fluorophore and therefore can remove artifacts due to the variation of concentration across the sample. This work further exploited the applicability of surface modified SiQDs for imaging purposes in the circumstance of FLIM-FRET (Figure 5.8). Here, SiQDs were used as a donor and conjugated to a dye acceptor (DY485) (Figure 5.8A). This particular dye acceptor was chosen due to its good spectral overlap with the SiQDs (Figure 5.9), and its large Stokes shift (85 nm) so that signals between the donor/acceptor were separated. The SiQDs were coupled to the dye via amide linkage using a single coupling step. Before conjugation, the self-excitation of the dye exhibited weak photoluminescence at 560 nm. After conjugation, the intensity of photoluminescence observed at 560 nm was increased by approximately two folds, which was accompanied by quenched intensity of emission peak from the SiQDs at 450 nm by ~20 % and the resulting solution showing orange under UV excitation (Figure 5.8B-C). This first evidence of FRET between SiQDs and DY485 was further confirmed by lifetime studies using FLIM (Figure 5.8D-H). The acceptor dye (DY485) had a much shorter lifetime (<2.5 ns) than the donor SiQDs (>4 ns). After conjugation, there was a significant decrease of fluorescence lifetime of the SiQDs (Figure 5.8D-H). When observed from the donor channel at 450 nm, the phasor cluster corresponding to the conjugate could be found along a phasor trajectory (black curve) between the SiQDs and the dye, which was distinct from the linear combination seen in previous

cases (Figure 5.3 and Figure 5.6).

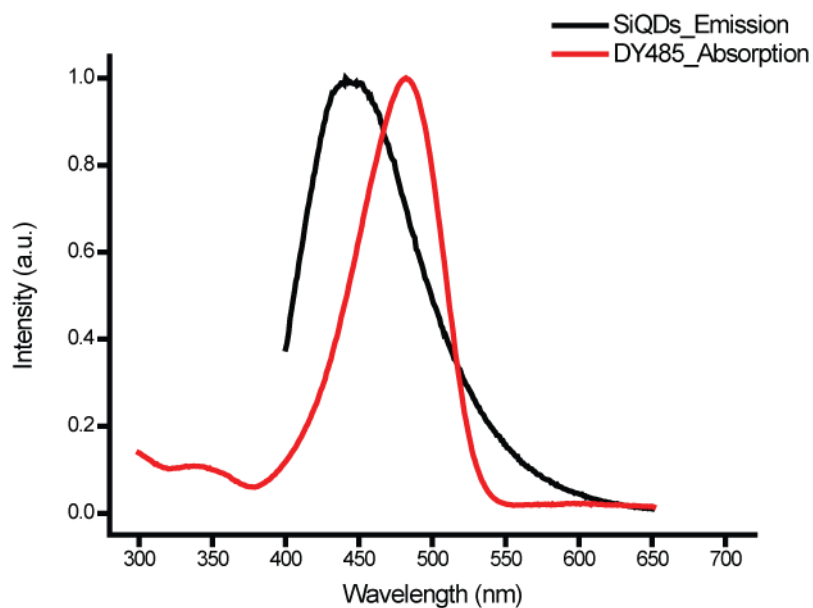


Figure 5.9 Absorption spectrum of dye and emission spectra of SiQDs, showing good spectral overlap between the donor-acceptor pair. Excitation wavelength: 375 nm.

The FRET efficiency was determined by observing the drop of donor lifetime using the phasor plot<sup>24,26</sup>. It needs to be highlighted here that the conventional method of determining FRET efficiency requires the measuring of the actual lifetime change of the fluorophore. However, using the phasor approach of FLIM data analysis, the FRET efficiency can be obtained without such a measurement. For instance, when the lifetime of the SiQDs (donor) was changed upon interaction with the dye molecule (acceptor), the realization of all possible FRET phasors with the different efficiencies was described with a curved trajectory in the phasor plot (black curve in Figure 5.8D-H). The experimental position of the phasor of a given pixel was then plotted directly onto the trajectory, and from this the FRET efficiencies were determined. The contributions of the background and of the donor without acceptor were evaluated using the rule of the linear combination (Eq. 5.5

and Eq. 5.6), when the background phasor and the donor alone (SiQDs alone) recorded in an independent measurement comparable to FRET studies of molecular species<sup>26</sup>.

By this method, the FRET efficiencies between SiQDs and DY485 were calculated to be between 1.6% and 10.6 %, using dye concentration from 5  $\mu\text{M}$  to 20  $\mu\text{M}$ . It needs to be mention here that the indicated amount of dye used refers to the concentration used during the modification step with no purification procedure afterwards, as in practice it was difficult to measure the amount of dye that were surface bound. However, if the silicon quantum dots had an average ‘molecular weight’ of 3000 g/mol (based on TEM results), the indicated concentration of the dye suggests the ‘molar ratio’ of SiQDs and DY485 was in the range of  $\sim 1:1-1:6$  if all dye are surface bound. Nevertheless, in practice it is impossible for a surface reaction to happen in 100 % yield, this estimation is tentative and a detailed study is beyond the scope of the current work.

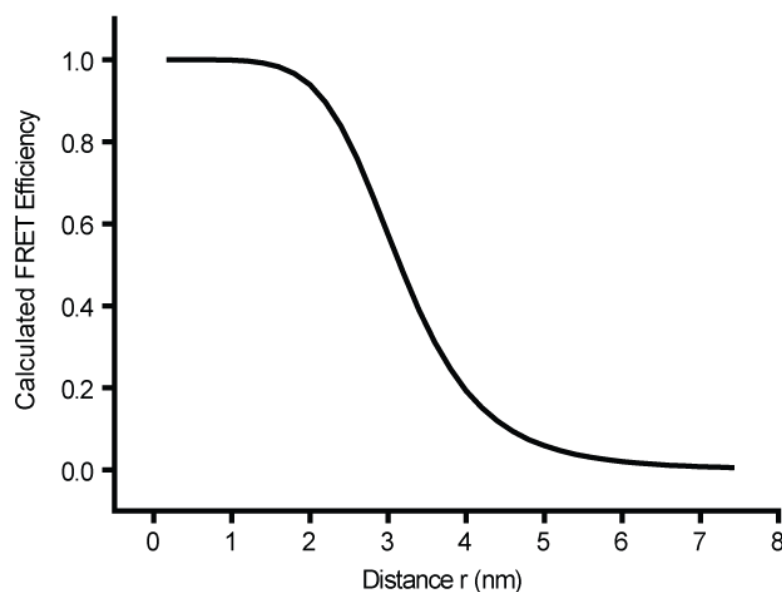


Figure 5.10 Calculation of FRET efficiency in respect to distance between SiQDs

and DY485. The Förster distance  $R_0 = 3.2$  nm, where the FRET efficiency is at 50 %.

Since the FRET process is strongly distance dependent<sup>35,36</sup>, the Förster distance at an efficiency of 50 % was calculated to be  $\sim 3.2$  nm (Eq. 5.8, Figure 5.8). In this case, the linker between the donor (SiQDs) and the acceptor (dye) was less than 1 nm, indicating higher than 90 % FRET efficiency. The discrepancy between the experimental value and theoretical value is two folds. Firstly, the calculation of Förster distance is based on the centres of the fluorophores. Here, the ‘centre’ needs to take into account the radius of the nanoparticles. From the TEM results (Figure 5.1) and comparable reports<sup>11,28</sup>, the SiQDs made by the reduction route used in this study had an average diameter of 1.5 – 3 nm, which increased spatial distance of the donor-acceptor pair to  $\sim 2.5 - 4$  nm. Secondly, the empirical estimation of FRET efficiency was derived from molecular species, such as dyes and proteins, where multiple assumptions were made (i.e. the dipole orientation factor,  $\kappa^2$ , was assumed to be  $\sim 0.67$  for randomly oriented molecules). In the case presented in this study these assumptions may or may not be true.

## 5.4 Conclusions

In this work, the application of FLIM in the context of photoluminescent SiQDs is demonstrated. The long fluorescence lifetime of SiQDs allowed easy deconvolution of fluorescence signals from the nanoparticles from their biological backgrounds, regardless of their comparable blue colour. Analysis of FLIM was performed in the phasor space with only

limited photon counts recorded in each pixel. It was further demonstrated that the FLIM method and phasor approach of FLIM analysis could be applied in the study of energy transfer process involving SiQDs, especially FRET. These advancements provided additional utilities for SiQDs for fluorescent bio-imaging applications in the future.

## 5.5 References

- (1) Hessel, C. M.; Reid, D.; Panthani, M. G.; Rasch, M. R.; Goodfellow, B. W.; Wei, J.; Fujii, H.; Akhavan, V.; Korgel, B. A. Synthesis of Ligand-Stabilized Silicon Nanocrystals with Size-Dependent Photoluminescence Spanning Visible to Near-Infrared Wavelengths. *Chem Mater* **2011**, *24*, 393-401.
- (2) Holmes, J. D.; Ziegler, K. J.; Doty, R. C.; Pell, L. E.; Johnston, K. P.; Korgel, B. A. Highly luminescent silicon nanocrystals with discrete optical transitions. *Journal of the American Chemical Society* **2001**, *123*, 3743-3748.
- (3) English, D. S.; Pell, L. E.; Yu, Z. H.; Barbara, P. F.; Korgel, B. A. Size tunable visible luminescence from individual organic monolayer stabilized silicon nanocrystal quantum dots. *Nano Letters* **2002**, *2*, 681-685.
- (4) Tilley, R. D.; Yamamoto, K. The microemulsion synthesis of hydrophobic and hydrophilic silicon nanocrystals. *Advanced Materials* **2006**, *18*, 2053-2056.
- (5) Li, Q.; He, Y.; Chang, J.; Wang, L.; Chen, H.; Tan, Y.-W.; Wang, H.; Shao, Z. Surface-Modified Silicon Nanoparticles with Ultrabright Photoluminescence and Single-Exponential Decay for Nanoscale Fluorescence Lifetime Imaging of Temperature. *Journal of the American Chemical Society* **2013**, *135*, 14924-14927.
- (6) Jurbergs, D.; Rogojina, E.; Mangolini, L.; Kortshagen, U. Silicon nanocrystals with ensemble quantum yields exceeding 60%. *Appl Phys Lett* **2006**, *88*.
- (7) Baldwin, R. K.; Pettigrew, K. A.; Garno, J. C.; Power, P. P.; Liu, G. Y.; Kauzlarich, S. M. Room temperature solution synthesis of alkyl-capped tetrahedral shaped silicon nanocrystals. *Journal of the American Chemical Society* **2002**, *124*, 1150-1151.
- (8) Hessel, C. M.; Henderson, E. J.; Veinot, J. G. C. Hydrogen silsesquioxane: A molecular precursor for nanocrystalline Si-SiO<sub>2</sub> composites and freestanding hydride-surface-terminated silicon nanoparticles. *Chem Mater* **2006**, *18*, 6139-6146.
- (9) Heath, J. R. A LIQUID-SOLUTION-PHASE SYNTHESIS OF CRYSTALLINE SILICON. *Science* **1992**, *258*, 1131-1133.
- (10) HEINRICH, J. L.; CURTIS, C. L.; CREDO, G. M.; SAILOR, M. J.; KAVANAGH, K. L. Luminescent Colloidal Silicon Suspensions from Porous Silicon. *Science* **1992**, *255*, 66-68.
- (11) Tilley, R. D.; Warner, J. H.; Yamamoto, K.; Matsui, I.; Fujimori, H. Microemulsion synthesis of monodisperse surface stabilized silicon nanocrystals. *Chem*

*Commun* **2005**, *0*, 1833-1835.

(12)Li, X. G.; He, Y. Q.; Swihart, M. T. Surface functionalization of silicon nanoparticles produced by laser-driven pyrolysis of silane followed by HF-HNO<sub>3</sub> etching. *Langmuir* **2004**, *20*, 4720-4727.

(13)Mangolini, L.; Kortshagen, U. Plasma-assisted synthesis of silicon nanocrystal inks. *Advanced Materials* **2007**, *19*, 2513-+.

(14)Rodríguez Núñez, J. R.; Kelly, J. A.; Henderson, E. J.; Veinot, J. G. C. Wavelength-Controlled Etching of Silicon Nanocrystals. *Chem Mater* **2011**, *24*, 346-352.

(15)Wilcoxon, J. P.; Samara, G. A.; Provencio, P. N. Optical and electronic properties of Si nanoclusters synthesized in inverse micelles. *Phys Rev B* **1999**, *60*, 2704-2714.

(16)Warner, J. H.; Hoshino, A.; Yamamoto, K.; Tilley, R. D. Water-Soluble Photoluminescent Silicon Quantum Dots. *Angewandte Chemie International Edition* **2005**, *44*, 4550-4554.

(17)Cheng, X. Y.; Lowe, S. B.; Ciampi, S.; Magenau, A.; Gaus, K.; Reece, P. J.; Gooding, J. J. Versatile "Click Chemistry" Approach to Functionalizing Silicon Quantum Dots: Applications toward Fluorescent Cellular Imaging. *Langmuir* **2014**, *30*, 5209-5216.

(18)Dasog, M.; Yang, Z.; Regli, S.; Atkins, T. M.; Faramus, A.; Singh, M. P.; Muthuswamy, E.; Kauzlarich, S. M.; Tilley, R. D.; Veinot, J. G. C. Chemical Insight into the Origin of Red and Blue Photoluminescence Arising from Freestanding Silicon Nanocrystals. *ACS Nano* **2013**, *7*, 2676-2685.

(19)Cassette, E.; Helle, M.; Bezdetsnaya, L.; Marchal, F.; Dubertret, B.; Pons, T. Design of new quantum dot materials for deep tissue infrared imaging. *Adv Drug Deliver Rev* **2013**, *65*, 719-731.

(20)Mastronardi, M. L.; Henderson, E. J.; Puzzo, D. P.; Ozin, G. A. Small Silicon, Big Opportunities: The Development and Future of Colloidally-Stable Monodisperse Silicon Nanocrystals. *Advanced Materials* **2012**, *24*, 5890-5898.

(21)He, G. S.; Zheng, Q.; Yong, K.-T.; Erogbogbo, F.; Swihart, M. T.; Prasad, P. N. Two- and Three-Photon Absorption and Frequency Upconverted Emission of Silicon Quantum Dots. *Nano Letters* **2008**, *8*, 2688-2692.

(22)Tu, C. Q.; Ma, X. C.; Pantazis, P.; Kauzlarich, S. M.; Louie, A. Y. Paramagnetic, Silicon Quantum Dots for Magnetic Resonance and Two-Photon Imaging of Macrophages. *Journal of the American Chemical Society* **2010**, *132*, 2016-2023.

(23)Colyer, R. A.; Lee, C.; Gratton, E. A novel fluorescence lifetime imaging system that optimizes photon efficiency. *Microscopy Research and Technique* **2008**, *71*, 201-213.

(24)Digman, M. A.; Caiolfa, V. R.; Zamai, M.; Gratton, E. The Phasor Approach to Fluorescence Lifetime Imaging Analysis. *Biophysical Journal* **2008**, *94*, L14-L16.

(25)Stringari, C.; Cinquin, A.; Cinquin, O.; Digman, M. A.; Donovan, P. J.; Gratton, E. Phasor approach to fluorescence lifetime microscopy distinguishes different metabolic states of germ cells in a live tissue. *Proceedings of the National*

*Academy of Sciences* **2011**, *108*, 13582-13587.

(26)Hinde, E.; Digman, M. A.; Welch, C.; Hahn, K. M.; Gratton, E. Biosensor Förster resonance energy transfer detection by the phasor approach to fluorescence lifetime imaging microscopy. *Microscopy Research and Technique* **2012**, *75*, 271-281.

(27)Shiohara, A.; Hanada, S.; Prabakar, S.; Fujioka, K.; Lim, T. H.; Yamamoto, K.; Northcote, P. T.; Tilley, R. D. Chemical reactions on surface molecules attached to silicon quantum dots. *J Am Chem Soc* **2010**, *132*, 248-253.

(28)Cheng, X.; Lowe, S. B.; Ciampi, S.; Magenau, A.; Gaus, K.; Reece, P. J.; Gooding, J. J. Versatile “Click Chemistry” Approach to Functionalizing Silicon Quantum Dots: Applications toward Fluorescent Cellular Imaging. *Langmuir* **2014**, *30*, 5209-5216.

(29)Wallrabe, H.; Periasamy, A. Imaging protein molecules using FRET and FLIM microscopy. *Curr. Opin. Biotechnol.* **2005**, *16*, 19-27.

(30)Veinot, J. G. Synthesis, surface functionalization, and properties of freestanding silicon nanocrystals. *Chem Commun (Camb)* **2006**, 4160-4168.

(31)Dohnalová K.; Gregorkiewicz, T.; Kůsová, K. Silicon quantum dots: surface matters. *Journal of Physics: Condensed Matter* **2014**, *26*, 173201.

(32)Suhling, K.; French, P. M. W.; Phillips, D. Time-resolved fluorescence microscopy. *Photoch Photobio Sci* **2005**, *4*, 13-22.

(33)Erogbogbo, F.; Chang, C. W.; May, J.; Prasad, P. N.; Swihart, M. T. Energy transfer from a dye donor to enhance the luminescence of silicon quantum dots. *Nanoscale* **2012**, *4*, 5163-5168.

(34)Rosso-Vasic, M.; De Cola, L.; Zuilhof, H. Efficient Energy Transfer between Silicon Nanoparticles and a Ru–Polypyridine Complex. *The Journal of Physical Chemistry C* **2009**, *113*, 2235-2240.

(35)Medintz, I. L.; Clapp, A. R.; Mattoussi, H.; Goldman, E. R.; Fisher, B.; Mauro, J. M. Self-assembled nanoscale biosensors based on quantum dot FRET donors. *Nat Mater* **2003**, *2*, 630-638.

(36)Clapp, A. R.; Medintz, I. L.; Mauro, J. M.; Fisher, B. R.; Bawendi, M. G.; Mattoussi, H. Fluorescence Resonance Energy Transfer Between Quantum Dot Donors and Dye-Labeled Protein Acceptors. *Journal of the American Chemical Society* **2003**, *126*, 301-310.

**Chapter 6 A silicon quantum dots protease sensor  
based on Förster resonance energy transfer (FRET)**

## 6.1 Introduction

Previous studies with SiQDs have been mainly focused on the synthesis and surface functionalization, including bottom-up growth with silane<sup>1-6</sup> or zintl salts<sup>7-13</sup>, laser pyrolysis<sup>14-20</sup>, etching<sup>21-26</sup>, decomposing silsesquioxane<sup>27-36</sup> and plasma synthesis<sup>37-43</sup>. Chapter three and four of this thesis have also contributed to this area of research. In chapter five, the application of lifetime imaging microscopy (FLIM) of SiQDs in intracellular environments was demonstrated using one and two photon FLIM, as well as in the circumstance of FLIM-FRET. This chapter builds upon previous chapters by demonstrating the preparation of a SiQDs protease sensor based on FRET by controlling the surface chemistry of SiQDs.

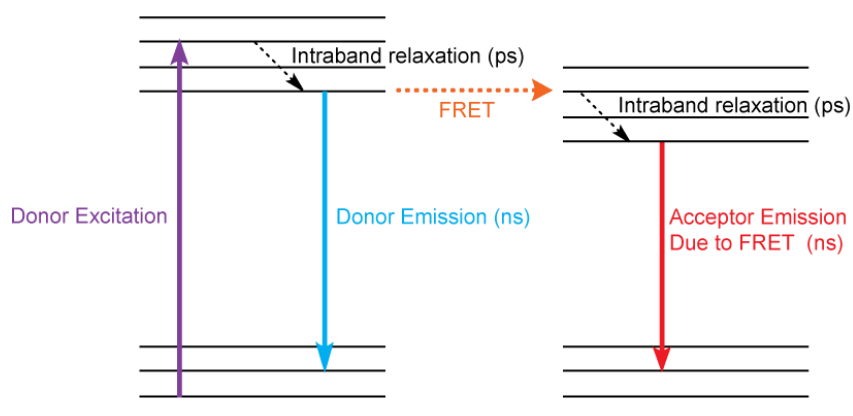


Figure 6.1 A simplified Jablonski diagram showing the basic mechanism of FRET.

The Förster resonance energy transfer (FRET) occurs between two fluorophores with overlapping energy states (Figure 6.1)<sup>44-46</sup>. In a typical FRET process, exciting the donor fluorophore allows transfer of its energy to the acceptor fluorophore via non-radiative dipole-dipole coupling, which then induces emission

from the acceptor<sup>44,46-48</sup>. The efficiency of energy transfer depends on the inverse power of six to the distance between the two fluorophores, as well as the band match. As the fluorescence of a fluorophore depends on both the radiative and non-radiative processes, the energy transfer in FRET leads to decreased lifetime of the acceptor and corresponding increased lifetime of the donor<sup>45,49-52</sup>.

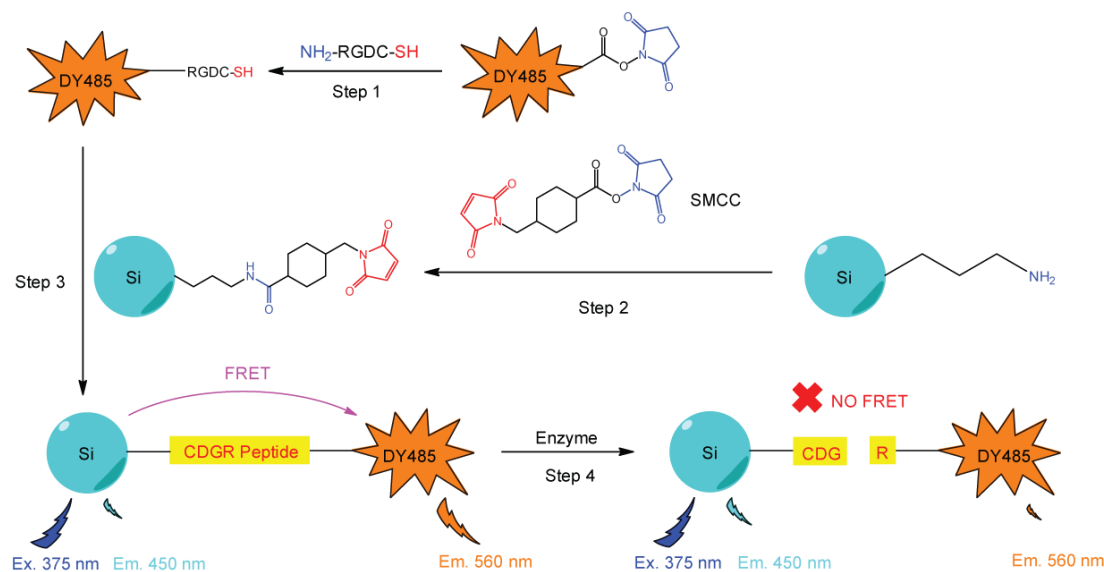


Figure 6.2 Schematics of a trypsin sensor involving SiQDs based on FRET. Step 1: dye (DY485) labelled peptide is prepared by coupling NHS activated dye and the free amine group at the N terminus of the peptide. Step 2: Surface functionalized SiQDs are prepared by activating the particle surface with a short heterobifunctional cross-linking reagent (SMCC) that contains a NHS ester end (blue) that reacts with primary amines and a maleimide end (red) that reacts with thiols. Step 3: the maleimide group reacts specifically with the thiol moiety of cysteine in the peptide covalently to allow energy transfer between the SiQDs and the dye. Step 4: The linker between the donor/acceptor is cleaved upon treatment of trypsin, with proteolysis takes place at the C terminus of Arg. The cleavage results in the disappearance of the FRET signal accompanied by decreased PL intensity of the acceptor dye.

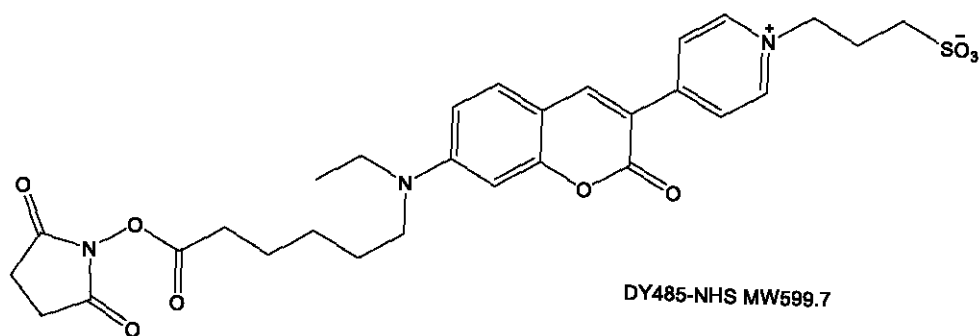
In this study, as illustrated in Figure 6.2, a trypsin sensor is designed based on FRET involving SiQDs (donor) linked with a dye acceptor (DY485) via an enzyme responsive peptide. Trypsin is a serine protease which cleaves peptide chains at the

C' terminal of lysine or arginine. Although a less interesting protease for disease diagnosis, trypsin is highly robust in physiological conditions, and due to its medium size (~23kDa), a good model protein for the study of quantum dots based FRET protease sensors.<sup>46</sup> The construct is prepared by first synthesizing a dye labelled peptide (step 1); The SiQDs surface is then activated with a heterobifunctional linker (SMCC), which shows differential reactivity towards amine and the sulfhydryl groups at either ends (step 2); The surface activated SiQDs then reacts with the dye labelled peptide, generating FRET signal due to the close distance and large spectral overlap between the SiQDs/DY485 (step 3). Upon enzymatic cleavage, the dye is removed from the surface of SiQDs, which is accompanied by the disappearance of the FRET signal and reduced PL from the dye (step 4).

## **6.2 Methods and Materials**

### **6.2.1 Chemicals and Materials**

All chemicals and solvent used were obtained and prepared as described in chapter 2 unless otherwise stated. All peptides used were purchased from Genscript. The organic dye acceptor DY485-NHS was purchased from Dyomics (GmbH) with the following structure:



## 6.2.2 Synthesis and purification of allylamine modified silicon quantum dots

### dots

Hydrogen terminated SiQDs were prepared as described in chapter 2. Surface modification and purification were prepared using procedures as described in chapter 2, using ~4 mL of allylamine ( $5.3 \times 10^{-2}$  mol) added per 100 mL of solution.

## 6.2.3 Preparation and characterization of dye labelled peptides

To prepare DY485 labelled peptides, 10  $\mu$ L of 10 mM DY485-NHS solution was mixed with 20  $\mu$ L 10 mM peptide solution (both in dry DMF) in an eppendorf tube to achieve a final molar ratio of peptide:dye of 2:1. The mixture was diluted with dry DMF to make a final stock solution containing 2.5 mM of the dye. The solution was left at room temperature for 2 hours to allow completion of the reaction and the final product was stored under argon at 4  $^{\circ}$ C until use. The cysteine residue in the RGDC peptide can easily form disulphide bonds upon exposure to air and water, therefore a fresh stock was made every two weeks<sup>53</sup>.

Electrospray ionisation (ESI) mass spectra and high performance liquid chromatograph (HPLC) traces were recorded on a Shimadzu HPLC mass spectrometer (MS) system (LCMS-2010EV) equipped with a quadrupole mass

analyser and prominence diode array detector (SPD-M20A, monitoring absorbance from 190 nm to 800 nm). Data was processed using the Shimadzu software package LCMS Solutions 3.60. HPLC was performed in a Phenomex Luna C8 column (250.00 × 4.60 mm column, 5 µm particle size) at a temperature of 40 °C flow rate of 1.0 mL min<sup>-1</sup>. The mobile phase consisted of solvents A (0.1% formic acid in water) and B (0.1% formic acid in acetonitrile). The solvent gradient was as follows: 5% solvent B for 5 min, a gentle increase from 5% to 100% solvent B over 35 min, 100% solvent B for 10 min, a decrease to 5% solvent B over 5 min, and 5% solvent B for a further 5 min. A splitter was used after HPLC to reduce the total flow into the ESI MS to 0.2 mL min<sup>-1</sup>. The MS detector voltage was set to 1.5 KV and 1 scan per second was completed over the range 200 m/z - 2000 m/z. 100 µL of sample solution was injected in each run.

#### **6.2.4 Preparation of the FRET conjugates**

To prepare FRET conjugates using SiQDs conjugated with DY485 labelled peptides, a solution of 10 mg/mL of allylamine functionalized SiQDs were prepared in 1×PBS at pH 7.4. Into the solution was then added with the dye labelled peptide with desired concentration, and the reaction was left overnight at room temperature. For every enzyme assay a fresh FRET conjugate is prepared.

#### **6.2.5 Characterization of optical properties of surface modified SiQDs**

Optical properties of synthesized silicon quantum dots, including UV-Vis

absorption and photoluminescence (PL) measurements were characterized as described in chapter 2.

### 6.2.6 Calculation of FRET efficiency and Förster distance

The theoretical FRET efficiency and Förster distance were determined according to a published method<sup>44,46,47,54</sup>. Specifically, the FRET efficiency depends on the distance between donor and acceptor:

$$E = \frac{1}{1+(r/R_0)^6} \quad (\text{Equ. 6.1), where:}$$

E = FRET efficiency

r = distance between the donor and acceptor

R<sub>0</sub> = Förster distance

The Förster distance is determined by the following relationship:

$$R_0 = 0.211 * [\kappa^2 n^{-4} Q_D \int_0^\infty F_D(\lambda) \epsilon_A(\lambda) \lambda^4 d\lambda]^{1/6} \quad (\text{Equ. 6.2), where}$$

$\kappa$  = dipole orientation factor,  $\kappa^2 \approx 2/3$  for randomly oriented molecules

n = refractive index of the medium ( n = 1.33 for H<sub>2</sub>O and PBS)

Q<sub>D</sub> = quantum yield of the donor (between 0 – 100 %, for SiQDs-allylamine 5%)

F<sub>D</sub>( $\lambda$ ) = normalized emission spectrum of the donor (unit: none)

$\epsilon_A(\lambda)$  = wavelength dependent extinction coefficient of the acceptor (unit: M<sup>-1</sup>\*cm<sup>-1</sup>)

1)

### 6.2.7 Trypsin enzyme assay

For a typical trypsin assay experiment, a stock solution of 10 times (1 mM)



passivated SiQDs, two observed features were related with the distal amine moiety: the first was the broad peak at  $3450\text{ cm}^{-1}$ (strong) caused by the N-H stretch; and the second feature was observed at  $1632\text{ cm}^{-1}$ (strong), assigned as the N-H bend. For SMCC modified SiQDs, the broad peak at  $3450\text{ cm}^{-1}$ (strong) was due to the N-H stretch. The two sharp peak at  $1698\text{ cm}^{-1}$ (strong) and  $1738\text{ cm}^{-1}$ (strong) were related to the two C=O groups in the maleimide group. It was noticed that the two peaks at  $1792\text{ cm}^{-1}$ (strong) and  $1879\text{ cm}^{-1}$ (strong), as well the peak at  $1220\text{ cm}^{-1}$ (strong), were seen in unbound molecules (Figure 6.4b), were not on SMCC modified SiQDs. These peaks were probably due to the C=O stretch and C-O stretch in the succinimide ester therefore were not present after the modification, similar to observation with porous silicon<sup>55</sup>. A peak at  $1644\text{ cm}^{-1}$  was observed probably due to the N-H bend. Since this peak was not observed in unbound molecules (Figure 6.4) and also not at the exact position as in allyamine modified SiQDs as seen in (a), but was attributed to the newly formed amide linkage after modification. Since the C=C stretch in alkene is usually not strong in FT-IR, here it can be seen that this feature from maleimide is partially covered by the neighbouring C=O signal, but can still be observed at  $1570\text{ cm}^{-1}$ (weak).

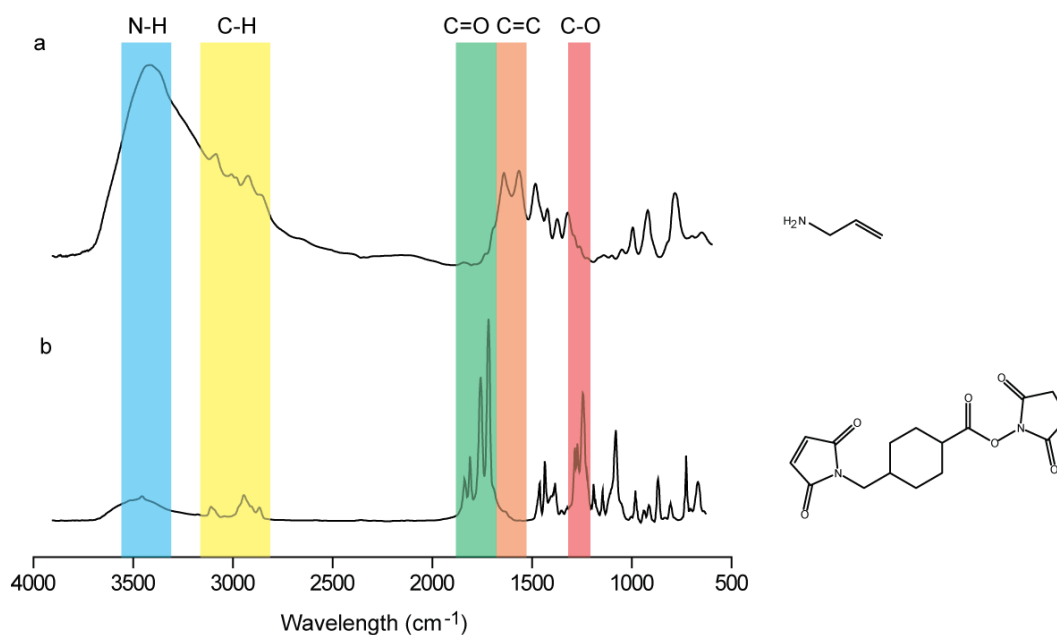


Figure 6.4 Characterization of molecules used for surface modification of SiQDs by FT-IR. Shown as (a) allylamine and (b) 4-(*N*-maleimidomethyl)cyclohexane carboxylic acid *N*-hydroxysuccinimide ester (SMCC). Characteristic peaks are highlighted for each surface modifying compound.

For comparison, molecules used for surface modifications of SiQDs were also characterized with FT-IR (Figure 6.4). A C-H feature observed slightly above 3050  $\text{cm}^{-1}$ (w) was seen in both cases. The high wavenumber of this peak was characteristic for alkene therefore confirmed the presence of allyl or maleimide group. For allylamine (a), two signature peaks were identified. The first was the broad band at 3450  $\text{cm}^{-1}$  corresponding to the N-H stretch in the amine group. The second was the peak at 1641  $\text{cm}^{-1}$ (m) which was related with the N-H bend. For SMCC (b), a set of peaks observed at 1819/1792  $\text{cm}^{-1}$ (m) and 1738/1698  $\text{cm}^{-1}$ (s) which were likely to be associated with the C=O stretches in succinimide ester and maleimide groups. A small peak was observed at 1570  $\text{cm}^{-1}$ (w) as a shoulder feature next to the C=O stretches, which was due to the C=C stretch in the maleimide group.

### 6.3.2 Characterization of DY485 labelled peptides

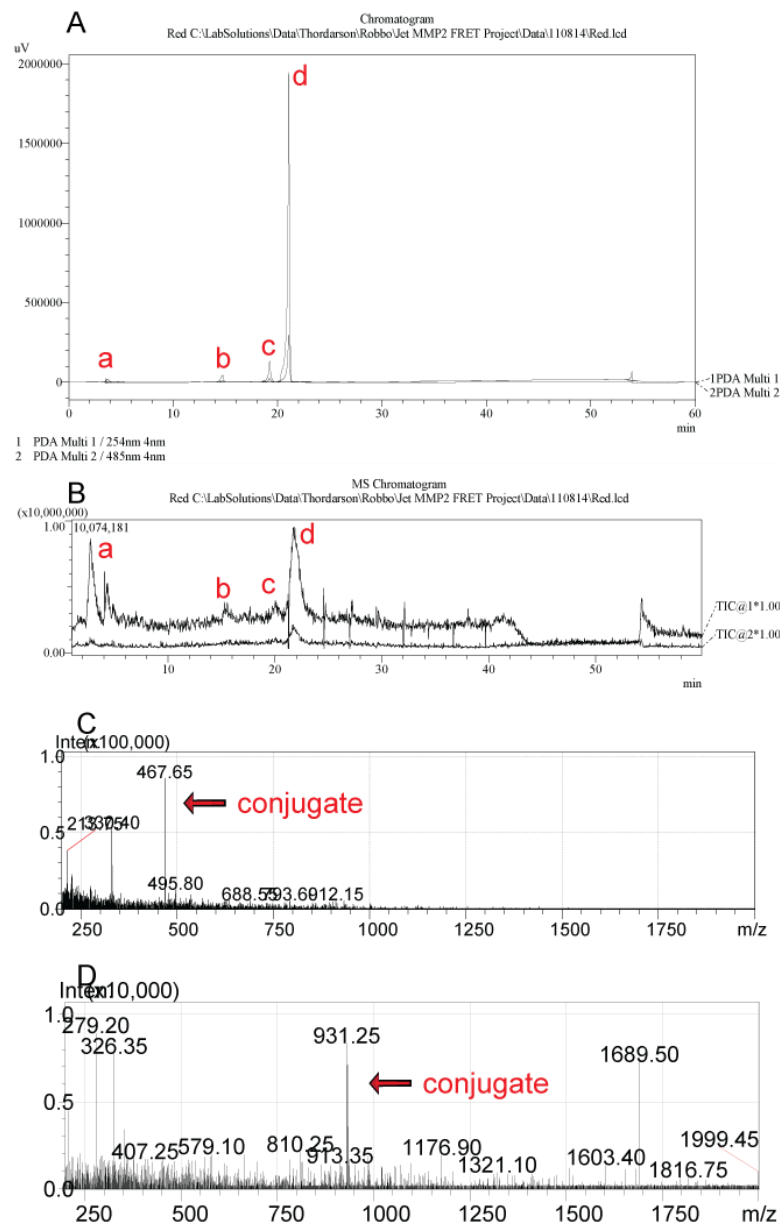


Figure 6.5 Characterization of DY485-RGDC conjugates by high performance liquid chromatography (HPLC) mass spectrometry (MS). From **A-D**: **A**: UV absorption profile measured at 485 nm; **B**: Total Ion Count (TIC) chromatogram; **C**: ESI+ MS spectrum at  $t_R$  12.2; **D**: ESI- MS spectrum at  $t_R$  12.2. From a-d: a: unreacted peptide, b: dye labelled peptide, c: hydrolyzed dye and d: unreacted dye.

Figure 6.5 shows the HPLC trace and corresponding MS profiles, showing the successful synthesis of the dye labelled peptide. From the 485 nm HPLC trace (A)

and TIC chromatogram (B) peak *a* at  $t_R$  2.0 min corresponds to the mass spectra of unreacted peptide, peak *b* at  $t_R$  12.2 min corresponds to the dye labelled peptide, peak *c* at  $t_R$  19.5 min corresponds to the hydrolyzed dye and peak *d* at  $t_R$  20.4 min corresponds to unreacted dye. C and D show the mass spectra of the conjugate in positive (C) and negative (D) modes respectively, with the large peak corresponding to the expected ion indicated with an arrow. The exact mass of the dye conjugate is 933.34 u. The observed signals in the MS (ESI +) at  $m/z$  467.65 ( $[M+2H]^{2+}$  requires 467.68) and in the MS (ESI -) at  $m/z$  932.25 ( $[M-H]^-$  requires 932.24). At  $t_R$  12.2 min we have identified both the dye UV absorbance at 485 nm, the parent ion in negative ESI MS, and the doubly charged species in positive ESI MS. This gave strong evidence to the successful synthesis of the DY485 labelled peptide. Comparable analyses of the other peaks are indicated in the appendix I

### 6.3.3 Optical properties of the FRET conjugate

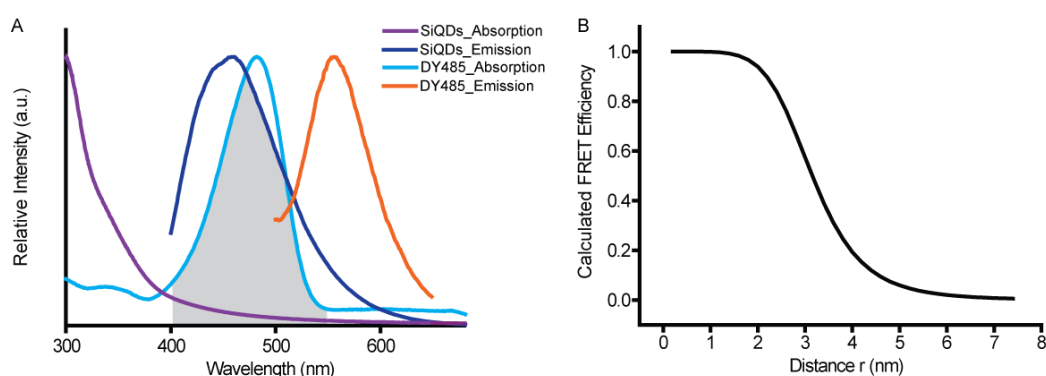


Figure 6.6 Spectral overlap of SiQDs/DY485 and calculated FRET efficiency of the conjugate. (A) Normalized absorption and emission spectrum of SiQDs and DY485, shown as purple (SiQDs absorption), blue (SiQDs emission), Cyan (DY485 absorption) and Orange (DY485 emission). The grey area indicates the overlapping region between the donor emission and the acceptor absorption spectrum. The emission spectra were measured with excitation wavelength of 375 nm. (B)

Calculated FRET efficiency based on the spectral overlap of SiQDs/DY485. The Förster distance where the transfer efficiency is at 50 % is determined to be 3.2 nm.

Figure 6.6 illustrates the absorption/emission profiles of the SiQDs/DY485 pair (A) and calculated FRET efficiency based on the spectral overlap (B). From Figure 6.6A, it can be seen that the SiQDs absorb mainly in the UV region, but emits at ~450 nm with FWHM of ~100 nm. Meanwhile, the absorption peak of the dye is located at 485 nm and the emission peak observed at 560 nm, with FWHM of ~70 nm. The first feature realized from measuring the absorption/emission profiles was that the emission peaks of SiQDs and DY485 had almost little overlap, therefore when measuring the acceptor (or donor) emission, the influence of the fluorescence from the other fluorophore was small. The second feature was that the emission of SiQDs and absorption of DY485 were well overlapped. This has led to good integral factor and therefore high theoretical transfer efficiency, as shown in Figure 6.6B. From the figure, it can be seen that the theoretical Förster distance where transfer efficiency is at 50% is ~3.2 nm.

It is worth mentioning that although the main absorption peak of the dye is at 485 nm, the dye still shows some level of absorptivity of lower wavelength and can be partially excited (i.e. ~15% in peak intensity at 375 nm compared with the main absorption peak at 485 nm). Based on the optical profiles of SiQDs/DY485, the relationship between the FRET efficiency and the distance between the centres of the fluorophores is determined (Figure 6.6B). From the graph, it can be seen that the Förster distance where the transfer efficiency is at 50 % is determined to be ~3.2 nm. When the distance between the fluorophores extends above this range, the

FRET efficiency rapidly drops and becomes almost negligible when reaches more than 5 nm.

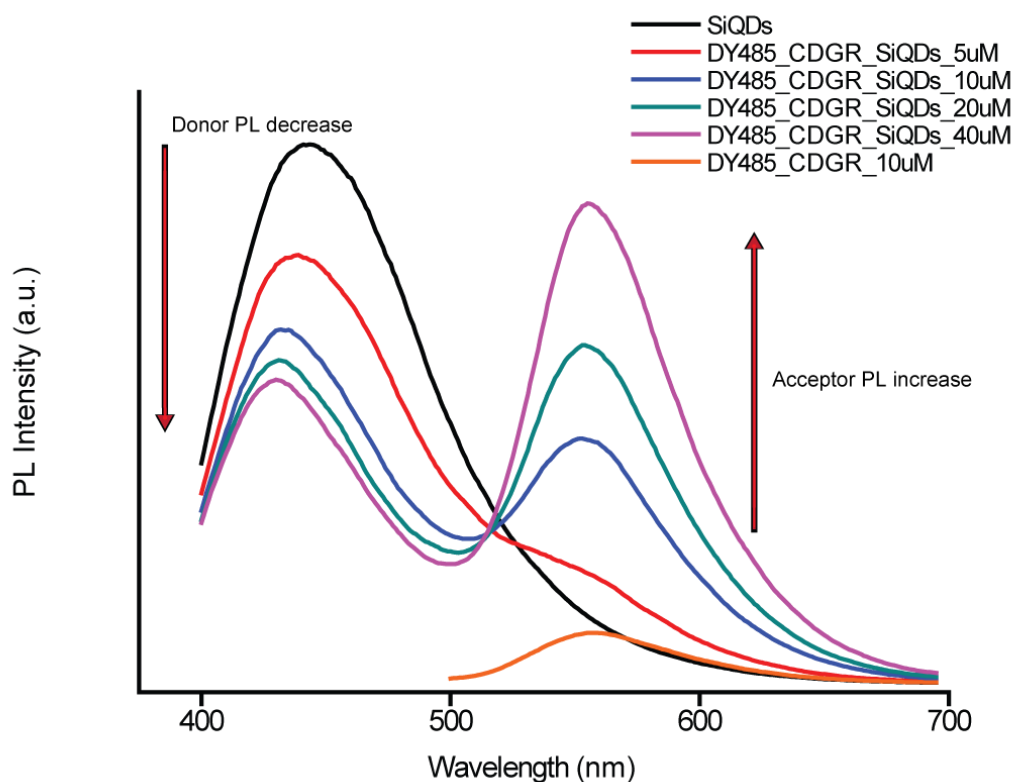


Figure 6.7 PL spectra of the FRET conjugates shown with increased concentration of the dye excited at 375 nm when the concentration of the SiQDs was kept constant. As the concentration of the dye increases, the emission from the SiQDs decreases steadily, this is accompanied by enhanced emission from the dye. The control group (orange) with 10  $\mu$ M of the dye labelled peptide used suggests self-excitation of the dye still can be observed without FRET, but conjugation with the donor enhanced its PL intensity significantly. The concentration of the dye used refers to the dye molecules present in the entire system without any purification step, rather than surface bound dyes.

After conjugating with the dye labelled peptide, as more dye labelled peptide is added, PL of SiQDs is gradually quenched and emission from the dye is increased (Figure 6.7). Here, the low emission from control group, using 10  $\mu$ M of dye-peptide (orange line) when excited at 375 nm, suggests that the observed increased emission from the dye is mainly from energy transfer from the particles, rather than

self-excitation of unbound dye molecules in solution. It was noticed that the quenched donor peak is slightly blue shifted with addition of the dye (i.e. by ~20 nm in the concentration range indicated). This is probably because the spectral overlap of SiQDs/DY485 is much better above 450 nm than below 430 nm (Figure 6.6B).

### 6.3.4 Trypsin assay with FRET conjugate

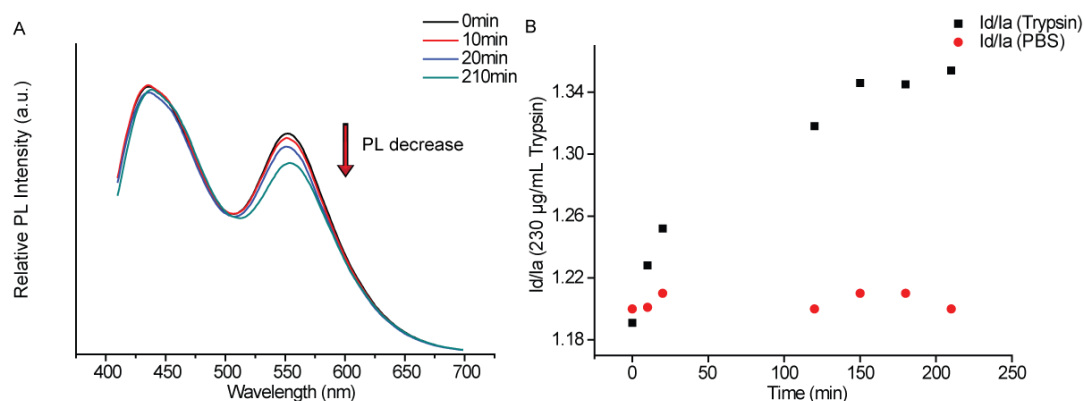


Figure 6.8 Change of PL for the FRET conjugate upon treatment of trypsin. (A) PL spectrum upon trypsin treatment monitored over time. Excitation wavelength: 375 nm. (B) Ratio of peak intensity of the donor SiQDs ( $I_d$ ) versus the acceptor DY485 ( $I_a$ ) monitored over time, shown as black square (treated with trypsin at 230  $\mu\text{g/mL}$ ) and red sphere (control group, treated with 1xPBS solution) over a period of three and half hours. When treated with trypsin, the ratio of  $I_d/I_a$  increase steadily, in comparison to the control group which remained stable during the period of measurement.

Figure 6.8 shows the impacts of trypsin treatment on the FRET conjugate. From panel A, it can be seen that the acceptor peak (DY485) gradually decreases over a period of 3.5 hours upon digestion with the enzyme at concentration of 230  $\mu\text{g/mL}$  (10  $\mu\text{M}$ ). This is in agreement with measurements of  $I_d/I_a$  (peak intensity of donor emission vs. acceptor emission, Figure 6.8B), where ratio of the peak intensity

increases steadily over time for enzyme treated construct but remained stable for the control group treated PBS solution.

Interestingly, unlike conventional quantum dots protease sensors based on FRET,<sup>46,56</sup> the donor peak in this study did not seem to recover upon the cleavage of the enzyme. The proposed reasons are twofold. The first is that the surface modification strategies of the two types of nanoparticles are completely different. For instance, for CdSe/ZnS quantum dots the attachment of dye labelled peptides is usually achieved via ligand exchange on the ZnS layer<sup>46,56</sup>. For SiQDs however, surface modification is done by the formation of covalent linkages directly attached to the Si surface. The lack of a lattice matched barrier for SiQDs has resulted in particularly significant role of surface chemistry on the PL properties of SiQDs, including peak shift and reduced  $\phi$ , particularly with thiol modified particles as seen in chapter three<sup>57,58</sup>. Therefore the PL emission from the particles could also have been influenced by the surface modification in addition to FRET. In fact, if the surface modification is the dominating factor for quenching the SiQDs emission then the effect of FRET at the donor channel could be almost completely covered. Second, as discussed in 6.3.3, since the dye still has 10-20% of absorptivity below 400 nm, this also contributed to the decreased PL intensity at the donor channel. For instance, if the absorption of the dye is strong enough, then the quenching effect from FRET would not be observable due to absorption of the dye (a different process compared with FRET with no energy transfer occurring). However, in the results presented, the only factor that allowed increased PL intensity of the dye is FRET from the SiQDs donor. Since trypsin has shown an effect towards reducing

the FRET signal, this gives evidence to the fact that the dye labelled peptide is attached on the particle surface via covalent linkage as illustrated in Figure 6.2.

Another observation from this study was that the trypsin efficiency seems to be fairly low. For CdSe based quantum dots enzyme sensor<sup>46,56</sup>, change of donor/acceptor intensity ratios were observed in a much shorter time period (i.e. 20 min) with much larger change of  $I_d/I_a$ . However, in this study the experiments were carried in room temperature at 25 °C to ensure temperature condition remains stable throughout the work, it is not the optimal condition for enzyme digestion. Furthermore, since the final FRET conjugate was not purified, it probably contained unbound dye labelled peptides and competition of digestion reaction could have also influenced enzyme efficiency. Nevertheless, for proof of concept purposes, the results presented above have demonstrated experimentally the preparation of a protease sensor based on SiQDs using FRET, which is the first of its kind to the best knowledge of the author.

### **6.3.5 *Ab initio* calculation of separation distance between donor/acceptor**

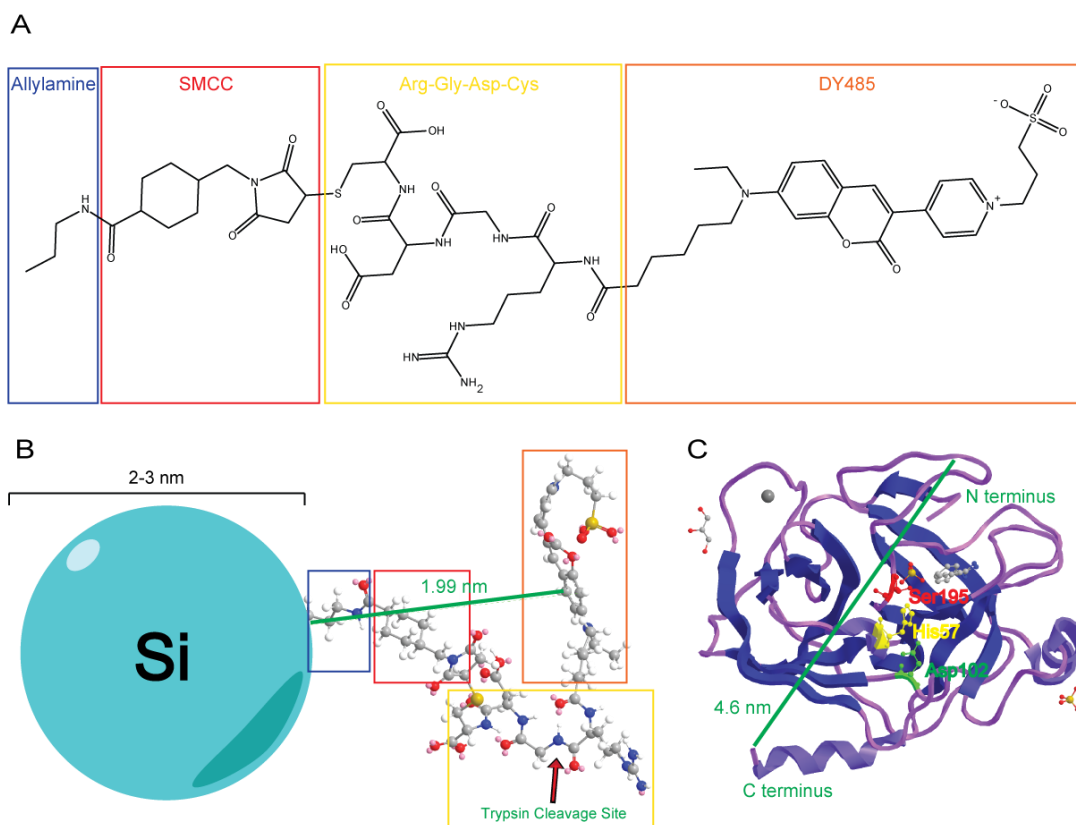


Figure 6.9 Modelling of the attachment of the surface group (i.e. DY485-RGDC-SMCC-allylamine) on SiQDs. (A) Structure of the entire surface group attached on SiQDs. (B) Illustration of the final surface modified SiQDs with the optimal molecular geometry with lowest energy calculated without considering the particles. The minimal energy calculation of the surface molecule is performed with the GAMESS interface using a semi-empirical method (PM3). The spacing distance between the surface of SiQDs and centre of the dye (i.e. length of allylamine+SMCC+ peptide, shown as green line in B) is calculated to be  $\sim 2$  nm. The trypsin cleavage site is illustrated with an arrow. Colours in the ball and stick model: grey: carbon, white: hydrogen, blue: nitrogen, red: oxygen, yellow: sulphur. (C) Crystal structure of trypsin. The enzyme is generally globular in shape, with a diameter of  $\sim 4.6$  nm (green line). The binding catalytic triad where cleavage occurs is highlighted in yellow. The crystal structure is obtained from the protein data bank (PDB code 4I8J with resolution of  $0.87\text{\AA}$ ).

Considering the FRET efficiency depends strongly on the distance between the donor/acceptor pair, the optimal geometry of the entire surface group was modelled. As the surface molecule was considerably large for high precision modelling (i.e. MW > 1000Da), calculation was performed with the GAMESS interface using a

semi-empirical method PM3 (Parameterized model number 3). Unsurprisingly, the modelling results suggested the surface molecule was bent in its lowest energy state (Figure 6.9B). Based on this model, the spatial distance between the surface of SiQDs and centre of the dye, was determined to be ~2 nm (Green line in Figure 6.9B). If considering the size of the SiQDs (i.e. 3 nm). The spatial distance between the centres of the fluorophores in the conjugate was in the range of ~3.5 nm.

The significance of this separation distance is two folds. First, assuming the PL properties of SiQDs are not affected by the peptides (hence Figure 6.6B is true), then the distance between the centres of fluorophores would be in the range of ~3.5 nm, and the FRET efficiency would be ~30% if there is only one dye molecule attached on each nanoparticle. Second, the spacing between SiQDs and DY485 is adequate for the enzyme digestion to occur. For instance, trypsin is a globular protein with diameter of ~4.6 nm (Figure 6.9C). When bound to the substrate peptide, the enzyme uses a catalytic triad consisting of His57, Asp102 and Ser195 (highlighted with yellow/green/red) located close to the surface of the protein. Therefore, the distance between the cleavage site and the surface of SiQDs should be long enough to allow digestion to occur. The calculation, however, is tentative and performed under solution environments. It does not include other factors that affect the on the surface when multiple neighbouring moieties are present which can increase steric hindrance between the chains. Other factors to consider include

## 6.4 Conclusions

This chapter has described a protease sensor using SiQDs based on FRET. This was done by conjugating the SiQDs as donor with a dye acceptor covalently via a short peptide linker. Both PL measurement and modelling suggested the large spectral overlap and close distance of SiQDs/dye would allow efficient energy transfer from the particles to the dye, leading to enhanced emission from the acceptor and quenched emission from SiQDs. Further treatment of the FRET conjugates with trypsin resulted in cleavage of the peptide linker between the donor/acceptor pair hence reduced acceptor PL. The results presented in this chapter were the first demonstration of a SiQDs protease sensor based on FRET to the best knowledge of the author.

## 6.5 References

- (1) Warner, J. H.; Hoshino, A.; Yamamoto, K.; Tilley, R. D. Water-soluble photoluminescent silicon quantum dots. *Angew Chem Int Ed Engl* **2005**, *44*, 4550-4554.
- (2) Warner, J. H.; Hoshino, A.; Shiohara, A.; Yamamoto, K.; Tilley, R. D. The synthesis of silicon and germanium quantum dots for biomedical applications - art. no. 609607. *Colloidal Quantum Dots for Biomedical Applications* **2006**, *6096*, 9607-9607.
- (3) Shiohara, A.; Hanada, S.; Prabakar, S.; Fujioka, K.; Lim, T. H.; Yamamoto, K.; Northcote, P. T.; Tilley, R. D. Chemical Reactions on Surface Molecules Attached to Silicon Quantum Dots. *Journal of the American Chemical Society* **2010**, *132*, 248-253.
- (4) Shiohara, A.; Prabakar, S.; Faramus, A.; Hsu, C. Y.; Lai, P. S.; Northcote, P. T.; Tilley, R. D. Sized controlled synthesis, purification, and cell studies with silicon quantum dots. *Nanoscale* **2011**, *3*, 3364-3370.
- (5) Wilcoxon, J. P.; Samara, G. A.; Provencio, P. N. Optical and electronic properties of Si nanoclusters synthesized in inverse micelles. *Phys Rev B* **1999**, *60*, 2704-2714.
- (6) Garoufalidis, C. S.; Zdetsis, A. D.; Grimme, S. High level ab initio

calculations of the optical gap of small silicon quantum dots. *Phys Rev Lett* **2001**, *87*, 276402.

(7) Bley, R. A.; Kauzlarich, S. M. A low-temperature solution phase route for the synthesis of silicon nanoclusters. *Journal of the American Chemical Society* **1996**, *118*, 12461-12462.

(8) Bley, R. A.; Yang, C. S.; Kauzlarich, S. M.; Delgado, G. R.; Lee, H. W. H. A low temperature solution phase synthesis for silicon quantum dots. *Abstr Pap Am Chem S* **1997**, *213*, 356-COLL.

(9) Yang, C. S.; Bley, R. A.; Kauzlarich, S. M.; Lee, H. W. H.; Delgado, G. R. Synthesis of alkyl-terminated silicon nanoclusters by a solution route. *Journal of the American Chemical Society* **1999**, *121*, 5191-5195.

(10) Mayeri, D.; Phillips, B. L.; Augustine, M. P.; Kauzlarich, S. M. NMR Study of the Synthesis of Alkyl-Terminated Silicon Nanoparticles from the Reaction of SiCl<sub>4</sub> with the Zintl Salt, NaSi. *Chem Mater* **2001**, *13*, 765-770.

(11) Baldwin, R. K.; Pettigrew, K. A.; Garno, J. C.; Power, P. P.; Liu, G. Y.; Kauzlarich, S. M. Room temperature solution synthesis of alkyl-capped tetrahedral shaped silicon nanocrystals. *Journal of the American Chemical Society* **2002**, *124*, 1150-1151.

(12) Zou, J.; Baldwin, R. K.; Pettigrew, K. A.; Kauzlarich, S. M. Solution synthesis of ultrastable luminescent siloxane-coated silicon nanoparticles. *Nano Letters* **2004**, *4*, 1181-1186.

(13) Zhang, X. M.; Neiner, D.; Wang, S. Z.; Louie, A. Y.; Kauzlarich, S. M. A new solution route to hydrogen-terminated silicon nanoparticles: synthesis, functionalization and water stability. *Nanotechnology* **2007**, *18*.

(14) Li, X. G.; He, Y. Q.; Swihart, M. T. Surface functionalization of silicon nanoparticles produced by laser-driven pyrolysis of silane followed by HF-HNO<sub>3</sub> etching. *Langmuir* **2004**, *20*, 4720-4727.

(15) Hua, F.; Swihart, M. T.; Ruckenstein, E. Efficient surface grafting of luminescent silicon quantum dots by photoinitiated hydrosilylation. *Langmuir* **2005**, *21*, 6054-6062.

(16) Erogbogbo, F.; Yong, K. T.; Roy, I.; Xu, G.; Prasad, P. N.; Swihart, M. T. Biocompatible luminescent silicon quantum dots for imaging of cancer cells. *ACS Nano* **2008**, *2*, 873-878.

(17) Erogbogbo, F.; Yong, K. T.; Hu, R.; Law, W. C.; Ding, H.; Chang, C. W.; Prasad, P. N.; Swihart, M. T. Biocompatible Magnetofluorescent Probes: Luminescent Silicon Quantum Dots Coupled with Superparamagnetic Iron(III) Oxide. *Acs Nano* **2010**, *4*, 5131-5138.

(18) Erogbogbo, F.; Tien, C. A.; Chang, C. W.; Yong, K. T.; Law, W. C.; Ding, H.; Roy, I.; Swihart, M. T.; Prasad, P. N. Bioconjugation of luminescent silicon quantum dots for selective uptake by cancer cells. *Bioconjug Chem* **2011**, *22*, 1081-1088.

(19) Erogbogbo, F.; Chang, C. W.; May, J. L.; Liu, L.; Kumar, R.; Law, W. C.; Ding, H.; Yong, K. T.; Roy, I.; Sheshadri, M.; Swihart, M. T.; Prasad, P. N. Bioconjugation of luminescent silicon quantum dots to gadolinium ions for bioimaging applications. *Nanoscale* **2012**, *4*, 5483-5489.

(20)Liu, J.; Erogbogbo, F.; Yong, K.-T.; Ye, L.; Liu, J.; Hu, R.; Chen, H.; Hu, Y.; Yang, Y.; Yang, J.; Roy, I.; Karker, N. A.; Swihart, M. T.; Prasad, P. N. Assessing Clinical Prospects of Silicon Quantum Dots: Studies in Mice and Monkeys. *ACS Nano* **2013**.

(21)Kang, Z.; Tsang, C. H.; Wong, N. B.; Zhang, Z.; Lee, S. T. Silicon quantum dots: a general photocatalyst for reduction, decomposition, and selective oxidation reactions. *J Am Chem Soc* **2007**, *129*, 12090-12091.

(22)Kang, Z.; Tsang, C. H. A.; Zhang, Z.; Zhang, M.; Wong, N.-b.; Zapien, J. A.; Shan, Y.; Lee, S.-T. A Polyoxometalate-Assisted Electrochemical Method for Silicon Nanostructures Preparation: From Quantum Dots to Nanowires. *Journal of the American Chemical Society* **2007**, *129*, 5326-5327.

(23)He, Y.; Kang, Z.-H.; Li, Q.-S.; Tsang, C. H. A.; Fan, C.-H.; Lee, S.-T. Ultrastable, Highly Fluorescent, and Water-Dispersed Silicon-Based Nanospheres as Cellular Probes. *Angewandte Chemie International Edition* **2009**, *48*, 128-132.

(24)He, Y.; Su, Y.; Yang, X.; Kang, Z.; Xu, T.; Zhang, R.; Fan, C.; Lee, S.-T. Photo and pH Stable, Highly-Luminescent Silicon Nanospheres and Their Bioconjugates for Immunofluorescent Cell Imaging. *Journal of the American Chemical Society* **2009**, *131*, 4434-4438.

(25)Kang, Z.; Liu, Y.; Tsang, C. H. A.; Ma, D. D. D.; Fan, X.; Wong, N.-B.; Lee, S.-T. Water-Soluble Silicon Quantum Dots with Wavelength-Tunable Photoluminescence. *Advanced Materials* **2009**, *21*, 661-664.

(26)Li, H. T.; He, X. D.; Kang, Z. H.; Huang, H.; Liu, Y.; Liu, J. L.; Lian, S. Y.; Tsang, C. H. A.; Yang, X. B.; Lee, S. T. Water-Soluble Fluorescent Carbon Quantum Dots and Photocatalyst Design. *Angew Chem Int Edit* **2010**, *49*, 4430-4434.

(27)Hessel, C. M.; Henderson, E. J.; Veinot, J. G. C. Hydrogen silsesquioxane: A molecular precursor for nanocrystalline Si-SiO<sub>2</sub> composites and freestanding hydride-surface-terminated silicon nanoparticles. *Chem Mater* **2006**, *18*, 6139-6146.

(28)Henderson, E. J.; Veinot, J. G. C. Synthesis of Oxide Encapsulated and Freestanding Hydride Surface Terminated Si<sub>1-x</sub>Ge<sub>x</sub> Nanocrystals. *Chem Mater* **2007**, *19*, 1886-1888.

(29)Hessel, C. M.; Henderson, E. J.; Veinot, J. G. C. An investigation of the formation and growth of oxide-embedded silicon nanocrystals in hydrogen silsesquioxane-derived nanocomposites. *J Phys Chem C* **2007**, *111*, 6956-6961.

(30)Hessel, C. M.; Henderson, E. J.; Kelly, J. A.; Cavell, R. G.; Sham, T. K.; Veinot, J. G. C. Origin of luminescence from silicon nanocrystals: a near edge X-ray absorption fine structure (NEXAFS) and X-ray excited optical luminescence (XEOL) study of oxide-embedded and free-standing systems. *J Phys Chem C* **2008**, *112*, 14247-14254.

(31)Kelly, J. A.; Henderson, E. J.; Veinot, J. G. Sol-gel precursors for group 14 nanocrystals. *Chem Commun (Camb)* **2010**, *46*, 8704-8718.

(32)Kelly, J. A.; Veinot, J. G. C. An Investigation into Near-UV Hydrosilylation of Freestanding Silicon Nanocrystals. *ACS Nano* **2010**, *4*, 4645-4656.

(33)Kelly, J. A.; Shukaliak, A. M.; Fleischauer, M. D.; Veinot, J. G. C. Size-

Dependent Reactivity in Hydrosilylation of Silicon Nanocrystals. *Journal of the American Chemical Society* **2011**, *133*, 9564-9571.

(34)Rodríguez Núñez, J. R.; Kelly, J. A.; Henderson, E. J.; Veinot, J. G. C. Wavelength-Controlled Etching of Silicon Nanocrystals. *Chem Mater* **2011**, *24*, 346-352.

(35)Dasog, M.; Yang, Z.; Regli, S.; Atkins, T. M.; Faramus, A.; Singh, M. P.; Muthuswamy, E.; Kauzlarich, S. M.; Tilley, R. D.; Veinot, J. G. C. Chemical Insight into the Origin of Red and Blue Photoluminescence Arising from Freestanding Silicon Nanocrystals. *ACS Nano* **2013**, *7*, 2676-2685.

(36)Yang, Z.; Iqbal, M.; Dobbie, A. R.; Veinot, J. G. C. Surface-Induced Alkene Oligomerization: Does Thermal Hydrosilylation Really Lead to Monolayer Protected Silicon Nanocrystals? *Journal of the American Chemical Society* **2013**, *135*, 17595-17601.

(37)Mangolini, L.; Thimsen, E.; Kortshagen, U. High-yield synthesis of luminescent silicon quantum dots in a continuous flow non-thermal plasma reactor. *Amorphous and Nanocrystalline Silicon Science and Technology-2005* **2005**, *862*, 307-312.

(38)Jurbergs, D.; Rogojina, E.; Mangolini, L.; Kortshagen, U. Silicon nanocrystals with ensemble quantum yields exceeding 60%. *Appl Phys Lett* **2006**, *88*.

(39)Mangolini, L.; Jurbergs, D.; Rogojina, E.; Kortshagen, U. Plasma synthesis and liquid-phase surface passivation of brightly luminescent Si nanocrystals. *J Lumin* **2006**, *121*, 327-334.

(40)Mangolini, L.; Kortshagen, U. Plasma-assisted synthesis of silicon nanocrystal inks. *Advanced Materials* **2007**, *19*, 2513-+.

(41)Kortshagen, U. Nonthermal plasma synthesis of semiconductor nanocrystals. *J Phys D Appl Phys* **2009**, *42*.

(42)Pereira, R. N.; Rowe, D. J.; Anthony, R. J.; Kortshagen, U. Freestanding silicon nanocrystals with extremely low defect content. *Phys Rev B* **2012**, *86*, 085449.

(43)Wheeler, L. M.; Neale, N. R.; Chen, T.; Kortshagen, U. R. Hypervalent surface interactions for colloidal stability and doping of silicon nanocrystals. *Nat Commun* **2013**, *4*.

(44)Medintz, I. L.; Clapp, A. R.; Mattoussi, H.; Goldman, E. R.; Fisher, B.; Mauro, J. M. Self-assembled nanoscale biosensors based on quantum dot FRET donors. *Nat Mater* **2003**, *2*, 630-638.

(45)Medintz, I. L.; Mattoussi, H.; Clapp, A. R. Potential clinical applications of quantum dots. *Int J Nanomed* **2008**, *3*, 151-167.

(46)Shi, L.; De Paoli, V.; Rosenzweig, N.; Rosenzweig, Z. Synthesis and Application of Quantum Dots FRET-Based Protease Sensors. *Journal of the American Chemical Society* **2006**, *128*, 10378-10379.

(47)Suhling, K.; French, P. M. W.; Phillips, D. Time-resolved fluorescence microscopy. *Photoch Photobio Sci* **2005**, *4*, 13-22.

(48)Wallrabe, H.; Periasamy, A. Imaging protein molecules using FRET and FLIM microscopy. *Curr. Opin. Biotechnol.* **2005**, *16*, 19-27.

(49) Achatz, D. E.; Mező, G.; Kele, P.; Wolfbeis, O. S. Probing the Activity of Matrix Metalloproteinase II with a Sequentially Click-Labeled Silica Nanoparticle FRET Probe. *ChemBioChem* **2009**, *10*, 2316-2320.

(50) Janczewski, D.; Tomczak, N.; Han, M. Y.; Vancso, G. J. Synthesis of functionalized amphiphilic polymers for coating quantum dots. *Nature Protocols* **2011**, *6*, 1546-1553.

(51) Dennis, A. M.; Rhee, W. J.; Sotto, D.; Dublin, S. N.; Bao, G. Quantum Dot-Fluorescent Protein FRET Probes for Sensing Intracellular pH. *ACS Nano* **2012**, *6*, 2917-2924.

(52) Erogbogbo, F.; Chang, C. W.; May, J.; Prasad, P. N.; Swihart, M. T. Energy transfer from a dye donor to enhance the luminescence of silicon quantum dots. *Nanoscale* **2012**, *4*, 5163-5168.

(53) Vincent, J. P.; Lazdunski, M. Trypsin-pancreatic trypsin inhibitor association. Dynamics of the interaction and role of disulfide bridges. *Biochemistry-Us* **1972**, *11*, 2967-2977.

(54) Albani, J. R. Principles and Applications of Fluorescence Spectroscopy. *Principles and Applications of Fluorescence Spectroscopy* **2007**, 1-255.

(55) Bocking, T.; Kilian, K. A.; Reece, P. J.; Gaus, K.; Gal, M.; Gooding, J. J. Biofunctionalization of free-standing porous silicon films for self-assembly of photonic devices. *Soft Matter* **2012**, *8*, 360-366.

(56) Shi, L.; Rosenzweig, N.; Rosenzweig, Z. Luminescent Quantum Dots Fluorescence Resonance Energy Transfer-Based Probes for Enzymatic Activity and Enzyme Inhibitors. *Analytical Chemistry* **2006**, *79*, 208-214.

(57) Cheng, X. Y.; Gondosiswanto, R.; Ciampi, S.; Reece, P. J.; Gooding, J. J. One-pot synthesis of colloidal silicon quantum dots and surface functionalization via thiol-ene click chemistry. *Chem Commun* **2012**, *48*, 11874-11876.

(58) Cheng, X.; Lowe, S. B.; Ciampi, S.; Magenau, A.; Gaus, K.; Reece, P. J.; Gooding, J. J. Versatile "Click Chemistry" Approach to Functionalizing Silicon Quantum Dots: Applications toward Fluorescent Cellular Imaging. *Langmuir* **2014**, *30*, 5209-5216.

## **Chapter 7 Conclusions and future perspectives**

Even though some of the early reports on SiQDs were published almost twenty years ago<sup>1,2</sup>, acceleration of research was not seen until in recent years (Figure 7.1). This thesis has aimed to expand the current knowledge on the preparation, surface modification and biological applications of colloidal SiQDs. To conclude this thesis, this section summarizes previous chapters and suggests future work on the basis of the results obtained.

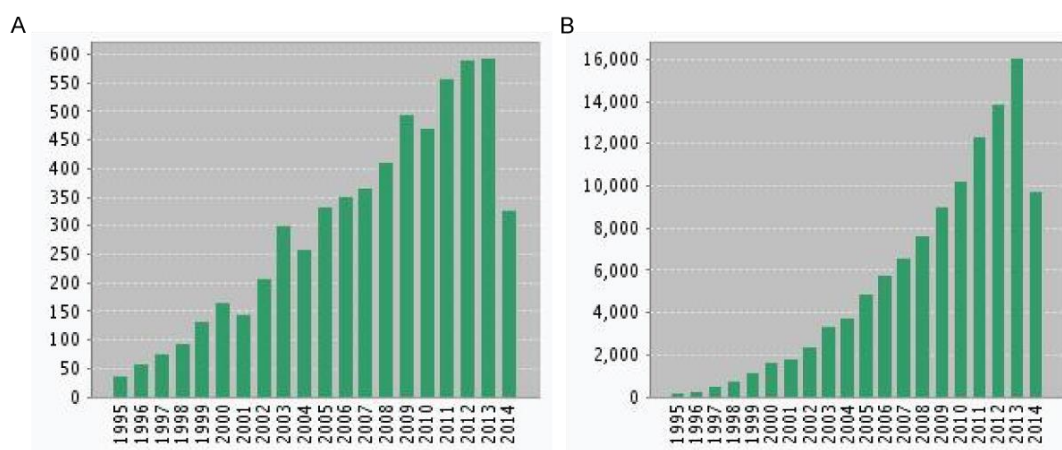


Figure 7.1 Search results analysis with the topic of ‘silicon quantum dots’ using Web of Science. Shown as (A) total number of publications and (B) citations per year.

## 7.1 Summary of results

Chapter three of this thesis showed an efficient one-pot, solution based synthetic method of preparing colloidal SiQDs. The initial alkene passivated particle surface was further functionalized with thiol molecules by thiol-ene ‘click’ reactions. The importance of this advance was that it provided a simple route of fabricating SiQDs with a range of choice of surface functionalities without the need of using surfactants. This progress simplified the current procedure of preparing SiQDs considering the surfactants were difficult to remove and usually involves

column chromatography. However, two problems were identified with this method. The first was that aggregation still occurred to some extent and synthesized SiQDs were not completely monodisperse. The second was that the further modification of SiQDs by thiol-ene click reaction with different organic derivatives bearing different thiol molecules seemed to decrease quantum yield from the nanoparticles.

Chapter four demonstrated a two-step method of preparing and modifying SiQDs by CuAAC ‘click’ reaction. It was shown that the synthesized water soluble SiQDs were suitable for fluorescent imaging using HeLa cells. The functionalized SiQDs exhibited high monodispersity, reasonable quantum yield, and strong PL stability against photobleaching in biological relevant environments. Cell viability studies indicated that the prepared SiQDs had low cytotoxicity even at very high concentrations. The importance of this work was that the high specificity and versatility of azide-alkyne coupling would allow functionalization of SiQDs with a azide molecules of choice with good colloidal stability and PL stability. However, similar to the thiol-ene modification strategy, further attachment of surface molecules bearing azide groups reduced the brightness of SiQDs, although the colloidal stability was less affected compared with the one-pot synthesis.

In chapter five, the FLIM technique was demonstrated using SiQDs with one-photon excitation, two-photon excitation and in the context of FLIM-FRET. The long fluorescence lifetime of SiQDs allowed easy deconvolution of fluorescence signals from the nanoparticles from their biological backgrounds, regardless of their comparable blue colour. It was further demonstrated that the FLIM analysis could be performed using the phasor approach with only limited photons available in each

pixel. In general, this work was developed a new method of working with chemically synthesized SiQDs in intracellular environments in addition to exploring the synthesis strategy.

Chapter six described a protease sensor using SiQDs based on FRET. This was achieved by conjugating the SiQDs donor to a dye acceptor covalently via a short peptide linker. Both PL measurement and modelling suggested the large spectral overlap and close distance of SiQDs/dye would allow energy transfer from the particles to the dye, generating enhanced emission from the acceptor and quenched emission from the donor. Treatment of the FRET conjugates with enzyme resulted in cleavage of the peptide linker between the donor/acceptor pair hence reduced acceptor PL. The results presented in this chapter gave the first experimental demonstration of a SiQDs protease sensor based on FRET.

## **7.2 Future work**

For future work on preparation and surface modifications of SiQDs, the first area to work in is to further explore the impact of surface modification on the colloidal stability of the particles. The results from this thesis indicate that colloidal stability is governed by steric interactions or chain length. Although this conclusion is in agreement with several previous studies<sup>3-5</sup>, a recent report of modifying SiQDs with hard Lewis base suggesting hypervalent interaction is the key factor of stabilizing the particles by ruling out steric or electrostatic effects<sup>6</sup>. Considering the role of surfactant molecules used in this thesis that may also coordinate with silicon surface, this suggests the colloidal stability of SiQDs can be maintained even with

very short, inorganic ligand based surface groups. The short, inorganic ligand based surface groups may significantly improve the charge carrier transport properties within the SiQDs while introducing surface doping at the same time. Both are essential for device fabrication, such as in thin film based SiQDs solar cells or various optoelectronic devices.

The second area of interest is to investigate the relationship between surface modifications and PL properties. Both chapter three and chapter four reported the change of PL properties upon surface modification where decreased quantum yield was observed. For comparison, a recent study by Li *et. al.* showed that attaching certain electron donating species, such as diphenylamine and carbazole on SiQDs surface<sup>7</sup>, significantly increased the quantum yields and fluorescence lifetime of SiQDs by approximately ten folds. Therefore, the relationship between the PL properties of SiQDs and surface modification particularly with electron donating (withdrawing) groups is of great interest. If PL properties (i.e. quantum yield, fluorescence lifetime) can be controlled by varying the surface groups, this will give another method of manipulating the PL properties of the dots in addition to size control.

The third area of interest is to work with the doped SiQDs. Recently, phosphorous doped SiQDs were prepared with plasma synthesis using silane precursors<sup>8</sup>. It was shown for the first time that SiQDs exhibited localized surface plasmon resonance (LSPR) in the near-mid infrared region ( $600\text{-}2500\text{ cm}^{-1}$ ) where optical signature of the particles was tuned by varying carrier concentration<sup>8</sup>. This advancement was important as it paved the way for using doped SiQDs for

applications in plasmonic based bioimaging and photothermal therapies, a new research area currently dominated by metal containing nanocrystals with rare reports seen with semiconductor quantum dots.

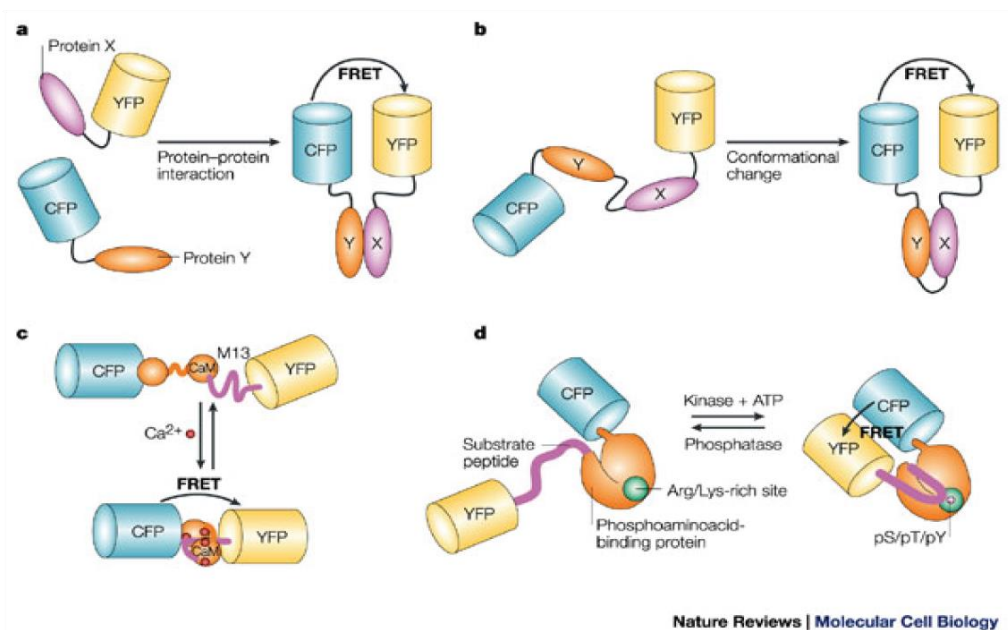


Figure 7.2 Several applications of FRET based probes for cellular biology, demonstrated with a typical FRET pair using cyan fluorescent protein (CFP) and yellow fluorescent protein (YFP). From a-d: a: two proteins (X and Y) labelled with CFP and YFP respectively interact to bring CFP/YFP together to induce FRET; b- c conformational change of a conjugates labelled with CFP/YFP at two ends respond to environmental factors to induce conformation change thus FRET; d: Sensing of intramolecular phosphorylation using FRET. Figure adapted from Zhang *et. al.*<sup>9</sup>

For future work based on the bio-applications using SiQDs, further work can be carried out in both *in situ* or intracellular environments. It is realized that exploiting the interface of SiQDs and their surrounding environments will greatly extend the applications of the dots in biological applications. For *in situ* studies, since the enzyme trypsin used in this thesis had limited clinical significance, an immediate next step is to perform the study with other disease related enzymes, such as the

matrix metalloprotease (MMP) family that are overexpressed in a number of cancers<sup>10,11</sup>. In addition, as FRET is a distance dependent mechanism that does not rely on the chemical nature of the linker between the donor/acceptor, it has been used for investigating processes such as inter molecular interactions (where two interacting molecules are labelled with the FRET pair respectively, Figure 7.2a), intra molecular interactions (where a conjugate is made with ends labelled with the donor/acceptor, Figure 7.2b), and sensing of certain ions or the phosphorylation processes (Figure 7.2c-d). It is suggested that further work based on chapter six can be carried out in those specific applications. An extension of these studies can be carried out in the corresponding intracellular environments utilizing FLIM, where the long fluorescence lifetime, stable PL and low toxicity of SiQDs is most distinctive compared with other fluorophores and quantum dots, to allow tracking of slow biological processes which are otherwise hard to achieve.

### **7.3 Concluding remarks**

Quantum dots that do not contain heavy metal elements are vital to the further developments of this class of nanomaterials for bio-applications. For this purpose, SiQDs are highly desirable due to their non-toxic nature for biological systems. This thesis has developed two new approaches of preparing surface modified SiQDs, proposed the use of FLIM in observing SiQDs, and showed the preparation of a SiQDs protease sensor based on FRET. However, more detailed investigations need to be performed before SiQDs can be translated into clinical settings. It is hoped

that with the continued efforts contributed into these areas, SiQDs will have a bright future of applications at the interface of material science, physics and biomedicine.

#### 7.4 References

- (1) Heath, J. R.: A LIQUID-SOLUTION-PHASE SYNTHESIS OF CRYSTALLINE SILICON. *Science* **1992**, 258, 1131-1133.
- (2) Delley, B.; Steigmeier, E. F.: QUANTUM CONFINEMENT IN SI NANOCRYSTALS. *Phys Rev B* **1993**, 47, 1397-1400.
- (3) Kelly, J. A.; Henderson, E. J.; Veinot, J. G.: Sol-gel precursors for group 14 nanocrystals. *Chem Commun (Camb)* **2010**, 46, 8704-18.
- (4) Veinot, J. G.: Synthesis, surface functionalization, and properties of freestanding silicon nanocrystals. *Chem Commun (Camb)* **2006**, 4160-8.
- (5) Cheng, X.; Lowe, S. B.; Reece, P. J.; Gooding, J. J.: Colloidal silicon quantum dots: from preparation to the modification of self-assembled monolayers (SAMs) for bio-applications. *Chem. Soc. Rev.* **2014**, 43, 2680-2700.
- (6) Wheeler, L. M.; Neale, N. R.; Chen, T.; Kortshagen, U. R.: Hypervalent surface interactions for colloidal stability and doping of silicon nanocrystals. *Nat Commun* **2013**, 4.
- (7) Li, Q.; He, Y.; Chang, J.; Wang, L.; Chen, H.; Tan, Y.-W.; Wang, H.; Shao, Z.: Surface-Modified Silicon Nanoparticles with Ultrabright Photoluminescence and Single-Exponential Decay for Nanoscale Fluorescence Lifetime Imaging of Temperature. *Journal of the American Chemical Society* **2013**, 135, 14924-14927.
- (8) Rowe, D. J.; Jeong, J. S.; Mkhoyan, K. A.; Kortshagen, U. R.: Phosphorus-Doped Silicon Nanocrystals Exhibiting Mid-Infrared Localized Surface Plasmon Resonance. *Nano Letters* **2013**, 13, 1317-1322.
- (9) Zhang, J.; Campbell, R. E.; Ting, A. Y.; Tsien, R. Y.: Creating new fluorescent probes for cell biology. *Nat Rev Mol Cell Biol* **2002**, 3, 906-918.
- (10) McIntyre, J. O.; Fingleton, B.; Wells, K. S.; Piston, D. W.; Lynch, C. C.; Gautam, S.; Matrisian, L. M.: Development of a novel fluorogenic proteolytic beacon for in vivo detection and imaging of tumour-associated matrix metalloproteinase-7 activity. *Biochemical Journal* **2004**, 377, 617-628.
- (11) Xia, Z.; Xing, Y.; So, M.-K.; Koh, A. L.; Sinclair, R.; Rao, J.: Multiplex Detection of Protease Activity with Quantum Dot Nanosensors Prepared by Intein-Mediated Specific Bioconjugation. *Analytical Chemistry* **2008**, 80, 8649-8655.

# Appendix

## Appendix I Characterization of dye labelled peptides by HPLC-MS

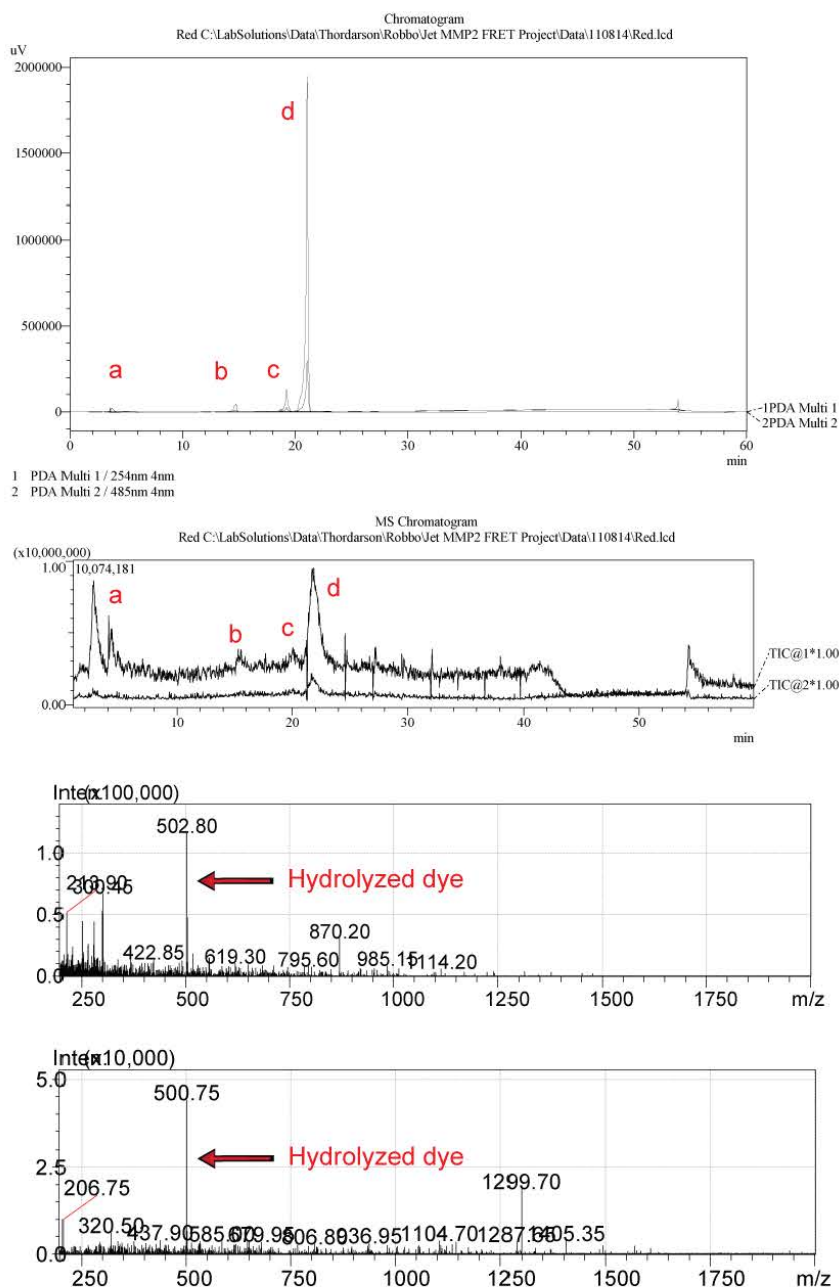


Figure A.1 The exact mass of the hydrolyzed dye is 502.59 u (peak c in MS chromatogram). The observed signals were in the MS (ESI +) at m/z 502.80 and in the MS (ESI -) at m/z 500.75. At  $t_R$  20.0 min we have identified both the dye UV

absorbance at 485 nm, the parent ion in positive ESI MS, and the doubly negative charged species in negative ESI MS.

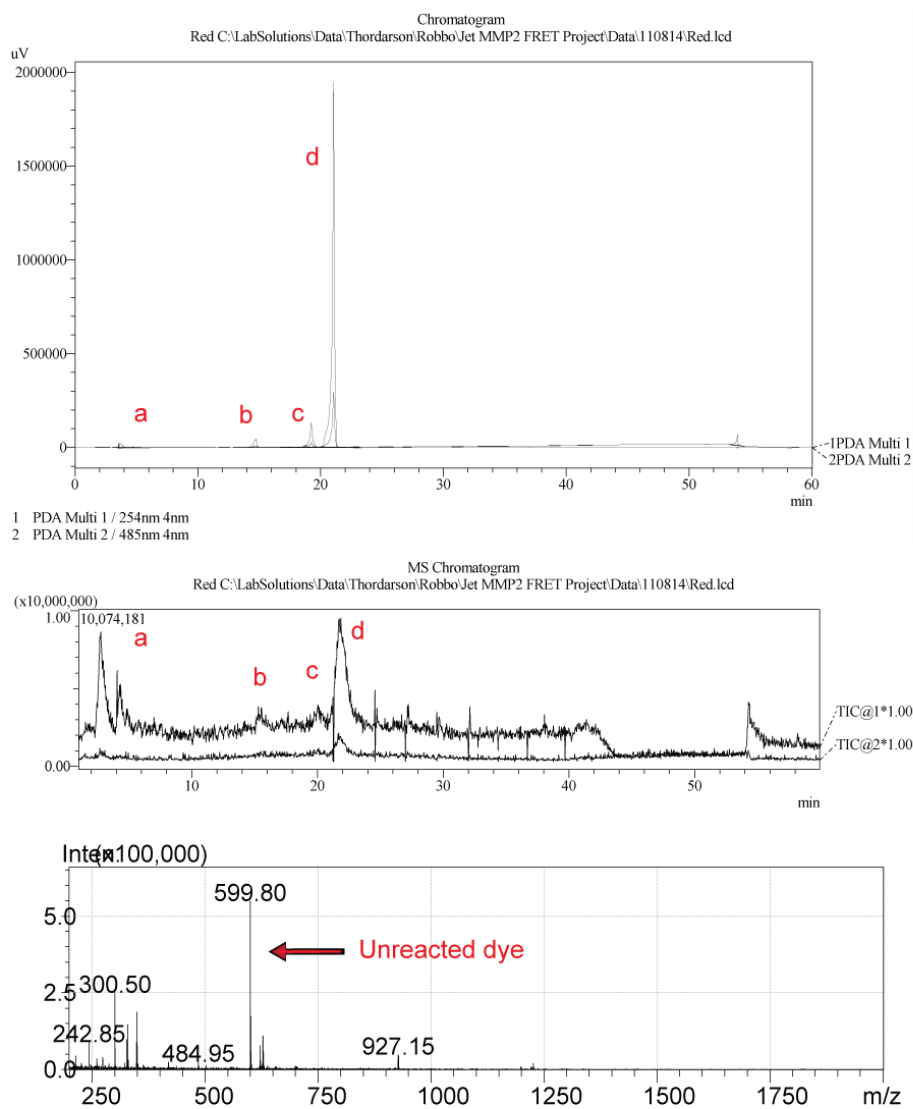


Figure A.2 The exact mass of the unreacted dye is 599.67 u (peak d in MS chromatogram). The observed signals were in the MS at  $m/z$  599.80. At  $t_R$  21.0 min we have identified both the dye UV absorbance at 485 nm.

## Appendix II Optical properties of SiQDs-porphyrin conjugates

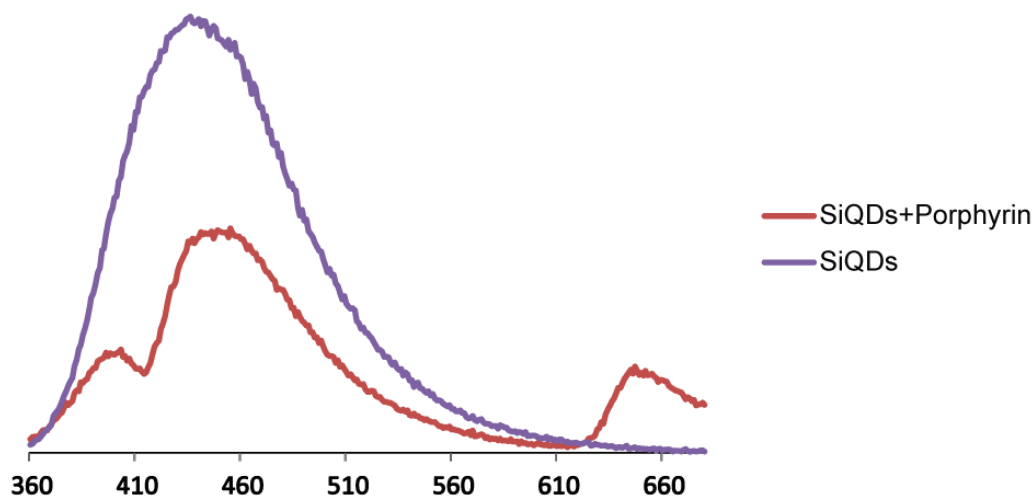


Figure A.3 PL emission spectra of SiQDs-porphyrin conjugates upon EDC/NHS coupling. The dye (*meso*-tetra(4-carboxyphenyl)porphyrine) absorbs at 420 nm and emits at 650 nm. The presence of porphyrin induced quenched PL from the nanoparticles, which is particularly obvious at 420 nm where dye absorbs most strongly.

## Appendix III FLIM study of SiQDs-porphyrin conjugates

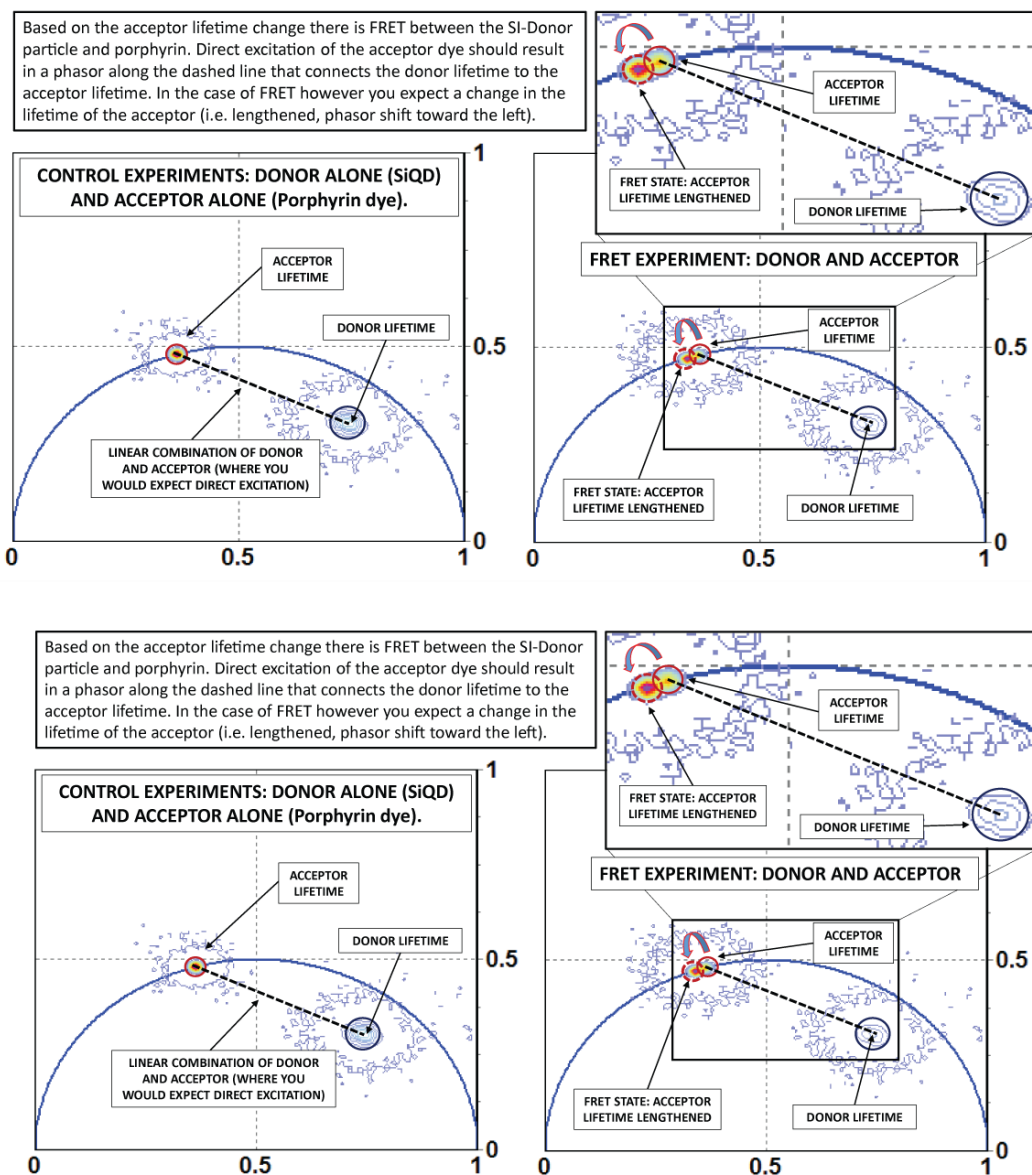


Figure A. 4 FLIM study of SiQDs porphyrin conjugates. The attachment of porphyrin to SiQDs resulted in increased lifetime of the acceptor porphyrin, suggesting FRET between the two fluorophores. The experiments were carried out with both one photon (above) and two photon (below) excitations.